

CONCEPTS AND TOOLS TO IMPROVE THE THERMAL ENERGY PERFORMANCE OF BUILDINGS AND URBAN DISTRICTS

**DIAGNOSIS, ASSESSMENT, IMPROVEMENT STRATEGIES,
AND COST-BENEFIT ANALYSES**

Zur Erlangung des akademischen Grades eines

Doktors der Ingenieurwissenschaften
(Dr.-Ing.)

von der KIT-Fakultät für Wirtschaftswissenschaften
des Karlsruher Instituts für Technologie (KIT)

genehmigte

Dissertation

von

Zoe Mayer M. Sc.

Tag der mündlichen Prüfung: 01.02.2023

Referent: Prof. Dr. Frank Schultmann

Korreferent: Prof. Dr. Thomas Lützkendorf

Lizenzierung

Das vorliegende Werk darf von der KIT-Bibliothek frei im Internet angeboten werden. Die Nutzung erfolgt ausschließlich zu wissenschaftlichen Zwecken und zum Eigengebrauch. Die Urheberrechte liegen bei den Autorinnen bzw. Autoren. Für den Inhalt sind alleine die Autorinnen und Autoren verantwortlich. Jegliche Formen der kommerziellen Nutzung und Abänderung der Publikation sind ohne vorherige Zustimmung und Absprache mit den Autorinnen bzw. Autoren ausdrücklich verboten, es sei denn, sie sind durch eine Creative-Commons- oder vergleichbare Lizenz explizit gestattet. Die Namen der Autorinnen und Autoren müssen stets genannt werden. Die Nutzerinnen und Nutzer sind für die Einhaltung der Rechtsvorschriften selbst verantwortlich und können bei Missbrauch haftbar gemacht werden.

Acknowledgements

I would like to take this opportunity to acknowledge the people and institutions that have supported me while working on this dissertation.

First, I want to thank my supervisor Prof Dr. Frank Schultmann and Dr. Rebekka Volk, the head of my research lab, for their help and patience. I thank Prof. Dr. Thomas Lützkendorf, Prof. Dr. Gerhard Satzger, and Prof. Dr. Ingrid Ott for reviewing my dissertation and being a part of my examination committee. I am grateful to all my co-authors, Prof. Dr. Lucio Soibelman, Prof. Dr. Achim Streit, Dr. James Kahn, Dr. Yu Hou, Dr. Markus Götz, Elena Vollmer, Julia Heuer, Tobias Beiersdörfer, Nicolas Blumenröhr, and Zhaoyang Li, for their collaboration on the research projects, papers, and publications, which are part of this cumulative dissertation. I thank Harald Schneider for supporting and advising me during my research. The time spent together with my colleagues at the Institute for Industrial Production is invaluable for me, and I am grateful for the same. Further, I sincerely thank Marinus Vogl and the Air Bavarian GmbH for supporting me with the collection and development of usable datasets. My family and friends constantly encouraged and stood by me during my work on this dissertation. For that, I am forever grateful.

This research would not have been possible without the support provided by the Landesgraduiertenförderung (State Postgraduate Fellowship Programme) of the Karlsruhe Institute of Technology (KIT) and the Studienstiftung des Deutschen Volkes (German Academic Scholarship Foundation).

Karlsruhe, May 2023
Zoe Mayer

Abstract

Retrofitting existing buildings to optimize their thermal energy performance is a key factor in achieving climate neutrality by 2045 in Germany. Analyzing buildings in their current condition is the first step toward preparing effective and efficient energy retrofit measures. A high-quality building analysis helps to evaluate whether a building or its components are suitable for retrofitting or replacement. Subsequently, appropriate combinations of retrofit measures that create financial and environmental synergies can be determined.

This dissertation is a cumulative work based on nine papers on the thermal analysis of existing buildings. The focus of this work and related papers is on thermography with drones for building audits, intelligent processing of thermographic images to detect and assess thermal weaknesses, and building modeling approaches to evaluate thermal retrofit options. While individual buildings are usually the focus of retrofit planning, this dissertation also examines the role of buildings in the urban context, particularly on a district level. Multiple adjacent buildings offer numerous possibilities for further improving retrofits, such as the economies of scale for planning services and material procurement, neighborhood dynamics, and exchange of experiences between familiar building owners.

This work reveals the opportunities and obstacles for panorama drone thermography for building audits. It shows that drones can contribute to a quick and structured data collection, particularly for large building stocks, and thus complement current approaches for district-scale analysis. However, the significant distance between the drone camera and building, which is necessary for automated flight routes, and varying recording angles limit the quantitative interpretability of thermographic images. Therefore, innovative approaches were developed to process image datasets generated using drones. A newly designed AI-based approach can automate the detection of thermal bridges on rooftops. Using generalizations about certain building classes as demonstrated by buildings from the 1950s and 1960s, a novel interpretation method for drone images is suggested. It enables decision-making regarding the need to retrofit thermal bridges of recorded buildings. A novel optimization model for German single-family houses was developed and applied in a case study to investigate the financial and ecological benefits of different thermal retrofit measures. The results showed that the retrofitting of building façades can significantly save energy. However, they also revealed that replacing the heating systems turns out to be more cost-effective for carbon dioxide savings.

Small datasets, limited availability of technical equipment, and the need for simplified assumptions for building characteristics without any information were the main challenges of the approaches in this dissertation.

Contents

Acknowledgements	i
Abstract	ii
Contents	iii
Figures	v
Tables	vi
Abbreviations	vii
Part I: Framework, Foundations, and Implications	1
1 Introduction	2
1.1 Motivation	2
1.2 Objective and Research Questions	3
1.3 Structure of the Dissertation	3
2 Theoretical Foundations	7
2.1 The German Building Stock.....	7
2.2 Buildings and Thermal Energy	9
2.3 Energy Retrofits of Buildings.....	10
2.4 Different Urban Scales for Planning Energy Retrofits.....	12
2.5 Thermal Analysis and Retrofit Planning Approaches for Buildings.....	16
3 Summary of the Studies and Key Results	19
3.1 Paper A: Building Analysis Approaches for Planning Energy Retrofits on District Scale	19
3.2 Paper B: Evaluating the Quality of Aerial and Terrestrial Building Thermography for the Thermal Analysis of Buildings.....	21
3.3 Paper C: Further Investigations to Evaluate the Quality of Aerial and Terrestrial Thermographic Images	23
3.4 Paper D: Building Façade Component Segmentation for Drone-Based Building Analysis Approaches	25
3.5 Paper E: Automated Thermal Bridge Detection of Building Rooftops on District Scale Using Aerial Thermographic Images.....	27
3.6 Paper F: Improving the Automated Thermal Bridge Detection of Building Rooftops Using Aerial Thermographic Images	28
3.7 Paper G: Dataset of Thermal Bridges on Building Rooftops.....	31
3.8 Paper H: Thermographic Image-Based Assessment for Thermal Bridges on District Scale.....	32

3.9 Paper I: Planning Thermal Retrofits for Single Buildings	35
4 Conclusion and Discussion.....	39
References	42
Part II Companion Articles	52
Evaluation of Building Analysis Approaches as a Basis for the Energy Improvement of City Districts.....	Paper A
Comparison of Building Thermography Approaches Using Terrestrial and Aerial Thermographic Images	Paper B
Investigating the Quality of Thermographic Drone Images for the Analysis of Buildings.....	Paper C
A Computer Vision Approach for Building Façade Component Segmentation on 3D Point Cloud Models Reconstructed by Aerial Images.....	Paper D
AI-Based Thermal Bridge Detection of Building Rooftops on District Scale Using Aerial Images.....	Paper E
Deep Learning Approaches to Building Rooftop Thermal Bridge Detection from Aerial Images.....	Paper F
Thermal Bridges on Building Rooftops (TBBR).....	Paper G
Aerial Thermographic Image-Based Assessment of Thermal Bridges Using Representative Classifications and Calculations.....	Paper H
Analysis of Financial Benefits for Energy Retrofits of Owner-Occupied Single-Family Houses in Germany.....	Paper I

Figures

Figure 1: Research questions addressed by the research papers included in this dissertation (Mayer et al., 2021 – Paper A; Mayer et al., 2022 – Paper B; Mayer et al., 2022 – Paper C; Hou et al., 2021 – Paper D; Mayer et al., 2021 – Paper E; Mayer et al., 2022 – Paper F; Mayer et al., 2023 – Paper G; Mayer et al., 2021 – Paper H; Mayer et al., 2022 – Paper I)	6
Figure 2: Research fields of the research papers included in this dissertation (Mayer et al., 2021 – Paper A; Mayer et al., 2022 – Paper B; Mayer et al., 2022 – Paper C; Hou et al., 2021 – Paper D; Mayer et al., 2021 – Paper E; Mayer et al., 2022 – Paper F; Mayer et al., 2023 – Paper G; Mayer et al., 2021 – Paper H; Mayer et al., 2022 – Paper I).....	6
Figure 3: Study design for the analysis of EQs presented in Paper A (Original source: Mayer et al., 2021 – Paper A).....	20
Figure 4: 3D point cloud reconstructions from thermal and RGB images presented in Paper D: (A) RGB and (B) thermal 3D model from a city area in Karlsruhe; (C) RGB and (D) thermal 3D model from a university campus in Karlsruhe (Original source: Hou et al., 2021 – Paper D).....	26
Figure 5: Drone images of the city center of Karlsruhe used for the TBBR dataset presented in Paper E: (A) thermal image, (B) RGB image, and (C) image with height information (Original source: Mayer et al., 2021 – Paper E)	28
Figure 6: Flowchart for the study design of Paper F (Mayer et al., 2022 – Paper F)	30
Figure 7: Research design of Paper H. For more details on references of the Figure see original paper. (Original source: Mayer et al., 2021 – Paper H).....	33
Figure 8: Model components of the optimization model including model input parameters, calculation modules, and model outputs presented in Paper I (Original source: Mayer et al., 2022 – Paper I)	36

Tables

Table 1: Characteristics of German buildings from the construction time between 1949 to 1978 (Loga et al., 2015).....	8
Table 2: Different urban scales for planning building energy retrofits (Dixon and Eames, 2013; Paiho et al., 2019; Riechel, 2016; Riechel and Koritkowski, 2016; Ruggeri et al., 2020; Images from Google Maps, 2021).....	16
Table 3: Experimental parameters for thermographic drone flights of Paper B (Original source: Mayer et al., 2022 – Paper B)	22
Table 4: Experimental parameters for thermographic drone flights of Paper C (Original source: Mayer et al., 2022 – Paper C)	24
Table 5: Tested neural network architectures and training configurations presented in Paper F (Mask RCNN-R18* indicated that the model was initialized with the identical random seed as used in Paper E) (Original source: Mayer et al., 2022 – Paper F)	30
Table 6: TBBR annotations and characteristics (Original source: Mayer et al., 2022 – Paper G).....	32
Table 7: Overview of thermal bridge types visible on thermographic drone images presented in Paper H (Original source: Mayer et al., 2021 – Paper H)	34

Abbreviations

2D	Two-dimensional
3D	Three-dimensional
AI	Artificial intelligence
AR	Average recall
BA	Bundesanzeiger (Federal Gazette)
BAFA	Bundesamt für Wirtschaft und Ausfuhrkontrolle (Federal Office for Economic Affairs and Export Control)
BBSR	Bundesinstitut für Stadt-, Bau-, und Raumforschung (Federal Institute for Research on Building, Urban Affairs and Spatial Development)
BDEW	Bundesverband der Energie- und Wasserwirtschaft (German Association of Energy and Water Industries)
BetrKV	Betriebskostenverordnung (Operating Costs Ordinance)
BGB	Bürgerliches Gesetzbuch (German Civil Code)
BT	Deutscher Bundestag (German Bundestag)
BMWi	Bundesministerium für Wirtschaft und Energie (Federal Ministry for Economic Affairs and Energy); since 2021: BMWK/ Bundesministerium für Wirtschaft und Klimaschutz (Federal Ministry for Economic Affairs and Climate Action)
BMWK	Bundesministerium für Wirtschaft und Klimaschutz (Federal Ministry for Economic Affairs and Climate Action)
BMWSB	Bundesministerium für Wohnen, Stadtentwicklung und Bauwesen (Federal Ministry for Housing, Urban Development and Building)
CA	Companion Article
CO ₂	Carbon dioxide
CEP	Community energy planning
CESP	Community energy strategic planning

dena	Deutsche Energie Agentur (German Energy Agency)
Destatis	Statistisches Bundesamt (Federal Statistical Office of Germany)
DIN	Deutsches Institut für Normung (German Institute for Standardization)
DOE	Department of Energy, United States of America
EEG	Erneuerbare Energien Gesetz (Renewable Energy Sources Act)
EG-ICE	European Group for Intelligent Computing in Engineering
EN	Europäische Norm (European Standard)
EStG	Einkommenssteuergesetz (Income Tax Act)
EQ	Energetisches Quartierskonzept (Energy District Plan)
ErbbauRG	Erbbaurechtsgesetz (Heritable Building Act)
FSAF	Feature selective anchor-free neural network architecture
GAMS	General algebraic modeling system
GAN	Generative adversarial networks
GEG	Gebäudeenergiegesetz (Buildings Energy Act)
GemO	Gemeindeordnung (Municipal Code of Baden-Wuerttemberg)
GPU	Graphic processing unit
HeizkostenV	Verordnung über Heizkostenabrechnung (Heating Costs Ordinance)
IIP	Institut für Industriebetriebslehre und Industrielle Produktion (Institute for Industrial Production)
IoU	Intersection over union
KfW	Kreditanstalt für Wiederaufbau (Credit Institute for Reconstruction)
KIT	Karlsruher Institut für Technologie (Karlsruhe Institute of Technology)
KPA	Kopernikus-Projekt Ariadne (Copernicus Project Ariadne)
KSG	Bundesklimaschutzgesetz (Federal Climate Change Act)
LBO BW	Landesbauordnung Baden-Württemberg (Baden-Wuerttemberg Building Ordinance)

Mask RCNN-18	Neural network architecture based on a region based convolutional neural network
Mask RCNN-R50	Neural network architecture based on a region based convolutional neural network
MFH	Multi-family house
PED	Positive energy district
PIB	Presse- und Informationsamt der Bundesregierung (Press and Information Office of the German Federal Government)
ResNet+9 blocks	Residual neural network architecture
RGB	Red green blue
SBE	Sustainable built environment
SFH	Single-family house
SR	Savills Research
Swin-T	Shifted windows transformer neural network architecture
SWOT	Strengths weaknesses opportunities and threats
TBBR	Thermal bridges on building rooftops (TBBR dataset)
TFH	Two-family house
ThermCAD	Software tool based on a computer-aided design (CAD) system
TridentNet	Trident network neural network architecture
UAV	Unmanned aerial vehicle
UAS	Unmanned aerial system
UE	Urban Europe
U-Net256	U-shaped neural network architecture
v1	Version 1
v2	Version 2

Part I: Framework, Foundations, and Implications

1 Introduction

1.1 Motivation

The Bundesklimaschutzgesetz (KSG) (Federal Climate Change Act) has set the target of climate-neutrality in Germany by 2045 (KSG, 2019). The energy consumption of buildings is crucial for achieving this goal. In Germany, approximately 17% of the total carbon dioxide (CO₂) emissions come directly from the building sector (BMW_i, 2015). This number rises to around 30% when also considering indirect CO₂ emissions, including those caused by the production of electricity and district heat for buildings, and to around 40% when considering the production, processing, and disposal of building materials as well (BBSR, 2020; BBSR, 2021; BMW_i, 2015).

Owing to the growing demand for living space and low reconstruction rates in Germany, high climate protection standards for new buildings alone are insufficient to significantly reduce the primary energy demand of buildings (dena, 2021). Of greater importance are energy retrofits of existing buildings, which modify them to improve their energy performance (Richarz et al., 2006). However, the retrofit rate in Germany has been stagnating at a consistently low level of approximately 1% for many years and steps need to be taken to increase it if Germany is to achieve its climate neutrality goals (BMW_i, 2015; KPA, 2021).

Individual buildings are usually the focus of the planning and implementation of energy retrofit measures (Ruggeri et al., 2020). New opportunities arise with the simultaneous consideration of multiple buildings (Riechel, 2016; Ruggeri et al., 2020). The urban level is particularly suitable for retrofitting multiple buildings. An urban district is a small subunit of the city (Riechel, 2016). Internationally, many approaches that push energy retrofits on a district scale, such as community energy strategic planning (CESP) in the USA, community energy planning (CEP) in Canada, and positive energy districts (PED) in Europe are prevalent (DOE, 2013; Littlejohn and Laszlo, 2015; Mayer et al., 2021 – Paper A; UE, 2013). In Germany, retrofits on a district scale are frequently planned as part of energetische Quartierskonzepte (EQs) (energy district plans) (KfW, 2015).

For effective and efficient retrofits of buildings, an analysis of the initial state before starting the retrofit process is crucial (Balaras, 2022). The initial condition of a building should be well recorded to deduce possible retrofit options that can be comprehensively weighed and prioritized. As detailed analysis and retrofit planning approaches for individual buildings cannot always be efficiently scaled up to entire districts, new approaches or further development of existing tools are required.

1.2 Objective and Research Questions

The aim of this dissertation is to investigate approaches for analyzing the thermal quality of buildings to optimally prepare for planning and implementing energy retrofits. The focus of this work is on the analysis of individual buildings and analysis approaches for multiple neighboring buildings and city districts. Both the technical and economic aspects of energy retrofitting were considered in this context. The focus is on German residential buildings built post war and before the first thermal insulation regulations between 1950 and 1978 (Loga et al, 2015). Due to a lack of energy quality standards, these buildings usually have high thermal deficits and require improvements (BMW, 2022). The overall goal is to identify, develop, and supplement existing building analysis approaches and make the energy retrofits for German buildings more efficient and effective. This work utilized terrestrial and airborne thermography with unmanned aerial vehicles (UVAs/drones) for this purpose.

The research questions addressed in this dissertation are listed as follows.

- 1) Which analytical approaches for buildings on a district scale are commonly used for planning thermal retrofits?
- 2) How can thermography with drones be used to analyze buildings on a district scale?
- 3) How can the processing of thermal images collected with a drone be automated for the detection of the thermal weaknesses of building envelopes?
- 4) How to plan efficient and effective thermal retrofit measures for buildings in Germany?

1.3 Structure of the Dissertation

This dissertation is cumulative. In addition to the comprehensive outline given in Part I, nine research papers are listed in Part II. They address the different research questions of this dissertation.

Part I begins with an introductory chapter that states the need to investigate thermal analysis approaches of buildings for planning energy retrofits for individual buildings, city districts, and entire cities. The second section of Part I provides the theoretical foundations required for a better understanding of this dissertation. This includes an overview of the German building stock and its thermal quality, a summary of thermal energy aspects relevant to buildings, the definition of thermal energy retrofits as used in this work, and an explanation of the different urban scales of interest for analyzing buildings and planning retrofits. This section also introduces different analysis approaches for the thermal performance of buildings. The third section of Part I summarizes the methods, materials and results of the nine research papers. The final section provides a critical discussion of the methods, materials, and results of this dissertation and points out changes in framework conditions and databases that occurred after the

publication of the single research papers. It also contains a conclusion on the main outcomes of this dissertation.

Part II contains the following scientific papers, ordered according to their main research questions as outlined in Figure 1. They are based on research collaborations with different co-authors. Figure 2 provides an overview of the different research areas that are covered in these papers.

- Paper A, “Evaluation of building analysis approaches as a basis for the energy improvement of city districts”: This article was published in 2021 in the Karlsruhe Institute of Technology (KIT) Working Paper Series in Production and Energy and gives an overview of current building analysis approaches. It reveals the strengths and weaknesses of the planning of thermal building retrofits on a district scale. This study was based on an analysis of 25 publicly available reports of German energy district plans (EQs). (Mayer et al., 2021 – Paper A)
- Paper B, “Comparison of building thermography approaches using terrestrial and aerial thermographic images”: This paper was presented in 2022 at the Sustainable Built Environment (SBE) Conference in Berlin. It compares the thermographic image quality of classical-terrestrial thermography and airborne thermography with drones for thermal audits of buildings. During the study, an image dataset of German buildings was collected with terrestrial and drone cameras varying in flight speed, angle, and height. The image data were evaluated according to different image quality characteristics. (Mayer et al., 2022 – Paper B)
- Paper C, “Investigating the quality of thermographic drone images for the analysis of buildings”: This paper was published by the journal Remote Sensing in 2023. This is a follow-up study to Paper B that expands its results with a novel improved dataset and more comprehensive quantitative analysis of the recorded aerial and terrestrial images. (Mayer et al., 2023 – Paper C)
- Paper D, “A computer vision approach for building façade component segmentation on 3D point cloud models reconstructed by aerial images”: This paper was presented in 2021 at the European Group for Intelligent Computing in Engineering (EG-ICE) Conference in Berlin. To improve image processing approaches for building audits working with aerial thermographic image data, this study introduces a segmentation approach using open-source training datasets. It segmented windows and doors on façade images rendered from three-dimensional (3D) point clouds. (Hou et al., 2021 – Paper D)
- Paper E, “AI-based thermal bridge detection of building rooftops on district scale using aerial images”: This contribution was presented in 2021 at the EG-ICE Conference in Berlin. It proposes a method to automatically detect thermal bridges on building roof-

tops from panorama drone images of city districts. This study used an image dataset containing thermal information and a height map for rooftop recognition in addition to the red green blue (RGB) information to train and evaluate a neural network. (Mayer et al., 2021 – Paper E)

- Paper F, “Deep learning approaches to building rooftop thermal bridge detection from aerial images”: This paper was published by the journal Automation in Construction in 2022. It improves the approach presented in Paper E. Using an updated thermal drone image dataset of thermal bridges on building rooftops, this study focused on enhancing the object detection quality. It compared multiple state-of-the-art neural networks. (Mayer et al., 2022 – Paper F)
- Paper G, “Thermal Bridges on Building Rooftops (TBBR)”: This paper was published in 2023 in the journal Nature Scientific Data. It provides a detailed description of a dataset of thermal bridges on building rooftops. The paper provided the basis for the studies presented in Papers E and F. (Mayer et al., 2023 – Paper G)
- Paper H, “Aerial thermographic image-based assessment of thermal bridges using representative classifications and calculations”: This paper was published in 2021 in the journal Energies. It describes an approach for identifying and characterizing thermal bridges on aerial thermographic images in terms of their risk for the formation of mold, energy losses, retrofit costs, and energy-saving related retrofit benefits. Based on a dataset of thermal drone images, thermal bridge types for the German building cohorts of the 1950s and 1960s were classified. (Mayer et al., 2021 – Paper H)
- Paper I, “Analysis of financial benefits for energy retrofits of owner-occupied single-family houses in Germany”: This paper was published in 2022 in the journal Building and Environment. It investigates the potential for saving CO₂ with financially optimal retrofits from the perspective of building owners. A mixed-integer economic optimization model was developed to determine the energy retrofit configurations for owner-occupied buildings. It was tested through case studies of two representative German single-family houses (SFHs) constructed in the 1960s and 1970s. (Mayer et al., 2022 – Paper I)

1) Which analytical approaches for buildings on a district scale are commonly used for planning thermal retrofits?	2) How can thermography with drones be used to analyze buildings on a district scale?	3) How can the processing of thermal images collected with a drone be automated for the detection of the thermal weaknesses of building envelopes?	4) How to plan efficient and effective thermal retrofit measures for buildings in Germany?
A	B C G H	D E F G	H I

Figure 1: Research questions addressed by the research papers included in this dissertation (Mayer et al., 2021 – Paper A; Mayer et al., 2022 – Paper B; Mayer et al., 2023 – Paper C; Hou et al., 2021 – Paper D; Mayer et al., 2021 – Paper E; Mayer et al., 2022 – Paper F; Mayer et al., 2023 – Paper G; Mayer et al., 2021 – Paper H; Mayer et al., 2022 – Paper I)

Individual buildings	Building stocks	German buildings (1949-1978)
I	A B C D E F G H	H I
Thermal bridges	Building rooftops	German framework conditions
E F G H	E F G	A H I
Thermographic building audits	Retrofit measure assessment	Building modeling
B C D E F G H	H I	H I
Economic perspective	Technical perspective	Aerial image datasets
H I	B C D E F G H I	B C D E F G H
Computer science approaches	Literature based study	Quantitative optimization study
D E F G I	A	D E F I

Figure 2: Research fields of the research papers included in this dissertation (Mayer et al., 2021 – Paper A; Mayer et al., 2022 – Paper B; Mayer et al., 2023 – Paper C; Hou et al., 2021 – Paper D; Mayer et al., 2021 – Paper E; Mayer et al., 2022 – Paper F; Mayer et al., 2023 – Paper G; Mayer et al., 2021 – Paper H; Mayer et al., 2022 – Paper I)

2 Theoretical Foundations

2.1 The German Building Stock

There are approximately 21 million buildings in Germany. They include 19 million residential buildings with 43 million residential units. This group of residential buildings can be broken down into three million apartment buildings/multi-family houses (MFHs), 16 million single-family houses (SFHs), and two-family houses (TFHs). SFHs and TFHs comprise half of all residential units and 60% of living space. MFHs comprise the other half of the residential units but only 40% of the living space. In contrast to residential buildings, there is no official number of non-residential buildings. However, approximately 2 million heated units are estimated to be in use. (dena, 2021; Loga et al, 2015)

Most residential buildings in Germany were built in the post-war period after 1945 (Loga et al, 2015). A significant number of buildings were constructed before the first thermal insulation regulations. Approximately 38% of all buildings, 43% of all residential units, and 41% of the total living space of the German building stock date from 1949–78 (Loga et al, 2015). According to the German building typology proposed by Loga et al. (2015), German buildings constructed between 1949 and 1978 can be divided into three subclasses based on their architectural styles and construction designs. A distinction is made between buildings constructed in 1949–57, 1958–68, and 1969–78. The main characteristics of these buildings are summarized in Table 1.

Table 1: Characteristics of German buildings from the construction time between 1949 to 1978 (Loga et al., 2015)

Period	General characteristics
1949–1957	<ul style="list-style-type: none"> • Simple construction styles during the post-war period (often with debris materials) were standard. • The requirements for social housing were introduced. • They had predominantly masonry constructions, single or double shell masonry made of solid bricks, and rubble hollow blocks. • Wooden beam ceilings were used only in single-family houses. • Top floor/ roof was often heated and used as a living space. • Constructions often had strong thermal bridges, especially on cantilevered balconies of apartment buildings. • There was an increase in the use of central heating (coke, gas, and oil), gas floor heating, or gas ovens instead of solid fuel ovens. • District heating systems were used in the German Democratic Republic.
1958–1968	<ul style="list-style-type: none"> • First residential tower blocks were built in multi-story housing. • Reinforced concrete constructions in many variations became increasingly dominant. • Plastered masonry made of hollow blocks, lattice bricks, chipboard blocks or similar material was used. • Constructions often had strong thermal bridges, particularly on cantilevered concrete components. • Multi-family buildings were often constructed with masonry made of plastered lattice bricks, perforated sand-lime bricks, or panel constructions with concrete sandwich elements. • Top floor/ roof was often heated and used as a living space. • Coal, oil, and gas central heating or district heating was used commonly. • Running hot water became commonplace.
1969–1978	<ul style="list-style-type: none"> • New industrial construction methods (sandwich constructions) were used. • Prefabricated house concept was utilized in the single-family house sector. • Sometimes panels were constructed with lightweight or concrete sandwich elements. • Concrete ceilings became common. • Masonry was made of plastered lattice bricks, sand-lime perforated bricks, aerated concrete, or similar substances. • Constructions often contained strong thermal bridges, particularly on cantilevered concrete components. • Triggered by the first oil crisis, heat insulation gradually gained importance.

The German building stock accounts for 850 TWh of the energy usage annually (dena, 2021). For residential buildings, space heating and hot water account for the largest share of energy consumption (approximately 85%) (dena, 2021). Process heat including cooking, cooling, mechanical energy, information and communication technology, and lighting accounts for the rest (dena, 2021). Most residential buildings are heated using fossil fuels. Approximately half of the residential units operate with gas, a quarter with oil, 15% with district heat, and only 3% operate heat pumps (BDEW, 2022). Buildings built between 1949 and 1979 consume the highest amount of energy (BMW, 2022). Different stakeholders own the German residential building stock. In addition to private owners and owner associations, buildings are owned by municipalities, municipal building associations, housing associations, private housing companies, and investment funds (SR, 2019). Approximately 45% of all residential units in Germany are occupied by the owners, and 55% are rented (Destatis, 2019). Private ownership is concentrated in SFHs and TFHs. While approximately 85% of all SFHs and 55% of all TFHs are occupied by private owners, most rental units are in apartment buildings (Destatis, 2019).

2.2 Buildings and Thermal Energy

When considering buildings and thermal energy, two aspects are important: supply and demand. The supply side is determined by the heating and cooling system of the building and its energy source. Conversely, the demand side is determined by the thermal quality of the building envelope. (Chwieduk, 2003)

Neglecting cooling energy, which is not in the focus of this dissertation, the demand side of a building can be characterized by its heating energy requirements. A distinction is made between the Heizenergiebedarf (heating energy needs) and the Heizenergieverbrauch (heating energy consumption) of a building. Heating energy needs are theoretically determined under standard conditions. Heating energy consumption is the actual measurable demand of a building. Along with other factors, it depends on the behavior of the building inhabitants and fluctuating weather conditions. (DIN V 18599, 2021)

The heating energy requirements of a building depend on the following factors (DIN V 18599, 2021):

- transmission heat losses through the building envelope;
- ventilation heat losses caused by the building ventilation and leaks in the building envelope;
- solar heat gains caused by the solar radiation through transparent components or radiation absorption on the surfaces of nontransparent envelope components;
- internal heat gains from people/animals and devices in a household.

In particular, heat gains are independent of the building fabric¹. The heat losses characterize the thermal quality of a building. The ventilation heat loss of a building is determined by the ventilation system. A building can be ventilated freely through windows and mechanical ventilation. A higher ventilation-heat loss occurs if the building envelope is not airtight and has leaks through which heated air is lost. The heat losses of a building envelope are determined by its transmission heat loss. The total losses are the sum of the heat losses through the single envelope components and heat losses through thermal bridges. These heat losses depend on the area size and thermal quality of a building's envelope components and vary considerably between buildings². (DIN V 18599, 2021; Schild, 2018) A thermal bridge is an area of the building envelope that conducts heat more easily from the warmer inside to the colder outside than the adjacent areas (Schild, 2018). This is due to the different thermal conductivities of the materials used or geometry of the construction (Schmidt and Windhausen, 2017). Thermal bridges can be either linear/ 2D (two-dimensional) (2D thermal bridges) or punctual/ 3D (3D thermal bridges) (Schild, 2018). The heat losses of linear thermal bridges can account for up to one-third of the transmission heat losses of the entire building (Schild, 2018; Theodosiou and Papadopoulos, 2008). Contrarily, the influence of punctual thermal bridges is negligible (Schild, 2018). Therefore, they are neglected in most analyses. Only frequently-occurring punctual thermal bridges should be considered when evaluating the thermal characteristics of buildings (Schild, 2018). Moreover, thermal bridges significantly increase the risk for the accumulation of moisture and formation of mold (Vereecken and Roels, 2012).

To compensate for heat energy losses through the building envelope and to heat up water, the heating system of a building plays a key role. The economic and ecological performance of a heating system depends on the efficiency of the heat generation, the distribution system, and the energy sources used. (DIN V 18599, 2021)

2.3 Energy Retrofits of Buildings

Within the context of a building environment, the term “retrofit” is used to describe substantive physical changes to buildings. A building retrofit is often linked to adaptation, which is an intervention to adjust, reuse, or upgrade a building to suit new conditions or requirements. (Dixon and Eames, 2013)

¹ Solar heat gains can be influenced by changing the building components (e.g., larger window areas) along with a significant change in the architecture.

² In Germany, the average proportion of the building envelope is 53% for walls (including windows and doors), 27% for the rooftops, and 20% for the base. (Holm and Maderspacher, 2018). Assuming similar heat transfer coefficients of the single envelope components, transmission heat losses through the individual components can also be expected to be in this percentage range.

In building retrofitting, energy retrofits and conventional (non-energy-related) retrofits should be distinguished. Conventional retrofits are optical or functional modifications to a building or its parts that do not necessarily improve or at times even worsen its energy performance (Kumbaroğlu and Madlener, 2012). Energy retrofits are modifications to existing buildings that improve their energy performance for the remainder of their operating life (Richarz et al., 2006). This improvement targets the thermal (heating, hot water, and cooling) and electric (lighting and additional electricity generation through e.g. building-related photovoltaics) performances of a building (Richarz et al., 2006). This dissertation refers exclusively to modifications that improve the thermal quality of a building. Thus, in this work, the term “energy retrofit” only refers to thermal energy-related modifications of buildings.

An energy retrofit can target the thermal supply and demand sides of a building (see Section 2.2). A well-coordinated improvement of the building envelope and/or its operation technology is required for this (Shellong, 2016). Hernández et al. (2012) described three main strategies that can be used to upgrade the thermal performance of existing buildings:

- reduction of on-site energy requirements through low-energy building technologies such as high-efficiency heating equipment, high insulation thickness, and passive design;
- using on-site supply options such as renewable energy (including solar thermal panels and ground heat sources) available within the building’s footprint;
- using off-site supply options. For example, renewable energy sources available off-site, such as importing wood pellets and renewable district heat, can be used to generate energy on-site.

According to Ma et al. (2012), the process of a building retrofit can be divided into five major phases. In the first phase, the building owners or other relevant stakeholders define the targets of a retrofit project. The primary reasons for planning energy retrofits are energy savings, heating costs, greater thermal comfort, and creating a healthy environment (Ipsos, 2018). In addition, other criteria, such as protecting the environment and climate or to comply with legal requirements, can be relevant to stakeholders (Ipsos, 2018; GEG, 2022). The second phase comprises an energy audit and performance assessment of the considered building. This includes analyzing the building energy data, understanding building energy use, identifying areas wherein energy is wasted, and proposing low-cost energy conservation measures. In the third phase, the retrofit options are identified and prioritized. In this phase, energy models, economic analysis tools, and risk assessment methods are used to assess the performance of different retrofit options. The fourth phase focuses on the implementation of optimal retrofit measures. The fifth and final phases should validate and verify the retrofit targets after the implementation.

In Germany, the Gebäudeenergiegesetz (GEG) sets the legal framework for the energy retrofit of buildings (GEG, 2022). It came into force in November 2020 and will be updated in 2023 (BMWSB, 2022; GEG, 2022). The GEG covers the replacement and retrofit regulations of ener-

gy-relevant building components, as well as the minimum energy standards for new and existing buildings. For existing buildings, some aspects of the GEG are relevant, as specified in §46 to §56. These are the requirements of retrofitting and maintaining existing buildings, as well as conditional requirements. For all existing buildings, insulation of the top floor ceiling of the highest-heated floor or roof is required. The conditional requirements of GEG are explained in §48. If a building component is changed because of a repair or modernization measure, the minimum energy standards must be fulfilled for the entire component if the area of the changed component exceeds 10% of the total component area. Decreasing the energy quality of the existing building is forbidden in all types of construction measures. Non-residential public buildings must use renewable energy sources if more than 20% of the outside area of a building is retrofitted or if the heating system of the building is changed. The legal framework also covers the cost allocation of the retrofits. This aspect is only relevant for rented buildings, as tenants save heating costs and landlords pay for the energy retrofit to refine the investments and running costs for a retrofit. These restrictions are included in the Betriebskostenverordnung (BetrKV) (Operating Costs Ordinance), the Verordnung über Heizkostenabrechnung (HeizkostenV), (Heating Costs Ordinance) and the Bürgerliches Gesetzbuch (BGB) (German Civil Code). According to §559 BGB, landlords are allowed to pass on a maximum of 8% of the retrofit costs to tenants per year. However, they are only allowed to allocate the costs that have arisen from the construction work and increasing the quality of the building (not just maintenance construction costs). Public subsidies, loan interests, and savings on maintenance costs must be excluded. (BetrKV, 2021; BGB, 2022; GEG, 2022; HeizkostenV, 2021)

Technical standards for retrofitting buildings in Germany are specified in detail using standards from the Deutsches Institut für Normung (DIN) (German Institute for Standardization) (DIN, 2021). They arise from national, European, and international standards through a consensus process in which experts agree on a common version of the content, considering the state of the art (DIN, 2021). DIN standards are checked at least every five years to ensure that they are up-to-date (DIN, 2021). If a standard no longer corresponds to the state of the art, the standards are revised (DIN, 2021). DIN standards are a suitable data source for scientific work and reflect the technology and technical framework conditions. Examples of standards relevant for the thermal energy analysis and retrofit of buildings include DIN V 18599 and DIN 4108, which are also listed in the GEG (GEG, 2022). DIN V 18599 standardizes the calculation of the net, final, and primary energy demand for heating, cooling, ventilation, domestic hot water, and lighting (DIN V 18599, 2021). DIN 4108 standardizes the essential requirements for thermal insulation for buildings (DIN 4108, 2021).

2.4 Different Urban Scales for Planning Energy Retrofits

According to Riechel (2016), three urban scales can be distinguished for planning energy retrofits: single buildings, districts, and whole cities.

In the context of this work the terms “cities” and “municipalities” are equivalent. In this sense, a “city” is guided by the concept of a *Kommune* (municipality) as specified in the *Gemeindeordnung (GemO)* (Municipal Code of Baden-Wuerttemberg) (GemO, 2018). It is an independent administrative unit below the federal and state levels (GemO, 2018). Municipalities manage and are responsible for all public tasks in their area unless federal or state laws restrict them (GemO, 2018). Municipalities have their own political council (city council) that enables local authorities to make decisions and an administration unit for implementing decisions and performing mandatory tasks (GemO, 2018).

The term “district” in the context of this work corresponds to the German term “*Quartier*” and can be translated to English as “neighborhood,” “community,” “quarter,” or “part of a city.” In some scientific publications, there is no distinction between these terms (e.g., Bourdic and Salat, 2012; Paiho et al. 2019). In some publications, a distinction is made between a neighborhood and district. The former is a smaller unit, and the latter is a larger, specified urban administration unit (e.g., Fonseca and Schlueter, 2015). However, in this work, both concepts are represented by the term “district.” The district scale is defined as the intermediate scale between the city and building scale (Riechel, 2016). A district consists of several connected private and/or public buildings and infrastructure (e.g., streets, green spaces, gas pipes, etc.) (KfW, 2015). Going beyond the formal definition, a characteristic of districts is their close connection to everyday life for the residents (Riechel, 2016). This underlines the idea of a “neighborhood” as a place where various urban functions such as living, services, trade, and traffic are related to one another (Riechel, 2016). Essential characteristic features for districts are, for example, ownership structures, socio-spatial parameters, and location within the city as a whole (Riechel, 2016).

According to the *Landesbauordnung Baden-Württemberg (LBO BW)* (Baden-Wuerttemberg Building Ordinance), “buildings” are structures that can be used independently, entered by people, and are suitable for protecting people, animals, or property (LBO BW, 2017). Residential buildings are primarily used for residential purposes and in addition to apartments, may contain rooms for freelancing professionals or similar workers and their associated garages and ancillary rooms (LBO BW, 2017). A building is part of a property as it is “an essential component of a property [...] that is firmly connected to the land”³ according to §94 BGB (BGB, 2022). In the case of a building inheritance, according to §11 *Erbbaurechtsgesetz (Erbbaurechtsgesetz)* (Heritable Building Act), a building can be constructed on someone else’s property (Erbbaurechtsgesetz, 2013). A property and the building on it can be the sole or shared property of individuals or groups. In a shared ownership, individuals or groups are entitled to specified shares of the property according to §747 BGB (BGB, 2022).

³ Translation from German original citation “Zu den wesentlichen Bestandteilen eines Grundstücks gehören die mit dem Grund und Boden fest verbundenen Sachen, insbesondere Gebäude, sowie die Erzeugnisse des Grundstücks, solange sie mit dem Boden zusammenhängen.” (BGB, 2022)

Considering these three different scales (building, district, and city) for the energy retrofitting of buildings, studies by Dixon and Eames (2013), Paiho et al. (2019), Riechel (2016), Riechel and Koritkowski (2016), and Ruggeri et al. (2020) highlight the various advantages and disadvantages of action at the different scales.

(1) Building scale offers the advantage of a concrete and precise planning option that can address the specific framework conditions of a building and its relevant stakeholders. In this way, all the financial, ecological, and other interests of the building owners (and other stakeholders) can be included when planning retrofit measures. The specific architectural and constructional features of a building can only be determined by examining individual buildings in detail (Ruggeri et al., 2020). Building scale is a key factor in the implementation of suitable retrofit measures. In particular, for historic buildings that require unusual energy-efficiency measures, retrofits are considerably complex and individualistic because of the heritage protection regulations (Ruggeri et al., 2020). Dixon and Eames (2013), however, stress that an over-focus on the building scale “risks fragmentation and overreliance on individual building owners and tenants”.




(2) The advantage of the city scale is its ability to manage policies. At the city scale, climate and energy-saving goals can be formulated, and strategies can be developed and politically controlled (Riechel, 2016). At the city scale, it is also possible to address and involve a range of stakeholders, such as developers and financiers, to create systematic and long-term retrofit visions (Riechel, 2016). Moreover, the city scale can push for retrofits by understanding the city as a historically grown entity with specific governance structures and social, environmental, and economic framework conditions (Dixon and Eames, 2013). However, the city level is too large and complex to implement coordinated and concrete measures for the retrofitting of buildings and approach the stakeholders (Riechel, 2016).

(3) The district scale is large enough to identify the patterns of energy consumption and supply beyond the boundaries of a single building, however, small enough to implement concrete solutions (Fonseca and Schlueter, 2015). It is in fact the scale where the most urban transformations in Europe occur (Fonseca and Schlueter, 2015). Compared to the building scale, planning at the district scale can increase technical flexibility for operation (Riechel, 2016). The focus goes beyond measures such as insulating the building envelope and replacing the heating system. The district approach for heating creates new technical solutions (e.g., district heating networks) that can improve the energy efficiency and planning design. District heating systems are more efficient and economical with higher load densities and can be better planned for than those for single buildings (Paiho et al. 2019). The district level is also suitable for integrating renewable energies (e.g., near-surface or deep geothermal energy and district-level solar thermal systems) (Riechel, 2016). The retrofit measures can be planned on a district scale to benefit economically compared to that for single buildings. Cost can be reduced in the procurement of services such as energy analysis, design, and construction when simultaneously conducting retrofit projects for several buildings in the district (Paiho et al, 2019). Cost

advantages do not necessarily optimize the technical infrastructure. Scale effects, such as volume discounts on the purchase of building materials for purchasing groups, are also relevant (Riechel, 2016). As buildings are primarily under private ownership, municipalities must promote and accelerate the energy retrofits of buildings. Paiho et al. (2019) highlight that the district-scale approach was the most effective in encouraging different stakeholders to utilize and benefit from synergies of concurrent retrofits of buildings. In this context, Riechel (2016) points out that the close connection between the district and daily lives of inhabitants and owners is beneficial for targeted addressing and activation of stakeholders. He emphasizes that the district scale is better suited for this than the city level, and furthermore, that communication among stakeholders can dynamically occur in districts. For example, informal communication among neighbors (neighborhood gossip) or looking at and imitating an exemplary building modernization in the neighborhood by other building owners push retrofit motivations. Riechel (2016) further emphasizes that the district scale is more concrete than the city scale. Strategies and models for the whole city become more tangible by translating them to a district level where they are related to the living environment of the stakeholders. The neighborhood level is suitable for clarifying the organizational issues related to implementation (e.g., responsibilities and implementation models). This also includes the timing of the implementation of the measures. However, approaches on the district and city scales require more coordination with a wide range of stakeholders (Riechel, 2016). This increases the effort for the coordination of measures as compared to the single-building scale (Riechel, 2016; Riechel and Koritkowski, 2016).

A summary of the various key functions of different urban scales for the energy retrofit of buildings is presented in Table 2.

Table 2: Different urban scales for planning building energy retrofits (Dixon and Eames, 2013; Paiho et al., 2019; Riechel, 2016; Riechel and Koritkowski, 2016; Ruggeri et al., 2020; Images from Google Maps, 2021)

Scale	City	District	Building
Example			
	Karlsruhe city (Germany)	District (Innenstadt-Ost)	Building (Kaiserstr. 18)
Function for energy retrofits	Strategic unit	Operating unit	Implementation unit
Suitable energy retrofit approaches	Suitable for the development and management of city strategies and urban climate/ energy goals	Suitable for retrofit approaches that rely on the specifics of a certain district (cross-building infrastructure, neighborhood dynamics, economies of scale, etc.)	Suitable for the concrete implementation of retrofit measures that fulfill the individual needs of concerned building stakeholders (building owners, tenants, other building users, etc.)
Primary decision makers	Politicians and city administrations	District managers, city administrations, and building stakeholders	Building owners and other building stakeholders

2.5 Thermal Analysis and Retrofit Planning Approaches for Buildings

The auditing and analysis of buildings and possible retrofitting options are key steps for planning the retrofitting of buildings. They determine whether and how a building can be retrofitted. Describing the value of building audits, Balaras (2022) characterizes them as the following: “Building audits, in one form or another, can be used to systematically collect the necessary data, in order to gain adequate knowledge and a better understanding on the operations, energy use and prevailing indoor conditions of buildings. The data can be used to identify, quantify and prioritize renovation measures for reaching higher energy efficiency, lowering emissions and improving indoor environmental quality.” According to Ma et al. (2012), energy assessments of buildings vary in range and depth. Energy analyses can be classified into three

levels, “including Level 1: walk through assessment, Level 2: energy survey and analysis, and Level 3: detailed energy analysis.” The more comprehensive the data for a building/building stock, the more precisely a retrofit plan can be tailored to individual and social goals. In addition to evaluating retrofit options for buildings on a district scale, the audits and analyses of buildings are also essential for identifying districts with high demands for retrofits. Riechel (2016) criticizes that only rarely the selection of districts for retrofit plans on a district scale (EQs) follows a systematic, holistic search process.

The thermal quality of a building can be assessed using various approaches. One non-invasive auditing approach to determine the thermal condition of building envelopes and envelope components that is crucial for this dissertation is infrared thermography. By recording thermographic images, the thermal weaknesses of building envelopes related to heat, water, and airflow can be identified Lucchi (2018). Applications of thermography include the thermal characterization of walls, glazing, and windows; detecting areas with excessive heat loss; inspecting thermal insulation and air leakages; detecting moisture and water; measuring U-values; and determining areas with thermal anomalies (Lucchi, 2018). According to Lucchi (2018) thermography can be divided into active and passive methods. Passive thermography focuses on the entire building envelope to identify thermal weaknesses, whereas active thermography focuses only on thermal weaknesses and provides more details (Lucchi, 2018). In addition, a distinction can be made between indoor and outdoor thermography, depending on whether recordings are made from the inside of the building or from the outside. The influence of weather conditions on outdoor thermography is relevant for good thermographic practices (Volland et al., 2012). In Germany, DIN EN 13187 (DIN EN 13187, 1999) defines the thermography requirements (primarily for outdoor thermography) that must be considered for professional evaluation: For good thermographic practice, the temperature difference between the inside and outside of the building must be sufficiently large. Direct sunlight, strong temperature fluctuations, and wind changes must be avoided. Accordingly, during thermographic recording, climatic and environmental factors must be documented. This dissertation focuses only on passive thermography from the outside. Both classical-terrestrial thermography recorded with handheld cameras and airborne thermography using drones are covered under this dissertation.

The processing and analysis of thermographic images can be performed manually or automatically using thermographic images or 3D models derived from multiple images (Hou et al., 2021; Hou et al., 2022). Computer vision and deep-learning approaches can be used to automatically detect thermal patterns in thermographic images. A key concept for this dissertation is the use of neural networks for the processing of thermographic images. One of the greatest advantages of neural networks is their ability to learn effective representations for a given task, such as the recognition of thermal bridges in images of buildings (Leo et al., 2018). Such a neural network model must be trained using examples of labeled thermal bridges. Modern graphic processing units (GPUs) enable the processing of large image datasets and can deal with high image resolutions (Liu et al., 2017). Standard neural networks utilize neurons to

produce real-valued activations and adjust the weights to connect neurons to solve a specific task (Liu et al., 2017). When only small datasets are available, more powerful neural network architectures are required to achieve good results (Liu et al., 2017).

Based on the information about the initial condition of buildings gained during audits, software or manual approaches can be used to create building models and calculate the energy consumption requirements. These building models and retrofit measures can be examined and optimized by simulating their effects on the building and its performance. (Deb and Schlueter, 2021)

3 Summary of the Studies and Key Results

3.1 Paper A: Building Analysis Approaches for Planning Energy Retrofits on District Scale

This section refers to the content of the paper “Evaluation of building analysis approaches as a basis for the energy improvement of city districts”, which was published in 2021 in the KIT Working Paper Series in Production and Energy. It was written in collaboration with Rebekka Volk, and Frank Schultmann. (Mayer et al., 2021 – Paper A)

Study context and design:

The basis for planning retrofits on a district scale, as intended by EQs, is the analysis of the existing building stock. The initial analysis of a district’s buildings is the most time- and resource-intensive step. It accounts for 40% of the time on average (Riechel and Koritkowski, 2016) and 50–80% of the financial resources needed to develop an EQ (Neußer, 2017).

The objective of this study was to provide an overview of the existing building analysis approaches on a district scale, which are commonly used in Germany. The basis of this study was an analysis of 25 publicly available EQ reports from Germany published between 2013 and 2018. The sizes of the districts covered by the EQ reports varied in the range 4.6–235.5 ha, 393–12,440 inhabitants, and 20–1,135 buildings, respectively. All considered districts contain mixed types of buildings with a significant share of residential buildings, as well as non-residential building such as commerce, offices, industry, and schools.

All the building analysis approaches mentioned in the studied reports were identified. Moreover, to investigate strengths, weaknesses, and potential improvements of existing approaches, short strengths weaknesses opportunities and threats (SWOT) analyses for the individual approaches were performed using the information given in the EQ reports. In this context, strengths were enhancers of an effective and efficient building energy analysis and weaknesses were inhibitors leading to high costs, long analysis times, and inaccurate results. Opportunities are possible ways of mitigating weaknesses. Conversely, threats are risks that need to be considered when improving analytical approaches. The research design of this study is illustrated in Figure 3.

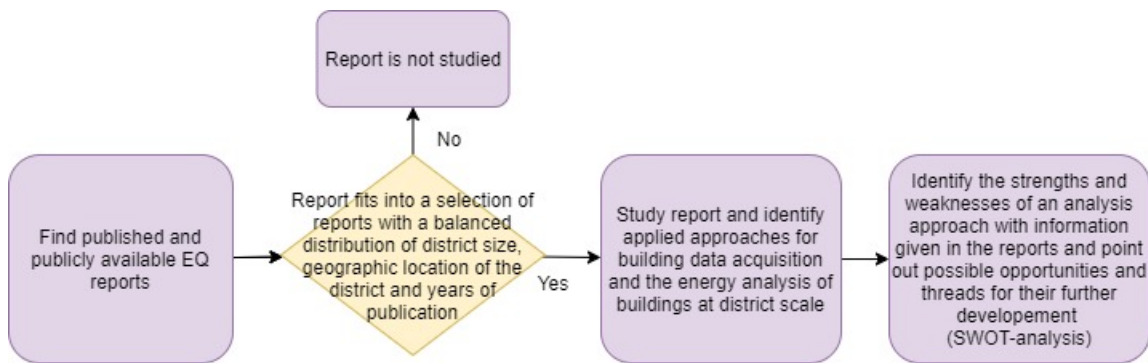


Figure 3: Study design for the analysis of EQs presented in Paper A (Original source: Mayer et al., 2021 – Paper A)

Results and discussion:

In all studies, a total of ten different approaches for analyzing buildings on a district scale were identified. These approaches are as follows: (1) the application of building typologies to obtain information for certain recurring building classes; (2) conducting expert interviews with local architects; (3) recording and processing of thermographic images for façade analysis; (4) analyzing building stocks of homogeneous sub-districts; (5) analyzing aerial images of building façades; (6) collecting data provided by chimney sweep associations; (7) analyzing building data from existing city databases such as monument registers; (8) using energy consumption data from local network operators; (9) surveying habitants and building owners; and (10) collecting data through on-site inspections.

Current analytical approaches for districts require many resources for various reasons. For example, many existing databases containing information on the thermal quality of buildings are subject to strict data protection requirements. To obtain information from citizens, well-informed building stakeholders need to be motivated to participate in the early stages of EQ development. Information available in existing building databases has no uniform formats. Thus, processing existing data is difficult. A combination of multiple approaches is commonly used to compensate for the weaknesses of individual analysis approaches. Some approaches are well-suited for the analyses of buildings with typical and recurring characteristics such as the building typologies. Other resource-intensive approaches such as expert interviews or thermography are suitable for the detailed analysis of buildings that are unique in their design and use. More precise analysis results require complex data acquisition, which is not always scalable for districts. To improve building analyses on a district scale, more research and further development of the scalability of existing approaches and improvement of legal and organizational framework conditions at the state and municipality levels are needed.

An important limitation of this study was that a relatively small number of EQ reports were studied due to limited accessibility. Moreover, EQ reports do not always provide complete information on the approaches used. Conversely, they focus more on presenting the results.

Expert interviews with developers of EQs, such as local energy agencies, are suitable for improving the study design.

3.2 Paper B: Evaluating the Quality of Aerial and Terrestrial Building Thermography for the Thermal Analysis of Buildings

This section summarizes the contents of the paper “Comparison of building thermography approaches using terrestrial and aerial thermographic images”, which was presented in 2022 at the SBE conference for the sustainable built environment in Berlin. It was written in collaboration with Andres Epperlein, Rebekka Volk, Elena Vollmer, and Frank Schultmann. (Mayer et al., 2022 – Paper B)

Study context and design:

Due to the time-consuming nature of manual image recordings with handheld cameras, classical-terrestrial thermography reaches its limits when a significant number of buildings or whole city districts need to be audited (Bitelli et al., 2015). Further limitations of terrestrial thermography are high buildings, recording of rooftops, and property rights that do not always allow comprehensive recordings from all building perspectives (Previtali et al., 2013). Thermographic cameras mounted on drones enable large-scale building audits. The collection of images can be automated with faster completion and lower cost (Krawczyk et al., 2015). Advantages of airborne thermography include the possibility of different recording angles and capturing images of tall buildings. In practice, thermographic images recorded using drones can also be used to generate 3D models (Hou et al., 2021).

Entrop and Vasenev (2017) and Daffara et al. (2020), among others, have published studies dealing with optimal settings for drone thermography in building audits. However, they do not provide information on the thermographic image quality compared to static thermography.

This study presented a structured approach to evaluate different flight settings by varying the distance between the drone and building, flight speed, and recording angles of a UAV-based thermal image (see Table 3). Additional terrestrial images were manually recorded using a handheld camera for quality comparisons. In summary, the dataset investigated consisted of 140 aerial images and 249 terrestrial images of two multi-family buildings.

Table 3: Experimental parameters for thermographic drone flights of Paper B (Original source: Mayer et al., 2022 – Paper B)

Flight	Viewing angle [°]	Height above ground [m]	Height above building [m]	Flight speed [m/s]
Flight 1	90	60	42	1
Flight 2	90	60	42	3
Flight 3	90	30	12	1
Flight 4	45	60	42	3
Flight 5	45	30	12	3
Flight 6	45	60	42	1
Flight 7	45	30	12	1

The quality of images in this study's dataset was evaluated using four qualitative and one quantitative quality criteria. The qualitative criteria were motion blur, contrast, visibility of image details, and perspective covered by the recording angle. The quantitative criterion was the comparative temperature difference. It was defined as the temperature difference between the central point of a thermal anomaly of an aerial thermographic image and terrestrial/other aerial thermographic image recorded with different flight settings. To evaluate the temperature difference, three points of interest with elevated temperatures in the building were considered.

Results and discussion:

The results of the study showed that for the analyzed dataset, the flight speed of the drone while recording images did not influence the image quality. Flight speeds did not cause motion blur varying in the range 1–3 m/s. Even greater flight speeds could be suitable, in contrast to the findings of Entrop and Vasenev (2017) who recommended speeds lower than 1.5 m/s for their technical equipment. Moreover, the study found that varying the distances and angles between the thermal camera and building can falsify quantitative temperature information, lower contrast, and decrease the visibility of image details. These effects are caused by a weakening of the returning infrared radiation or emissivity level. Considering the pros and cons of different distances (30 m/ 60 m above the ground which is 12 m/42 m above the building) and flight angles (90°/ 45°), the 90° perspective is suitable for analyzing rooftops. However, in this study, it was not advantageous as compared to a flight angle of 45°, which additionally enabled an analysis of façade areas. The analysis of rooftops was the best at a medium flight distance (12 m) above the building. However, a quantitative temperature study and detailed façade analysis were not possible at this distance. Additionally, the study found that a flight height of 42 m above the building is not recommended for quantitative studies. However, a distance of 42 m enabled the identification of large thermal bridges and leakages, which are distinctly visible in the images obtained in this study. This setting can be advantageous for projects such as the analysis of whole districts, targeting the identification of the largest thermal leak, and providing a rough overview of multiple buildings.

The limitation of this study was the small number of images showing only two large buildings recorded on the same day under similar weather conditions. Quantitative analysis of the images was limited to three different points. A technical problem faced in the study was the strong vignette effect on the images. The camera caused a shadowing toward the edge of the images. Based on the results of this study, subsequent research performed in Paper C improved the findings with a more comprehensive dataset, a reduced vignette effect, and more quantitative information.

3.3 Paper C: Further Investigations to Evaluate the Quality of Aerial and Terrestrial Thermographic Images

This section refers to the content of the paper “Investigating the quality of thermographic drone images for the analysis of buildings” published by the journal *Remote Sensing* in 2023 and written in collaboration with Andres Epperlein, Elena Vollmer, Rebekka Volk, and Frank Schultmann. It builds on the insights and extends the research approach of Paper B “Comparison of building thermography approaches using terrestrial and aerial thermographic images”. (Mayer et al., 2023 – Paper C)

Study context and design:

This study was based on the research approach of Paper B (Mayer et al., 2022 – Paper B). It extended the methodology of Paper B by working with a more comprehensive dataset and introducing modified and improved quality criteria for thermographic images. The examined quality criteria were motion blur (already considered in Paper B), feature discernibility, and accessibility of areas under scrutiny. Moreover, two quantitative criteria were examined. They are the comparative temperature difference as introduced in Paper B and the comparative contrast that compared temperature contrasts for different recording settings. The dataset consisted of 968 thermographic images with 136 and 139 images that were automatically and manually recorded with a drone, respectively, and 693 manually recorded terrestrial images. The images were collected over two days and showed three large German MFHs. The thermographic images recorded with a drone were collected manually by a drone pilot to allow closer distances to the buildings and automatically by preprogrammed flight routes. Different flight speeds, camera distances, and camera angles were tested. The drone settings are presented in Table 4. For the evaluation of the quantitative criteria, 112 areas of interest showing an increased temperature on the images, such as thermal bridges, rooftop opening vents, and other thermal anomalies, were analyzed and compared. In addition, the time efficiency of the recording process for aerial and terrestrial images was considered.

Table 4: Experimental parameters for thermographic drone flights of Paper C (Original source: Mayer et al., 2023 – Paper C)

Flight	Building	Automatically/ manually performed flight route	Camera angle [°]	Height above ground [m]	Height above building [m]	Distance to façade [m]	Flight speed [m/s]
1	Full area	Automatically	45	40	22	Varying	1
2	Full area	Automatically	45	40	22	Varying	3
3	Full area	Automatically	45	40	22	Varying	5
4	Full area	Automatically	45	60	42	Varying	3
5	Full area	Automatically	90	40	22	Varying	3
6	Full area	Automatically	90	60	42	Varying	3
7	Wichernstr. 4	Manually	0	4–12	Varying	15	0
8	Wichernstr. 4	Manually	0	4–12	Varying	8	0
9	Wichernstr. 4	Manually	0	4–12	Varying	4	0
10	Wichernstr. 10-18	Manually	0	4–12	Varying	15	0

Results and discussion:

In this study, flight speeds between 1–5 m/s did not decrease the image quality. Accordingly, a higher flight speed than that evaluated in Paper B did not have a negative impact. Increasing camera distance and the changing angles of the drone with respect to the building, however, created a significant negative impact by decreasing contrast, falsifying temperatures, and reducing feature discernibility. The 90° perspective provided a complete overview of rooftops. However, it excluded the façade and created a lower contrast due to reflections of the sky when recording at night. Recordings with a 45° camera angle enabled the analysis of both the rooftop and façade. Manual drone flights enabled high-quality recordings of high-façade sections that were not possible with terrestrial recordings or automated flight routes. With a flight height of 42 m above the building, areas larger than those with a flight height of 22 m were recorded within a shorter time. Quantitative information on contrast and temperature was falsified, which became evident in the quantitative analysis. Furthermore, with a 22 m recording distance above the building, quantitative studies of building façades, such as the calculation of U-values of building envelopes, are not recommended. The time efficiency of automatically recorded drone images was positively influenced by the dynamic recordings taken while flying. Conversely, larger flight distances and preparation times negatively impacted the time efficiency.

The limitation of this study was that it only evaluated ten different flight settings recorded on two days. The flight settings were limited by the equipment and obstacles such as trees in the recording area. Future studies could use larger datasets recorded on more days, different

weather conditions, and at various times of the day, with additional flight settings for more buildings, and analyze more thermal anomalies to achieve better quantitative results. The dataset contained a negligible vignette effect in the images, which was considerably reduced compared to the dataset used in Paper B. To determine the exact influence of angle and recording distance on the quality of images, future studies should determine the camera angle and distance of the drone with respect to the building, which is always changing during flight and could be calculated with photogrammetry approaches.

3.4 Paper D: Building Façade Component Segmentation for Drone-Based Building Analysis Approaches

This section refers to the paper “A computer vision approach for building façade component segmentation on 3D point cloud models reconstructed by aerial images”. It was presented at the EG-ICE 2021 Workshop on Intelligent Computing in Engineering and written in collaboration with Yu Hou, Zhaoyang Li, Rebekka Volk, and Lucio Soibelman. (Hou et al., 2021 – Paper D)

Study context and design:

Thermal images of buildings can be used for training and testing computer vision approaches that automatically detect thermal bridges in certain building parts or automatically identify building parts with high energy losses. Most of the available databases of thermal images contain terrestrial images of buildings. They contain segmentation information and labels to distinguish between different building parts, such as windows and rooftops. These image databases cannot be directly used for training models to segment building parts on aerial images or in point-cloud models obtained with drones. As the labeling of newly captured aerial images is time-consuming and labor-intensive, it is valuable to find ways using existing terrestrial datasets for aerial image processing. Thus, this study proposed a framework for training image segmentation models using terrestrial images to predict the semantic information on building façades. The results were tested on two datasets from the German city of Karlsruhe: one of the inner-city districts and the other of the university campus of the KIT.

As a first step, 3D point cloud models were reconstructed using the ContextCapture software (Bentley, 2021) from aerial images obtained with drones. Examples of the reconstructed 3D models from Karlsruhe are shown in Figure 4. Next, 2D images were rendered from the reconstructed 3D model. Then, semantic segmentation models based on two neural network architectures (ResNet+9 blocks and U-Net256 versions) of the generative adversarial networks (GAN) (Goodfellow et al., 2014) were trained for door and window segmentations with open source datasets. Finally, segmentation results were predicted based on the rendered 2D images for the university campus, inner-city area, and a test set of the open-source dataset.

Two evaluation criteria were used to evaluate the performance of the methodology: an accuracy analysis of the segmentation performance on the open-source dataset and a performance

analysis for the rendered images. For the performance analysis, four metrics were used: precision, recall, intersection over union (IoU), and Dice coefficient.

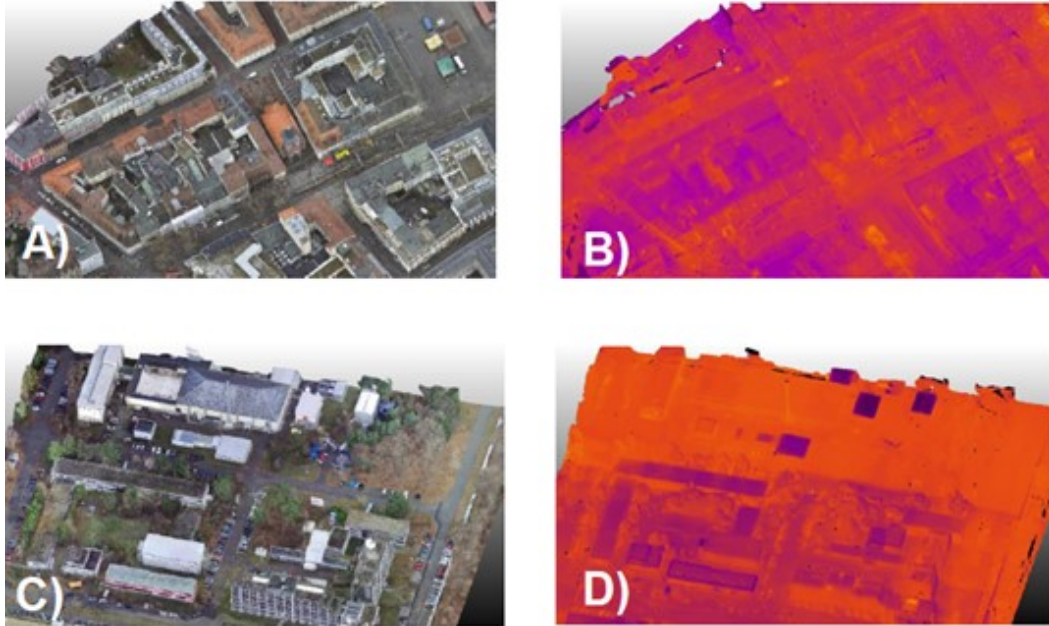


Figure 4: 3D point cloud reconstructions from thermal and RGB images presented in Paper D: (A) RGB and (B) thermal 3D model from a city area in Karlsruhe; (C) RGB and (D) thermal 3D model from a university campus in Karlsruhe (Original source: Hou et al., 2021 – Paper D)

Results and discussion:

The results showed the possibility of creating a 3D point cloud model created using aerial images, and that façade images can be rendered for segmentation using a virtual camera within the model. The segmentation accuracy decreased when using the images rendered from the 3D model compared to those of the open-source dataset. The important finding of this study was that segmenting windows is more accurate than segmenting doors. The methodology also performed better for city data than for campus data, potentially because the building styles in the open-source dataset used for training were closer to the styles in the city images. In all cases except for predicting the door class in rendered images from the campus datasets, ResNet+9 blocks outperformed U-Net256.

A limitation of the study was that for the test and training images, there were more pixels belonging to windows than to doors. Datasets with more door labels could be beneficial for a more balanced training. Moreover, there are two main ways to improve segmentation performance: either by improving the quality of the rendered images or improving the segmentation algorithms.

3.5 Paper E: Automated Thermal Bridge Detection of Building Rooftops on District Scale Using Aerial Thermographic Images

This section summarizes the contents of the paper “AI-based thermal bridge detection of building rooftops on district scale using aerial images”. It was presented at the EG-ICE 2021 Workshop on Intelligent Computing in Engineering and was written in collaboration with James Kahn, Yu Hou, Rebekka Volk, and Frank Schultmann. The dataset used in this study is described in more detail in Paper G “Thermal Bridges on Building Rooftops (TBBR)”. (Mayer et al., 2021 – Paper E)

Study context and design:

To automatically detect thermal bridges on thermographic images with artificial intelligence (AI), previous studies worked with close-up images of single buildings and used threshold approaches to spot significant temperature differences in the images (Garrido et al., 2018; Macher et al., 2020; Martinez-de Dios and Ollero, 2006; Rakha et al., 2018). Unlike close-up images, panorama images covering whole districts contain different buildings from different angles and surroundings, such as streets, cars, humans, and traffic lights. For these images, threshold approaches are unsuitable for the reliable automatic detection of thermal bridges. This is because thermal bridges change their shape from different angles, and high temperature differences also occur in surrounding objects that are not buildings.

This study analyzed the thermal quality of buildings on a district scale. The focus was on how thermal bridges on buildings can be quickly and easily identified within an entire district using aerial panorama images. The focus of this study was exclusively on building rooftops, which are particularly difficult to record using classical-terrestrial thermography and require aerial recordings. To accelerate the evaluation procedure, the potential of a deep learning approach was investigated.

For this, a neural network (Mask RCNN-R18 (He et al., 2017) from the Detectron 2 library (Wu et al., 2019)) was trained and tested on thermal bridges on building rooftops (TBBR dataset). The TBBR dataset was created for this study in cooperation with Yu Hou, James Kahn, Tobias Beiersdörfer, and Rebekka Volk in 2021. It is available as an open source publication on Zenodo (Mayer et al., 2021) and described in more detail in Paper G. TBBR contains panorama images of buildings with five channels (RGB, thermal, and a height map) and includes annotations of thermal bridges. An example of an image from the TBBR dataset is shown in Figure 5. The average recall (AR) was used to score the detection results of the thermal bridges.



Figure 5: Drone images of the city center of Karlsruhe used for the TBBR dataset presented in Paper E: (A) thermal image, (B) RGB image, and (C) image with height information (Original source: Mayer et al., 2021 – Paper E)

Results and discussion:

The results of this study for detecting thermal bridges on building rooftops are comparably poor. The best results were achieved for the TBBR dataset for large objects, which achieved a maximum AR of less than 20%. A key limitation of this study was the relatively small number of images available in the dataset because of the time-consuming process of manually annotating thermal bridges in images. In addition, inaccuracies were found in the TBBR dataset resulting from the misalignment of the RGB and thermal layers. A promising result of this study is the good performance for thermal bridge location, which was reliably detected on building rooftops and not on other building parts, such as façades, or the surroundings at street level. A hypothesis drawn from this study is the benefit of height maps for the computational learning process of rooftops. Based on the results of this study, a follow-up work evolved exploring this hypothesis, along with different neural network approaches to improve the automated detection results given the small amount of data. It is presented in Paper F.

3.6 Paper F: Improving the Automated Thermal Bridge Detection of Building Rooftops Using Aerial Thermographic Images

This section refers to the paper “Deep learning approaches to building rooftop thermal bridge detection from aerial images” which was published in 2022 by the journal Automation in Construction. It was written in collaboration with James Kahn, Yu Hou, Markus Götz, Rebekka Volk, and Frank Schultmann. It builds on the insights of Paper E “AI-based thermal bridge detection of building rooftops on district scale using aerial images” and extends the research approach. The dataset used in this study is an improved version of the dataset used in Paper E and is described in more detail in Paper G “Thermal Bridges on Building Rooftops (TBBR)”. (Mayer et al., 2022 – Paper F)

Study context and design:

This study built on the findings of Paper E and extends its methodology (Mayer et al., 2021 – Paper E). It also evaluated thermal bridge detection on building rooftops of panorama drone images using deep learning approaches. As Paper E did not show sufficiently satisfactory results for the detection of thermal bridges, this study investigated ways to improve automatic thermal bridge detection results. For this, the accuracy of the TBBR dataset annotations was improved with an updated version of 2.0, by creating a more precise alignment of the RGB, height, and thermal image channels. Moreover, different neural network architectures were tested on the improved dataset to compare their performance.

The study is divided into two parts that use different computer vision frameworks. The first part works with the Detectron 2 library (Wu et al, 2019), which is consistent with the study design of Paper E. The first part has two goals: investigating the benefit of the height map for training the neural network and verifying the benefits of the updated TBBR v2 dataset. The second part worked with OpenMMLab’s MMDetection library (Chen et al., 2019). Both libraries, Detectron 2 and MMDetection, were chosen as they are well-known frameworks that focus on a mix of accessibility and demonstrated performance. The goal of the second part is to investigate the performance of different neural networks in automatically detecting thermal bridges on building rooftops on the TBBR v2 dataset. Four different architectures were considered. In addition, all models were trained with and without pre-training. All studied model configurations are listed in Table 5 to compare their performance in line with Paper E. For each configuration, five trainings with different random seeds were trained and tested to obtain the mean and standard deviation of the AR scores. Figure 6 illustrates the research approach.

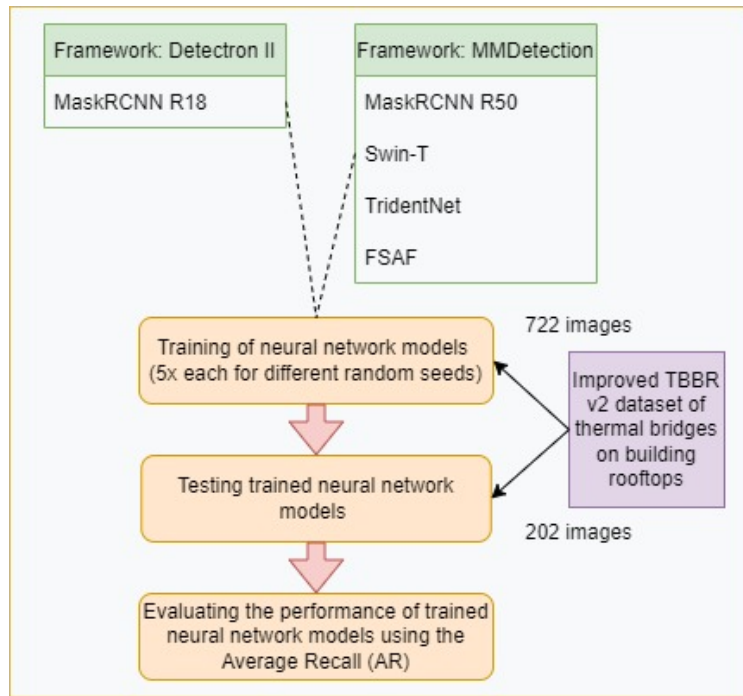


Figure 6: Flowchart for the study design of Paper F (Mayer et al., 2022 – Paper F)

Table 5: Tested neural network architectures and training configurations presented in Paper F (Mask RCNN-R18* indicated that the model was initialized with the identical random seed as used in Paper E) (Original source: Mayer et al., 2022 – Paper F)

Framework	Architecture	Pre-trained	Ablation (without height map)
Detectron 2	Mask RCNN-18	-	-
		-	X
	Mask RCNN-18*	-	-
MMDetection	Mask RCNN-R50	-	-
		X	-
		-	X
		X	X
	Swin-T	-	-
		X	-
	TridentNet	-	-
		X	-
	FSAF	-	-
		X	-

Results and discussion:

For the first part of the study, comparing the second version of the TBBR dataset with the old version from Paper E, the results for the automatic detection of thermal bridges improved considerably. The test-time performance approximately doubled using an identical Mask RCNN-18 configuration. For the ablation study without height map information, the test results for detecting thermal bridges on rooftops did not show worse AR scores than the models trained with height information. Nevertheless, more falsely detected thermal bridges appeared on the ground and components that were not building rooftops in the ablation study. This is consistent with the results presented in Paper E.

The results of the second part of the study showed which neural network architectures work best for detecting thermal bridges on rooftops for the TBBR v2 dataset. The best AR scores were achieved with the MMDetection framework, particularly with the pre-trained Swin-T transformer models. An AR of approximately 50% was achieved for large thermal bridges with a pre-trained configuration. Overall, the pre-trained models showed better scores than the non-pre-trained models.

The limitation of the study was the small size of the TBBR dataset. It only contained images of the German city of Karlsruhe. In addition, the images in the dataset showed a significant overlap. For future studies, the scoring of detected thermal bridges should consider scores across all instances of the same thermal bridges and not only those of individual images. Although the results of this study were promising (especially compared to the poor results of Paper E scoring a maximum AR of less than 20% for large thermal bridges), better results are likely possible with larger datasets.

3.7 Paper G: Dataset of Thermal Bridges on Building Rooftops

This section refers to the paper “Thermal Bridges on Building Rooftops (TBBR)”, which was published in 2023 in the journal Nature Scientific Data and written in collaboration with James Kahn, Markus Götz, Yu Hou, Tobias Beiersdörfer, Nicolas Blumenröhr, Rebekka Volk, Achim Streit, and Frank Schultmann. It provides the data descriptor for Paper E “AI-based thermal bridge detection of building rooftops on district scale using aerial images” and Paper F “Deep learning approaches to building rooftop thermal bridge detection from aerial images”. (Mayer et al., 2023 – Paper G)

Dataset information:

This paper afforded a detailed description of a dataset of thermal bridges on building rooftops (TBBR). The TBBR dataset contains 926 images of six large building blocks located in the city center of Karlsruhe. The images were recorded from different angles at flight heights in the

range 60–80 m above ground in March 2019. They contain 6895 annotations of thermal bridges in the COCO JSON format (Lin et al., 2014) that were created using the VGG Image Annotator software (Ditta and Zisserman, 2019). All images consist of five channels: three channels for RGB information, thermal information, and a height map generated from a 3D building model. This dataset can be used to train and evaluate neural networks. For this purpose, the dataset was divided into a training subset of 723 images containing 5614 annotations of thermal bridges and a test subset of 203 images containing 1313 annotations of thermal bridges. Table 6 provides an overview of the dataset for the annotations of the thermal bridges and rooftops at which they occur.

Table 6: TBRR annotations and characteristics (Original source: Mayer et al., 2023 – Paper G)

Criterion	Characteristic	Train	Test	Total
Rooftop shape	Steep roof	3939	895	4834
	Flat roof	524	379	903
	Mixed shape	1151	39	1190
Rooftop component	Rooftop surfaces	437	185	622
	Component connections	3977	842	4819
	Cantilevers	640	149	789
	Windows	560	137	697

3.8 Paper H: Thermographic Image-Based Assessment for Thermal Bridges on District Scale

This section refers to the contents of the paper “Aerial thermographic image-based assessment of thermal bridges using representative classifications and calculations” which was published in 2021 in the journal *Energies*. It was written in collaboration with Julia Heuer, Rebekka Volk, and Frank Schultmann. (Mayer et al., 2021 – Paper H)

Study context and design:

The prime disadvantage of large-area thermography using drones is generally a lack of detailed background information on individual building materials and construction methods. This study examined a methodology for identifying thermal bridges in thermographic drone images and rating them with regard to their retrofit potential using simplifications for building classes of interest. For this, the procedure for identifying and assessing thermal bridges was developed as follows and tested for German buildings constructed in 1950–69. First, a comprehensive dataset of thermographic images of the building type of interest was collected. Preprocessing software was used to enhance the quality of thermographic images and optimize the color scheme. The dataset was manually analyzed for thermal bridges, which in the next step could be classified as recurring patterns. To ensure that the thermal anomalies in images were real thermal bridges and not caused by open windows or moisture on specific building parts, these

thermographic images were compared with simultaneously collected RGB images. The different identified thermal bridge classes were then characterized using representative building information for materials and construction methods. Size related retrofit costs for each thermal bridge class were subsequently calculated. The procedure is summarized in Figure 7.

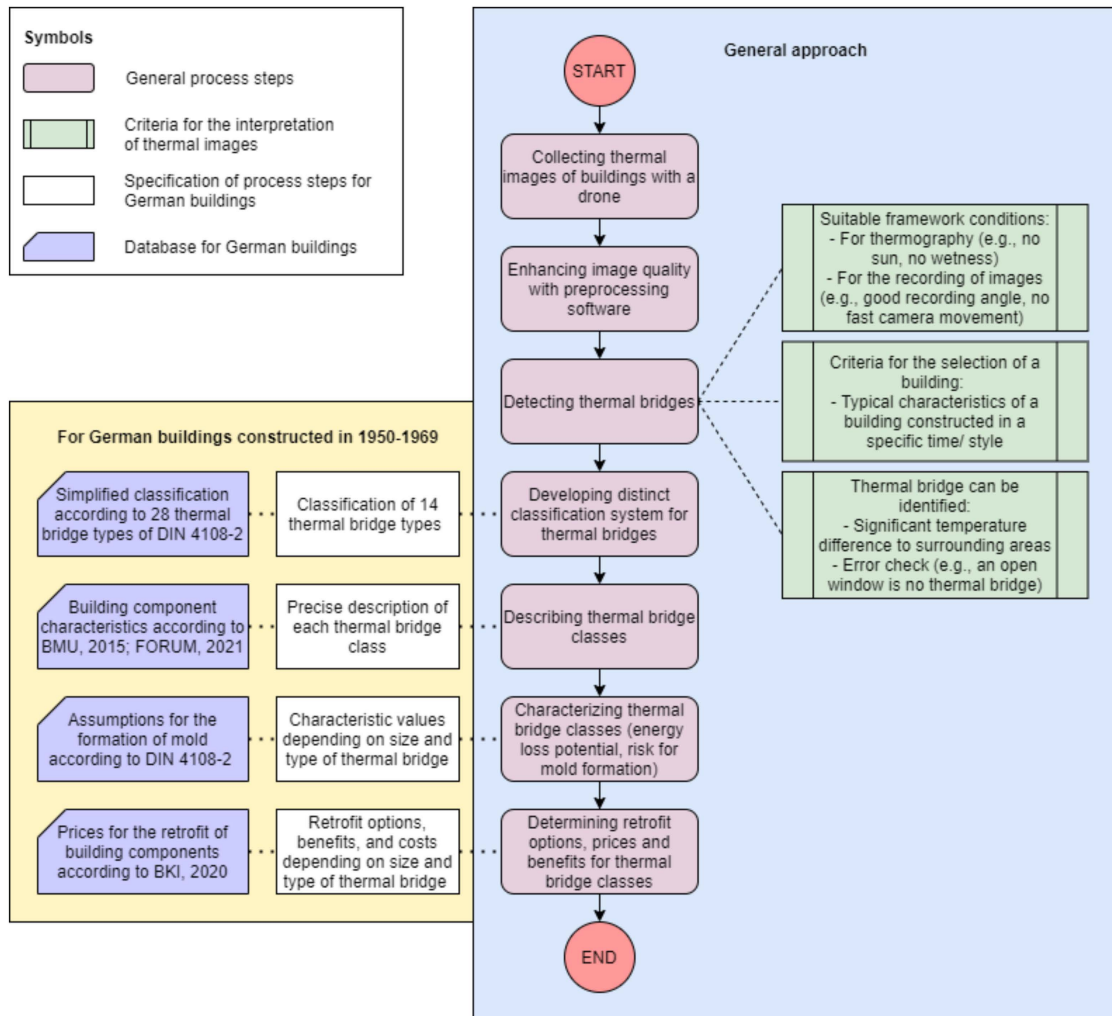
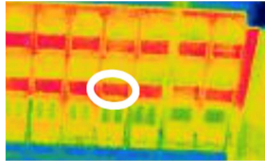
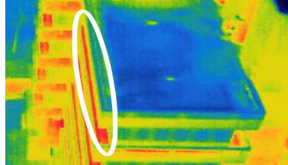
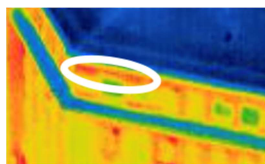
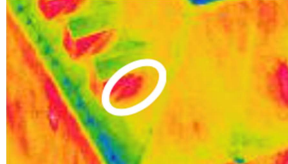
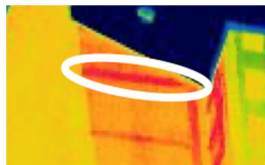
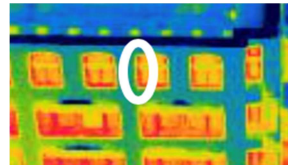
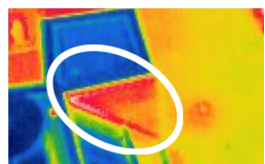
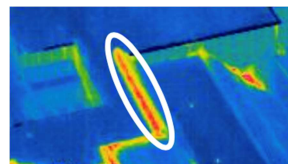
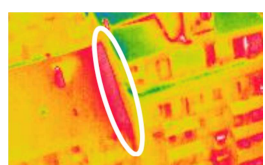
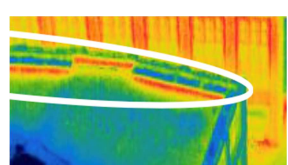
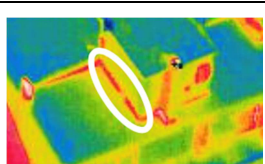
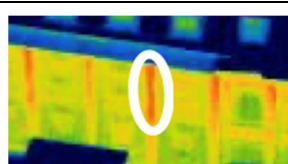
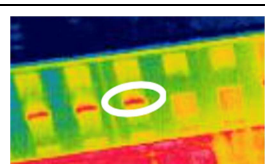
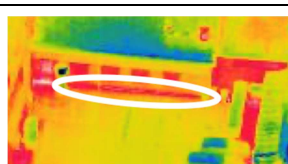


Figure 7: Research design of Paper H. For more details on references of the Figure see original paper. (Original source: Mayer et al., 2021 – Paper H)

This study focused on German buildings constructed between 1950 and 1969. For this building class, a comprehensive dataset of thermographic drone images from Karlsruhe, Germany, was studied. A total of 14 relevant and recurring thermal bridge types were identified. They were based on the classification of 28 thermal bridge types according to the Supplementary Sheet 2 of DIN 4108 (DIN 4108, 2021). These thermal bridge types were summarized and illustrated using representative thermographic images from the dataset used in Table 7. To characterize the 14 thermal bridge types for their risk of mold growth, potential heat losses, and retrofit potentials, representative thermal bridges and typical retrofit options were simulated using

the software ThermCad from ROWA-Soft (Thermcad) (ROWA soft, 2021). The costs of the possible retrofits were also calculated.

Table 7: Overview of thermal bridge types visible on thermographic drone images presented in Paper H (Original source: Mayer et al., 2021 – Paper H)

Type of thermal bridge	Example image	Type of thermal bridge	Example image
Window sill		Balcony slab	
Window lintel		Dormer	
Floor slab		Window reveal	
Connection wall and rooftop		Roof ridge	
Connection rooftop on wall		Attic	
Staggered story		Inside wall	
Roller shutter casing		Basement ceiling slab	

Results and discussion:

Thermographic drone images enabled the identification of thermal bridges on a district scale. Recurring thermal bridge types were detected and interpreted. This study provided a catalogue of thermal bridge types for German buildings from the 1950s and 1960s, with exemplary thermographic panorama images and information on mold growth risks, energy losses, and retrofit potentials. This catalogue is suitable for practical applications. In this study, retrofits of thermal bridges with window components, basement ceiling slabs, balcony slabs, floor slabs, and attics were relevant for preventing mold growth. To save energy, on the other hand, thermal bridges of window sills, window lintels, and attics were relevant.

Building analysis approaches at the district scale, such as those introduced in this study, need to work with simplifying assumptions, which can be imprecise in practice. Thus, the approach presented in this study did not replace the detailed analyses of buildings and comprehensive planning efforts for the retrofitting of thermal bridges. Conversely, it provided the first indication of which structures need to be assessed in more detail when considering the thermal quality of the entire district. Future studies can use this methodology to further develop thermal bridge catalogs. Furthermore, the detection and measurement of certain easily identifiable thermal bridge types can be automated in the future (e.g., using deep learning approaches). Potential energy-saving can be automatically estimated through size-related systematics.

3.9 Paper I: Planning Thermal Retrofits for Single Buildings

The contents of the paper “Analysis of financial benefits for energy retrofits of owner-occupied single-family houses in Germany”, published in 2022 in the Journal Building and Environment, are discussed herein. It was written in collaboration with Rebekka Volk, and Frank Schultmann. (Mayer et al., 2022 – Paper I)

Study context and design:

Germany provides comprehensive financial incentives for energy retrofits of SFHs, which motivates people to take retrofit measures for their buildings. An optimization model can help weigh various retrofit measures against each other by considering the financial incentives provided by the state. To date, many retrofit measure optimization models exist, such as those by Antipova et al. (2014), Jafari and Valentin (2017), Kumbaroğlu and Madlener (2012), Ruparathna et al. (2017), Wang et al. (2014), and Wu et al. (2016). No existing model at the time of the study was found that economically optimized German buildings and German framework conditions of energy standards, retrofit costs, different financing alternatives, and German funding schemes.

Thus, this study presented a planning optimization model for the thermal retrofitting measures for SFHs. As financial profitability is a major decision criterion for performing retrofits in Germany (Gossen and Nischan, 2014; Renz and Hacke, 2016; Stieß et al. 2010), a model was developed to optimize the monetary savings of building operations for different time periods for hot water and space heating through different retrofit options. The calculation developed considers funding schemes for supporting energy retrofits and allows conclusions to be drawn regarding whether funding instruments offer sufficient incentives for comprehensive, climate-friendly retrofits. The model is based on a mixed-integer economic optimization. All the components of the optimization model are illustrated in Figure 8.

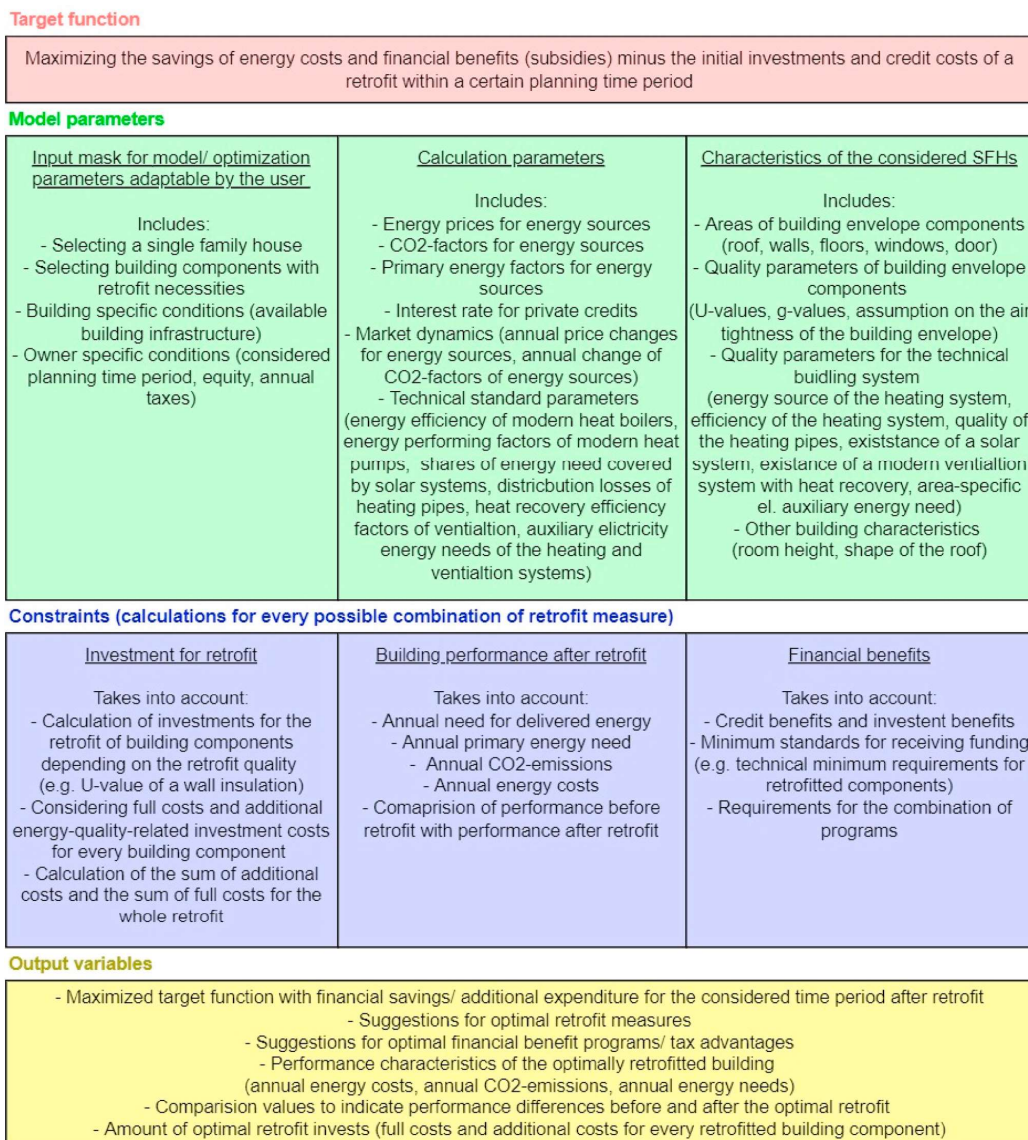


Figure 8: Model components of the optimization model including model input parameters, calculation modules, and model outputs presented in Paper I (Original source: Mayer et al., 2022 – Paper I)

In a case study, all components of the model were implemented using the German framework conditions in the general algebraic modeling system (GAMS) programming language (GAMS, 2021) and tested for different retrofit scenarios. Two SFHs constructed in the 1960s and 1970s, modeled according to the representative buildings, described by Loga et al. (2015), were the focus of the case study. The German funding instruments of Kreditanstalt für Wiederaufbau (KfW) (Credit Institute for Reconstruction), of Bundesamt für Wirtschaft und Ausfuhrkontrolle (BAFA) (Federal Office for Economic Affairs and Export Control), and tax benefits according to Einkommenssteuergesetz (EStG) (Income Tax Act) §35c as of 2020 were examined (BAFA, 2020; EStG, 2020; KfW, 2020).⁴

Results and discussion:

The model presented in this study complements existing models by introducing a simple approach to approximate the heating energy needs of SFHs. Owing to its mathematical implementation, it operates with fast computing time. It provides decision support for financially optimal retrofit measures from the perspective of self-using SFH owners and covers the German framework conditions.

The results of the case study indicate that considerable CO₂ reductions for building operations are possible. Within a 20 years planning period, all energy retrofits of the two SFH representatives reached a point where retrofit investments were amortized or approximately amortized through energy savings. Even with comprehensive retrofit necessities of the buildings, energy retrofits showed short time spans of 10–20 years for positive returns on investments. Under the German framework conditions, retrofit measures that exceeded the regulated minimum energy standard of building components proved to be optimal in approximately all scenarios that were studied in this paper. Regarding the funding schemes of KfW, BAFA, and tax benefits, this study showed that the funding conditions are not designed to maximize the CO₂ savings of an energy retrofit. Instead, the funding efficiencies of funds ranging from 493-3747 € differ considerably in reducing one ton of CO₂ annually. This is because the German funding system focuses on reducing the primary energy use and not CO₂. The replacement of the heating system leads to significant CO₂ savings, whereas measures on the building envelope only lead to relatively small reductions.

This study had various shortcomings and possible improvements. The developed model leads to a systematic overestimation of financial, energy, and CO₂ savings. This is because of the assumption of standardized user behavior that overestimated the heating energy needs compared to the empirically measured heating energy consumptions. For the comprehensive database of the study, some values used in the calculations, such as prices for retrofit measures that were only adapted with adjustment factors, should be updated. The study was

⁴ There was a revision of the subsidies for energy retrofits after the publication of the study in 2022. More information on this is provided in the Discussion Section.

limited to only operational performance and cost savings and did not consider grey energy for retrofit measures, life cycle assessment, and increased asset values of investments. With nonlinear equations and more precise energy simulations, the reliability of the model can be increased when fast computing times are not prioritized.

4 Conclusion and Discussion

This dissertation investigated the potential and limitations of different thermal analysis approaches for existing buildings, which can help prepare suitable energy retrofits. For this purpose, nine papers (Papers A, B, C, D, E, F, G, H, and I) focused on individual buildings as well as multiple buildings on a district scale. The important concepts of this work were thermography with drones for building envelope auditing, automated processing of thermographic images, and modeling and optimizing energy retrofit measures. Both technical and economic criteria were examined in this study in the context of the German standards and framework conditions.

While a conclusion, discussion, and critical appraisal were provided for each individual study in the corresponding papers, the overall picture of the dissertation is concluded and critically discussed in this section. It also refers to the initial research questions of this work, asking 1) which analysis approaches for buildings on a district scale are commonly used for planning thermal retrofits, 2) how can thermography instruments with drones be used to analyze buildings on a district scale, 3) how can the processing of thermal images collected with a drone be automated for the detection of thermal weaknesses of building envelopes, and 4) how can efficient and effective thermal retrofit measures be planned for buildings in Germany.

The popularity of energy retrofit plans at the district scale is growing in Germany. This is demonstrated by the large number of current EQs. As of mid-2021, KfW has approved more than 1,550 funding applications for EQs since it was introduced in 2011 compared to the 850 EQs as of 2019 mentioned in Paper A (ES, 2022). Different approaches are commonly used to analyze buildings on district scales to prepare retrofits, such as citizen surveys, expert interviews, the use of energy consumption information from network operators, and building typologies. Thermography is also currently used for EQs in audit buildings but is usually limited to individual buildings because of the resource-intensive nature of this approach.

A key approach for auditing multiple buildings on a district scale for the development of EQs considered in this study is the aerial thermography with drones. In contrast to classical-terrestrial thermography, there are considerable possibilities of scaling to entire districts and even cities. Airborne thermography offers novel opportunities for auditing buildings and rooftops that are otherwise hardly accessible. However, for the automation of drone recordings, the current state-of-the-art equipment requires that a sufficient safety distance from obstacles be maintained. In practice, larger distances to buildings are usually necessary compared to that for handheld cameras. Additionally, varying recording angles may occur for automated flight routes when covering large areas. Due to these recording conditions, the quality of images suffers, as shown in Papers B and C. The quantitative evaluation of thermographic images is associated with considerable quantitative falsifications in contrast and temperature. Converse-

ly, airborne thermography is considerably efficient for the qualitative investigation of a building stock's thermal constitution.

When recording areas with thermographic cameras using drones, buildings with unexpected relative heat losses or relevant thermal bridges can be detected and interpreted, as shown in Paper H. The detection of thermal bridges can be automated using 3D models and deep learning approaches. These approaches can achieve good results as demonstrated in Papers E and F. To further develop airborne thermography, technical innovations such as drones that automatically keep certain however small distances from buildings and can fly around obstacles would be an advantage. A decisive limitation of Papers B, C, D, E, F, and H dealing with thermographic images is that the datasets used for drone images (such as that presented in Paper G) only contained a comparably small number of images and were recorded on only a few days for a limited number of buildings. For the improved qualitative evaluation of thermographic image datasets, more comprehensive, more diverse datasets, and new evaluation methods, such as through further developed neural networks are required.

Building models, such as those presented in Paper I, are suitable for a precise analysis of the individual energy requirements of buildings. Here, the economic, technical, and ecological possibilities were evaluated. In Paper I, which is based on the German framework conditions for owner-occupied SFHs as of 2020, for example, the replacement of the building heating system was more attractive than the retrofit of the building envelope.

Many results of this work, such as in Paper H and I, are applicable for framework conditions in Germany or are based on datasets of German buildings. However, most of the findings are transferable and adaptable to the framework conditions of other countries. This is important as there are a significant number of old buildings constructed with low thermal quality in other parts of Europe and the world. In addition, in Germany, some framework conditions have changed since the publication of the studies presented in this work or will change in near future. This is particularly true regarding the political conditions and funding schemes for buildings that are part of Paper I. With the coalition agreement of the German federal government from 2021 to 2025, changes in the legal framework are planned that are intended to mitigate the effects of climate change in the building sector. Changes in the GEG increase the standards for every newly installed heating system that must be operated on the basis of 65% renewable energy. The standards for significant building extensions, conversions, and retrofits of existing buildings in the GEG will be adjusted so that the parts to be replaced correspond to a higher quality standard called the Effizienzhausstandard 70 (efficiency house standard 70)⁵ (PIB, 2021). Moreover, the funding schemes for energy retrofits investigated in Paper I were changed in 2022 (BA, 2022a).

⁵ For more explanations on efficiency house standards see Paper I

In addition to the German policy, international conditions have evolved considerably and have impacted the German market. During the preparation of this dissertation, Russia's war of aggression against Ukraine drastically influenced the world economy (Mbah and Wasum, 2022). In Germany, this had a particular impact on thermal energy. For example, in the gas sector, there has been a significant and constantly changing price increase and scarcity, which is also reflected in energy supply systems, such as district heating (BA, 2022 b). Legal requirements that have already been initiated by the new federal government also lead to price distortions in the profitability calculations, as considered in Papers H and I. For example, electricity prices changed through a new law "Gesetz zur Absenkung der Kostenbelastungen durch die EEG-Umlage und zur Weitergabe dieser Absenkung an die Letztverbraucher," reducing the cost burden through the Renewable Energy Law surcharge to zero (BT, 2022). Consequently, geopolitical factors also play a role in the design of funding schemes, not only to focus exclusively on the CO₂ saving potential of retrofit measures, but also on the security of supply chains. In addition to ecological, geopolitical, and financial factors, the availability of skilled workers is a challenge for energy retrofits in Germany. Thus, from the perspective of the German government it is stated: "There is often a lack of available capacity in the trade to implement retrofit measures, and construction companies report capacity bottlenecks due to the increasing shortage of skilled workers. Overall, this leads to increasing construction costs, delays, and implementations with suboptimal energy quality"⁶ (BMWK, 2022).

Despite numerous challenges and constantly changing political, economic, ecological, and technical framework conditions, thermal retrofitting of buildings will be a decisive step toward climate neutrality. Analysis methods and modeling approaches must be adapted to these volatile conditions. In conclusion, despite the limitations of this work for datasets and methodology, relevant new insights were provided in this dissertation and its corresponding papers. They have provided the basis for further development of building analysis approaches for single buildings and those on a district scale.

⁶ Translation from German original citation "Oftmals fehlen im Handwerk verfügbare Kapazitäten, um die Maßnahmen umzusetzen, und Baufirmen melden Kapazitätsengpässe durch den zunehmenden Fachkräftemangel. In Summe führt das zu steigenden Baukosten, -verzögerungen und Umsetzungen mit suboptimaler energetischer Qualität. Insgesamt verharrt die Sanierungsquote auf einem Niveau, das, gemessen an den Klimaschutzziele im Gebäudebereich, zu gering ist." (BMWK, 2022)

References

- Antipova, E., Boer, D., Guillén-Gosálbez, G., Cabeza, L., Jiménez, L. (2014). Multi-objective optimization coupled with life cycle assessment for retrofitting buildings. *Energy and Buildings*, 82, 92-99. Doi: <https://doi.org/10.1016/j.enbuild.2014.07.001>
- Balaras, C. A. (2022). Building Energy Audits—Diagnosis and Retrofitting towards Decarbonization and Sustainable Cities. *Energies*, 15(6), 2039. Doi: <https://doi.org/10.3390/en15062039>
- Bundesverband der Energie- und Wasserwirtschaft (BDEW) (2022). Beheizungsstruktur des Wohnungsbestandes in Deutschland 2021. Online 30.08.2022: https://www.bdew.de/media/documents/Wohnungsbestand_Beheizungsstruktur_2021_online_o_dw_jaehrlich_CMi_18072022.pdf
- Bentley Systems (2021). ContextCapture. Online 08.08.2022: <https://www.bentley.com/de/products/brands/contextcapture>
- Betriebskostenverordnung (BetrKV) (2021). Betriebskostenverordnung vom 25. November 2003 (BGBl. I S. 2346, 2347), die zuletzt durch Artikel 15 des Gesetzes vom 23. Juni 2021 (BGBl. I S. 1858) geändert worden ist. Online 15.08.2022: <https://www.gesetze-im-internet.de/betrkv/BetrKV.pdf>
- Bitelli, G., Conte, P., Csoknyai, T., Franci, F., Girelli, V., Mandanici, E. (2015). Aerial thermography for energetic modelling of cities. *Remote Sensing*, 7(2), 2152-2170. Doi: [10.3390/rs70202152](https://doi.org/10.3390/rs70202152)
- Bourdic, L., Salat, S. (2012). Building energy models and assessment systems at the district and city scales: a review. *Building Research & Information*, 40(4), 518-526. Doi: <https://doi.org/10.1080/09613218.2012.690951>
- Bundesamt für Wirtschaft und Ausfuhrkontrolle (BAFA) (2020). Heizen mit Erneuerbaren Energien. Online 28.07.2021: https://www.bafa.de/DE/Energie/Heizen_mit_Erneuerbaren_Energien/heizen_mit_erneuerbaren_energien_node.html;jsessionid=EAA4476C1EBD21FBC7040BF8BE972452.1_cid362
- Bundesanzeiger (BA) (2022 a). Bekanntmachung Änderungen von Richtlinien vom 21. Juli betreffend die Richtlinie für die Bundesförderung für effiziente Gebäude (BEG). *BAnz AT 27.07.2022 B1*. Online 15.08.2022: <https://www.bundesanzeiger.de/pub/publication/PUX896vgdokcHa8nOHT/content/PUX896vgdokcHa8nOHT/BAnz%20AT%2027.07.2022%20B1.pdf?inline>
- Bundesanzeiger (BA) (2022 b). Erste Verordnung zur Änderung der Verordnung über Allgemeine Bedingungen für die Versorgung mit Fernwärme vom 13. Juli 2022. *Bundesgesetzblatt Teil I, 2022, Nr. 25*. Online 25.08.2022: https://www.bgbl.de/xaver/bgbl/start.xav#__bgbl__%2F%2F%5B%40attr_id%3D%27bgbl122s1134.pdf%27%5D__1659618413928
- Bundesinstitut für Stadt-, Bau-, und Raumforschung (BBSR) (2020). Umweltfußabdruck von Gebäuden in Deutschland. Kurzstudie zu sektorübergreifenden Wirkungen des Handlungsfelds

“Errichtung und Nutzung von Hochbauten” auf Klima und Umwelt. BBSR-Online-Publikation Nr. 17/2020. Online 15.08.2022: https://www.bbsr.bund.de/BBSR/DE/veroeffentlichungen/bbsr-online/2020/bbsr-online-17-2020-dl.pdf?__blob=publicationFile&v=3

Bundesinstitut für Stadt-, Bau-, und Raumforschung (BBSR) (2020). Klimaschutz im Gebäudebereich - Grundlagen, Anforderungen und Nachweismöglichkeiten für klimaneutrale Gebäude – ein Diskussionsbeitrag. BBSR-Online-Publikation Nr. 33/2021. Online 30.11.2022: <https://www.bbsr.bund.de/BBSR/DE/veroeffentlichungen/bbsr-online/2021/bbsr-online-33-2021.html>

Bundesklimaschutzgesetz (KSG) (2019). Bundes-Klimaschutzgesetz vom 12. Dezember 2019 (BGBl. I S. 2513), das durch Artikel 1 des Gesetzes vom 18. August 2021 (BGBl. I S. 3905) geändert worden ist. Online 15.08.2022: <http://www.gesetze-im-internet.de/ksg/KSG.pdf>

Bundesministerium für Wirtschaft (BMWi) (2015). Energieeffizienzstrategie Gebäude. Berlin. Online 15.08.2022: https://www.bmwi.de/Redaktion/DE/Publikationen/Energie/energieeffizienzstrategie-gebaeude.pdf?__blob=publicationFile&v=25

Bundesministerium für Wirtschaft (BMWi) (2022): Wohngebäude: Baujahre 1949-79 haben höchsten Energieverbrauch. Berlin. Online 15.08.2022: <https://www.bmwi.de/Redaktion/DE/Infografiken/Energie/energieverbrauch-wohngebaeude.html>

Bundesministerium für Wirtschaft und Klimaschutz (BMWK) (2022). Effiziente Gebäude. Online 15.08.2022: <https://www.bmwk.de/Redaktion/DE/Dossier/energiewende-im-gebaeudebereich.html>

Bundesministerium für Wohnen, Stadtentwicklung und Bauwesen (BMWSB) (2022). Das Gebäudeenergiegesetz. Online 15.08.2022: <https://www.bmwsb.bund.de/Webs/BMWSB/DE/themen/bauen/energieeffizientes-bauen-sanieren/gebaeudeenergiegesetz/gebaeudeenergiegesetz-artikel.html>

Bürgerliches Gesetzbuch (BGB) (2022). Bürgerliches Gesetzbuch in der Fassung der Bekanntmachung vom 2. Januar 2002 (BGBl. I S. 42, 2909; 2003 I S. 738), das zuletzt durch Artikel 4 des Gesetzes vom 15. Juli 2022 (BGBl. I S. 1146) geändert worden ist. Online 17.08.2021: <https://www.gesetze-im-internet.de/bgb/BGB.pdf>

Chen, K., Wang, J., Pang, J., Cao, Y., Xiong, Y., Li, X., ..., Lin, D. (2019). MMDetection: Open mmlab detection toolbox and benchmark. arXiv preprint arXiv:1906.07155.

Chwieduk, D. (2003). Towards sustainable-energy buildings. *Applied energy*, 76(1-3), 211-217. Doi: [https://doi.org/10.1016/S0306-2619\(03\)00059-X](https://doi.org/10.1016/S0306-2619(03)00059-X)

Daffara, C., Muradore, R., Piccinelli, N., Gaburro, N., de Rubeis, T., Ambrosini, D. (2020). A cost-effective system for aerial 3D thermography of buildings. *Journal of Imaging*, 6(8), 76. Doi: 10.3390/jimaging6080076

Deb, C., Schlueter, A. (2021). Review of data-driven energy modelling techniques for building retrofit. *Renewable and Sustainable Energy Reviews*, 144, 110990. Doi: <https://doi.org/10.1016/j.rser.2021.110990>

Deutsche Energie-Agentur (dena) (2021). DENA-GEBÄUDEREPORT 2022. Zahlen, Daten, Fakten. Online 15.08.2022: https://www.dena.de/fileadmin/dena/Publikationen/PDFs/2021/dena-Gebaudereport_2022.pdf

Deutscher Bundestag (BT) (2022). Gesetz zur Absenkung der Kostenbelastungen durch die EEG-Umlage und zur Weitergabe dieser Absenkung an die Letztverbraucher. 20.05.2022 Durchgang BR-Plenarprotokoll 1021, 172-172, TOP 4. Online 15.08.2022: <https://dip.bundestag.de/vorgang/gesetz-zur-absenkung-der-kostenbelastungen-durch-die-eeq-umlage-und-zur/285356?f.wahlperiode=20&rows=25&pos=24>

Department of Energy (DOE) (2013). Guide to Community Energy Strategic Planning. Online 15.08.2022: https://www.energy.gov/sites/prod/files/2014/05/f15/cesp_guide.pdf

Deutsches Institut für Normung (DIN) (1999). DIN EN 13187:1999-05. Wärmetechnisches Verhalten von Gebäuden - Nachweis von Wärmebrücken in Gebäudehüllen - Infrarot-Verfahren (ISO 6781:1983, modifiziert); Deutsche Fassung EN 13187:1998.

Deutsches Institut für Normung (DIN) (2021). DIN 4108. Wärmeschutz und Energieeinsparung in Gebäuden.

Deutsches Institut für Normung (DIN) (2021). DIN V 18599. Energetische Bewertung von Gebäuden - Berechnung des Nutz-, End- und Primärenergiebedarfs für Heizung, Kühlung, Lüftung, Trinkwarmwasser und Beleuchtung.

Deutsches Institut für Normung (DIN) (2022). DIN-Norm. Online 15.08.2022: <https://www.din.de/de/ueber-normen-und-standards/din-norm>

Dixon, T., Eames, M. (2013). Scaling up: the challenges of urban retrofit, *Building Research & Information*, 41:5, 499-503. Doi: 10.1080/09613218.2013.812432

Dutta, A., Zisserman, A. (2019). The VIA annotation software for images, audio and video. *Proceedings of the 27th ACM international conference on multimedia*, 2276-2279. Doi: <https://doi.org/10.1145/3343031.3350535>

Einkommensteuergesetz (EStG) (2020). Einkommensteuergesetz in der Fassung der Bekanntmachung vom 8. Oktober 2009 (BGBl. I S. 3366, 3862) zum Änderungsstand 01.01.2020. Online 28.07.2021: <https://www.gesetze-im-internet.de/estg/EstG.pdf>

Energetische Stadtsanierung (ES) (2022). Den Quartiersansatz fördern. Online 15.08.2022: <https://www.energetische-stadtsanierung.info/energetische-stadtsanierung/programmkefw/>

Entrop, A., Vasenev, A. (2017). Infrared drones in the construction industry: designing a protocol for building thermography procedures. *Energy Procedia* 132 (4), 63–8. Doi: 10.1016/j.egypro.2017.09.636

Erbbaurechtsgesetz (Erbbaurechtsgesetz) (2013). Erbbaurechtsgesetz in der im Bundesgesetzblatt Teil III, Gliederungsnummer 403-6, veröffentlichten bereinigten Fassung, das zuletzt durch Artikel 4 Absatz 7 des Gesetzes vom 1. Oktober 2013 (BGBl. I S. 3719) geändert worden ist. Online 08.08.2022: <https://www.gesetze-im-internet.de/erbbauv/ErbbauRG.pdf>

Fonseca, J., Schlueter, A. (2015). Integrated model for characterization of spatiotemporal building energy consumption patterns in neighborhoods and city districts. *Applied Energy*, 142, 247-265. Doi: <https://doi.org/10.1016/j.apenergy.2014.12.068>

- GAMS Development Corp. (2021). GAMS Studio. Online 10.12.2021: <https://www.gams.com/products/gams/gams-language/>
- Garrido, I., Lagüela, S., Arias, P., Balado, J. (2018). Thermal-based analysis for the automatic detection and characterization of thermal bridges in buildings. *Energy and Buildings*, 158, 1358-1367. Doi: <https://doi.org/10.1016/j.enbuild.2017.11.031>
- Gebäudeenergiegesetz (GEG) (2022). Gebäudeenergiegesetz vom 8. August 2020 (BGBl. I S. 1728), das durch Artikel 18a des Gesetzes vom 20. Juli. 2022 (BGBl. I S. 1237) geändert worden ist. Online 15.08.2022: <https://www.gesetze-im-internet.de/geg/GEG.pdf>
- Gemeindeordnung (GemO) (2018). Gemeindeordnung für Baden-Württemberg (Gemeindeordnung - GemO) in der Fassung vom 24. Juli 2000 (Fassung vom 19.06.2018). Online 15.08.2022: https://www.landesrecht-bw.de/jportal/portal/t/dqi/page/bsbawueprod.psml/screen/JWPDFScreen/Inhaltsverzeichnis_GemO_BW_jlr-GemOBWV23IVZ.pdf;jsessionid=B5C59FCC13E912708B240EB68162BBCB.jp90
- Goodfellow, I., Pouget-Abadie, J., Mirza, M., Xu, B., Warde-Farley, D., Ozair, S., ..., Bengio, Y. (2014). Generative Adversarial Networks. *Advances in neural information processing systems*, pp.2672–2680. Doi: 10.1109/ICCVW.2019.00369
- Google Maps (2021). Karlsruhe. Online 06.06.2021: <https://www.google.com/maps/place/Karlsruhe/@49.0111519,8.3914946,3821m/data=!3m1!1e3!4m5!3m4!1s0x47970648a2e07809:0xb6fc55734cb7ee7f!8m2!3d49.0068901!4d8.4036527>
- Gossen, M., Nischan, C. (2014). Regionale Differenzen in der Wahrnehmung von energetischen Sanierungen. Ergebnisse einer qualitativen Befragung von privaten GebäudeeigentümerInnen zu energetischer Sanierung in zwei unterschiedlichen Regionen, Gebäude-Energiewende, Arbeitspapier, 1. Online 28.07.2021: https://www.gebaeude-energie-wende.de/de/data/gebEner/user_upload/Dateien/GEW_AP1_Ergebnisbericht_Interviews_final_141126.pdf
- He, K., Gkioxari, G., Dollár, P., Girshick, R. (2017). Mask r-cnn. *Proceedings of the IEEE international conference on computer vision*, 2961-2969. Online 01.09.2022: https://openaccess.thecvf.com/content_iccv_2017/html/He_Mask_R-CNN_ICCV_2017_paper.html
- Heizkostenverordnung (HeizkostenV) (2021). Verordnung über Heizkostenabrechnung in der Fassung der Bekanntmachung vom 5. Oktober 2009 (BGBl. I S.3250), die durch Artikel 1 der Verordnung vom 24. November 2021 (BGBl. I S. 4964) geändert worden ist. Online 08.08.2022: <https://www.gesetze-im-internet.de/heizkostenv/HeizkostenV.pdf>
- Hernández, P., Oregi, X., Fitcher, J., Campos, G. (2012). Paper 687: Strategies for upgrading energy performance of buildings in existing urban areas. *Oeste*, 3141(22), 2. Online 15.08.2022: https://www.researchgate.net/profile/Xabat-Oregi/publication/288839008_Strategies_for_upgrading_energy_performance_of_buildings_in_existing_urban_areas/links/5686bdeb08ae1e63f1f5aa3a/Strategies-for-upgrading-energy-performance-of-buildings-in-existing-urban-areas.pdf

Holm, A., Maderspacher, C. (2018). Wirtschaftliche Bedeutung der Gebäudehülle im Wohnungsbau, Forschungsinstitut für Wärmeschutz. Gräfelfing. Online 30.11.2022:

[https://daemmt-](https://daemmt-besser.de/fileadmin/user_upload/Downloads/Studien/FIW_Studie_Wirtschaftliche-Bedeutung-der-Geba__udehu__lle-im-Wohnungsbau_2018.pdf)

[besser.de/fileadmin/user_upload/Downloads/Studien/FIW_Studie_Wirtschaftliche-Bedeutung-der-Geba__udehu__lle-im-Wohnungsbau_2018.pdf](https://daemmt-besser.de/fileadmin/user_upload/Downloads/Studien/FIW_Studie_Wirtschaftliche-Bedeutung-der-Geba__udehu__lle-im-Wohnungsbau_2018.pdf)

Hou, Y., Chen, M., Volk, R., Soibelman, L. (2022). Investigation on performance of RGB point cloud and thermal information data fusion for 3D building thermal map modeling using aerial images under different experimental conditions. *Journal of Building Engineering*, 45, 103380.

Doi: <https://doi.org/10.1016/j.job.2021.103380>

Hou, Y., Mayer, Z., Li, Z., Volk, R., Soibelman, L. (2021 - Paper D). A Computer Vision Approach for Building Façade Component Segmentation on 3D Point Cloud Models Reconstructed by Aerial Images. *EG-ICE 2021 Proceedings: Workshop on Intelligent Computing in Engineering*, 561. Online 18.08.2021: https://www.researchgate.net/profile/Rebekka-Volk/publication/353768665_A_Computer_Vision_Approach_for_Building_Facade_Component_Segmentation_on_3D_Point_Cloud_Models_Reconstructed_by_Aerial_Images/links/6110f75d1e95fe241abb1b49/A-Computer-Vision-Approach-for-Building-Facade-Component-Segmentation-on-3D-Point-Cloud-Models-Reconstructed-by-Aerial-Images.pdf

Hou, Y., Volk, R., Chen, M., Soibelman, L. (2021). Fusing tie points' RGB and thermal information for mapping large areas based on aerial images: A study of fusion performance under different flight configurations and experimental conditions. *Automation in Construction*, 124, 103554. Doi: [10.1016/j.autcon.2021.103554](https://doi.org/10.1016/j.autcon.2021.103554)

Ipsos (2018). Beweggründe und Hindernisse für energetische Sanierung. Umfrage im Auftrag der European Climate Foundation. Ipsos SA, Paris. Online 08.08.2022:

<https://europeanclimate.org/wp-content/uploads/2019/03/Ipsos-full-report-DE.pdf>

Jafari, A., Valentin, V. (2017). An optimization framework for building energy retrofits decision-making, *Build. Environ.* 115. 118–129. Doi: <https://doi.org/10.1016/j.buildenv.2017.01.020>

Kopernikus-Projekt Ariadne (KPA) (2021). Ariadne-Report: Deutschland auf dem Weg zur Klimaneutralität 2045 - Szenarien und Pfade im Modellvergleich. Doi:

<https://doi.org/10.48485/pik.2021.006>

Krawczyk, J. M., Mazur, A. M., Sasin, T., Stokłosa, A. (2015). Infrared building inspection with unmanned aerial vehicles. *Prace Instytutu Lotnictwa*. Doi: [10.5604/05096669.1194965](https://doi.org/10.5604/05096669.1194965)

Kreditanstalt für Wiederaufbau (KfW) (2015). Merkblatt Energetische Stadtsanierung - Zuschuss. 432 Zuschüsse für Quartierskonzepte und Sanierungsmanager. Frankfurt. Online 12.1.2021: [https://www.kfw.de/PDF/Download-Center/F%C3%B6rderprogramme-\(Inlandsf%C3%B6rderung\)/PDFDokumente/6000002110_M_432_Energetische_Stadtsanierung_Zuschuss.pdf](https://www.kfw.de/PDF/Download-Center/F%C3%B6rderprogramme-(Inlandsf%C3%B6rderung)/PDFDokumente/6000002110_M_432_Energetische_Stadtsanierung_Zuschuss.pdf)

Kreditanstalt für Wiederaufbau (KfW) (2020). Förderkredite und Zuschüsse für bestehende Immobilien. Online 28.07.2021: <https://www.kfw.de/inlandsfoerderung/Privatepersonen/Bestandsimmobilie/F%C3%B6rderprodukte/F%C3%B6rderprodukte-f%C3%BCr-Bestandsimmobilien.html>

- Kumbaroğlu, G., Madlener, R. (2012). Evaluation of economically optimal retrofit investment options for energy savings in buildings. *Energy and Buildings*, 49, 327-334. Doi: <https://doi.org/10.1016/j.enbuild.2012.02.022>
- Landesbauordnung für Baden-Württemberg (LBO BW) (2017). Landesbauordnung BW: Landesbauordnung für Baden-Württemberg (LBO) in der Fassung vom 5. März 2010 (Fassung vom 21.11.2017). Online 20.08.2022: https://www.landesrecht-bw.de/jportal/portal/t/ex2/page/bsbawueprod.psml/screen/JWPDFScreen/filename/Inhaltsverzeichnis_BauO_BW_2010_jlr-BauOBW2010V7IVZ.pdf
- Leo, M., Furnari, A., Medioni, G., Trivedi, M., Farinella, G. (2018). Deep learning for assistive computer vision. *Proceedings of the European Conference on Computer Vision (ECCV) Workshops*. Online 15.08.2022: https://openaccess.thecvf.com/content_ECCVW_2018/papers/11134/Leo_Deep_Learning_for_Assistive_Computer_Vision_ECCVW_2018_paper.pdf
- Lin, T., Maire, M., Belongie, S., Hays, J., Perona, P., Ramanan, D., ..., Zitnick, C. (2014). Microsoft coco: Common objects in context. *European conference on computer vision*, 740-755. Springer, Cham. Doi: https://doi.org/10.1007/978-3-319-10602-1_48
- Littlejohn, D., Laszlo, R. (2015). National report on community energy plan implementation. *Quality Urban Energy Systems of Tomorrow*. Online 15.08.2022: https://questcanada.org/wp-content/uploads/2018/08/National-Report-on-Community-Energy-Plan-Implementation_Full_Report_2015.pdf
- Liu, W., Wang, Z., Liu, X., Zeng, N., Liu, Y., Alsaadi, F. (2017). A survey of deep neural network architectures and their applications. *Neurocomputing*, 234, 11-26. Doi: <https://doi.org/https://doi.org/10.1016/j.neucom.2016.12.038>
- Loga, T., Stein, B., Diefenbach, N., Born, R. (2015). Deutsche Wohngebäudetypologie: Beispielhafte Maßnahmen zur Verbesserung der Energieeffizienz von typischen Wohngebäuden. Institut Wohnen und Umwelt GmbH (IWU): Darmstadt, Germany, 18. Online 15.08.2022: https://www.iwu.de/fileadmin/publikationen/gebaeudebestand/episcopes/2015_IWU_LogeEtAl_Deutsche-Wohngeb%C3%A4udetypologie.pdf
- Lucchi, E. (2018). Applications of the infrared thermography in the energy audit of buildings: a review. *Renewable and Sustainable Energy Reviews* 82, 3077–90. Doi: [10.1016/j.rser.2017.10.031](https://doi.org/10.1016/j.rser.2017.10.031)
- Ma, Z., Cooper, P., Daly, D., Ledo, L. (2012). Existing building retrofits: Methodology and state-of-the-art. *Energy and buildings*, 55, 889-902. Doi: <https://doi.org/10.1016/j.enbuild.2012.08.018>
- Macher, H., Landes, T., Grussenmeyer, P. (2020). Automation of Thermal Point Clouds Analysis for the Extraction of Windows and Thermal Bridges of Building Facades. *The International Archives of Photogrammetry, Remote Sensing and Spatial Information Sciences*, 43, 287-292. Doi: <https://doi.org/10.5194/isprsarchives-XLIII-B2-2020-287-2020>
- Martinez-De Dios, J., Ollero, A. (2006). Automatic detection of windows thermal heat losses in buildings using UAVs. *World automation congress*, 1–6. IEEE. Doi: [10.1109/WAC.2006.375998](https://doi.org/10.1109/WAC.2006.375998)

-
- Mayer, Z., Epperlein, A., Volk, R., Vollmer, E., Schultmann, F. (2022 - Paper B). Comparison of building thermography approaches using terrestrial and aerial thermographic images. IOP Conference Series: Earth and Environmental Science, 1078, 012026. IOP Publishing. Online 21.09.2022: <https://iopscience.iop.org/article/10.1088/1755-1315/1078/1/012026/meta>
- Mayer, Z., Epperlein, A., Vollmer, E., Volk, R., Schultmann, F. (2023 - Paper C). Investigating the quality of thermographic drone images for the analysis of buildings. Remote Sensing, 15, 301. Doi: <https://doi.org/10.3390/rs15020301>
- Mayer, Z., Heuer, J., Volk, R., Schultmann, F. (2021 - Paper H). Aerial thermographic image-based assessment of thermal bridges using representative classifications and calculations. Energies, 14(21), 7360. Doi: <https://doi.org/10.3390/en14217360>
- Mayer, Z., Hou, Y., Kahn, J., Beiersdörfer, T., Volk, R. (2021). Thermal Bridges on Building Rooftops - Hyperspectral (RGB + Thermal + Height) drone images of Karlsruhe, Germany, with thermal bridge annotations (Version 0.1.0) [Dataset]. Zenodo. Doi: <http://doi.org/10.5281/zenodo.4767772>
- Mayer, Z., Hou, Y., Kahn, J., Beiersdörfer, T., Volk, R. (2022). Thermal Bridges on Building Rooftops - Hyperspectral (RGB + Thermal + Height) drone images of Karlsruhe, Germany, with thermal bridge annotations (Version 0.2.0) [Dataset]. Zenodo. Doi: <https://doi.org/10.5281/zenodo.6517768>
- Mayer, Z., Kahn, J., Götz, M., Hou, Y., Beiersdörfer, T., Blumenröhr, N., ..., Schultmann, F. (2023 - Paper G). Thermal Bridges on Building Rooftops (TBBR). Nature Scientific Data. Doi: <https://doi.org/10.1038/s41597-023-02140-z>
- Mayer, Z., Kahn, J., Hou, Y., Götz, M., Volk, R., Schultmann, F. (2022 - Paper F). Deep learning approaches to building rooftop thermal bridge detection from aerial images. Automation in Construction. Doi: <https://doi.org/10.1016/j.autcon.2022.104690>
- Mayer, Z., Kahn, J., Hou, Y., Volk, R. (2021 - Paper E). AI-based thermal bridge detection of building rooftops on district scale using aerial images. Proceedings of the EG-ICE 2021 Workshop on Intelligent Computing in Engineering proceedings, Berlin, Germany (Vol. 30). Online 18.08.2021: https://www.researchgate.net/profile/Rebekka-Volk/publication/353768496_AI-based_thermal_bridge_detection_of_building_rooftops_on_district_scale_using_aerial_images/links/6110f63f1ca20f6f860ba438/AI-based-thermal-bridge-detection-of-building-rooftops-on-district-scale-using-aerial-images.pdf
- Mayer, Z., Volk, R., Schultmann, F. (2021 - Paper A). Evaluation of building analysis approaches as a basis for the energy improvement of city districts (No. 61). Working Paper Series in Production and Energy. Doi: 10.5445/IR/1000139091
- Mayer, Z., Volk, R., Schultmann, F. (2022 - Paper I). Analysis of financial benefits for energy retrofits of owner-occupied single-family houses in Germany. Building and Environment, 211, 108722. Doi: <https://doi.org/10.1016/j.buildenv.2021.108722>
- Mbah, R., Wasum, D. (2022). Russian-Ukraine 2022 War: A review of the economic impact of Russian-Ukraine crisis on the USA, UK, Canada, and Europe. Advances in Social Sciences Research Journal, 9(3), 144-153. Doi: 10.14738/assrj.93.12005.

Neußner, W. (2017). Energetische Quartierssanierung - Ausblick und externe Rahmenbedingungen. *Information zur Raumentwicklung*, 4/2017. BBSR. Online 10.08.2022: https://www.bbsr.bund.de/BBSR/DE/veroeffentlichungen/izr/2017/4/downloads/energetische-quartierssanierung-ausblick-dl.pdf?__blob=publicationFile&v=1

Paiho, S., Ketomäki, J., Kannari, L., Häkkinen, T., Shemeikka, J. (2019). A new procedure for assessing the energy-efficient refurbishment of buildings on district scale. *Sustainable Cities and Society*, 46, 101454. Doi: <https://doi.org/10.1016/j.scs.2019.101454>

Presse- und Informationsamt der Bundesregierung (PIB) (2021). Koalitionsvertrag zwischen SPD, Bündnis 90/Die Grünen und FDP. Online 15.08.2022: <https://www.bundesregierung.de/breg-de/service/gesetzesvorhaben/koalitionsvertrag-2021-1990800>

Previtali, M., Barazzetti, L., Brumana, R., Roncoroni, F. (2013). Thermographic analysis from UAV platforms for energy efficiency retrofit applications. *Journal of Mobile Multimedia*, 066-082. Online 08.08.2022: <https://journals.riverpublishers.com/index.php/JMM/article/view/4641>

Rakha, T., Liberty, A., Gorodetsky, A., Kakillioglu, B., Velipasalar, S. (2018). Heat mapping drones: an autonomous computer-vision-based procedure for building envelope inspection using unmanned aerial systems (UAS). *Technology| Architecture+ Design*, 2(1), 30-44. Doi: <https://doi.org/10.1080/24751448.2018.1420963>

Renz, I., Hacke, U. (2016). Einflussfaktoren auf die Sanierung im deutschen Wohngebäudebestand. Ergebnisse einer qualitativen Studie zu Sanierungsanreizen und-hemmnissen privater und institutioneller Eigentümer. IWU, Darmstadt. Online 28.08.2022: https://www.kfw.de/PDF/Download-Center/Konzernthemen/Research/PDF-Dokumente-alle-Evaluationen/Einflussfaktoren-auf-die-Sanierung-im-deutschen-Wohngeb%C3%A4udebestand_2016.pdf

Richarz, C., Schulz, C., Zeitler, F. (2006). Energetische Sanierung: Grundlagen, Details, Beispiele (Vol. 1). Inst. für Internat. Architektur-Dokumentation. ISBN-10: 3920034511

Riechel, R. (2016). Zwischen Gebäude und Gesamtstadt: das Quartier als Handlungsraum in der lokalen Wärmewende. *Vierteljahrshefte zur Wirtschaftsforschung*, 85(4), 89-101. Doi: [doi:10.3790/vjh.85.4.89](https://doi.org/10.3790/vjh.85.4.89)

Riechel, R., Koritkowski, S. (2016). Wärmewende im Quartier. Hemmnisse bei der Umsetzung am Beispiel energetischer Quartierskonzepte. Online 15.08.2022: <https://repository.difu.de/jspui/bitstream/difu/227696/1/DM16100667.pdf>

ROWA Soft GmbH (2021). ThermCAD Wärmebrückensimulationsberechnung. Altenburg, Germany, 2021. Online 15.08.2022: <http://www.rowasoftgmbh.de/de/produkte/produktdetails/thermcad>

Ruggeri, A., Gabrielli, L., Scarpa, M. (2020). Energy retrofit in European building portfolios: A review of five key aspects. *Sustainability*, 12(18), 7465. Doi: [10.3390/su12187465](https://doi.org/10.3390/su12187465)

-
- Ruparathna, R., Hewage, K., Sadiq, R. (2017). Economic evaluation of building energy retrofits: A fuzzy based approach. *Energy and Buildings*, 139, 395-406. Doi: <https://doi.org/10.1016/j.enbuild.2017.01.031>
- Savills Research (SR) (2019). Eigentümerstruktur am Wohnungsmarkt. SPOTLIGHT, Savills Research. Online: 15.08.2022: <https://pdf.euro.savills.co.uk/germany-research/ger-2019/spotlight-eigentumerstruktur-am-wohnungsmarkt.pdf>
- Schild, K. (2018): Wärmebrücken: Berechnung und Mindestwärmeschutz; 1. Aufl. Springer Fachmedien Wiesbaden GmbH, Wiesbaden. ISBN-10: 3658207086
- Schmidt, P., Windhausen, S. (2017): Bauphysik-Lehrbuch: Wärmeschutz – Energieeinsparung – Feuchte- und Tauwasserschutz – Schallschutz – Raumakustik. Bundesanzeiger Verlag GmbH, Köln. ISBN: 978-3-8462-0407-8
- Shellong, W. (2016). Analyse und Optimierung von Energieverbundsystemen. Springer-Verlag. ISBN: 978-3-662-49463-9
- Statistisches Bundesamt (Destatis) (2019). Statistisches Jahrbuch 2019 - Wohnen. ISBN: 978-3-8246-1086-0. Online 08.08.2022: https://www.destatis.de/DE/Themen/Querschnitt/Jahrbuch/jb-wohnen.pdf?__blob=publicationFile
- Stieß, I., van der Land, V., Birzle-Harder, B., Deffner, J. (2010). Handlungsmotive, -hemmnisse und Zielgruppen für eine energetische Gebäudesanierung. Ergebnisse einer standardisierten Befragung von Eigenheimsanierern. Frankfurt am Main. Online 28.07.2021: http://www.isoepublikationen.de/publikationen/publikation-de-tail/?tx_refman_pi1%5Brefman%5D=354&tx_refman_pi1%5Bcontroller%5D=Refman&tx_refman_pi1%5Baction%5D=detail&cHash=75e2c320a175a52f327e678e4bdd61dc
- Theodosiou, T., Papadopoulos, A. (2008). The impact of thermal bridges on the energy demand of buildings with double brick wall constructions, *Energy and Buildings* 40 (2008) 2083–2089. Doi: 10.1016/j.enbuild.2008.06.006.
- Urban Europe (UE) (2020). White Paper on PED Reference Framework for Positive Energy Districts and Neighbourhoods. Online 15.08.2022: <https://jpi-urbaneurope.eu/ped/>
- Vereecken, E., Roels, S. (2012). Review of mould prediction models and their influence on mould risk evaluation. *Building and Environment*, 51, 296-310. Doi: <https://doi.org/10.1016/j.buildenv.2011.11.003>
- Volland, J., Pils, M., Skora, T. (2016). Wärmebrücken: erkennen – optimieren – berechnen – vermeiden; 2. Auflage. Verlagsgesellschaft Rudolf Müller GmbH & Co KG, Köln. ISBN: 978-3-481-03365-1
- Wang, B., Xia, X., Zhang, J. (2014). A multi-objective optimization model for the life-cycle cost analysis and retrofitting planning of buildings. *Energy and Buildings*, 77, 227-235. Doi: <https://doi.org/10.1016/j.enbuild.2014.03.025>

Wu, R., Mavromatidis, G., Orehounig, K., Carmeliet, J. (2017). Multiobjective optimisation of energy systems and building envelope retrofit in a residential community. *Applied Energy*, 190, 634-649. Doi: <https://doi.org/10.1016/j.apenergy.2016.12.161>

Wu, Y., vkhalidov, Castro, S., Wang, G., wuyuanyi135, Pepose, S. (Kirk), ..., Bozkurt, A. (2019). Nncrystals/Detectron2 v0.0.1. Doi: <https://doi.org/10.5281/ZENODO.3550121>

Part II Companion Articles

Paper A: Evaluation of Building Analysis Approaches as a Basis for the Energy Improvement of City Districts

This paper was reproduced in its original format with permission from KITopen:

Mayer, Z., Volk, R., Schultmann, F. (2021 - Paper A). Evaluation of building analysis approaches as a basis for the energy improvement of city districts (No. 61). Working Paper Series in Production and Energy. Doi: [10.5445/IR/1000139091](https://doi.org/10.5445/IR/1000139091)

Evaluation of Building Analysis Approaches as a Basis for the Energy Improvement of City Districts

Zoe Mayer, Rebekka Volk, Frank Schultmann

Chair of Energy Economics, Institute for Industrial Production (IIP)
at the Karlsruhe Institute for Technology (KIT),
Hertzstr. 16, building 06.33, 76187 Karlsruhe,
email: zoe.mayer@partner.kit.edu

Summary

Municipalities in Germany develop policy plans referred to as 'Energetische Quartierskonzepte' (EQ, pl. EQs) to lower and decarbonize the energy consumption of existing buildings in whole city districts. These EQs describe the status-quo, a strategy, and measures for the energy-related improvement of a district based on an initial analysis of the buildings in the considered area. We study 25 publicly available reports of German EQs to identify common state-of-the-art approaches for the analysis of buildings on district scale, summarizing their strengths and weaknesses. We extract ten approaches that are currently applied in practice. Overall, we could not find any connection between the year of the EQ publication, the district size, and the type and quantity of analysis approaches used. The most common approaches for obtaining data for building analyses are the use of representative building typologies, on-site inspections of buildings, datasets from network-operators, and citizen surveys. The main weaknesses of the assessed approaches are for example inaccuracies due to simplifying assumptions, inconsistent data formats from different data sources, and problems due to data protection restrictions. The standardization, combination, and further development of the assessed approaches are recommended.

Evaluation of Building Analysis Approaches as a Basis for the Energy Improvement of City Districts

Zoe Mayer , Rebekka Volk and Frank Schultmann

Keywords: heating, building retrofits, urban transition, district analysis, building inspection, neighborhood

1. Introduction

The Paris agreement of 2015 obliges the signing nations to restrict the rise in global average temperature well below 2°C compared to pre-industrial levels and to pursue efforts to limit it to 1.5°C [1]. To achieve such goals, urban areas play a key role. Today, more than half of the world's population lives in urban areas that contain the majority of the world's built assets and economic entities [2].

In 2018, the building sector accounted for the largest share of both global final energy use (36%) and energy-related CO₂ emissions (39%), and thus possesses a high potential for energy savings [3]. The Intergovernmental Panel on Climate Change (IPCC) summary for urban policy makers highlights the key role of the transformation and retrofitting of building stocks in urban areas for the achievement of climate goals [2]. This role is also emphasized by the New Urban Agenda [4], envisaging cities as part of the solution for sustainable development and climate protection. A part of this agenda focuses on the renewal, regeneration, and retrofitting of urban areas, and the provision of "high-quality buildings and public spaces, promoting integrated and participatory approaches involving all relevant stakeholders and inhabitants and avoiding spatial and socioeconomic segregation and gentrification".

To push a sustainable urban transition in the building sector, there are three main levels of action: the city scale, the district scale, and the building scale [5]. The district scale (neighborhood/ community scale) is the intermediate level between the city and the building scale, a spatially narrow area consisting of several private and/or public buildings, including public infrastructure [6, 7].

The district scale has certain advantages for the development of energy improvement approaches and their implementation and is also emphasized by the New Urban Agenda [4]. Riechel [5] summarizes different advantages of the district scale: Compared to action plans for single buildings, plans on district scale provide the possibility of cost digressions and other economies of scale for procurement, installation, or energy improvements. The closeness between inhabitants and other stakeholders in a neighborhood is an advantage compared to the development of strategies on city scale. Communication in a district takes place with its own dynamics: for example, informal communication among neighbors ("neighborhood gossip") or copying of building modernization in the neighborhood by other owners. Moreover, approaches on district scale do not only focus on buildings, but also on framework conditions of a district such as the optimization of infrastructure in a district. When planning building retrofits and the optimization of a district heating network there can be relevant efficiencies which can't be taken into account in practicable way at the city- or building scale [8]. Approaches on district scale can also take into account the local stakeholders (e.g. inhabitants and building owners) and their individual preferences in a more targeted way than on city scale. This is relevant, for example, when retrofitting multi-occupancy residential buildings with multi-property ownerships, which often requires special efforts for the coordination and participation of owners [9].

In order to systematically use the advantages of the district scale for the energy retrofit of buildings, there are various standardized approaches that are supported and funded by governments. Examples are the Community Energy Strategic Planning (CESP) in the USA [10], Community Energy Planning (CEP) in Canada [11], Positive Energy Districts (PED, pl. PEDs) in Europe [12] and “energetische Quartierskonzepte” (EQ, pl. EQs) in Germany [7]. CESP, CEP and EQs intend to reduce the energy use and increase the use of renewable, low carbon energy sources of buildings [7, 10, 11]. PEDs are energy-efficient and energy-flexible urban areas or groups of buildings which have net zero greenhouse gas emissions and contribute to a surplus production of renewable energy [12]. Moreover, there are countries (e.g. China) where district energy planning is not established yet, primarily because there are no clear standards and specifications for these plans, but emphasized as beneficial in future by researchers [13].

While the development of 100 total PEDs is targeted by 2050 [12], already 150 CEP projects have been developed as of 2015 [11], and even 850 EQs in Germany as of 2019 [14]. For the USA, the authors could not find any official figures on the progress of the development of CESP.

There is no generic approach for the improvement of existing building stocks on district scale known to the authors that has been performed as frequently and has a broad, often publicly accessible reporting system as German EQs. EQ reports are documents that are authored by energy agencies, universities and scientific research institutions and are usually commissioned and published by municipalities. They describe the process and the results of an EQ development. The German government supports municipalities in developing EQs with financial incentives by Kreditanstalt für Wiederaufbau¹ (KfW). KfW offers financial support via its program 432 for energy-focused city district optimization. The amount of the financial support of the KfW bank is between 5,000 euros and 350,000 euros per EQ and includes personnel and material costs for the development of an EQ and its implementation for the duration of maximum 5 years. [7]

KfW defines minimum requirements, procedures, and standards for the development of an EQ. Following the KfW definition [7], an EQ has to include six planning steps to receive funding, shown in Figure 1. The first step is the initial analysis of the district, its buildings, and infrastructure to identify large energy consumers and potential for energy savings. The second step is the development of an action plan, including specific measures and goals for the reduction and decarbonization of energy consumption in the district. An effective and efficient action plan depends significantly on a well-founded analysis of the initial state. The third step includes a plan for financing all planned actions. It must be clarified how much the municipalities pay themselves or through third parties and how much funding from KfW is needed. The fourth step targets the stakeholders (e.g. inhabitants, building owners, and local business people) of the district. With public participation measures and active energy consulting, the aim is to address and motivate these stakeholders to participate in the EQ process. This is a key step for the success of an EQ as the implementation of all measures depends on the participation of the stakeholders, especially the building owners and their willingness to invest own money, time, and effort. Concrete analysis results and the clarification of identified weak points in the individual buildings of the district can help for the mobilization of building owners. The fifth step is an implementation strategy, including a timetable and priorities for the implementation of actions. The final step is a plan for the long-term evaluation, performance monitoring, and assessment of success during the implementation of the EQ. [7,15]

¹ (engl. German Reconstruction Loan Corporation)

The specifics of individual steps are largely not specified by the KfW. Each municipality can/must find its own ways of designing them in the context of each individual district.

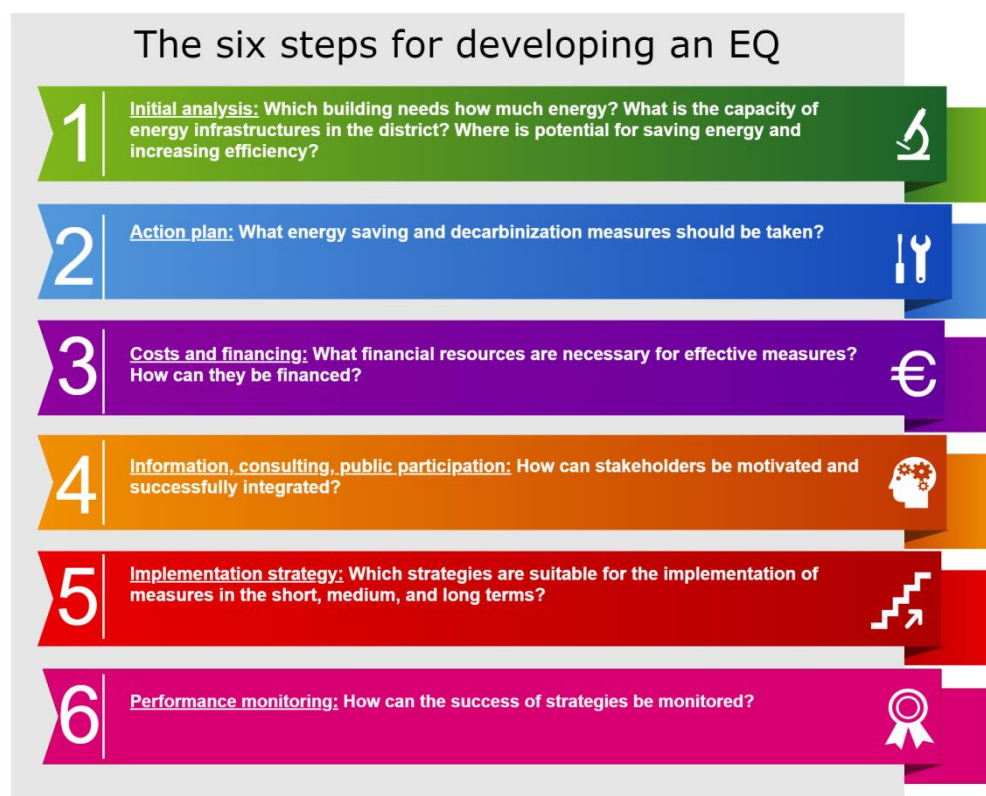


Figure 1. Planning steps of an EQ as outlined by KfW [7, 15]

The initial analysis of the district's buildings is the first step in the development of an EQ and the basis for all further steps. It is also the most resource-intensive step. Riechel and Koritkowski [16] state that the time required for collection of the data of a district can account for up to 65% of the total EQ development. On average, they estimate that the time share of this step is about 40%. For the pilot projects of the KfW program 432, Neußer [17] shows that a major share of 50% to 80% of the funding amount and time is spent for the analysis of the initial energy situation of buildings and facilities. This shows that the analysis step is decisive in order to reduce costs and time required for the development of EQs which could lower barriers for municipalities to invest in EQs and push climate protection measures for buildings on the district scale.

In this study, we address the following research questions on the analysis of districts for the development of EQs: Which approaches form the current practices for the analysis of districts in EQs? What are the strengths and weaknesses of current analysis approaches to analyze buildings on a district scale? What improvements of current approaches are possible and necessary for increasing EQ uptake?

2. Related work

In Germany, many recent publications and guidelines deal with the development of EQs and the initial analysis of a district. Early research goes back to the research program ExWoSt² dealing with innovative housing and urban development of the Federal Ministry of Transport, Building, and Urban Affairs [18]. Numerous projects in the field of the energy-related optimization of districts, such as “Energetische Stadterneuerung”³, “EnEff:Stadt”⁴, “Anforderungen an energieeffiziente und klimaneutrale Quartiere”⁵ (EQ-project), as well as guidelines at state level have emerged from this program [18-21].

The EQ-project deals with requirements for energy-efficient and climate-neutral districts on the basis of five sample districts that were among the first EQs in Germany following the KfW standards [18, 21]. The EQ-project investigates EQs and evaluates them with a view to their components and instruments for the climate-friendly improvement of urban districts. The research approach uses a qualitative analysis of impact relationships and a quantitative evaluation of energy saving measures. It focuses on the energy performance of buildings as well as in the transport sector of a district. For the initial analysis of a district, it highlights that good ways of aggregation (e.g. via building typologies) help keep initial data collection to a reasonable level of effort. This study is a good first approach to evaluating EQ practices, but is superficial regarding the initial district analysis and is based on only five early EQs.

More recent research on the quality of EQs is currently done by the BES project⁶ [22]. It evaluates EQs supported by the KfW program 432 with different subprojects and approaches to improve the program in line with practical needs, as well as to support the targeted knowledge transfer and the public communication of results. Up to 70 reference EQs are being examined within the framework of the research project. Final results are not available yet. So far, the BES project provides a short overview of planning tools for district analysis [23]. A more in-depth examination of current district analysis approaches in EQs and a consideration of their strengths and weaknesses are missing.

Neußer [17], who also takes part in the BES project, deals among other topics with the quality of databases for the analysis of districts. He criticizes the lack of standards for the collection and use of basic information in EQs, and thus the lack of comparability between EQs. Neußer also mentions the heterogeneity of districts as a challenge for the development of EQs, but neither specifies his critique nor proposes solutions.

The project “TransStadt” examines 15 districts that developed EQs with respect to local transformation paths in the context of a strategically oriented integrated urban development mix [5, 16, 24]. Riechel and Koritowski [16] focus on the obstacles and conflicts at municipal level that make it difficult or impossible to achieve national climate protection goals. Moreover, they identify the weaknesses of several components of existing EQs. For the initial analysis, Riechel and Koritowski state difficulties in collecting heat data in districts due to data protection regulations, and criticize the inconsistency of data used in the developed EQs such as CO₂ equivalents or the share of renewable energies in the electricity mix. The “TransStadt” project also developed a guideline to municipal transformation management for local heat transition [24]. This guideline includes advice on collecting technical data for the heating system and thermal

² ExWoSt: Experimenteller Wohnungs- und Städtebau (engl. Experimental urban development)

³ (engl. Energy renewal of cities)

⁴ EnEff:Stadt: Energieeffiziente Stadt (engl. Energy efficient city)

⁵ (engl. Requirements for energy-efficient and climate-neutral districts)

⁶ BES: Begleitforschung zur Energetischen Stadtsanierung (engl. Accompanying research on urban energy renewal)

quality of a district. It also mentions some weaknesses of current analysis tools, data protection requirements, and the integration of different data formats.

International research on the energy performance analysis of districts is summarized by Aghamolaei et al. [25]. They reviewed approaches in three sections: (1) approaches defining district energy performance, (2) approaches to and methodologies for district energy performance evaluation, and (3) system interactions between district entities. They state that few of the reviewed studies investigated the challenges in the initial stages of designing different steps of energy performance analysis in districts. However, inaccurate or imprecise assumptions in the basic steps of energy performance analysis can lead to expensive and irreversible consequences such as waste of project resources or unreliable results and solutions.

This literature overview shows that, particularly for German EQs, there is already research covering the topic of the analysis of city districts. However, there is no publication providing a comprehensive list of current approaches and focusing on their quality for the energy analysis of buildings in a structured way. So far, it has not been possible to conclude from existing publications what the reasons for the enormous resource consumption in the analysis step of the EQ development are and how in the future the use of time and costs can be reduced in order to make EQs more practicable in Germany.

3. Materials and methods

In this study, we summarize how EQs deal with the initial analysis of city districts and identify strengths and weaknesses as well as potential improvements of these approaches.

For this, we work with information that we gain from the comprehensive database of existing EQ reports. We first search for publicly available EQ reports in Google, Google Scholar, and on official websites of German municipalities and of local energy agencies. The reports we find, we sort according to their year of publication, the geographical location, and size of the investigated district. For this study we selected 25 EQ reports that attempt to balance the distribution of these three characteristics. We preference districts with a heterogeneous building stock, as a large diversity of buildings complicates analysis on district scale. The building stock heterogeneity includes the aesthetic, physical, and thermal quality of buildings with features like year of construction, building materials, size, restoration and maintenance quality including quality of thermal building envelopes, as well as heating systems and energy sources. There is also a broad heterogeneity of usage. Besides housing, most urban districts also include public buildings, such as schools or hospitals, and commercial buildings, such as offices, stores/trades, and different forms of handicraft and industry. In addition, we ensure that the reports are detailed enough to obtain information on the applied building analysis approaches.

When studying the selected EQ reports, we first examine the role of residential and non-residential buildings in the analysis of the district's building stocks. We look for information in the reports on whether the EQs differentiate between residential and non-residential buildings and whether special approaches are used for the analysis of non-residential buildings. We summarize all approaches mentioned in the reports for the acquisition of building data and the energy analysis of buildings on district scale. To investigate strengths, weaknesses, and potential improvements of building analysis approaches on district scale, we provide short SWOT⁷ analyses for each approach mentioned in the studied reports. In this context we consider strengths as enhancers of an effective and efficient building energy analysis and weaknesses as inhibitors leading to high costs, analysis times, and inaccurate results of a building energy analysis.

⁷ SWOT: Strengths, Weaknesses, Opportunities, and Threats

Opportunities are possible ways of mitigating weaknesses. Threats are risks having to be considered when improving analysis approaches. To find strengths and weaknesses, we extract know-how from the experiences described in the 25 EQ reports on the used building analysis approaches and point out opportunities and threats.

All results in Section 4 rely exclusively on information extracted from the analysis of the 25 EQ reports. Additional literature used for more precise explanations is explicitly indicated.

The research approach of this study is illustrated and summarized in the flowchart in Figure 2.

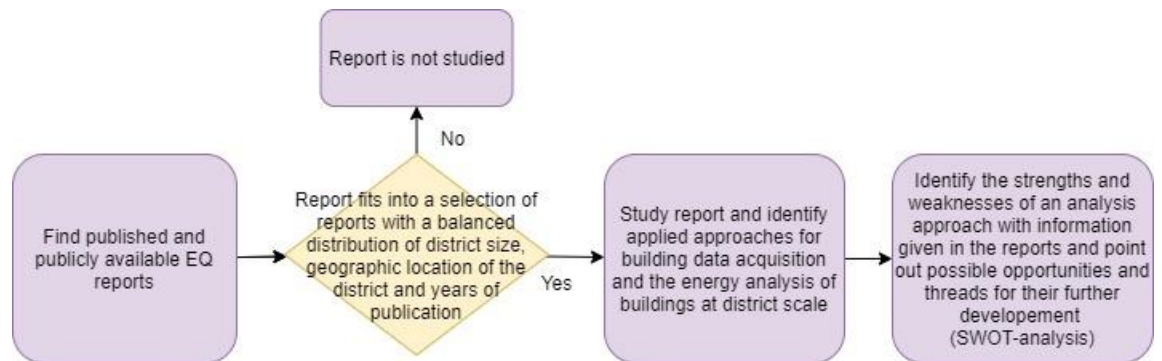


Figure 2. Flowchart for the study design

4. Review results

4.1. Database

Of the existing 850 German EQs as of 2019 [14], we found around 50 publicly accessible EQ reports that were published between 2013 and 2018 and do not violate data protection requirements. During our investigation, we could not find any reports published before 2013. All EQs fulfill the German “standards” (funding requirements of the KfW bank) and thus follow the same structure as described in Section 1. Of these 50 EQ reports, we selected 25 reports that correspond to as balanced a distribution as possible of the characteristics outlined in the beginning of Section 3, namely the geographical, temporal, and district size features of the considered districts (Figure 3, Figure 4, and Figure 5).

Since an EQ is often developed by local or regional stakeholders, such as local energy agencies, the selection process of the reviewed EQs was designed to cover as best as possible all federal states of Germany. Except for the federal states of Bremen, Saxony-Anhalt, and Mecklenburg-Western Pomerania, we found publicly accessible reports in all states. We selected a widespread geographical distribution of the considered EQs between Northern and Southern Germany as well as laterally and of districts of different sizes. The sizes of the districts’ covered areas vary between 4.6 ha and 235.5 ha, with an approximately balanced distribution between the sizes in the range between 4.6 ha and 100 ha, excluding two large outliers with 173 ha and 235.5 ha (Figure 5a). The number of district inhabitants varies between 393 and 12,440 with an approximately balanced distribution in the range of 393 to 8,900, excluding a slightly larger outlier with 12,440 (Figure 5b). The number of considered buildings in the reviewed EQs varies between 20 and 1,135, with an approximately balanced distribution in the range of 20 to 900, excluding one outlier with 1,135 (Figure 5c).

A detailed overview of the considered EQ reports shows information about the area size, number of inhabitants, and number of buildings (Table 1).

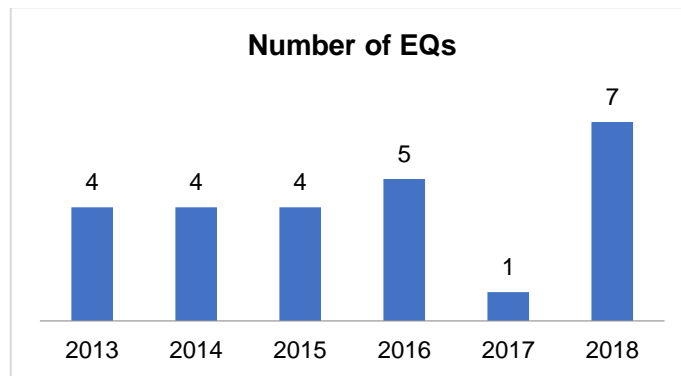


Figure 3. Number of reviewed and analyzed EQs according to their years of issue in the period of 2013 to 2018



Figure 4. Distribution of selected and reviewed EQs in Germany (created with Google Maps [26])

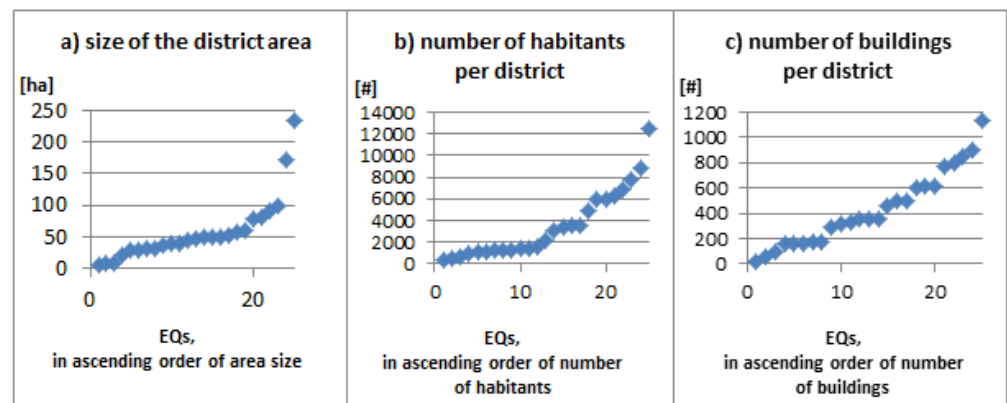


Figure 5. Selected and reviewed EQs sorted according to their characteristics of the considered EQs in ascending order: (a) Size of the district area, (b) Number of citizens, (c) Number of buildings in the district

Table 1. Overview of the considered plans for the energy improvement of districts (EQ) with Information about the area size, number of inhabitants, and number of buildings

District	Municipality	State	Year	Area [ha]	Inhabitants [#]	Buildings [#]	Area-related population density [inhabitants/ha]	Building-related population density [inhabitants/building]	Area-related building density [buildings/ha]	Remarks
Altchemnitz	Chemnitz	Saxony	2018	80	6003	460	75	13.1	5.8	*** [27]
Eichkamp und Heerstr	Berlin	Berlin	2016	60	3090	767	51.5	4	12.8	* [28]
Engeo	Bremervörde	Lower Saxony	2014	50	1272	350	25.4	3.6	7	** [29]
Gartenberg	Sömmerda	Thuringia	2013	37	894	320	24.2	2.8	8.6	[30]
Gibitzenhof	Nuremberg	Bavaria	2018	79	12440	800	157.5	15.6	10.1	** [31]
Hainholz	Hannover	Lower Saxony	2015	173	6821	850	39.4	8	4.9	** [32]
Hillscheid	Höhr-Grenzhausen	Rhineland-Palatinate	2014	47	1312	500	27.9	2.6	10.6	** [33]
Historische Innenstadt	Neuruppin	Brandenburg	2015	100	4933	900	49.3	5.5	9	[34]
Innenstadt	Nord Völklingen	Saarland	2017	32	3600	618	112.5	5.8	19.3	[35]
Innenstadt	Geldern	North Rhine-Westphalia	2016	40	2208	609	55.2	3.6	15.2	* [36]
Innenstadt	Baunatal	Hessen	2016	50	3450	285	69	12.1	5.7	[37]
Lerchenberg	Mainz	Rhineland-Palatinate	2014	235.5	6305	1135	26.8	5.6	4.8	[38]
Moabit-West	Berlin	Berlin	2013	8.3	8900	500	1072.3	17.8	60.2	** [39]
Mollerstadt	Darmstadt	Hessen	2013	30	3500	325	116.7	10.8	10.8	[40]
Nettersheim	Nettersheim	North Rhine-Westphalia	2018	50	393	155	7.9	2.5	3.1	* [41]
Neue Mitte	Grenzach-Whylen	Baden-Württemberg	2018	90	1431	163	15.9	8.8	1.8	[42]
Neumünden Fuldablick	Hann Münden	Lower Saxony	2018	52	1609	350	30.9	4.6	6.7	[43]
Nörd. Festplatz	Mörfelden-Walldorf	Hessen	2015	32.4	1157	176	35.7	6.6	5.4	[44]
Ostrow	Cottbus	Brandenburg	2016	40	1192	167	29.8	7.1	4.2	[45]
Schilksee	Kiel	Schleswig-Holstein	2018	8	5907	20	738.4	295.4	2.5	** [46]
südöstliches Eisendorf und Bremerstr	Hamburg	Hamburg	2018	58	7800	600	134.5	13	10.3	[47]
Unsere Stadt	Altensteig	Baden-Württemberg	2016	22	616	162	28	3.8	7.4	* [48]
Weinberg-Dichterviertel	Roßleben	Thuringia	2015	28	1152	101	41.1	11.4	3.6	[49]
Wengenviertel	Ulm	Baden-Württemberg	2013	4.6	480	60	104.3	8	13	** [50]
Weststadt	Steinheim	Baden-Württemberg	2014	45	1400	349	31.1	4	7.8	[51]

Data sources:

(-): data explicitly mentioned in the EQ reports

*: area size approximately calculated with Google Maps [26],

**: number of buildings approximately estimated on the basis of maps shown in the EQ reports;

***: number of inhabitants in 2016 according to information by the city of Chemnitz and its districts [52]

4.2. Study of applied building analysis approaches

4.2.1. Preliminary remarks for dealing with residential and nonresidential buildings

The studied EQ reports refer to districts that have mixed types of buildings with a large share of residential buildings, as well as nonresidential buildings such as commerce, offices, industry, and schools. In the initial analysis, the majority of 16 EQs focus almost exclusively or exclusively on residential buildings. Seven EQs consider the analysis of residential and nonresidential buildings in the reports equally or in a close to equal way. Only two EQs put nonresidential buildings in the focus of the analysis.

With regard to different building types, 15 EQ reports describe the use of analysis tools that differ from the standard analysis tools which are especially suitable for residential buildings described in the following subsection (4.2.2). These differing tools are, for example, transferable industrial value estimates, comparative values for nonresidential buildings of the German energy saving guideline (Energieeinsparverordnung, EnEV), or other scientific indicators for nonresidential buildings. For public buildings, ten EQs work with consumption data and building information collected and provided by municipalities.

An overview of this subsection on the single EQ reports is summarized in the Appendix Table 3.

4.2.2. Overview of building analysis approaches

In the 25 EQ reports, ten approaches for analyzing buildings on district scale are mentioned (Figure 6).

19 EQs describe on-site inspections to analyze the considered area and buildings. This involves recording basic building information such as the size dimensions of buildings, along with structural conditions of buildings such as the visible thermal quality of building envelopes or of individual envelope components. In most cases, on-site inspections are limited exclusively to inspections from the outdoor perspective. Also concerning the inspection of buildings from the outside (envelope qualities and size dimensions), eight EQs work with aerial images from Google Maps or other image data providers.

19 EQs work with consumption data obtained from the local network operator for heating (gas, district heating). Nine EQs mention the possibility of working with data from the district chimney sweep association. These datasets often contain additional information on the age of heating systems that are mentioned in some EQ reports. Another way of collecting real consumption data is to work with citizen surveys, which are performed in 19 EQ reports. Some survey sheets are provided as additional material in the EQ reports. These surveys not only include questions concerning energy consumption data, but also the size and shape of the buildings and their parts, current restoration and reconstruction information, the building architecture, the year of construction, the energy system and energy source of the building, as well as personal data of the building owners and tenants. In the EQs, these data are partly used directly and partly for post-survey calculations of the theoretical energy demands of buildings (if the consumption values are not specified) and for identification of the structural weaknesses of a building. The surveys are usually addressed to the building owners, but sometimes also to the tenants. Expert interviews are mentioned in four EQ reports. Experts mentioned in the studied EQ reports are for example important stakeholders in a district with a large property portfolio or stakeholders who combine building knowledge with local knowledge, such as local planning offices.

In order to calculate the theoretical demand for the heating of buildings, 21 EQs use existing or self-made building typologies and standard energy demand values per occupant, residential unit, building, or square meter heated area. The use of building typologies is the most common analysis approach across all studied EQ reports. Typologies define representative buildings for specific years of construction, refurbishment statuses, as well as form and design characteristics. The theoretical

thermal energy demand for such representative buildings can be derived in relation to parameters such as the building size (mostly depending on the number of floors, the number of residential units, and the living area size). A popular building typology for the German building stock named TABULA combines the fields of housing and urban development with energy efficiency and climate protection [53].

17 EQs work with information from building-related data sources and documents, often stored in GIS formats. Such databases are monument protection documents, energy performance certificates, construction files, development plans, real estate registers, or other databases such as destruction maps from World War II or previous energy analyses of buildings. To detect the structural weaknesses of a building envelope, four EQs work with thermal images of buildings from the inside and/or outside.

A holistic approach is the analysis of homogeneous sub-districts. This approach is mentioned in six EQ reports. The entire district can be divided into homogeneous small areas, for which individual representative buildings are then analyzed.

An overview of this subsection on the single EQ reports is summarized in the Appendix in Table 4.

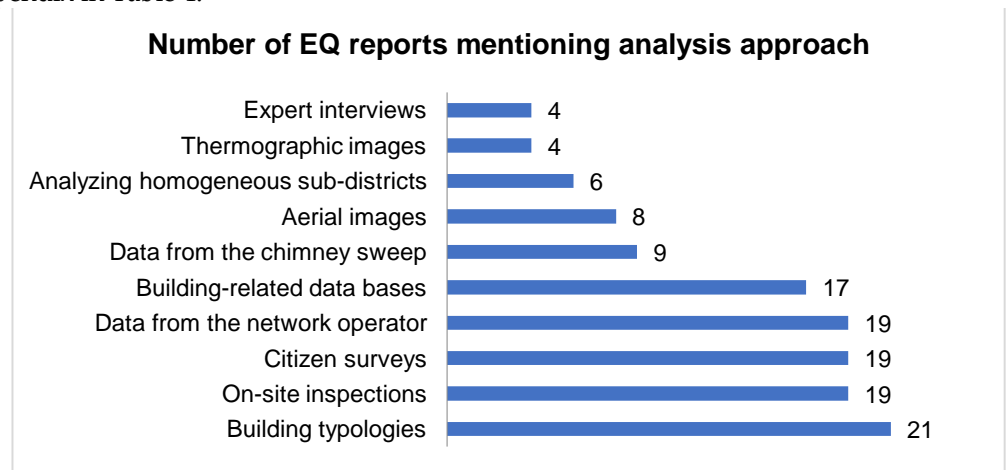


Figure 6. Frequency of used analysis approaches in the studied EQs

4.2.3. Evaluation of common analysis approaches in EQs

The advantage of building typologies is that they do not need much specific data or detailed calculations for each individual building to approximate the energy demand of a whole building stock [e.g. 47, p. 24]. For a very heterogeneous building stock, however, the limited number of building classes in a typology can lead to a problematic simplification. For example, the EQ report of Nord Völklingen criticizes the most frequently used TABULA typology. It states that the building classes of the typology, which are based on the year of construction, allow only limited conclusions about the current thermal quality of a building. Neither retrofits and reconstructions nor extensions of buildings are included in the cataloging [35, p. 21]. The extent to which the use of building typologies leads to a false description of the building stock depends on the used typology and the difference between real buildings and building class typologies. Better analysis results can be achieved with the detailing and expansion of typologies, with the trade-off of increased analysis effort.

On-site inspections can consider the individuality of each building and the heterogeneity of districts. Inspections are particularly suitable for analyzing complex and highly specific buildings with significant energy consumption. In Nuremberg, a production plant [31, p. 74] and in Hannover, important architectural monuments [32, p. 45] are on-site-inspected in depth. The more detailed on-site inspections are, the more complex they become which is why they can often not be carried out for a whole district. For example, Hamburg's EQ report states that a detailed inspection of all buildings in the district (over 500) would have required a considerable amount of time (the amount

of time is not specified in the report). Thus, they just limited on-site inspections to the documentation of a few criteria [47, p.30]. The accessibility of properties is also usually limited due to property rights. Inspections are therefore often limited to the perspective from the street if no agreements have been arranged with building owners and tenants beforehand [37, p. 49]. In order to keep the inspection effort of a district low, inspections can only be limited to special buildings that are difficult to analyze with other approaches.

To detect structural weaknesses of building envelopes in detail, thermal images of buildings provide timely and high-quality information. As part of on-site inspections these are usually also just recorded for individual complex buildings and/or limited to the street perspective. The analysis of roofs from the ground perspective is often limited by conventional thermographic recordings [28, p. 33]. For the EQ of Cottbus, for example, aerial thermographic images are taken into account [45].

Aerial images from providers like Google are easily accessible and can be used to supplement missing information from on-site inspections [40, p. 51]. All sides of the buildings and roofs are visible. Nevertheless, in contrast to on-site inspections, up to date images and high image quality are not always available.

In order to increase the quality and timeliness of aerial images, and to extend inspections and thermographs to all building perspectives, drones could be used in the future. With programmed flight routes and automated image processing, the effort of collecting high-resolution and timely drone images would be manageable. Nevertheless, data protection must be taken into account when recording images with high resolution.

Citizen surveys allow responding to the heterogeneity of buildings in a district and can also be used to collect information about the heating technology of buildings. However, problems arise in the activation of participants at the beginning and during the EQ development. Different response rates have shown that not all EQs have been successful with activating participants. Ten of the 19 EQs describe the response rate of surveys in more detail. They state response rates between 3% up to a peak value of 50%.⁸ Potential reasons for the different rates are not explained in the reports. Another possible obstacle for the use of questionnaires is that building owners and tenants need to be well informed about their buildings. In some cases, the questionnaires ask very detailed information concerning the thermal quality of buildings and use technical terms. For example, the survey of Altensteig asks for the wattage of the heating system and the thickness of building components such as the floor slab [48, p.109]. Another citizen survey in Chemnitz asked for the usable building area (“Nutzfläche”⁹) [27]. It is unlikely that all participants have sufficient knowledge to answer such questionnaires correctly and in a consistent way. A simplification of questionnaires could increase the response rate and the correctness of information, but it is questionable to what extent simplified surveys are helpful for a meaningful analysis.

Like surveys, expert interviews can also provide detailed information. Compared to surveys, more detailed, extensive, and targeted questions are possible in direct interviews. However, organizing and conducting expert interviews can require significant effort. Therefore, they can be seen as a targeted supplement to information gaps [35, p. 41].

⁸ Response rates of citizen surveys: Ulm (Wengenviertel): 50%, Höhr-Grenzhausen (Hillscheid): 50%, Steinheim (Weststadt): 43%, Grenzach-Whylen (Neue Mitte): 42%, Berlin (Eichkamp und Heerstr.): 25%, Hannover (Hainholz): 15%, Chemnitz (Altchemnitz): 13%, Nord Völkingen (Innenstadt): 12%, Hann Münden (Neumünden Fuldablick): 3%

⁹ The “Nutzfläche” of a building is the proportion of the floor area that is used in accordance with its intended purpose. Traffic areas (e.g. entrances, stairwells, lifts, corridors) and functional areas (heating room, machine rooms, technical operating rooms) are not included in the usable area [54].

Data provided by network operators and chimney sweeps have the same strengths and weaknesses. These data can have a high value for the analysis of individual heterogeneous buildings, they provide an indication of the thermal quality of a building without further building information. However, these approaches bring up the topic of data protection. In many districts, network operators and chimney sweep associations do not cooperate or just provide incomplete data about heating technologies and/or consumption data. Usually, suppliers in Germany are only allowed to provide consumption data on an aggregated scale like from distribution points at street level, building block level, or just for the whole district [43, p. 21; 40, p. 56; 27, p. 36; 36, p. 10]. Due to the high aggregation levels of data on block or street levels, statements for individual buildings become difficult if buildings within the aggregation differ from one another. A relaxation of data protection guidelines could be helpful for scientific or EQ development purposes, but conflicts with individual data rights and the developers of EQs have no influence on this. Furthermore, aggregated consumption data does not provide any information on the reason for energy consumption. High consumption can be attributed either to the thermal weaknesses of the building or to specific user behavior. Thus, the comparability of consumption data with calculated demand values must be taken into account when comparing different analysis approaches. Experience mentioned in the EQ report of Darmstadt has shown that consumption in buildings with poor energy performance is usually lower than the calculated energy demand, as people seem to be aware of it and aim to save heating costs [40, p. 68].

Building-related databases have the advantage that they are usually already available to EQ developers and do not have to be collected separately for the EQ development. However, the data is often not up-to-date due to the high effort of maintaining databases [45, p. 132]. Generalizable statements about the data quality of such databases are also difficult. The quality of data varies a lot between different sources and can only be checked in each individual case. When integrating various sources, problems with different standards and calculation databases can arise. Municipalities should have an interest in using uniform formats and standards for all processes and documentations. The goal to standardize data formats for a better integration and the reuse of data is, for example, explicitly mentioned in the EQ report of Cottbus [45, p. 139].

The holistic approach to define and then analyze homogeneous sub-districts of a district simplifies the analysis of complex heterogeneous structures. In the EQ report of Baunatal, neighboring buildings with a similar structure were clustered. Individual clusters were examined independently and with specific approaches (e.g. different approaches and responsibilities for residential and commercial clusters) [37, p. 50]. The division into homogeneous sub-districts can be very detailed, for example in Hann Münden with 37 clusters [43, p. 29]. The division into homogeneous sub-districts does not always make sense and depends highly on the degree of heterogeneity and the layout of a district.

Table 2 summarizes the described strengths, weaknesses, opportunities, and threats of the common district analysis approaches.

Table 2. SWOT analyses for common thermal analysis approaches for buildings on district scaleBuilding typologies:

Strengths (+): Small amount of data required to model many different kinds of buildings; Suitable for homogeneous buildings with properties in accordance with common typological characteristics and few special design features

Weaknesses (-): Simplification of the approach makes it difficult to include all kinds of specific characteristics of buildings like extensions and retrofit modifications

Opportunities (↑): Typologies with many modifications and options to take into account many specific characteristics of buildings and the considered district

Threats (↓): The advantage of small effort due to the simplicity of the approach can be lost with too many modifications and options to include specific characteristics of buildings

On-site inspections:

Strengths (+): Any kind of specific characteristic of buildings can be taken into account

Weaknesses (-): Property rights restrict the access and visibility of buildings and building parts

Opportunities (↑): Limitation of detailed inspections to special buildings which are difficult to determine with other analytical approaches

Threats (↓): High efforts for the EQ developers which increase when asking stakeholders for cooperation and access

Terrestrial thermographic images:

Strengths (+): Provide detailed information on the thermal quality of building envelopes

Weaknesses (-): High effort; For images from the inside, cooperation with building stakeholders is necessary

Opportunities (↑): New technologies like drones can help to collect images of many buildings from the outside with lower effort

Threats (↓): Thermographic images only from the outside provide less information than detailed thermographic analyses; Lower image qualities due to a higher distance between the camera and buildings when using drones

Aerial photographic images:

Strengths (+): Inspections from all sides are possible with less effort than in the case of on-site inspections

Weaknesses (-): Aerial satellite images have a too low resolution to see details; Partly outdated databases

Opportunities (↑): New technologies like drones can help to collect aerial images with a high quality and timeliness

Threats (↓): Collecting images of buildings with a high resolution could be a problem for data protection and privacy; Increased effort in collecting data compared to existing databases

Citizen surveys:

Strengths (+): Any kind of specific characteristic of buildings can be taken into account

Weaknesses (-): Difficulties of motivating stakeholders to participate in surveys; stakeholders should be well informed about their buildings and technically understand the questions asked

Opportunities (↑): Social science research can provide better strategies for motivating stakeholders to participate; Development of simple and easily understandable surveys

Threats (↓): Increasing effort to activate stakeholders; Too simple surveys do not provide good data

Expert interviews:

Strengths (+): Targeted, extensive, and detailed questions are possible

Weaknesses (-): High effort for organizing and conducting high-quality expert interviews

Opportunities (↑): Focusing on the possibility to complement specific missing information

Threats (↓): Depending on the availability, willingness to cooperate and quality of experts in individual districts

Data from network operators and chimney sweeps:

Strengths (+): Simple indicator of the thermal quality of a building without many further building data

Weaknesses (-): Data protection regulations prevent building-specific use of data; Limited comparability of consumption data and calculated energy needs; Network operators must be willing to cooperate

Opportunities (↑): Relaxed data protection regulations for research purposes can increase the quality of available data

Threats (↓): The willingness of network operators to cooperate and the relaxation of data protection conditions are difficult to influence by EQ developers; Individual data rights conflict with relaxed data protection requirements

Building-related databases:

Strengths (+): No additional effort of data collection if data sources already exist

Weaknesses (-): Depending on the quality of the individual database

Opportunities (↑): Uniform data standards across different data sources simplify cross-project data processing also for EQs

Threats (↓): The effort/possibility for the unification of data depends on the individual processes of municipalities

Analyzing homogeneous sub-districts:

Strengths (+): Simplifies the analysis of heterogeneous structures

Weaknesses (-): Not suitable for very heterogeneous districts; Practicability depending on the district layout

Opportunities (↑): Smaller sub-districts for more detailed analysis results; Clustering only for very homogeneous parts of the district

Threats (↓): A greater level of detail increasingly reduces the benefit of this approach

5. Results and discussion

In order to answer the research questions of our work and investigate current building analysis approaches on district scale, their strengths, weaknesses, and potential for improvement, our most important findings based on the analysis of 25 EQ reports are:

- Currently ten analysis approaches for the thermal quality of buildings in a district are frequently used in EQ practice. The most frequently applied approaches in our study for obtaining data for building analyses are: the use of representative building typologies, on-site inspections of buildings, datasets from network-operators and citizen surveys. Overall, we could not find any connection between the year of the publication of the EQ report and the type and quantity of analysis approaches used. We compared the approaches used for all newer EQs (2016-2018) and older EQs (2013-2015) and did not identify any significant differences in this regard. Furthermore, we could not find a connection between the size of the districts and the types of the used approaches.

- In order to compensate for weaknesses in the individual analysis approaches, EQs commonly rely on a combination of multiple approaches and accept deficits in the analysis. There are approaches that are well suited for the analysis of buildings with typical and recurring characteristics such as the use of building typologies and the analysis of homogeneous sub-districts. Other, more resource-intensive approaches are suitable for the detailed analysis of buildings that are individual in their design and use, such as expert interviews or thermography. For practical purposes, detailed analyses should only be carried out for special buildings without reference values and large energy consumers in a district. In addition, there are approaches that are generally suitable for obtaining building data, such as the use of existing building databases, energy consumption values from municipal utilities or chimney sweep associations, and the use of aerial photographs to measure building and component dimensions.

- Current analysis approaches for districts are resource-intensive and complicated for many reasons. Existing databases including information on the thermal quality of buildings are often subject to strict data protection requirements and not always accessible. Well-informed and participating building stakeholders are needed for data collection at early stages of the EQ development. Different file formats make it

difficult to combine different data sources, and for adequately modeling buildings (e.g. according to building typologies) lots of data is necessary. The more precise and usable analysis results should be, the more complex the data acquisition becomes.

- To improve building analyses on district scale for the development of EQs to make them faster, cheaper, and more accurate in the future, we see a need for action in two main areas: (1) the research and further development of existing approaches, and (2) the improvement of legal and organizational framework conditions at the state and municipality level.

Research to improve analytical approaches can lead to better analysis tools such as more detailed building typologies, but should consider the trade-off between better results and more complex analyses or data demand. In some cases, new technologies offer the possibility of improvement without additional effort, such as the use of drones to obtain thermographic aerial images of buildings and automated image processing/assessment or other data analytics approaches.

Further improvement of such approaches is also dependent on external factors that cannot be influenced by EQ developers, but by state governments and municipalities, such as relaxed data protection guidelines for energy consumption data from network operators and chimney sweep associations. Governments that want to push energy retrofits on district scale already (e.g. Germany) or pondering introducing retrofit plans on district scale (e.g. China) could rethink data protection standards for research purposes. Also, the inconsistency of data formats of existing databases in municipalities (e.g. of property land registers, monument protection catalogs, district heating maps) hampers exchanges between individual databases and complicates analysis processes of districts. Uniform data structures and/or open-source software in administrations is a necessity for simple data processing in future.

We also note a distinct lack of uniform standards regarding the procedure for developing EQs and the structure of reports, complicating the comparability of the results of different EQ reports. In Germany, clear instructions should be defined in the KfW funding conditions for this purpose regarding a clear and uniform presentation of the results of the initial analysis of buildings in EQ reports. It should contain information on basic characteristics of the district, such as the number of residents, the number of residential units, the number of owners, the energy demand/energy consumption of the entire district and the individual buildings and the types of heating systems used. It should be shown clearly and transparently how the energy requirements of the individual buildings and the district were calculated, and, if possible, a uniform method should be chosen for all EQs.

Finally, we would like to discuss possible criticisms of our research approach:

First, the major drawback of this study is the limited availability and the limited number of studied EQs. Like all literature-based research, we cannot guarantee to have identified all relevant publicly available EQ reports as well as all strengths or weaknesses in the analysis. However, with our analysis we provide a first comparative insight into these reports. Seeing 850 EQ as the population, 63 randomly sampled EQs would have been a representative sample (with confidence level: 90%, margin error: 10%). However, as the analysis of EQ reports is very complex and we only found around 50 publicly available EQ reports in our extensive research, we studied a sample of 25 appropriate reports taking into account as best as possible a mix of size, geographical aspects, and year of publication. We see this method as suitable and regard the added benefit of examining a higher number of EQ reports as small for answering our research questions. With a higher number of analyzed EQ reports the results about the frequency of applied analysis approaches would, however, become more reliable.

Second, we would like to point out that we used only published EQ reports as the basis for our research approach. To a large extent, the information provided in the 25 analyzed EQ reports regarding the used analysis approaches is not detailed. EQ reports focus more on the presentation of the analysis results and less on the procedure or

quality of used approaches. We also see that the analysis of the initial state of a district is often not a structurally delimited unit in the reports and sometimes merges into other parts of the EQ, such as the sections for the action plan or for the public participation process. This makes it more difficult to identify the used approaches and to analyze how they are implemented in the individual EQs.

Third, we want to emphasize that there are ways for improving the methodology of our SWOT analyses. For more results with further details of the SWOT analyses, expert interviews with the developers of EQs, such as local energy agencies, would be suitable. The use of supplementary literature, e.g. scientific publications on building typologies or guidelines for creating expert interviews for EQs, would also be beneficial and provide additional information.

Nevertheless, we believe that our study was able to identify the main analysis approaches used in practice in Germany to gain information on the thermal quality of buildings on district scale and gave insight into some of their essential shortcomings, and strengths for the development of EQs.

6. Conclusions

The district scale (neighborhood/ community scale) has many advantages for the energy retrofit of buildings. It does not focus on buildings as individual, independent objects, but rather in their urban context. In this way, for example, local social dynamics can be specifically addressed when motivating building stakeholders in the planning and implementation of retrofit measures. Economies of scale can be realized when retrofitting many buildings in a small area at the same time, while the district scale is smaller and easier to coordinate than the higher-level city scale. We thus expect that the district scale will gain in importance in the next years worldwide.

In Germany, the development and implementation of EQs is already a popular instrument for decreasing and decarbonizing the energy consumption of existing buildings in urban areas, and is readily funded by the German government. EQs have been very frequently applied already and EQ reports are documented for each individual district. However, a holistic and comprehensive evaluation of the long-term benefits of EQs after the implementation of developed measures with regard to ecological, social, and emission-related criteria has been lacking so far in research. It is necessary for urban policy makers to invest high costs and effort for analysing buildings and developing appropriate retrofit strategies for whole districts. The actual participation of the various different district stakeholders in the implementation process, however, is essential for the success of EQs and cannot be precisely quantified in the planning process.

To reduce the time and costs of retrofit plans on district scale we have identified a need for more research in the field of energy building analysis. We see our work as a basic overview of current building analysis on district scale with the intention of motivating further research in this field, especially to develop energy improvement strategies in urban areas.

With regard to EQs, we see a need for action for standardizations in Germany on the national level. To deal with different forms of buildings, uniform guidelines (both in data collection, assessment, and reference values) would be beneficial for analyses on district scale and lead to a better comparability of EQ report analysis and implementation results.

Funding information: The paper was created during a doctoral project financed with a scholarship at Karlsruhe Institute of Technology (KIT) according to the Landesgraduiertenförderungsgesetz - LGFG (State Postgraduate Fellowship Program).

Conflicts of Interest: The authors declare no conflict of interest. The funders had no role in the design of the study; in the collection, analyses, or interpretation of data; in the writing of the manuscript, or in the decision to publish the results.

Appendix

Table 3. Overview for dealing with residential and nonresidential buildings (1: used in EQ, 0: not used in EQ)

District		Specific analysis tools for nonresidential buildings	Data of public buildings from local administration	Focus on residential buildings	Focus roughly equally on residential and nonresidential build- ings	Focus on nonresiden- tial buildings
Eichkamp und Heerstr	Berlin	0	0	1	0	0
Moabit-West	Berlin	1	0	0	0	1
Ostrow	Cottbus	0	0	1	0	0
Historische Innenstadt	Neuruppin	0	0	1	0	0
sö Eisendorf und Bremerstr	Hamburg	1	1	1	0	0
Mollerstadt	Darmstadt	1	0	0	1	0
Innenstadt	Baunatal	1	0	1	0	0
Nettersheim	Nettersheim	0	1	1	0	0
Altchemnitz	Chemnitz	1	0	0	1	0
Neumünden Fuldablick	Hann Münden	1	0	1	0	0
Innenstadt	Nord Völklingen	1	0	1	0	0
Gartenberg	Sömmerda	0	0	1	0	0
Enego	Bremervörde	0	1	1	0	0
Schilksee	Kiel	0	1	0	1	0
Lerchenberg	Mainz	1	1	1	0	0
Gibitzenhof	Nuremberg	1	1	0	0	1
Weststadt	Steinheim	1	0	0	1	0
Wengenviertel	Ulm	0	0	1	0	0
Neue Mitte	Grenzach-Whylen	0	1	1	0	0
Unsere Stadt	Altensteig	1	1	0	1	0
Innenstadt	Geldern	0	0	1	0	0
Nörd. Festplatz	Mörfelden-Walldorf	1	1	0	1	0
Weinberg- Dichterviertel	Roßleben	1	0	1	0	0
Hainholz	Hannover	1	0	0	1	0
Hillscheid	Höhr-Grenzhausen	1	1	1	0	0
Total		15	10	16	7	2

Table 4. Overview for analysis approaches for the building stock (1: used in EQ, 0: not used in EQ)

District	Building typologies	On-site inspections	Citizen surveys	Data from the network operator	Building-related databases	Data from the chimney sweep	Aerial images	Analyzing homogeneous sub-districts	Thermographic images	Expert interviews
Eichkamp und Heerstr	Berlin	1	0	1	0	1	0	0	1	0
Moabit-West	Berlin	0	0	1	1	1	0	1	0	0
Ostrow	Cottbus	1	1	1	1	0	1	0	1	0
Historische Innenstadt	Neuruppin	1	0	0	1	0	0	1	0	0
sö Eisendorf und Bremerstr	Hamburg	1	1	0	1	1	0	0	0	0
Mollerstadt	Darmstadt	1	1	1	1	0	1	0	0	0
Innenstadt	Baunatal	1	1	1	0	0	1	1	0	0
Nettersheim	Nettersheim	1	1	0	1	1	0	1	0	0
Altchemnitz	Chemnitz	0	1	1	1	0	1	0	0	0
Neumünden	Hann Münden	1	1	1	1	1	0	1	0	0
Fuldablick	Nord Völklingen	0	1	1	1	0	1	0	0	1
Innenstadt	Sömmerda	1	1	1	1	0	1	0	1	0
Gartenberg	Bremervörde	1	0	1	1	0	0	0	0	0
Enego	Kiel	1	1	0	0	1	0	0	0	0
Schilksee	Mainz	1	1	1	1	1	1	0	0	0
Lerchenberg	Nuremberg	1	1	1	1	0	0	0	0	1
Gibitzenhof	Steinheim	1	1	1	1	0	1	0	0	0
Weststadt	Ulm	0	0	1	1	0	0	0	0	0
Wengenviertel	Grenzach-Whylen	1	1	1	0	1	0	0	0	0
Neue Mitte	Altensteig	1	1	1	0	1	0	0	0	1
Unsere Stadt	Geldern	1	1	1	1	0	0	1	0	1
Innenstadt	Mörfelden-Walldorf	1	0	0	1	1	0	1	1	0
Nörd. Festplatz	Roßleben	1	1	1	0	1	1	0	0	0
Weinberg-Dichterviertel	Hannover	1	1	0	1	1	0	1	0	0
Hainholz	Höhr-Grenzhausen	1	1	1	1	1	0	1	0	0
Hillscheid										
Total		21	19	19	19	17	9	8	6	4

References

1. United Nations (UN) (2015). Paris Agreement. UNFCCC secretariat. Online 5.3.2020: https://unfccc.int/files/essential_background/convention/application/pdf/english_paris_agreement.pdf
2. Bazaz, A. et al. (2018). Summary for urban policymakers: What the IPCC Special Report on global warming of 1.5° means for cities. Doi: <https://doi.org/10.24943/SCPM.2018>
3. International Energy Agency (IEA) (2019). 2019 Global Status Report for Buildings and Construction: Towards a zero-emissions, efficient and resilient buildings and construction sector. UN Environment program, 224. ISBN: 978-92-807-3768-4
4. United Nations (UN) (2017). New Urban Agenda. United Nations Conference on Housing and Sustainable Urban Development (Habitat III) in Quito, Ecuador, on 20 October 2016. ISBN: 978-92-1-132731-1
5. Riechel, R. (2016). Zwischen Gebäude und Gesamtstadt: das Quartier als Handlungsraum in der lokalen Wärmewende. (Analogous translation: Between the building and the city as a whole: the district as field for action in the local heat transition.) Vierteljahrshefte zur Wirtschaftsforschung, 85(4), 89-101. Online 2.9.2021: <https://www.econstor.eu/bitstream/10419/180141/1/vjh.85.4.089.pdf>
6. Huang, Z. et al. (2015). Methods and tools for community energy planning: A review. Renewable and sustainable energy reviews, 42, 1335-1348. <https://doi.org/10.1016/j.rser.2014.11.042>
7. Kreditanstalt für Wiederaufbau (KfW) (2015). Merkblatt Energetische Stadtsanierung - Zuschuss. 432 Zuschüsse für Quartierskonzepte und Sanierungsmanager. (Analogous translation: Leaflet on urban energy improvement - grant. 432 grants for district plans and redevelopment managers.) Frankfurt. Online 12.1.2021: [https://www.kfw.de/PDF/Download-Center/F%C3%B6rderprogramme-\(Inlandsf%C3%B6rderung\)/PDF-Dokumente/6000002110_M_432_Energetische_Stadtsanierung_Zuschuss.pdf](https://www.kfw.de/PDF/Download-Center/F%C3%B6rderprogramme-(Inlandsf%C3%B6rderung)/PDF-Dokumente/6000002110_M_432_Energetische_Stadtsanierung_Zuschuss.pdf)
8. Delmastro, C. et al. (2017). Sustainable urban heat strategies: Perspectives from integrated district energy choices and energy conservation in buildings. Case studies in Torino and Stockholm. Energy, 138, 1209-1220. Doi: <https://doi.org/10.1016/j.energy.2017.08.019>
9. Pardo-Bosch, F. et al. (2019). Key aspects of building retrofitting: Strategizing sustainable cities. Journal of environmental management, 248, 109247. Doi: <https://doi.org/10.1016/j.jenvman.2019.07.018>
10. US Department of Energy (DOE) (2013). Guide to Community Energy Strategic Planning. Online 30.8.2021: https://www.energy.gov/sites/prod/files/2014/05/f15/cesp_guide.pdf
11. Littlejohn, D., Laszlo, R. (2015). National report on community energy plan implementation. Quality Urban Energy Systems of Tomorrow (QUEST). Online 12.9.2021: https://questcanada.org/wp-content/uploads/2018/08/National-Report-on-Community-Energy-Plan-Implementation_Full_Report_2015.pdf
12. Urban Europe (UE) (2020). White Paper on PED Reference Framework for Positive Energy Districts and Neighborhoods. Online 30.8.2021: <https://jpi-urbaneurope.eu/ped/>
13. Xu, B. et al. (2015). Approach and practices of district energy planning to achieve low carbon outcomes in China. Energy Policy, 83, 109-122. Doi: <https://doi.org/10.1016/j.enpol.2015.04.008>
14. Begleitforschung Energetische Stadtsanierung (BES) (2019): Den Quartiersansatz fördern. (Analogous translation: Push the district approach.) Online 08.1.2021: <https://www.energetische-stadtsanierung.info/energetische-stadtsanierung/programmekfw/>
15. Begleitforschung Energetische Stadtsanierung (BES) (2021): Ein Quartierskonzept erstellen. (Analogous translation: Develop an energy improvement district plan.) Online 12.1.2021: <https://www.energetische-stadtsanierung.info/infothek/quartierskonzept/>
16. Riechel, R., Koritkowski, S. (2016). Wärmewende im Quartier. Hemmnisse bei der Umsetzung am Beispiel energetischer Quartierskonzepte. (Analogous translation: Heat transition in districts. Obstacles to implementation using the example of EQs.) Online 12.6.2021: <https://repository.difu.de/jspui/bitstream/difu/227696/1/DM16100667.pdf>
17. Neußer, W. (2017). Energetische Quartierssanierung - Ausblick und externe Rahmenbedingungen. (Analogous translation: District energy improvement - outlook and external conditions.) Information zur Raumentwicklung, 4/2017. BBSR. Online 12.6.2021: https://www.bbsr.bund.de/BBSR/DE/Veroeffentlichungen/lzR/2017/4/Inhalt/downloads/einfuehrung-dl.pdf?__blob=publicationFile&v=2
18. Bundesministerium für Verkehr, Bau und Stadtentwicklung (BMVBS) (2012). EQ - Anforderungen an energieeffiziente und klimaneutrale Quartiere (03/2012). (Analogous translation: Requirements for energy-efficient and climate-neutral neighborhoods.) Berlin. Online 12.1.2021: https://www.bbsr.bund.de/BBSR/DE/veroeffentlichungen/exwost/42/exwost42_1.pdf?__blob=publicationFile&v=1
19. Bundesamt für Bauwesen und Raumordnung (BBSR) (2007): Energetische Stadterneuerung. (Analogous translation: Energy related urban renovation.) Online 19.6.2021: https://www.bbsr.bund.de/BBSR/DE/FP/ExWoSt/Forschungsfelder/2007/EnergetischeStadterneuerung/energetischeStadterneuerung_node.html
20. Erhorn-Kluttig, H., Erhorn, H. (2016): Energetische Bilanzierung von Quartieren in der BMWi-Forschungsinitiative EnEff:Stadt. (Analogous translation: Energy balancing of districts in the BMWi research initiative EnEff:Stadt.) ISBN: 978-3-8167-9629-9

21. Bundesministerium für Verkehr, Bau und Stadtentwicklung (BMVBS) (2012). EQ - Anforderungen an energieeffiziente und klimaneutrale Quartiere (08/2012). (Analogous translation: Requirements for energy-efficient and climate-neutral neighborhoods.) Berlin. Online 12.1.2021: https://www.bbsr.bund.de/BBSR/DE/veroeffentlichungen/exwost/42/exwost42_2.pdf?__blob=publicationFile&v=2
22. Begleitforschung Energetische Stadtsanierung (BES) (2019): Begleitforschung. Ein lernendes Programm. (Analogous translation: Accompanying research. A learning program.) Online 12.6.2021: <https://www.energetische-stadtsanierung.info/begleitforschung/>
23. Begleitforschung Energetische Stadtsanierung (BES) (2021): Bestandsaufnahme zur energetischen Ausgangssituation auf Quartiersebene – Arbeitshilfen für die Praxis. (Analogous translation: Analysis of the initial energy situation at the district level - practical advices.) Online 20.7.2021: https://www.energetische-stadtsanierung.info/wp-content/uploads/2019/08/00_Arbeitshilfe_EnSa_Datenerhebung.pdf
24. Riechel, R. et al. (2017). Kommunales Transformationsmanagement für die lokale Wärmewende. (Analogous translation: Municipal transformation management for the local heat transition.) TransStadt-Leitfaden. Online 12.7.2021: <https://repository.difu.de/jspui/bitstream/difu/241699/1/DM17060254.pdf>
25. Aghamolaei, R. et al. (2018). Review of district scale energy performance analysis: Outlooks towards holistic urban frameworks. *Sustainable cities and society*, 41, 252-264. Doi: <https://doi.org/10.1016/j.scs.2018.05.048>
26. Google Maps (2021): Map of Germany. Online 10.9.2021: <https://www.google.com/maps/place/Germany/@51.096745,5.9659499,6z/data=!3m1!4b1!4m5!3m4!1s0x479a721ec2b1be6b:0x75e85d6b8e91e55b!8m2!3d51.165691!4d10.451526?hl=en>
27. City of Chemnitz (2018). Gewerbestandort Altchemnitz – Energetisches Quartierskonzept – Abschlussbericht. (Analogous translation: Commercial park Altchemnitz – district energy plan - final report.) Online 10.9.2021: https://www.altchemnitz.de/wp-content/uploads/2019/02/2018-08-31_QK-Altchemnitz_Abschlussbericht_ohne_AnhangB.pdf
28. Citizens Energy Association Eichkamp (2016). Energiekonzept für die Siedlungen Eichkamp und Heerstraße (Analogous translation: District energy plan for Eichkamp and Heerstraße.) Online 10.9.2021: http://hauseichkamp.de/energie/Abschlussbericht_Eichkamp%20Heerstrasse.pdf
29. City of Bremervörde (2014). Integriertes energetisches Quartierskonzept „Engeo“. (Analogous translation: District energy plan “Engeo”.) Online 10.9.2021: https://enerko.de/wp-content/uploads/2015/11/Energetisches_Quartierskonzept_Engeo_final.pdf
30. City of Sömmerda (2013). Integriertes Quartierskonzept “Gartenberg“. (Analogous translation: District energy plan „Gartenberg“.) Online 10.9.2021: http://gartenberg.klimaquartier-soemmerda.de/files/2013/02/Konzept_Gartenberg_kopiergeschuetzt.pdf
31. City of Nuremberg (2018). Energetische Quartierskonzepte Quartier Gibitzenhof - Überarbeiteter Abschlussbericht (Analogous translation: District energy plan for the district Gibitzenhof - Revised final report.) Online 10.9.2021: https://www.nuernberg.de/imperia/md/stadtentwicklung/dokumente/publikationen/final_quartierskonzept_gibitzenhof_kfw.pdf
32. City of Hannover (2015). Mit Vielfalt zur energetischen Stadterneuerung – Energetisches Quartierskonzept Hainholz. (Analogous translation: With diversity for energetic urban renewal – District energy plan Hainholz.) Online 10.9.2021: https://www.hannover.de/content/download/582262/file/Energet%20Konzept_Hainholz.pdf
33. Association municipality of Höhr-Grenzhausen (2014). Integriertes energetisches Quartierskonzept für das Fördergebiet in der Ortsgemeinde Hillscheid. (Analogous translation: Energy district plan for the funding area in the local community of Hillscheid.) Online 10.9.2021: <https://www.hoehr-grenzhausen.de/themen-die-uns-bewegen/energetische-stadtsanierung/ieqk-hillscheid-web.pdf?cid=e2>
34. Stadtwerke Neuruppin (2015). Dokumentation - Integriertes Quartierskonzept Historische Innenstadt Neuruppin. (Analogous translation: Documentation – District energy plan for the historic city center of Neuruppin.) No public link available.
35. City of Nord Völklingen (2017). Integriertes energetisches Quartierskonzept – Innenstadt Nord Völklingen (Analogous translation: District energy plan – City center of Nord Völklingen.) Online 10.9.2021: https://www.voelklingen.de/fileadmin/user_upload/Wirtschaft/Stadtplanung/Projekte_Nord_Innenstadt/180403_IEQK_VK_Innenstadt-Nord_Endfassung.pdf
36. City of Geldern (2016). Energetische Quartierssanierung – Innenstadt Geldern. (Analogous translation: Retrofitting districts – City center of Geldern.) Online 10.9.2021: [https://www.geldern.de/C125721A002E05DC/files/energetische_quartierssanierung_innenstadt.pdf/\\$file/energetische_quartierssanierung_innenstadt.pdf?OpenElement](https://www.geldern.de/C125721A002E05DC/files/energetische_quartierssanierung_innenstadt.pdf/$file/energetische_quartierssanierung_innenstadt.pdf?OpenElement)
37. City of Baunatal (2016). Energetisches Quartierskonzept - Innenstadt Baunatal (Analogous translation: District energy plan – city center of Baunatal.) Online 10.9.2021: https://www.baunatal.de/de-wAssets/docs/rathaus-und-politik/rathaus/klimaschutz/Quartierskonzept-Innenstadt-Endbericht_Endfassung_2016_08_05.pdf
38. City of Mainz (2014). Energetische Stadtsanierung – Integriertes Quartierskonzept Mainz-Lerchenberg. (Analogous translation: Energetic urban renewal – District energy plan Mainz-Lerchenberg.) Online 10.9.2021: https://www.mainz.de/medien/internet/downloads/20140129_QuartierskonzeptEndbericht.pdf

-
39. City of Berlin (2013). Stadtteilentwicklungskonzept Green Moabit - Bericht (Analogous translation: District transition plan Green Moabit – Report.) Online 10.9.2021: https://sustainum.de/wp-content/uploads/2015/10/Green_Moabit_Bericht-1.pdf
 40. City of Darmstadt (2013). Mollerstadt 2.0. – Energetische Stadtsanierung Darmstadt, Mollerstadt. (Analogous translation: Mollerstadt 2.0. - Energetic urban redevelopment Darmstadt, Mollerstadt.) Online 10.9.2021: <https://www.darmstadt.de/standort/stadtentwicklung-und-stadtplanung/stadtplanung/sanierung-soziale-stadt-stadtumbau/mollerstadt/mollerstadt-energetische-stadtsanierung>
 41. City of Nettersheim (2018). Integriertes energetisches Quartierskonzept „Sanierungsgebiet Nettersheim“. (Analogous translation: District energy plan „Retrofit area Nettersheim“.) Online 10.9.2021: https://www.nettersheim.de/fileadmin/user_upload/nettersheim/documents/FBIII/2018-04-12_ja_bericht_eqk.pdf
 42. Municipality Grenzach-Whylen (2018). Energetische Stadtsanierung Quartierskonzept - Neue Mitte Grenzach – Abschlussbericht. (Analogous translation: Urban energy transition district energy plan – new center Grenzach – final report.) Online 10.9.2021 <https://www.grenzach-wyhlen.de/ceasy/resource/?id=5132&download=1>
 43. City of Hann Münden (2018). Integriertes Energetisches Quartierskonzept Hann Münden, Neumünden/Fuldablick. (Analogous translation: District energy plan of Hann Münden, Neumünden/Fuldablick.) Online 10.9.2021: https://www.hann.muenden.de/media/custom/2759_1179_1.PDF?1552909852
 44. City of Mörfelden-Walldorf (2015). Integriertes energetisches Quartierskonzept „Okrifteler Straße/ nördlich Festplatz“. (Analogous translation: District energy plan „Okrifteler Straße/ nördlich Festplatz“.) Online 10.9.2021: http://klimaquartier-walldorf.de/files/2014/10/quartierskonzept_moerfelden_walldorf1.pdf
 45. City of Cottbus (2016). Energetisches Quartierskonzept Cottbus – Ostrow. (Analogous translation: District energy plan Cottbus – Ostrow.) Online 10.9.2021: https://www.cottbus.de/.files/storage/file/331455c3-c52c-476c-9513-5866aad0fdd6/Energetisches_Quartierskonzept_Cottbus-Ostrow.pdf
 46. City of Kiel (2018).Endbericht zur Quartierssanierung - Olympiazentrum in Kiel-Schilksee. (Analogous translation: Final report on the district energy plan - Olympic Center in Kiel-Schilksee.) Online 10.9.2021: https://www.kiel.de/de/umwelt_verkehr/klimaschutz/verwaltung/energiequartier_olympiazentrum_schilksee/Endbericht_Energiequartier_Schilksee.pdf
 47. City of Hamburg (2018).Integriertes Quartierskonzept „Südöstliches Eißendorf/Bremer Straße“. (Analogous translation: Energy district plan „Südöstliches Eißendorf/Bremer Straße“.) Online 10.9.2021: <https://www.hamburg.de/contentblob/11622512/83cab01385e919079d8bab6a78e17a8/data/download-bericht-langfassung.pdf>
 48. City of Altensteig (2015). Quartierkonzept “Unsere Stadt” - Stadt Altensteig. (Analogous translation: District energy plan “Our city” – city of Altensteig.) Online 10.9.2021: <https://www.altensteig.de/ceasy/resource/?id=8162-0&download=1>
 49. City of Roßleben (2016). Energetische Stadtsanierung - Integriertes Quartierskonzept Weinberg-Dichterviertel (Analogous translation: Energetic urban redevelopment - District energy plan Weinberg – Dichterviertel.) Online 10.9.2021: <http://stadt-rossleben.klimaquartier.de/files/2016/02/Klimaquartier-Rossleben-Konzept.pdf>
 50. City of Ulm (2013). Integriertes Quartierskonzept für die energetische Stadtsanierung Wengenviertel – Ulm. (Analogous translation: District energy plan for the energy-related urban redevelopment Wengenviertel – Ulm.) Online 10.9.2021: <https://san-ulm.de/wp-content/uploads/KfW-Konzept.pdf>
 51. City of Steinheim (2014). Integriertes energetisches Quartierskonzept „KlimaQuartier Weststadt“. (Analogous translation: Energy district plan „Klimaquartier Weststadt“.) Online 10.9.2021 <https://docplayer.org/4546989-Stadt-steinheim-integriertes-energetisches-quartierskonzept-klimaquartier-weststadt.html>
 52. FOG-Institut für Markt- und Sozialforschung (FOG) (2018). Entwicklung der Einwohnerzahlen der Stadtteile von Chemnitz 2013-2018. (Analogous translation: Development of the population of the Chemnitz city districts 2013-2018.) Online 14.6.2021: <https://www.fog-institut.de/2018/11/27/entwicklung-der-einwohnerzahlen-der-stadtteile-von-chemnitz-2013-2018/>
 53. Loga, T. et al. (2015). Deutsche Wohngebäudetypologie: Beispielhafte Maßnahmen zur Verbesserung der Energieeffizienz von typischen Wohngebäuden. (Analogous translation: German residential building typology: Exemplary measures to improve the energy efficiency of typical residential buildings.) Institut Wohnen und Umwelt GmbH (IWU): Darmstadt, Germany, 18. Online 12.5.2021: https://www.iwu.de/fileadmin/user_upload/dateien/gebaeudebestand/episcopo/DE_TABULA_TypologyBrochure_IWU.pdf
 54. DIN 277-1, Ausgabe 2016-01; Grundflächen und Rauminhalte im Bauwesen - Teil 1: Hochbau. (Analogous translation: DIN 277-1, edition 2016-01; basic areas and volumes in construction - part 1: building construction.)

Paper B: Comparison of Building Thermography Approaches Using Terrestrial and Aerial Thermographic Images

This paper was reproduced in its original format with permission from IOP Publishing:

Mayer, Z., Epperlein, A., Volk, R., Vollmer, E., Schultmann, F. (2022 - Paper B). Comparison of building thermography approaches using terrestrial and aerial thermographic images. IOP Conference Series: Earth and Environmental Science, 1078, 012026. IOP Publishing. Online 21.09.2022: <https://iopscience.iop.org/article/10.1088/1755-1315/1078/1/012026/meta>

Comparison of building thermography approaches using terrestrial and aerial thermographic images

Z Mayer¹*, A Epperlein¹, R Volk¹, E Vollmer¹ and F Schultmann¹

¹ Karlsruhe Institute of Technology (KIT), Institute for Industrial Production (IIP),
Hertzstr. 16, 76187 Karlsruhe

* zoe.mayer@partner.kit.edu

Abstract. Thermography is commonly used for auditing buildings. Classical manual terrestrial thermography records images of individual buildings at a short distance. When auditing a large number of buildings (e.g. whole city districts) this approach reaches its limits. Using drones with thermographic cameras allows images to be recorded automatically from different angles, with faster speed and without violating property rights. However, an airborne camera has a significantly greater distance and more varied angles to a building compared to terrestrial thermography. To investigate the influence of these factors for building auditing, we perform a study evaluating seven different drone settings of varying flight speed, angle, and altitude. A comparison is drawn to manually recorded terrestrial thermographic images. While we find that a flight speed between 1m/s and 3m/s does not influence the thermographic quality, high flight altitudes and steep viewing angles lead to a significant reduction of visible details, contrast, and to falsified temperatures. A flight altitude of 12m over buildings is found to be the most suitable for the qualitative and quantitative analysis of rooftops and a qualitative analysis of façades. A flight altitude of 42m over buildings can only be used for qualitative audits with little detail.

Keywords: Building audits, aerial thermography, drones, urban areas

1. Introduction

The New Urban Agenda declared by the United Nations in 2016 emphasizes the key role of cities in promoting sustainable development and climate protection throughout the building sector [1]. Districts, such as communities or neighborhoods, are easier to coordinate than entire cities when planning energy retrofitting strategies of multiple buildings at once [2]. Numerous international approaches deal with retrofitting buildings on district scale, like Community Energy Strategic Planning (USA) [3], Community Energy Planning (Canada) [4], Positive Energy Districts (Europe) [5] and “energetische Quartierskonzepte” (Germany) [6]. These approaches are planned and coordinated by municipalities in cooperation with institutions like local energy agencies or urban research institutions.

In order to develop a targeted retrofit plan for a whole district, the first step is to document and analyze the thermal quality of existing buildings. A well-established, non-invasive tool for such an audit is thermography, which can be used to monitor and analyze the condition of building envelopes by means of infrared images [7]. Thermographic imaging is capable of identifying thermal weaknesses related to heat-, water-, and airflows through the building envelope. Lucchi [8] summarized the



different applications of thermography in building auditing, which include the thermal characterization of walls, glazing, and windows; thermal bridging and the detection of areas with excessive heat loss; the inspection of thermal insulation and air leakages; detecting moisture and water; measuring U-values; and determining the percentage of the areas with thermal anomalies [8].

Classical thermography studies use hand-held cameras on eye-level to obtain thermographic images of high quality [8]. However, stationary terrestrial thermography reaches its limits in the analysis of entire city districts due to the time-consuming nature of the method where large numbers of buildings of various heights are concerned [9]. Additionally, not all components of a building façade (such as the roof or upper floors) can be captured properly from the ground [10].

Using unmanned aerial vehicles (UAVs), colloq. drones, equipped with thermographic cameras can help implement large scale building audits [11]. The image acquisition process can be automated, allowing for faster completion at lower costs [12]. It becomes possible to obtain images at different angles (not just eye-level) and of high buildings that remain inaccessible via terrestrial thermography. Moreover, the thusly acquired images can easily be used to generate 3D models to provide a good overview of a whole district [13].

Nevertheless, only few scientific publications thus far discuss the use of airborne thermography for building audits. Entrop and Vasenev [14] provide initial research on the basics and possible flight patterns to reduce both time and cost of such a process. They consider a flight distance of between 5m and 10m to a building and use a flight speed of 1m/s after finding image quality to be insufficient when recorded at 1.5m/s. Although they give instructions on how best to perform building audits via UAV-based thermography, they do not specify the means by which thermal image quality is assessed [14]. Rakha and Gorodetsky [15] analyze suitable drone flight settings to create thermographic 3D models of individual buildings. They investigate different settings such as flight path, image overlap, and distance between infrared camera and building. The optimal flight route is found to be a strip pattern at a distance of 12m. Suitable altitudes above ground are chosen as 18m, 22m, and 27m – or twice the building height – to achieve a high enough overlap for 3D model generation. The authors conclude that thermographic drone imagery offers many new possibilities in automating building audits owing to its reduced effort and simplified post-processing [15]. Daffara et al. [16] also investigate suitable flight settings for the development of thermographic 3D building models. For this, they examine a distance of 10m to the building, a maximum height of 8m above the ground, and a high image overlap. They highlight the benefit of drone thermography for building energy audits, particularly of otherwise inaccessible building parts like rooftops [16]. Most recently, Hou et al. [13] explore an approach for thermographic 3D model development of entire city districts using UAVs. Different flight patterns such as vertical grid, horizontal grid, and mesh grid, as well as 90° (nadir) and 45° viewing angles in combination with a high image overlap are analyzed. The authors find that nadir flight captures more details on the roof, while a viewing angle of 45° is more suitable for detecting façade features [13].

In summary, there are no studies known to the authors that document quality criteria for thermographic images acquired via UAV. We therefore present a structured approach to evaluate different flight settings of a UAV-based thermal imager and compare the resulting images to those recorded via terrestrial infrared camera. We derive general statements about the quality, benefits, and deficits of the individual flight settings for building audits.

2. Methods and Materials

2.1. Image Dataset

The dataset used to evaluate the quality of airborne thermography consists of 140 aerial images of two German multi-family buildings. Seven different flight settings were implemented, resulting in ten images per building and setting. An additional set of 249 thermographic images depicting the same buildings were recorded from the ground perspective with a standard handheld camera.

Both buildings are located in the Sophienstrasse 195-197 and 201-203 in the medium sized city Karlsruhe (Germany), have a height of 18m, and belong to the building stock of the municipal housing association Volkswohnung GmbH. Both buildings were constructed in 1957, have 30 and 20 apartments respectively and are fully rented out.

Aerial images were acquired using a “DJI Matrice 600” drone equipped with the “Zenmuse XT2”, a combination of FLIR’s “Duo Pro R” thermal and RGB camera and DJI’s gimbal [17]. The terrestrial images were recorded with a “FLIR T200” hand-held camera [18]. While the latter generates standard JPEG images, the UAV camera saves thermal data in FLIR’s proprietary image format RJPEG.

The thermographic image acquisition took place on January 16th, 2022, from 7pm to 1am. Atmospheric temperatures lay between +2° and +3°C with wind speeds of 2 to 11km/h [19]. It was cloudy throughout the recording timeframe with a slight drizzle between 9.50pm and 10.20pm. The day before exhibited similar weather without any precipitation [20]. The meteorological conditions present during our study therefore align with the best practice rules for thermography according to Fouad and Richter [21]: a sufficiently high temperature difference of at least 15K between in- and outdoors was present, assuming the room temperature of these heated residential buildings was given as the standard +18°C. The recommended maximum outdoor temperature of +5°C was not surpassed and the temperature remained stable for at least 24 hours before image acquisition, ranging from –2°C at its lowest to +3°C at its highest [20]. To avoid the effects of solar radiation, image recording was performed after sunset on a cloudy day. The wind speed ranged from 1m/s to 6.7m/s, thus preventing a considerable change of the heat transfer coefficient. Additionally, no moisture was discernible on either rooftops or building façades, ensuring no falsified temperature recordings ensued. Some best practice conditions mentioned by Fouad and Richter [21], such as a maximum distance of 20m between camera and building and a fixed camera position, are inherently problematic to fulfil in UAV-based applications. These two aspects require a structured analysis as is performed in this study to investigate the effects of both speed and distance on this form of thermography.

The seven different flight settings of the drone (summarized in Table 1) vary according to viewing angle, distance between camera and building, respective distance to the ground, and flight speed. During the first three flights, the viewing angle of the thermographic camera was set to 90° (nadir) to properly record the building rooftops. The other four flights were acquired at an oblique angle of 45° to record the façade. The flight heights were set at 30m (in flights 3, 5 and 7) and 60m (in flights 1, 2, 4, and 6), which correspond to a distance of 12m and 42m respectively between camera and building. Lower flight heights couldn’t be realized on account of nearby obstacles, most commonly trees. In practice, a larger distance to the ground is advantageous in terms of flight duration, as an area can be covered in a shorter period of time using a wider mesh pattern. The speed was set to 1m/s (in flights 1, 3, 6 and 7) and 3m/s (in flights 2, 4, and 5) and was based on experiences from other studies [14]. The camera emissivity was set to 0.95 during all flights, as suggested by Fouad and Richter [21].

Table 1. Experimental parameters used during UAV-based thermal image acquisition (seven different flight settings)

	Viewing angle	Altitude above ground	Altitude above building	Flight speed
	[°]	[m]	[m]	[m/s]
Flight 1	90	60	42	1
Flight 2	90	60	42	3
Flight 3	90	30	12	1
Flight 4	45	60	42	3
Flight 5	45	30	12	3
Flight 6	45	60	42	1
Flight 7	45	30	12	1

Thermal image acquisition via hand-held terrestrial camera was performed at a distance of 8 m to the building. The entire façade was imaged in small segments. Larger distances were not possible owing, again, to the presence of obstacles. As before, the emissivity of the camera was set to 0.95 [21].

To allow a better comparison of all captured thermographic images, we adapted their thermal coloring to an uniform temperature range of -8°C to $+8^{\circ}\text{C}$ using FLIR's Thermal Studio Suite software [22]. Figure 1 and 2 show examples of thermal images depicting the same building area, acquired via drone and hand-held camera respectively. Flights 1, 2 and 3 show the roof from nadir position, flights 4, 5 and 6 display the same façade, while flight 7 depicts the roof.

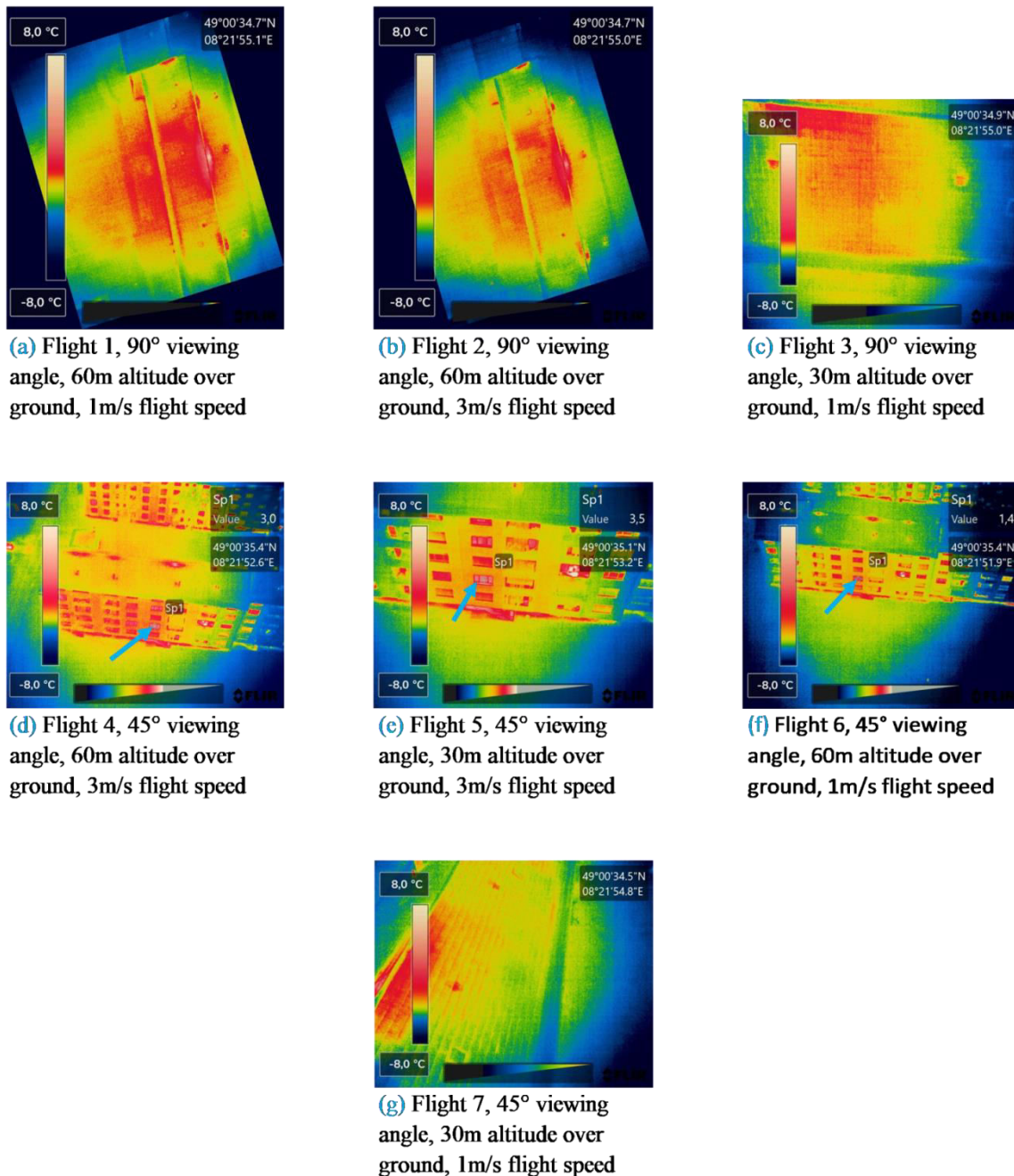


Figure 1. Aerial thermographic images of the building façade in Sophienstrasse 201-203 collected with a drone. The blue arrows in tiles (d, e, f) point to the same window as shown in Figure 2.

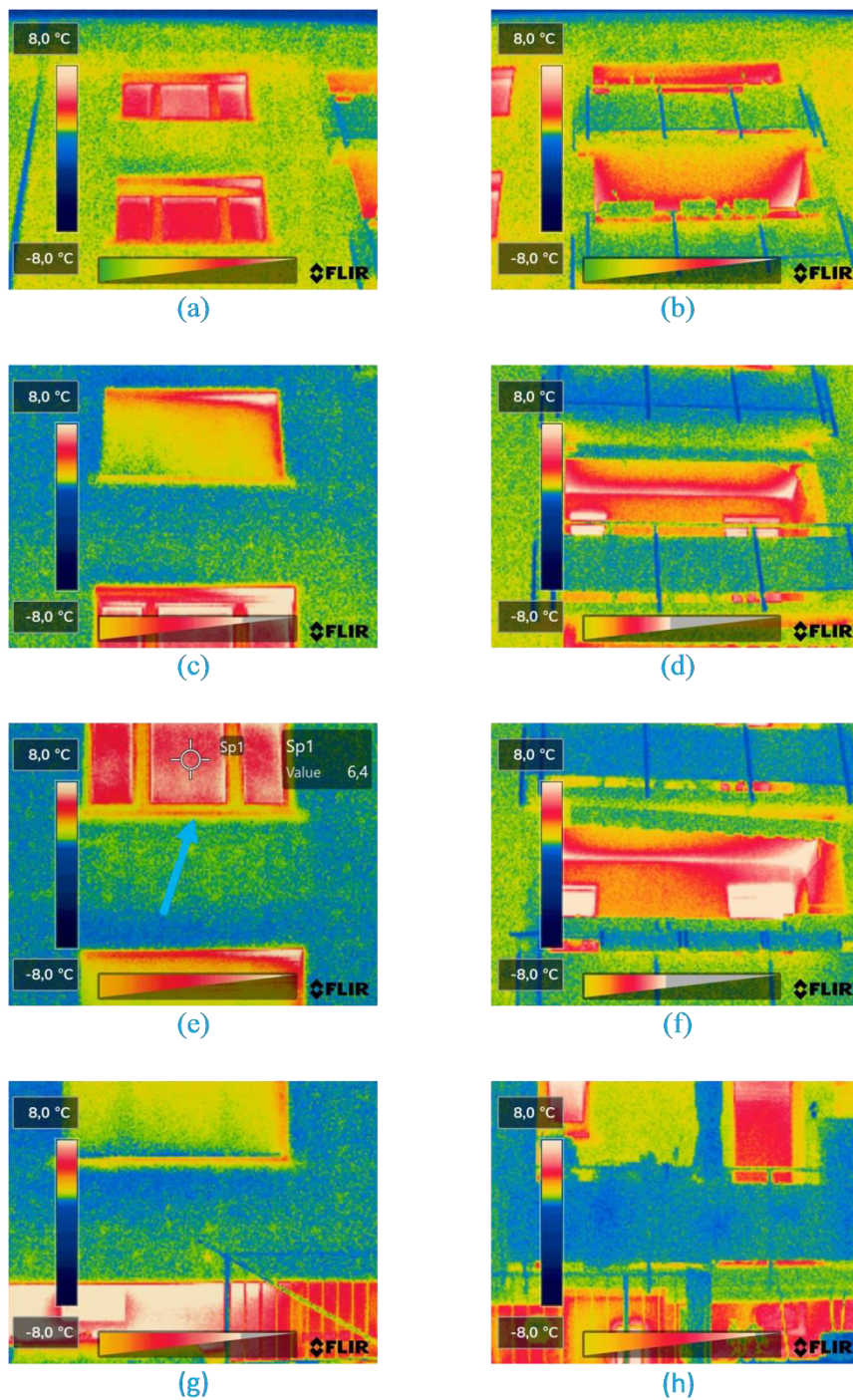


Figure 2. Terrestrial thermographic images recorded via hand-held camera showing the building façade in small segments at a distance of 8m. The blue arrow in the tile (e) shows the same window as the arrows in Figure 1.

2.2. Image Evaluation Criteria

We defined quality criteria to compare aerial and terrestrial thermographic images depending on motion, distance between camera and building, and the UAVs recording perspective:

- *Motion blur*: Motion blur occurs in image recording when the camera is moved during the capturing process. It leads to stripe-like, blurred areas in the images, which complicate the detection of thermal anomalies [23].
- *Contrast*: Contrast indicates differences in brightness and color within an image. The smaller an object appears on an image, the less contrast the image has, and the more difficult the detection of the object – as well as, in this instance, thermal anomalies upon it – becomes [24].
- *Visibility of image details*: The visibility of details can be influenced by the distance between the camera and a building as well as motion effects.³
- *Perspective*: The image perspective indicates which building parts can be recorded by a camera. It depends on the objects in the camera's field of view (e.g. trees), recording distance, and recording angle. The angle influences the visibility of certain thermal anomalies (e.g. those below eaves) and the reflection of infrared radiation (e.g. from windows).

Besides factors indicating the quality of the images, we defined a quantitative comparative criterium to identify thermal differences between terrestrial and aerial acquisition methods:

- *Comparative temperature difference*: The comparative temperature difference between the drone thermogram and terrestrial thermogram is defined as $\Delta T_{ij,kl} = T_{i,k} - T_{j,l}$, where $T_{i,k}$ is the temperature of the central point of a thermal anomaly on a thermographic image. Said image is recorded at a distance i of 8m (terrestrial), 12m, or 42m to the building, and viewing angle k defined as either t (terrestrial), o (oblique/45°), or n (nadir/90°). The temperature of the same point on another thermal image $T_{j,l}$ is defined by the distance j of 8m (terrestrial), 12m, or 42m to the building, and the viewing angle l – again either t (terrestrial), o (oblique/45°), or n (nadir/90°). Every such temperature value is determined using FLIR Thermal Studio's [22] Spot-function and denoted „Sp“ within the image. Since atmospheric air particles absorb infrared radiation, the temperature difference arises as a result of varying distances between building and camera. Greater distances can therefore distort image measurements. According to Fouad and Richter [21], the temperature deviation attributed to these factors is only negligible at distances of up to 20m. Another cause for thermal differences is the viewing angle; a steeper angle induces a change in emissivity. For angles greater than 60°, the emissivity becomes noticeably smaller and the temperature difference larger [21]. Quantifying the comparative temperature difference is important to deduce information on the usability of thermographic drone images for applications like the calculation of U-values (Section 1).

2.3. Image evaluation procedure

To evaluate the quality of the thermographic drone images, we manually checked all quality criteria according to Section 2.2. on the images of our dataset. For this, three exemplary building parts were selected, which are typically analyzed in thermographic building applications. We picked a window (indicated by the arrows in Figure 1 and Figure 2), a thermal anomaly located on the middle of the roof of Sophienstrasse 201-203, and a thermal bridge on the roof at the point where the building Sophienstrasse 201-203 connects to its neighbor. All three points are shown on exemplary thermal images in Figure 3. In total, we analyzed 21 aerial images and 24 terrestrial images in detail.

³ Besides physical influences, the visibility of details also depends on the resolution of an image. The UAV-based thermographic camera model is state-of-the-art and has an even better resolution than the hand-held one. The drone camera thus does not lead to a worse visibility of details than the hand-held camera (details on the camera models are given in Section 2.1.).

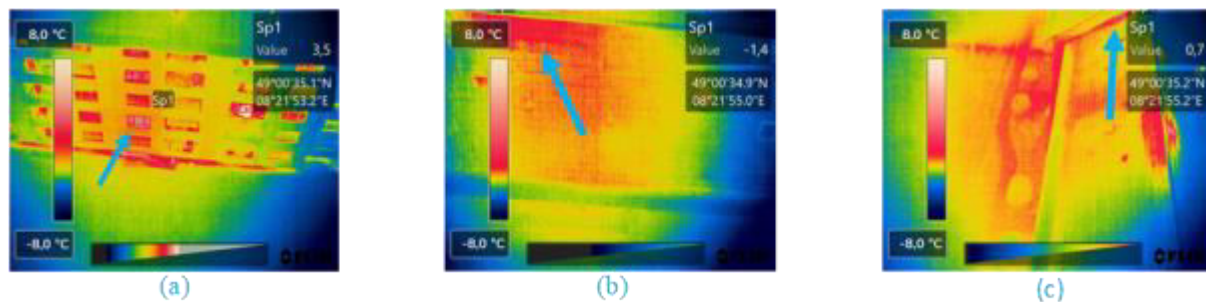


Figure 3. Three analyzed locations in Sophienstrasse 201-203 marked with blue arrows; (a) a window on the backside of the building; (b) a thermal anomaly on the roof near the ridge; (c) a thermal bridge below the eaves.

3. Results

For the analyzed dataset described in Section 2.1, we found the following results when considering the quality criteria defined in Section 2.2:

- *Motion blur*: In our dataset, none of the thermographic images show signs of blurriness in spite of the different flight speeds. We can therefore conclude that a flight speed between 1 and 3m/s allows for UAV-based thermal images without motion blur. For a greater efficiency during data collection, we recommend a speed of 3m/s instead of slower flight speeds.
- *Contrast*: The thermal color contrast in the images collected during flights 1 and 2 is weak and boundaries of the thermal anomalies can not be identified clearly. A reason for this could be the nadir viewing angle in combination with the large distance of at least 42m between camera and thermal anomaly. This value clearly exceeds the previously mentioned 20m limit above which a change in emissivity occurs. While inadequate contrast is given in all images recorded using those settings, the other flights display sufficient contrast.
- *Visibility of image details*: With increasing distance it becomes impossible to recognize certain details that are relevant for the interpretation of thermographic images. While thermal details like air leakages through window panes are clearly visible on terrestrial images, these details are not discernible at an altitude of more than 30m above ground. On images recorded with a flight height of 60m, it is not even possible to spot details like closed roller shutters (Figure 1 (d) and (f)). Other thermal anomalies solely visible on our terrestrial images include thermal bridges on the composite zone between window frames and panes as well as those on window sills. Thermal bridges on window frames themselves, however, can also be found in UAV-based images recorded at 30m (although they are indiscernible in those acquired at 60m).
- *Perspective*: All aerial thermographic images properly record building rooftops regardless of viewing angle. Flight 5 (minimal flight height, 45° angle) provides the best thermographic image of the rooftop, giving an optimal view of the full thermal bridge below the eaves. While the terrestrial perspective does not cover rooftops at all, it excels when used in window and building façade inspections. Window examinations can also be performed on images acquired at a 45° viewing angle, while the nadir perspective is not suitable for any façade analysis. As the results of both aerial flight modes do not differ in quality where roof inspections are concerned, the 45° viewing angle clearly is the more versatile option. It must be noted, however, that some examinations – for instance of balcony slabs and the underside of eaves – can only be performed on images recorded by hand-held camera.
- *Comparative temperature difference*: Regarding the analyzed window, a temperature difference $\Delta T_{60,8,o,t}$ of up to -5°C between the aerial (flight 6, $T_{60,o} = +1.4^{\circ}\text{C}$) and terrestrial ($T_{8,t} = +6.4^{\circ}\text{C}$) thermal images can be measured. A second comparison for the same window between an aerial image recorded at 30m altitude (flight 5, $T_{30,o} = +3.5^{\circ}\text{C}$) and the terrestrial one ($T_{8,t} = +6.4^{\circ}\text{C}$)

shows a temperature difference $\Delta T_{30,8,o,t}$ of up to -2.9°C . Where the rooftop anomaly near the ridge is concerned, a temperature difference $\Delta T_{60,30,n,o}$ of up to -1.7°C is measured between aerial images from flights 2 ($T_{60,n} = -1.1^{\circ}\text{C}$) and 7 ($T_{30,o} = +0.6^{\circ}\text{C}$). The thermal bridge on the roof displays a temperature difference $\Delta T_{60,30,o,o}$ of up to -3.4°C between aerial images from flights 6 ($T_{60,o} = -1.8^{\circ}\text{C}$) and 5 ($T_{30,o} = +1.6^{\circ}\text{C}$). All these examples show that larger distances lead to higher comparative temperature differences. This means that images recorded at 30m above ground (12m above the building) are preferable to those acquired at higher flight heights for rooftop and façade analyses via aerial thermography. For quantitative UAS-based thermographic applications, we see that a distance of 60m above ground (42 m above the building) leads to significant temperature falsification.

4. Discussion

Our study shows the influence of motion, distance, and recording angle of automated UAV-based thermal image acquisition on the quality of thermographic images. While the flight speed did not seem to have an influence on the image quality in our study, the distance and recording angle between the camera and building of interest can have a distinctly negative effect.

Our observations show thermal image quality to remain unchanged at low flight speeds of between 1 and 3m/s. We therefore suggest examining greater flight speeds to further increase the efficiency of the automated image acquisition process. While this contradicts Entrop and Vasenev's [14] experience of a 1.5m/s speed limit, recent advances in UAV technology may explain the new findings.

Varying distances and angles between thermal camera and investigated building surface can lead to a falsification of recorded temperature data, a lower contrast, and a decrease in visibility of image details, caused by a weakening of the returning infrared radiation or emissivity level. In our case study, we can clearly confirm the negative effect of increasing distances on these factors as described by Fouad and Richter [21]. Considering the pros and cons of different distances (30m and 60m above the ground) and flight angles (nadir and 45° angle), we can come to the following conclusion: The nadir perspective is suitable for analyzing rooftops, but provides no quality advantage compared to a flight angle of 45° , which additionally allows some façade analysis. Automated drone thermography is very suitable for the analysis of rooftops when choosing a medium flight distance such as 30m above ground (12m distance to the building). This setting (45° , 30m above ground) allows thermal patterns such as large thermal anomalies to be recognized. However, a quantitative temperature study and a detailed façade analysis is not possible owing to the comparatively large distance and steep angle of camera to building front. Images recorded at a 60m flight height (42m distance to the building) cannot be recommended for quantitative studies, although large thermal bridges and leakages are still discernible. This setting can still be advantageous if time constraints permit only a rough analysis of a district or building stock to identify larger areas of heat loss. Further statements on the thermal quality of specific buildings and areas then require more detailed analyses.

Despite the discussed revelations, our study suffers from some limitations. We only analyzed drone images of two buildings with merely seven different flight settings, all of which were recorded on the same day under similar weather conditions. On top of this, the quantitative analysis of the comparative temperature difference is only limited to three different points. Further comprehensive qualitative analyses are planned in follow-up work with more thermal images of buildings and additional evaluation criteria. We also intend to study different flight distances, higher flight speeds, and areas of different building types. Moreover, we want to structurally analyze the effort involved in UAV-based approaches compared to ground surveys by taking time and cost efficiency into account. Concerning our drone image data, it should be noted that all images include vignetting. The vignetting effect is a shadowing toward the edge of an image which falsely signals a higher intensity in the image's central region [25]. This is caused primarily by the camera itself. A technical optimization is planned to exclude this effect in future UAV-based images, for example by using a back-up aperture and thin rings as well as adapters to accommodate larger filters.

5. Conclusions

In this study, we compared the quality of automatically acquired UAV-based thermal images to classical terrestrial thermography via hand-held camera for building audits. For this, we collected a drone image dataset recorded using seven different flight settings of varying recording angle, flight speed, and distance above ground, as well as stationary terrestrial images with constant recording distance and angle. We investigated five quality criteria for thermographic images that we applied to three typical examples displaying thermal anomalies common to buildings.

We found that the studied flight speeds do not have a negative impact on the quality of thermography. On the other hand, large distances and steep angles to the building façade reduce the quality of thermographic images considerably. Automatic UAV-based thermography at a medium distance to buildings is especially suitable for the quantitative and qualitative analysis of rooftops. In this context, we see no advantage of the nadir perspective compared to a 45° angle. Analyses of images recorded at a very large distance are only suitable for efficient data collection and the qualitative recognition of patterns like large thermal bridges and air leakages. They do not allow for more detailed analyses nor give reliable quantitative information. Our results can be used for the structured planning of thermographic drone flights of large building stocks and will be improved upon by the authors in following studies.

Acknowledgements

The authors appreciate the support of Marinus Vogl (Air Bavarian GmbH) in acquiring the thermal images via UAV. Moreover, they thank Harald Schneider (Karlsruhe Institute of Technology) for his advice and assistance. Lastly, we gratefully acknowledge the consent and support of Karlsruher Volkswohnung GmbH within this research project.

References

- [1] United Nations 2017 New urban agenda *United Nations Conf. on Housing and Sustainable Urban Development* (Quito, Ecuador). ISBN: 978-92-1-132731-1
- [2] Riechel R 2016 Zwischen Gebäude und Gesamtstadt: das Quartier als Handlungsraum in der Lokalen Wärmewende *Vierteljahrshefte zur Wirtschaftsforschung* **85** (4) pp 89-101 (Berlin, Germany). DOI: 10.3790/vjh.85.4.89
- [3] US Department of Energy 2013 Guide to community energy strategic planning (Washington, USA). URL: https://www.energy.gov/sites/prod/files/2014/05/f15/cesp_guide.pdf (accessed 25 December 2021)
- [4] Littlejohn D and Laszlo R 2015 National report on community energy plan implementation *Quality Urban Energy Systems of Tomorrow* (Ottawa, Canada). URL: https://questcanada.org/wp-content/uploads/2018/08/National-Report-on-Community-Energy-Plan-Implementation_Full_Report_2015.pdf (accessed 10 January 2022)
- [5] JPI Urban Europe / SET Plan Action 3.2 2020 *White paper on PED reference framework for positive energy districts and neighbourhoods* (Vienna, Austria). URL: <https://jpi-urbaneurope.eu/ped/> (accessed 1 January 2022)
- [6] Kreditanstalt für Wiederaufbau 2015 Merkblatt Energetische Stadtsanierung - Zuschuss Klimaschutz und Klimaanpassung im Quartier URL: [https://www.kfw.de/PDF/Download-Center/F%C3%B6rderprogramme-\(Inlandsf%C3%B6rderung\)/PDF-Dokumente/6000002110_M_432_Energetische_Stadtsanierung_Zuschuss.pdf](https://www.kfw.de/PDF/Download-Center/F%C3%B6rderprogramme-(Inlandsf%C3%B6rderung)/PDF-Dokumente/6000002110_M_432_Energetische_Stadtsanierung_Zuschuss.pdf) (accessed 25 December 2021)
- [7] Vollmer M and Möllmann K P 2010 *Infrared Thermal Imaging* (Weinheim, Germany: Wiley-VCH). ISBN: 978-3-527-41351-5
- [8] Lucchi E 2018 Applications of the infrared thermography in the energy audit of buildings: a review *Renewable and Sustainable Energy Reviews* **82** pp 3077–90. DOI: 10.1016/j.rser.2017.10.031
- [9] Bitelli G, Conte P, Csoknyai T, Franci F, Girelli V and Mandanici E 2015 Aerial thermography

- for energetic modelling of cities *Remote Sens.* **7** (2) pp 2152–70. DOI: 10.3390/rs70202152
- [10] Previtali M, Barazzetti L, Brumana R and Roncoroni F 2013 Thermographic analysis from UAV platforms for energy efficiency retrofit applications *J. Mobile Multimedia* **9** (1) pp 66–82
- [11] Mayer Z, Kahn J, Hou Y and Volk R 2021 AI-based thermal bridge detection of building rooftops on district scale using aerial images *EG-ICE 2021 Workshop on Intelligent Computing in Engineering* vol 28, ed J Abualdenien et al (Berlin, Germany: Universitätsverlag der TU Berlin) pp 497–507. ISBN: 978-3-7983-3212-6
- [12] Krawczyk J, Mazur A, Sasin T and Stoklosa A W 2015 Infrared building inspection with unmanned aerial vehicles *Transactions of the Institute of Aviation* **240** (3) pp 32–48. DOI: 10.5604/05096669.1194965
- [13] Hou Y, Volk R, Chen M and Soibelman L 2021 Fusing tie points' RGB and thermal information for mapping large areas based on aerial images: a study of fusion performance under different flight configurations and experimental conditions *Automation in Construction* **124** (4) 103554. DOI: 10.1016/j.autcon.2021.103554
- [14] Entrop A G and Vasenev A 2017 Infrared drones in the construction industry: designing a protocol for building thermography procedures *Energy Procedia* **132** (4) pp 63–8. DOI: 10.1016/j.egypro.2017.09.636
- [15] Rakha T and Gorodetsky A 2018 Review of unmanned aerial system (UAS) applications in the built environment: towards automated building inspection procedures using drones *Automation in Construction* **93** (18) pp 252–64. DOI: 10.1016/j.autcon.2018.05.002.
- [16] Daffara C, Muradore R, Piccinelli N, Gaburro N, de Rubeis T and Ambrosini D 2020 A cost-effective system for aerial 3D thermography of buildings *J. Imaging* **6** (8) p 76. DOI: 10.3390/jimaging6080076
- [17] FLIR 2021 FLIR XT2 product information (Wilsonville, USA). URL: <https://www.flir.de/products/xt2/> (accessed 10 January 2022)
- [18] FLIR 2021 FLIR T-series (Wilsonville, USA). URL: <https://www.flir.com/instruments/t-series/> (accessed 10 January 2022)
- [19] Windfinder 2022 wind And weather report Karlsruhe/Lameyplatz (Hamburg, Germany). URL: https://de.windfinder.com/report/karlsruhe_lameyplatz/2022-01-16 (accessed 17 January 2022)
- [20] Timeanddate 2022 Wetterrückblick Karlsruhe, Baden-Württemberg, Deutschland – Wetter Gestern und Letzte Woche (Stavanger, Norway). URL: <https://www.timeanddate.de/wetter/deutschland/karlsruhe/rueckblick> (accessed 17 January 2022)
- [21] Fouad N A and Richter T 2012 *Leitfaden Thermografie im Bauwesen: Theorie, Anwendungsgebiete, Praktische Umsetzung* (Stuttgart, Germany: Fraunhofer IRB Verlag). ISBN: 381678456
- [22] FLIR 2021 FLIR Thermal Studio Suite. URL: <https://www.flir.de/products/flir-thermal-studio-suite/> (accessed 25 April 2022)
- [23] Sieberth T, Wackrow R and Chandler J H 2014 Motion Blur Disturbs - The Influence of Motion-blurred Images in Photogrammetry *Photogram. Rec.* **29** (148) pp 434–53. DOI: 10.1111/phor.12082
- [24] Böhringer J, Bühler P and Schlaich P 2008 *Kompendium der Mediengestaltung* (Heidelberg, Germany: Springer Berlin Heidelberg). DOI: 10.1007/978-3-642-54581-8
- [25] Mahmoodzadeh M, Gretka V, Hay K, Steele C and Mukhopadhyaya P 2021 Determining overall heat transfer coefficient (U-value) of wood-framed wall assemblies in Canada using external infrared thermography *Building and Environment* **199** (6) 107897. DOI: 10.1016/j.buildenv.2021.107897

Paper C: Investigating the Quality of Thermographic Drone Images for the Analysis of Buildings

This paper was reproduced in its original format with permission from MDPI:

Mayer, Z., Epperlein, A., Vollmer, E., Volk, R., Schultmann, F. (2023 - Paper C). Investigating the quality of thermographic drone images for the analysis of buildings. *Remote Sensing*, 15, 301. Doi: <https://doi.org/10.3390/rs15020301>



Article

Investigating the Quality of UAV-Based Images for the Thermographic Analysis of Buildings

Zoe Mayer *, Andres Epperlein, Elena Vollmer, Rebekka Volk and Frank Schultmann

Institute for Industrial Production, Karlsruhe Institute of Technology, 76187 Karlsruhe, Germany

* Correspondence: zoe.mayer@partner.kit.edu

Abstract: Thermography for building audits is commonly carried out by means of terrestrial recording processes with static cameras. The implementation of drones to automatically acquire images from various perspectives can speed up and facilitate the procedure but requires higher recording distances, utilizes changing recording angles and has to contend with the effects of movement during image capture. This study investigates the influence of different drone settings on the quality of thermographic images for building audits in comparison to ground-based acquisition. To this end, several buildings are photographically captured via unmanned aerial vehicle and classical terrestrial means to generate a dataset of 968 images in total. These are analyzed and compared according to five quality criteria that are explicitly chosen for this study to establish best-practice rules for thermal image acquisition. We discover that flight speeds of up to 5 m/s have no visible effects on the image quality. The combination of smaller distances (22 m above a building) and a 45° camera angle are found to allow for both the qualitative and quantitative analysis of rooftops as well as a qualitative screening of building façades. Greater distances of 42 m between camera and building may expedite the acquisition procedure for larger-scaled district coverage but cannot be relied upon for thermal analyses beyond qualitative studies.

Keywords: thermography; thermal imaging; building audits; remote sensing; UAV; energy analysis



Citation: Mayer, Z.; Epperlein, A.; Vollmer, E.; Volk, R.; Schultmann, F. Investigating the Quality of UAV-Based Images for the Thermographic Analysis of Buildings. *Remote Sens.* **2023**, *15*, 301. <https://doi.org/10.3390/rs15020301>

Academic Editor: Ji Zhou

Received: 2 November 2022

Revised: 29 December 2022

Accepted: 31 December 2022

Published: 4 January 2023



Copyright: © 2023 by the authors. Licensee MDPI, Basel, Switzerland. This article is an open access article distributed under the terms and conditions of the Creative Commons Attribution (CC BY) license (<https://creativecommons.org/licenses/by/4.0/>).

1. Introduction

Infrared thermography has gained prominence in the field of remote sensing due to the technology's reliability and versatility as well as non-contact and non-destructive qualities. It is implemented throughout a wide range of applications, including e.g., agricultural data collection, gas detection, industry monitoring, as well as identifying humans and animals [1–3].

Thermography has also proven to be very useful for the detection of thermal irregularities, air leakages and moisture abnormalities on building envelopes [4]. To this day, static setups or hand-held cameras are most common in the analysis of buildings [5]. However, performing thermography with a terrestrial camera reaches its limits in larger-scale projects due to its time-consuming nature [6] and inability to cover certain areas of the building envelope, such as the high façade elements of tall buildings [7]. It has therefore become increasingly popular for thermographic building audits on city- or district-scale to be performed by means of aircrafts, such as Unmanned Aerial Vehicles (UAVs) [5].

Aside from bypassing the aforementioned limitations of ground-based procedures, aerial methods additionally have the potential to streamline building auditing in the future scenarios, such as smart cities. Embedded into the broader context of urban data collection and processing approaches, they can improve the general sustainability of urban areas by providing vital information to governments and stakeholders, thus expediting lengthy decision-making processes [8]. UAVs can be used as relay stations for multiple Internet of Things devices, not just thermographic cameras. By including various kinds of sensors,

a broad range of environmental data can be collected, analyzed and communicated to a central station for reasons such as determining levels of pollution [9,10].

For these reasons, many recent scientific publications focus on establishing best practice rules for the recording and processing of UAV-based thermographic images. While numerous studies are devoted to identifying the various drone settings suitable for auditing buildings, they oftentimes fail to provide comprehensive information on the quality of the acquired images and assessment thereof. Krawczyk et al. [11], for instance, used UAV-based thermography to inspect a single-family house and named the aerial acquisition method the “optimum solution for inspections of buildings” because it permitted fast image recording and access to rooftops. However, the authors did not detail their chosen flight speeds nor any other drone settings, all of which greatly influenced the results. Entrop and Vasenev [12] studied various flight settings with the aim of reducing cost and time involved in drone-based thermography. They chose distances of between 5 m and 10 m to the object under scrutiny and a flight speed of 1.5 m/s, which they were later forced to lower to 1.0 m/s due to insufficient image quality. While they provided recommendations for UAV settings, they failed to specify the criteria used to assess the quality of their thermal images. The influence of certain flight settings on specific aspects of quality therefore remains unknown, making the discoveries difficult to transfer to other scenarios. Rakha and Gorodetsky [13] investigated suitable drone settings to create thermographic 3D models of buildings. They examined various parameters, such as flight path, overlap and distance between infrared camera and the building in question. While various flight heights of 18 m, 22 m, 27 m and twice the building height were all found to be suitable, the optimal set-up uses a 12 m distance to the building and a strip pattern flight path. Although the paper identifies new best practice rules for the creation of 3D models, it also fails to examine their concrete influence on the quality of the recorded thermographic data. Another paper to study the generation of 3D building models using UAV-based thermal images was conducted by Daffara et al. [14]. They performed drone flights at a distance of 10 m to the building façade and a maximum flight height of 8 m. No information was provided on the influence of their flight settings on image quality. The same can be said of Dahaghin et al. [15], who assessed the suitability of UAV-based thermal images in generating 3D models of building rooftops. Their images cover two different areas at comparatively large flight heights of 48.6 m and 160 m. Hou et al. [16] also developed a method to fuse point cloud data to create 3D thermal building models. The UAV flights for image acquisition were performed at different flight heights (60 m and 35 m above ground), angles (45° and 30°) and flight paths (mesh grid and Y path). The authors found that greater distances between camera and building induced more errors, while a 45° angle could capture more façade detail than the 30° alternative. Benz et al. [17] present a concept for the UAV-based assessments of buildings by estimating façade U-values from a generated 3D building model. Without providing an explanation for their choice of settings, they performed all flights at a 15 m distance to the building under scrutiny. They found that the quality of UAV-based thermography needs to be improved to allow for precise U-value calculations. Mayer et al. [18] developed a procedure for identifying, classifying and evaluating thermal bridges of buildings by means of drone-mounted thermographic camera. The images were acquired at heights of between 60 m and 80 m above ground. Using these settings, the authors were able to manually identify 14 different types of thermal bridges in the dataset. They found that thermal imaging performed in near parallel to a building façade (acute angle) often caused the thermal anomalies to be misinterpreted. For this reason, they excluded images that were recorded at a small angle (<70°) to the object under scrutiny. Another author to discuss thermal building anomalies is Zahradník [19], who showcased a UAV-based method for rooftop leakage detection. The data were acquired in nadir flight (camera pointing straight down) at a speed of 2 m/s and a constant distance of 20 m to the ground. Again, the reasoning for these specific settings was not provided in the paper. Mirzabeigi and Razkenari [20] explored a method for detecting thermal bridges on building envelopes which takes both UAV-based and terrestrial images into account.

For aerial acquisition, they chose a rectangular trajectory (strip pattern flight path) at a 6.5 m distance to the building. They failed to indicate on what grounds they assessed the quality of the thermal images acquired using the aforementioned methods. Gómez and Tascón [21] detailed best practice rules for using UAVs to detect thermal anomalies on agricultural building envelopes. The developed protocol is tested and validated on thermal video recordings of a new case study. The façade was inspected at a distance of 10 m and a flight height of 5 m above ground, the rooftop through images acquired at 20 m above the maximum building height and strip pattern flights. The authors defined these flight settings as suitable for their specific research aim without detailing the effects they had on image quality. Owing to the numerous and diverging recommendations for UAV set-ups provided in all manner of published thermographic case studies, Gómez and Tascón [21] concluded no generally applicable standard for best practices existed with regards to distance between UAV and object under scrutiny. Instead, they stated that flight settings must be chosen according to the specific objectives at hand.

Table 1 gives an overview of the aforementioned most recent studies concerned with building envelope analysis using UAV-based thermographic images. It also shows what, if any, information is provided on the chosen settings of the experimental flights conducted for said publications.

Table 1. Overview of recent studies in the field of UAV-based thermal building inspections [11–21].

Publication	Year	UAV Flight Settings
Krawczyk et al. [11]	2015	No information provided
Entrop and Vasenev [12]	2017	5–10 m vertical distance to building roof, 1 m/s flight speed
Rakha and Gorodetsky [13]	2018	12 m horizontal distance to building façade, 45° and 10° camera angle
Daffara et al. [14]	2020	10 m horizontal distance to building façade, 0° camera angle
Dahaghin et al. [15]	2021	48–218 m vertical distance to ground
Hou et al. [16]	2022	60 m and 35 m vertical distance to ground, 45° and 30° camera angles
Benz et al. [17]	2021	15 m distance to the building
Mayer et al. [18]	2021	60–80 m vertical distance to ground
Zahradník [19]	2022	20 m vertical distance to ground, 90° camera angle, 2 m/s flight speed
Mirzabeigi and Razkenari [20]	2022	6.5 m distance to building, ground-based terrestrial camera for comparison
Gómez and Tascón [21]	2021	10 m horizontal distance to building façade, 20 m vertical distance to building rooftop peak

A review of the cited papers revealed a considerable literary gap in the comprehensive assessment of the quality of thermal images and how they were influenced by various recording parameters. None of the named studies provide detailed descriptions of their thermographic images or criteria for evaluating their quality.

As high quality is of the utmost importance for the correct interpretation and quantitative assessment of the information provided in thermal images, this work aims to identify the benefits and drawbacks of different drone flight settings to formulate best practice rules for thermography in building auditing. Using a case study, we examine the impact of different modes of acquisition at varying camera speeds, recording angles and distances to the buildings under scrutiny to determine how these parameters influence the resulting images. To do so, we define and evaluate three qualitative and two quantitative criteria to indicate how recorded thermal information changes with different acquisition settings. This study builds on Mayer et al.'s [22] prospective conference contribution, which introduced four qualitative and one quantitative criteria for evaluating a small, exemplary dataset of automatically recorded UAV-based thermographic images as well as comparative images acquired by hand-held thermal camera. In total, Mayer et al. [22] analyzed 21 aerial and 24 terrestrial images in detail. The authors found image quality to be independent of flight

speeds of up to 3 m/s. Moreover, the study provides evidence that temperature values recorded in UAV-based thermographic images can significantly deviate from the values acquired by hand-held camera. Owing to the small case study size they did not, however, provide a comprehensive quantitative analysis to evaluate these findings in more detail.

Identifying the optimal settings for high quality thermography-based building audits requires a more in-depth, large-scaled analysis. This study therefore extends Mayer et al. [22] on four counts: (1) the new dataset is much broader, consisting of a significantly larger number of images collected in ideal weather conditions (complete absence of drizzle and rain); (2) an additional method of image acquisition—namely manual UAV flight—is included in the comparison; (3) the assessment is enhanced by a more quantitative-based set of criteria; and (4) mode-dependent recording times are examined to assess and compare the general efficiency of UAV-based and manual acquisition methods. In doing so, this paper aims to contribute an improved set of tools for assessing the quality of UAV-based thermographic building audits. It shows the comparative results of these applied to an extensive new case study, including images captured by three different means of acquisition. The results are discussed and compared to literature.

2. Materials and Methods

2.1. Research Approach

This study is split into three procedural parts, which are described in detail in the subsequent Sections 2.2–2.4. In a first step, data are acquired. The thermal images were collected by hand-held and UAV-based cameras using varying recording settings to cover four residential buildings. Next, quality criteria are defined to assess the usability of the recorded images for both a quantitative and qualitative analysis of the building envelopes. In a third step, the collected images are analyzed and compared according to the defined criteria. This allows for conclusions to be drawn about the benefits and drawbacks of the various tested settings for the thermal assessment of building envelopes. This research approach is illustrated in a flow chart in Figure 1.

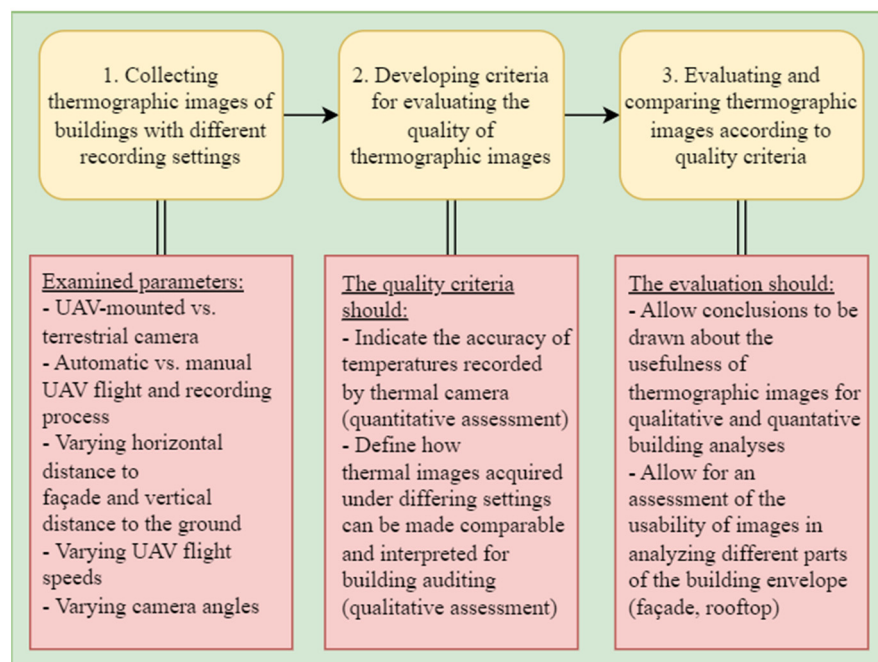


Figure 1. Flow chart of the research approach in this study.

2.2. Data Collection

The analyzed dataset consists of 968 thermal images: 693 captured on the ground and 275 via UAV. Of the aerial images, 139 were recorded manually and 136 in automatic

flight mode. As indicated in Figure 2, the case study covers four multi-family buildings in the German city of Karlsruhe, which belong to the local municipal housing association Volkswohnung Karlsruhe GmbH. The buildings are located in Sophienstr. 201–203, Volzstr. 2, Wichernstr. 4 and Wichernstr. 10–18. They were all constructed in the 1950s, stand 18 m tall and comprise between 12 and 47 apartments, all of which were fully rented out at the time of image acquisition.



Figure 2. Audited buildings in Sophienstr. 201–203, Volzstr. 2, Wichernstr. 4 and Wichernstr. 10–18, located in Karlsruhe, Germany [23].

The aerial images were acquired using a “DJI Matrice 300” UAV [24] equipped with the “Zenmuse XT2”, a combination of FLIR’s “Duo Pro R” thermal and RGB camera technology and DJI’s gimbal [25]. All thermal images were recorded in FLIR’s proprietary image format RJPEG. The terrestrial thermographic images were acquired using a “FLIR T200” hand-held camera [26] in the standard JPEG format. The emissivity was set to 0.95 throughout to remain within the recommended range of 0.90 to 0.98 [27].

Image acquisition took place on 28 February and 1 March 2022 between 8 p.m. and 1 a.m. On 28 February, the outside air temperature registered at between 1 °C and 3 °C. Wind speeds reached a maximum of 17 km/h. The sky was cloudless both during the flights and in the preceding 24 h. A maximum temperature of 11 °C was recorded by local weather stations in that time period. Very similar weather conditions were present on 1 March. The outside air temperature was recorded as being between −1 °C and 5 °C during acquisition, with wind speeds of max. 11 km/h. Again, the sky was entirely clear both during the flights and in the preceding 24 h, with a maximum temperature of 9 °C present in that time period. The sun set at around 6:10 p.m. on both days [28].

The meteorological conditions present during these UAV flights therefore align with Lucchi’s [29] and Fouad and Richter’s [27] recommendations: The temperature difference between indoor and outdoor areas was sufficiently high (Assuming a standard indoor room temperature of 19 °C [30], the requirement of a delta of more than 10 K was met.), and the recommended maximum outside temperature of 5 °C was not exceeded. Terrestrial and aerial images of the same building were recorded consecutively and on the same day to ensure near identical weather conditions, thus establishing a basis for comparisons between images and acquisition methods.

For a succinct comparison of UAV-based recording methods, nine different flight settings of varying speed (1 m/s, 3 m/s and 5 m/s), flight height (4 m to 60 m above ground), and camera angle (45°, 90°/nadir and 0°/facing the façade) were selected. Six

of these nine flights (flights 1 to 6) were carried out automatically; the rest (flights 7 to 9) were executed manually by a professional UAV pilot. All flight settings are summarized in Table 2.

Table 2. Flight settings for the case study (the presence of obstacles allowed only the buildings on Wichernstr. to be recorded via manual flights 7–9).

Flight	Building	Automatically/Manually Performed Flight Route	Camera Angle [°]	Height above Ground [m]	Height above Building [m]	Distance to Façade [m]	Flight Speed [m/s]
1	Full area	Automatically	45 (oblique)	40	22	-	1
2	Full area	Automatically	45 (oblique)	40	22	-	3
3	Full area	Automatically	45 (oblique)	40	22	-	5
4	Full area	Automatically	45 (oblique)	60	42	-	3
5	Full area	Automatically	90 (nadir)	40	22	-	3
6	Full area	Automatically	90 (nadir)	60	42	-	3
7	Wichernstr. 4	Manually	0 (manual)	4 to 12	-	4	-
8	Wichernstr. 4	Manually	0 (manual)	4 to 12	-	8	-
9	Wichernstr. 4, 10–18	Manually	0 (manual)	4 to 12	-	15	-

During automatic flights, a 45° camera angle was used to capture the façade (flights 1 to 4) and 90° (flights 5 and 6) to record rooftops. The flight heights were set to 60 m above the ground (flights 4 and 6)—corresponding to 42 m above the buildings—and 40 m (flights 1, 2, 3 and 5)—corresponding to 22 m above the buildings. Smaller distances proved impossible to realize due to the presence of natural obstacles, such as trees. To examine contrasting literary conclusions about the influence of camera velocity on image quality, the UAV’s flight speed was set to 1 m/s (flight 1) based on the experience of Entrop and Vasenev [12] and 3 m/s (flights 2, 4, 5, 6) as well as 5 m/s (flight 3) based on the findings of Mayer et al. [22]. A strip pattern flight path was used for all automated flights (flights 1 to 6) with a constant side and frontal overlap of 10%. Higher overlap is primarily required for tie point computations in the creation of mosaics or 3D models and is thus outside the scope of this work. The UAV-based thermal image dataset discussed in subsequent chapters consists of a pre-sorted selection of all images that were automatically captured along the flight route. Only those images depicting relevant building parts are included.

Operating the UAV in manual flight mode, as was done during flights 7 to 9, allows for much smaller flight heights and distances to the area of interest. It means entire building façades can be captured in close range without changing perspective. The lack of surrounding obstacles in Wichernstr. 4 and 10–18 allowed those buildings’ façades to be recorded at varying distances of 4 m, 8 m and 15 m. These images were taken in static flight, meaning the UAV was brought to a full-stop mid-air to avoid camera movement during acquisition. Terrestrial images were recorded at the same distances of 4 m, 8 m and 15 m to the buildings. The datasets from close-up acquisition methods are larger simply because each image only covers a small area, and therefore, a greater amount is required to capture a building envelope in its entirety.

FLIR’s “Thermal Studio” software [31] was utilized in the processing and analysis of all thermographic images. The temperature scale was chosen based on Fouad’s [32] recommendation to visualize thermal data using a range of at least 15 K. Set at −8 °C to +13 °C, it encompasses both the building’s warmest and coldest regions as well as the given surrounding temperatures. Color is assigned universally according to the “signal linear” function, which forces the color scale into a linear adaptation of the raw camera signals [33].

Figure 3 shows exemplary images acquired under the previously described settings of varying height, angle and recording method. Images depicting the same object at an

identical angle and distance may still vary owing to the different lenses of hand-held versus UAV-mounted thermal cameras. The full dataset being discussed in this paper is publicly available on Zenodo [34].

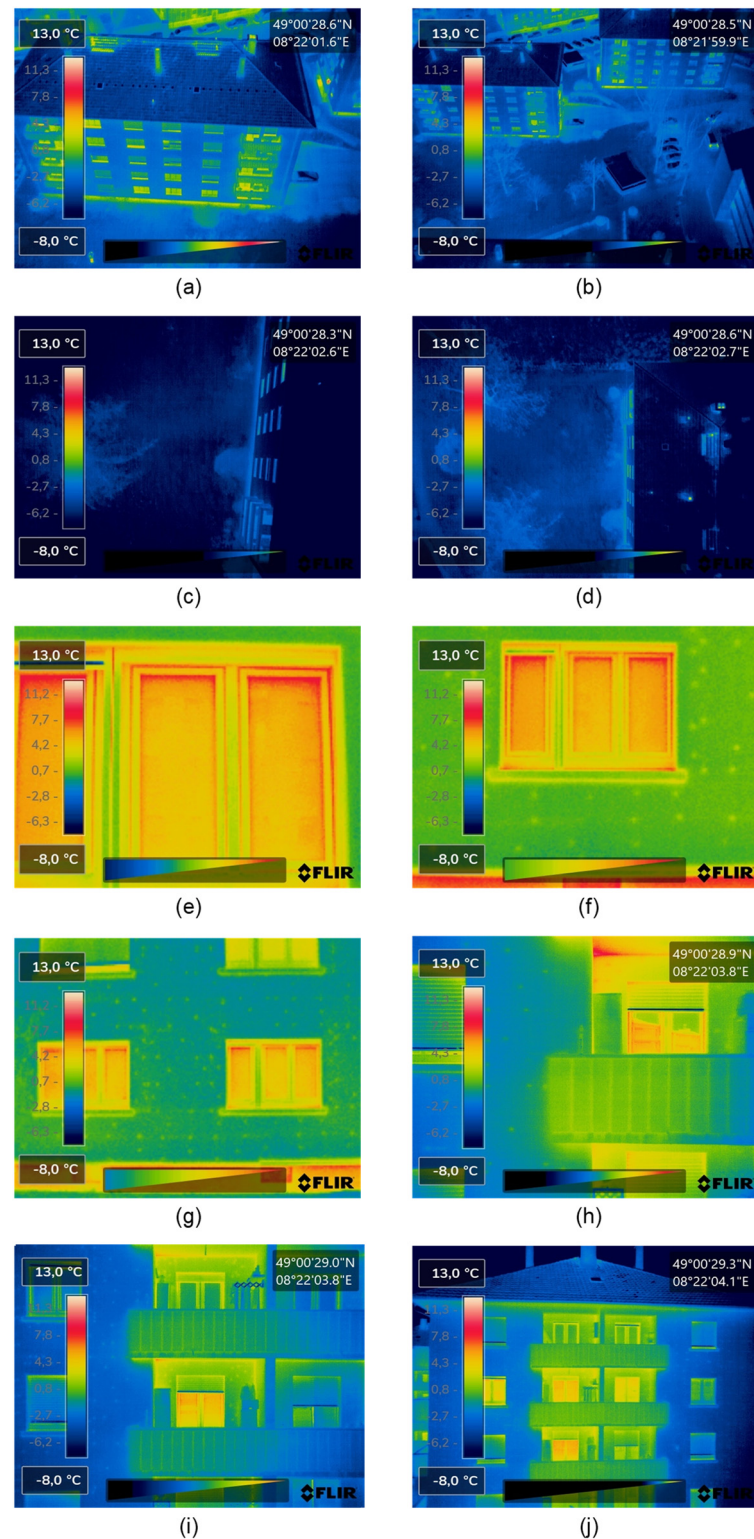


Figure 3. Thermographic images: (a–d) automatic UAV-based images; (e–g) terrestrial images; (h–j) manual UAV-based images; (a) oblique from 40 m above ground; (b) oblique from 60 m above ground; (c) nadir from 40 m above ground; (d) nadir from 60 m above ground; (e) 4 m distance; (f) 8 m distance; (g) 15 m distance; (h) 4 m distance; (i) 8 m distance; (j) 15 m distance.

2.3. Evaluation Criteria

This study presents select quantitative and qualitative criteria that can be used to compare and evaluate the quality of diversely acquired thermal images. To date, the authors know of no established set of criteria with which to assess the qualitative and quantitative usability of thermal images in building auditing and to make varying methods truly comparable. We therefore define them based on criteria common to photography and thermography, as described below. While the qualitative criteria are meant as tools to provide a general assessment of the achievable level of detail in thermal images, the quantitative criteria give insight specifically into the accuracy of temperature values recorded by the thermal camera in question. In addition to the aforementioned, the time required for image acquisition is taken into account as a separate indicator due to the relevance it has for the economic efficiency of a given method. The criteria can be influenced by constant parameters like those pertaining to the involved technology (This includes the thermal camera as well as implemented UAV technology.) and dynamic ones, such as camera speed, position in relation to the object of interest and atmospheric conditions as described by Fouad and Richter [27] (see Section 2.2).

Three qualitative criteria are defined for comparing the influence of different acquisition methods and settings on the visibility of details (such as thermal bridges) within the resulting thermal images. These are motion blur, feature discernibility and accessibility (of areas under scrutiny). While partially derived from Mayer et al. [22], these refined criteria place additional emphasis on an acquisition method's ability to reach all areas of interest. This is an aspect that must be considered for building auditing because if a method lacks the capability of capturing a building in its entirety, any adeptness it may have of capturing highly detailed images will be offset by the incompleteness of the resulting dataset and potential omission of important anomalies. The qualitative criteria used to evaluate the image dataset are:

- Motion blur: Motion blur occurs when a camera moves during the image recording process, resulting in stripe-like, blurred areas [35]. Camera speed, shutter speed and distance to the captured scene all influence how the effect manifests itself [35]. Camera speed and distance correlate in their influence on motion blur, particularly in UAV-based applications: The same amount of blur can be caused by a slower, close-up movement as well as a faster flight at greater distance [36]. Motion blur affects the detectability of thermally relevant areas and can falsify temperatures shown on thermographic images [35].
- Feature discernibility: The precise identification of thermal anomalies as part of the thermographic building auditing process vastly depends on the level of detail discernible within the recorded images. This aspect can be described on a qualitative level using the term spatial resolution: A common concept in remote sensing, it eludes to "the smallest object [or imaged ground area] that can be resolved by [a] sensor" [37]. Finer or greater spatial resolution means a higher level of detail is displayed in comparison to coarse or low resolution [38]. The size of recordable detail in a given scene depends on the instantaneous field of view (the camera-dependent angle through which radiation can be received) and the variable distance between camera and object of scrutiny [38]. The camera angle plays an influential role as well since the absolute distance to an object increases as soon as the optical axis is not perpendicular to its surface. Although such a change in perspective increases the capturable building surface area, it comes at the cost of lower resolution of the details being portrayed.
- Accessibility (of an area under scrutiny): While the previous factors describe the influences on the visibility of thermal anomalies in building auditing, this third criterion lays emphasis on what areas are even accessible to the various image acquisition methods. This depends on the camera pose and angle in relation to the inspected object as well as surface features and form. If the camera's optical axis is almost parallel to the building surface, the identification of thermal bridges will be nearly impossible.

Similarly, a building part might simply be inaccessible due to positional constraints or surface elements blocking the camera's view. This aspect is particularly relevant when the acquisition's aim lies in assessing the entire envelope of a given structure.

Additionally, two quantitative criteria strive to evaluate the recorded temperature values influenced by the different recording settings and means of acquisition. These are calculated through the thermal comparison of identical regions of interest in images acquired under varying settings. Quantitative analysis, as presented by Mayer et al. [22], is extended to further inspect the thermal difference between anomalies in comparison to the given surroundings and background. The two criteria are:

- Comparative temperature difference: As the name suggests, the comparative temperature difference means to indicate variations in recorded thermal values across different settings and acquisition methods. Quantifying this value allows the thermal images to be evaluated with regards to their usability in calculating U-values or energy losses [22]. The difference is defined as the delta in temperature of a certain area of interest across two comparable thermographic images:

$$\Delta T_{i,j,k,l}^A = T_{i,k}^A - T_{j,l}^A, \quad (1)$$

where $T_{i,k}^A$ corresponds to the maximum temperature of an area of interest A (a thermal anomaly) recorded at a distance i of up to 15 m (terrestrial and manual UAV), 22 m or 42 m (automatic UAV) to the building. The camera angle k is defined as either t (terrestrial), o (oblique/45°), n (nadir/90°) or m (manual/0°). $T_{j,l}^A$ is the maximum temperature of the same area of interest A within a second thermal image taken at a distance j of up to 15 m (terrestrial and manual UAV), 22 m or 42 m (automatic UAV) to the building and the camera angle l —again defined as either t, o, n or m. Changes in distance to the target object may lead to distortions in temperatures recorded by a thermal camera owing to intermediate air particles absorbing parts of the emitted infrared radiation [27]. Such atmospheric influences will likely have a noticeable effect as—according to Fouad and Richter [27]—the resulting temperature distortion remains neglectable only at distances of up to 20 m. In addition, the viewing angle k or l can further influence the calculated thermal difference. Emissivity decreases significantly at angles of more than 45°, thus causing larger temperature differences [39]. Quantifying the comparative temperature difference is important because it allows information to be derived about the ways in which thermographic UAV imagery can be used, e.g., in calculating U-values or energy losses [22].

- Comparative contrast: Contrast indicates differences in brightness and color within an image [40]. According to Ortiz-Sanz et al. [39] and Filippeschi and Leccese [41], this factor is mainly influenced by camera distance and angle to the object under scrutiny. A decrease in quantitative thermal contrast can be caused by signal degradation and increased reflections associated with lower emissivity levels [27,29]. For its use in thermal building auditing, contrast in an individual image can be defined as the temperature difference between a thermal anomaly (area of interest) and its surroundings (reference area). We, therefore, specify the comparative quantitative contrast as the difference in contrast of a specific area of interest between two thermographic images as follows:

$$\Delta T_{i,j,k,l}^C = \Delta T_{i,k}^C - \Delta T_{j,l}^C, \quad (2)$$

where $\Delta T_{i,k}^C$ and $\Delta T_{j,l}^C$ correspond to the quantitative contrasts of a thermal anomaly found in images recorded with different settings i, k and j, l (see comparative temperature difference). The contrast values themselves are defined as:

$$\Delta T_{i,k}^C = T_{i,k}^A - T_{i,k}^{RA}, \quad (3)$$

$$\Delta T_{j,l}^C = T_{j,l}^A - T_{j,l}^{RA}. \quad (4)$$

$T_{i,k}^A$ and $T_{j,l}^A$ thereby describe the temperatures of an area of interest A , while $T_{i,k}^{RA}$ and $T_{j,l}^{RA}$ represent the values measured at an adjacent reference area RA . The reference area is chosen as the nearest point to an area of increased temperature that is thermally monotonous, in other words constitutes an unaffected part of the building. The distances i and j between camera and building vary between up to 15 m for terrestrial and manually piloted UAV, as well as 22 m or 42 m for automatic UAV-based recordings. The camera angles k and l can once more be defined as either t , o , n or m .

2.4. Evaluation Procedure

This study examines 112 areas of increased temperature (e.g., thermal bridges) located on windows, (glazed) doors, roofs, façades, balconies, building bases, chimneys and vent openings. Examples of some of the inspected areas of interest are shown in Figure 4. A summary of all analysed thermal hotspots and their respective building parts is presented in Table 3.

For the two qualitative criteria, both of which relate to thermal differences, the maximum temperature of each of these areas of interest is utilized as a basis for the assessment. FLIR Thermal Studio's "ellipse" feature allows a user to trace anomalous areas within thermographic images and can determine said maximum. The nearest neighboring point that is part of the thermal background or surrounding average defines the reference temperature used to calculate the comparative quantitative contrast. As Fouad and Richter [27] found the effects of distance-dependent temperature distortions to be negligible at up to 20 m, we consolidate all terrestrial and manually piloted UAV acquisitions into two respective groups for the following quantitative analyses.

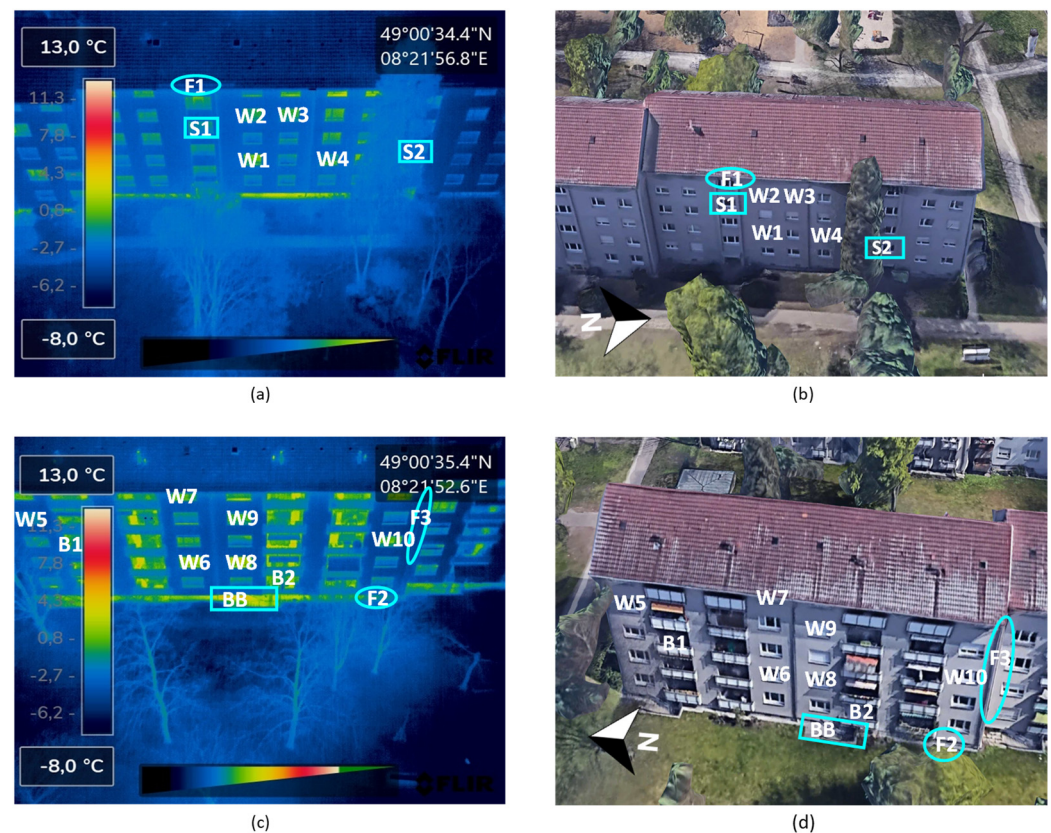


Figure 4. Example images: Areas of interest in Sophienstr. 201–203; left the thermographic images and right the corresponding RGB images from Google Earth [23]; (a,b) depict the east side of the building; (c,d) the west side; B1 and B2 show balconies; W1 to W10 windows; BB a building base; S1 and S2 staircases; F1 to F3 façade points.

Table 3. List of areas of interest for the case study per building and building part.

Building Part	Sophienstr. 201–203	Volzstr. 2	Wichernstr. 4	Wichernstr. 10–18
Balcony	2	8	7	4
Building base	1	-	2	-
Chimney	-	-	2	-
Door	-	1	-	-
Façade	3	4	2	6
Glass façade	-	2	-	-
Rooftop	-	3	4	7
Staircase	2	1	-	3
Vent opening	-	2	2	2
Window	10	4	19	9
Total	18	25	38	31

3. Results

Identified areas of interest must be analyzed according to the previously introduced quantitative and qualitative criteria to allow for conclusions to be drawn about the quality of the thermal images present in this case study dataset. The following results can be derived in doing so:

- Motion blur: Motion blur stems from movements of either the camera or objects in the field of view, making this criterion solely relevant to dynamic acquisition modes, seeing as the objects under scrutiny—namely buildings—are immobile. Acquisition via hand-held terrestrial camera or UAV in manual mode is considered static and therefore unaffected. In contrast, automatic UAV flight mode can be susceptible to motion blur. An evaluation of the case study images, however, shows that flight speeds of up to 5 m/s do not cause any visible blurring in all analyzed images. Figure 5 illustrates the absence of blurring effects in three exemplary images of the dataset.
- Feature discernibility: The distance between camera and target object, the angle and intrinsic camera-related properties all significantly influence resolution and the visibility of image details. This impact varies based on the mode of acquisition and implemented settings. UAV-based thermal images, recorded at a height of 22 m to 42 m above a building at a 45° camera angle, display discernible outlines of basement exits, base areas, windows, balconies and doors. However, a visibly greater accuracy can be achieved at a 22 m distance in comparison to 42 m with regards to details on windows and balconies. Thermal anomalies on window frames, sills and balconies, while clear at a closer range, are indistinguishable in images recorded at a distance of 42 m. Figure 6 exemplifies this observation by depicting the same building window captured through various methods and settings. As the same figure also demonstrates, such building elements can be seen in even greater detail in manually recorded images and terrestrial images owing to the smaller distances of 4 m to 15 m. On a ground-level altitude, hand-held cameras can capture images of comparable detail to a manual UAV-based camera at the same distance to the building. However, while manually piloted UAVs can cover upper areas of a building envelope with the same constant spatial resolution, the terrestrial acquisition mode requires changes in angle, thus causing a loss of discernible details. Nevertheless, a comparative analysis of the case study images shows that the terrestrial hand-held camera-based method records the following areas in greatest detail: geometric thermal bridges on balcony slabs, walls, between the building base and its façade, small windows close to ground level, window frame structures, air leakages between door and frame as well as window and sill and accumulated heat in upper window parts.
- Accessibility: The areas of a building's envelope that can be captured by thermal camera depend on the acquisition method and the achievable position-based field

of view. The nadir perspective, while allowing for a detailed view of rooftops, is ineffective at recording a building's façade, owing to the perpendicular angle between optical axis and normal on such a wall. In contrast, UAV-based images acquired automatically with a 45° pitch camera angle do show these kinds of details. In theory, this method allows for almost (Excepting minor blind spots such as those caused by building elements (like balconies) obscuring small façade parts from view) the entire building envelope to be screened. It must be noted, however, that the choice of flight pattern also plays an important role in how well the various building façades can be captured. As depicted in Figure 7a, a heading angle perpendicular to a wall will allow for the above described to be achieved with regards to this particular façade. However, assuming a rectangular building shape, the same angle will allow near to no clear view or access to both neighboring walls (s. Figure 7b). Flying solely with a strip pattern at such a heading angle needs to be cautioned against. Choosing a crosshatch pattern instead will ensure all four building façades are recorded with the same level of detail.

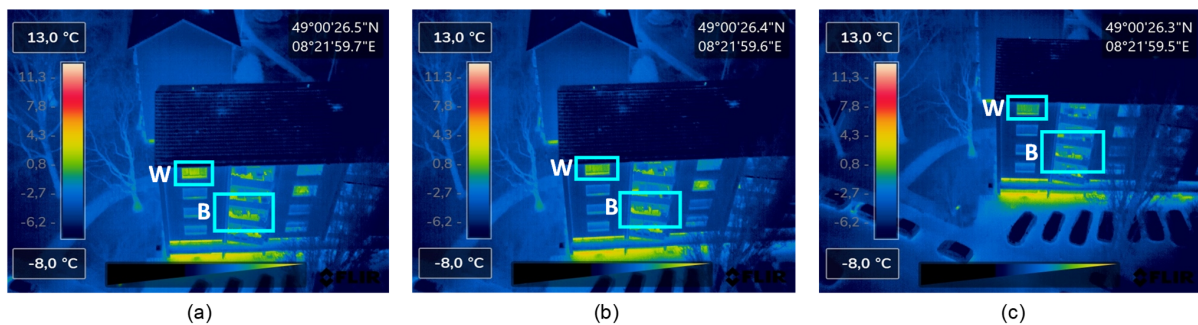


Figure 5. Comparison of thermographic images recorded at different flight speeds; (a–c) south side of Volzstr. 2; (a) at 1 m/s; (b) at 3 m/s; (c) at 5 m/s; B balcony; W window; B and W show no blur.

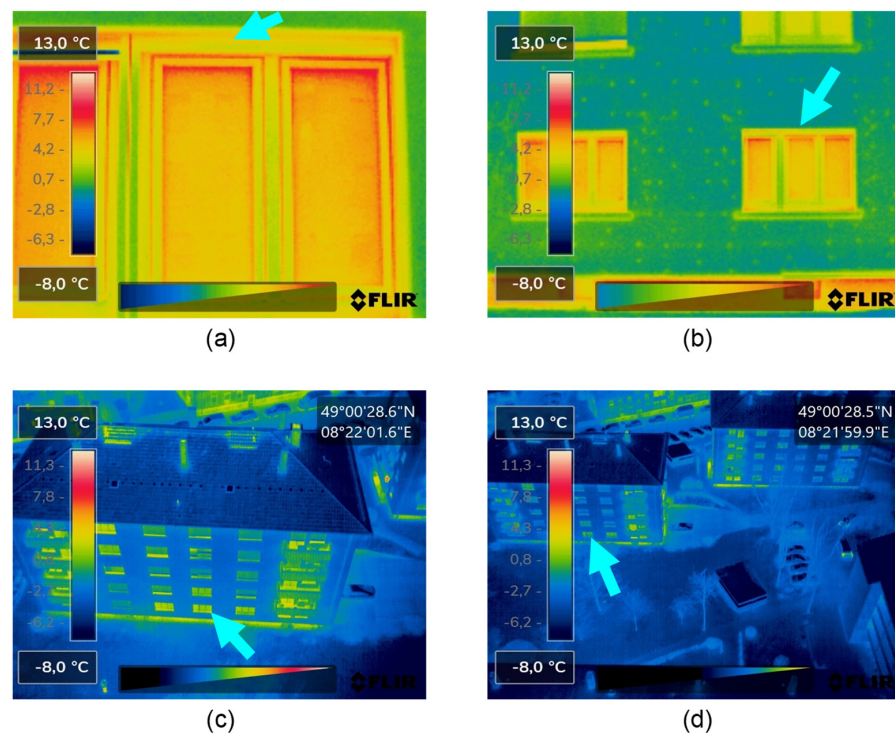


Figure 6. Comparison of the same window recorded with different settings; (a,b) terrestrial images recorded with a horizontal distance of (a) 4 m and (b) 15 m to the façade; (c,d) automatically recorded UAV images at a flight height of (c) 22 m and (d) 42 m above the building.

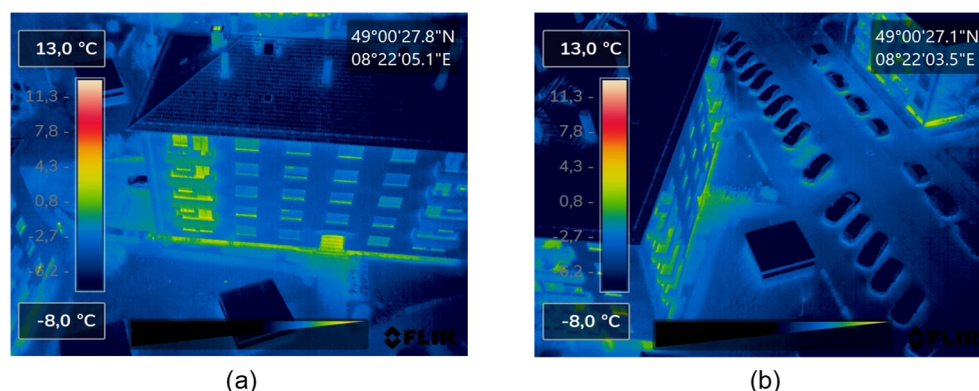


Figure 7. Flight with different heading angles relative to a building's façades/sides: (a) perpendicular to long side (b) perpendicular to short side (long side is obscured).

Acquisition by means of manually piloted UAV does not suffer from this methodological drawback, as the heading angle can be adapted to always assume the perpendicular to the wall in question. A combination of front-facing camera (0° pitch angle), small distance and the high degree of flexibility permitted by the UAV allow for the entire building envelope to be screened without similar blind spots occurring.

Compared to UAV-based images, hand-held cameras are far more restricted in their access to a building's envelope as they fail to capture rooftops of buildings as high as these. This means an entire area of the envelope may oftentimes be out of range for this acquisition method. Additionally, attaining views of areas higher up becomes more difficult the smaller the absolute distance between camera and building grows, owing to building features, such as balconies, obscuring the field of view. While this does improve at larger distances such as 8 m and 15 m, Figure 8 exemplifies how windows and their sills still remain concealed from the ground-based camera's view in comparison to images acquired by manual UAV. However, such an upward facing angle can also be advantageous for the inspection of eaves or the bottom of balcony slabs—for which Figure 8 shows the terrestrial method excels. Easily detectable areas by hand-held camera also include geometric anomalies in the joint area of two buildings between roof and façade, on side walls, and on the inside walls of balconies. However, the aforementioned limitation impacts these analyses with regards to areas of interest further above the ground.

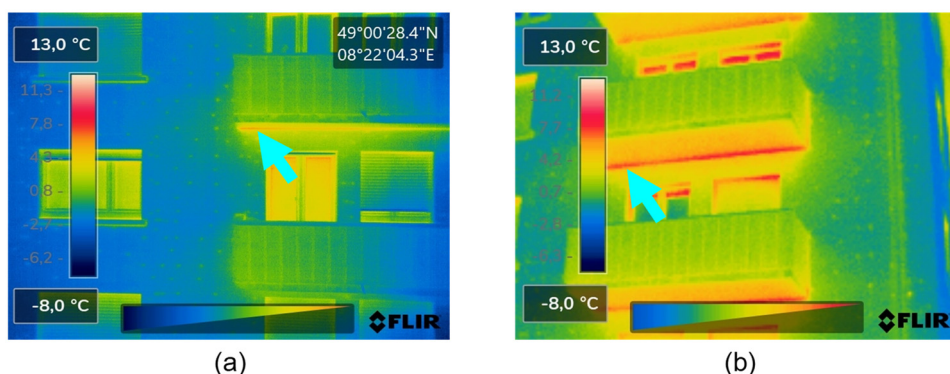


Figure 8. Thermographic images of a thermal bridge of a balcony slab recorded at an 8 m distance from a manual UAV's (a) and a ground-based hand-held camera's (b) perspective. Windows are more obscured in (b), while the thermal bridge under the balcony slab is more prominent. The same thermal bridge is inaccessible through automatically recorded aerial images.

- Comparative temperature difference: In addition to being influenced by camera-intrinsic parameters and atmospheric conditions, the measured temperature values can vary depending on the thermal camera's distance and angle to the object under

scrutiny [27]. The following box plots show a comparison of the acquisition methods (automatic and manual UAV-based and hand-held camera) at varying distances. While all plots in Figure 9 display both positive and negative temperature differences, the values are concentrated in the negative regions. This alludes to a general trend of decreasing distances leading to an increased recorded temperature. The box for $\Delta T_{o,o,42,22}^A$ (comparison of automatic UAV-based oblique images recorded at different heights of 22 m and 42 m) shows on average negative temperature differences. The positive temperature differences of $\Delta T_{o,o,42,22}^A$ may be a result of either a steep camera angle to the façade or a slight vignetting present in the collected images. The box plots for images from manual and automatic UAV flights at different distances show both positive and negative comparative temperature values. Positive values of up to +6 °C for $\Delta T_{o,t,22,15}^A$ are caused by window reflections as well as inexplicable distortions within manually UAV-based images. The negative values can be attributed to the variations in distance between camera and building. The final box plots again depict both negative and positive values with the negative maximum reaching −7.8 °C. This maximum of $\Delta T_{o,t,42,15}^A$ is likely caused by the largest possible difference in camera distance (UAV-based recording being at 42 m compared to terrestrial at up to 15 m). The positive temperature difference values between the terrestrial and UAV-based images ($\Delta T_{o,t,22,15}^A$, $\Delta T_{o,t,42,15}^A$) are again caused by window reflections which reduce recorded window temperatures in thermal images. Overall, it can be observed that larger differences in distance cause higher negative temperature deviations to occur. Additionally, the most conspicuous difference is found in the comparison of hand-held and UAV-based cameras. The more extreme ranges of both $\Delta T_{o,t}^A$ in comparison to the $\Delta T_{o,m}^A$ plots allude to the fact that distance itself might not be the only contributing factor—the different make and model of hand-held and UAV-based cameras as well as variations in angle and thus perspective of the ground-based acquisition method could be a cause for these observable variations.

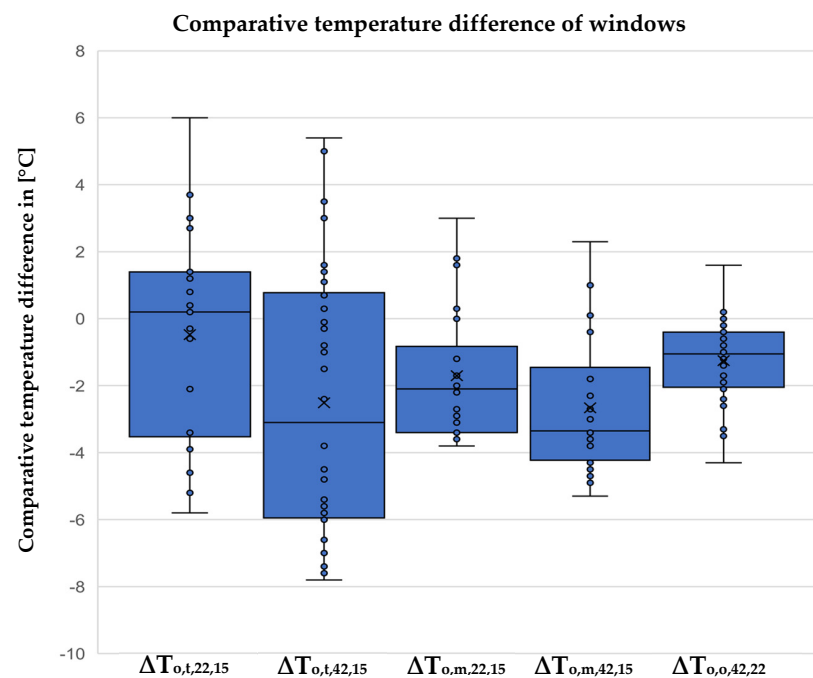


Figure 9. Box plots for the comparative temperature differences of windows: Comparative temperature differences between areas of interest of UAV-based images and terrestrial images.

Figure 10 illustrates a similar analysis of building rooftops, depicting the comparison of temperature differences in images acquired by oblique and nadir UAV-based methods. The calculated differences are found to be solely negative, which can again be explained by

the camera's disposition of recording lower temperatures at higher distances. Figure 11, for example, shows the same rooftop as having a different temperature when recorded at varying distances. $\Delta T_{0,0,42,22}^A$ exemplifies this fact as well, showing that a sole change in distance still causes a negative temperature difference. Another influencing factor can be determined when regarding the other box plots. Despite comparing the same distances, $\Delta T_{n,0,42,22}^A$ shows significantly lower temperature differences of up to $-6.5\text{ }^\circ\text{C}$. Simultaneously, $\Delta T_{n,0,42,42}^A$ displays differences between $0.3\text{ }^\circ\text{C}$ and $-3.5\text{ }^\circ\text{C}$, despite this being a purely methodological, distance- and camera-independent comparison. The temperature deviations occurring in $\Delta T_{n,0,42,42}^A$ must result from the only parameter that is varied here: the camera angle. This can be explained by the fact that the angle in nadir perspective lies outside the optimal angle range for image acquisition as defined by Ortiz-Sanz et al. [39]. Our findings therefore confirm Ortiz-Sanz et al.'s [39]: Reflections such as the aforementioned lead to the falsification of temperature values recorded in thermal images. Additionally, the increased negative temperature differences of $\Delta T_{n,0,42,22}^A$ occur both due to the change in distance to building as well as angle of camera.

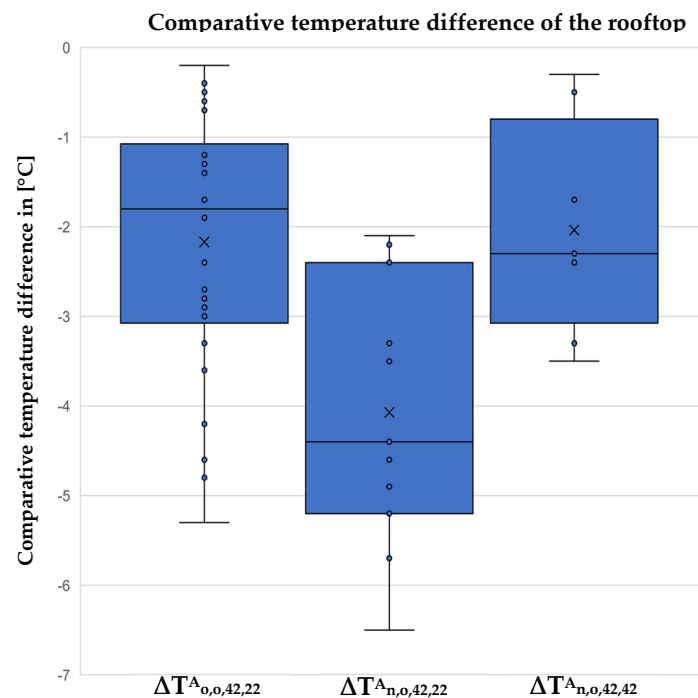


Figure 10. Box plots for the comparative temperature differences of rooftops: Comparative temperature differences between areas of interest of UAV-based images.

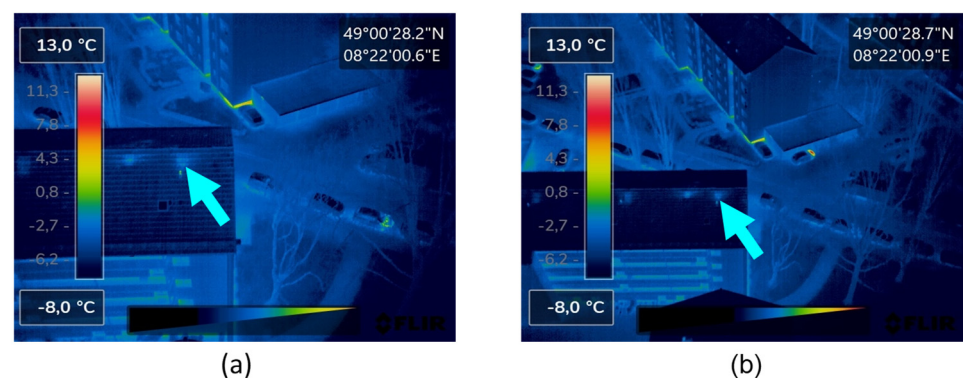


Figure 11. Thermographic images of the same rooftop recorded automatically with an oblique angle at (a) 22 m and (b) 42 m flight height above the building.

In summary, it can be said that the recorded temperature is influenced by distance. Precise quantitative statements about the influence of the recording settings on temperature distortions cannot be made on the basis of the small amount of analyzed data, even if a general trend has been identified. Smaller temperature deviations result from smaller changes in distance, such as in the comparison between 15 m and 22 m as opposed to 42 m. Window reflections are found to cause quantitative distortions within terrestrial thermographic recordings and manually flown UAV-based thermal images. It should be noted that the quantitative analysis of the rooftops using UAV-based images (at 22 m to 42 m flight height) seems more reliable than façade analyses at these distances, as the temperature deviations caused by camera distance are smaller in thermal rooftop anomalies than the inspected façade elements.

- Comparative contrast: The main factors that influence the contrast of thermographic images are camera angle and distance to the building under scrutiny. The effect of the camera angle becomes noticeable when comparing rooftops captured in nadir and 45° angle flight, with thermal anomalies displaying less contrast in images acquired at 90°. The cause of this lies with the prevalent weather conditions: clear, cloudless nights lead to increased reflections on rooftops [42]. As a result, the emissivity decreases and the contrast diminishes along with it. Figure 12 illustrates the described effect as it was observed on the rooftop of the building in Volzstr. 2.

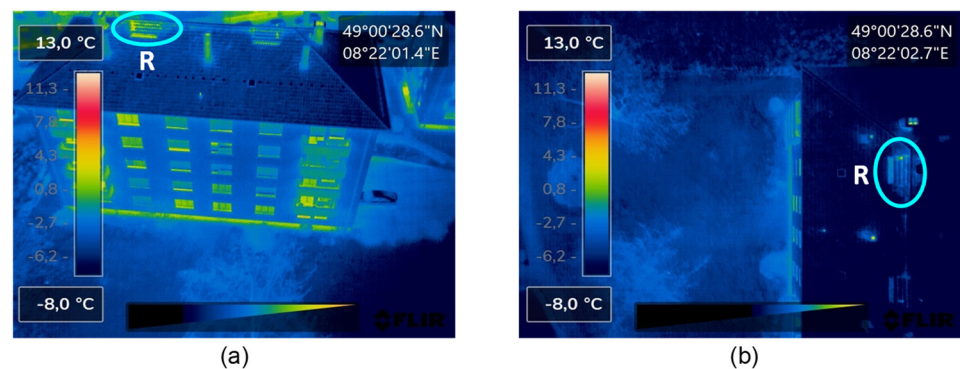


Figure 12. Influence of the camera angle on the contrast of drone-based thermographic images based on a roof anomaly R in Volzstr. 2; (a) in front view; (b) in nadir perspective. The contrast of R in (b) is weaker than in (a) due to increased reflections from the sky.

Windows can be similarly susceptible to angle-dependent reflections. These stem from surrounding buildings, trees and the sky itself, causing distortions in the calculated thermal contrast. However, such details are found to only be discernible in manually recorded UAV- or ground-based images—in other words at distances of 15 m and less to the building façade. In these modes of acquisition, more perceptible reflections are found to occur when recording images from below windows or on eye-level (at a 4 m distance), while no reflections are visible in images taken of a window from above. Figure 13 exemplifies the effects of window reflections depending on different camera angles.

While a change in distance between camera and target alters the perceived window reflections and therefore their effect as mentioned above, it also has a more general influence on thermal contrast. Measurable contrast is found to weaken with increasing distance. A comparison of automatic UAV-based images exemplifies this: The same windows, roof anomalies and other building elements are shown in greater contrast in images recorded at 22 m above the building than at a 42 m distance. In terrestrial images taken at distances of up to 15 m, this effect is even more pronounced, with thermal anomalies and bridges, balconies and windows displaying far greater contrast than at distances of both 22 m and 42 m.

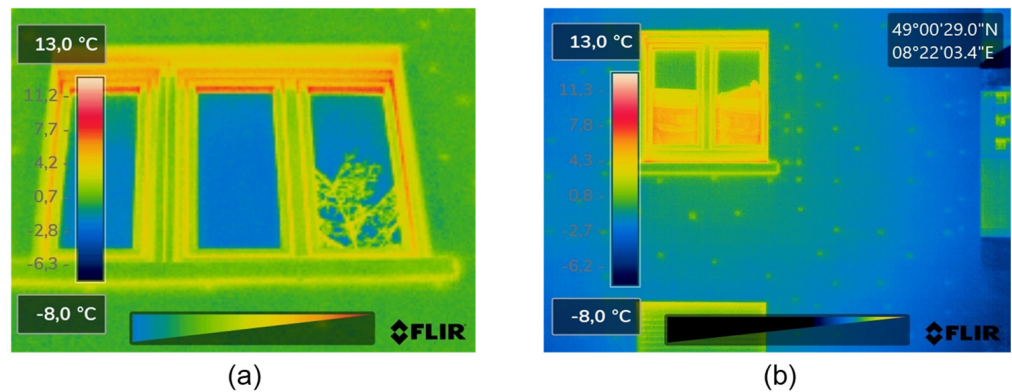


Figure 13. Window reflections recorded (a) with the terrestrial camera and (b) manually with the UAV-mounted camera at 4 m distance to the building façade.

Figures 14 and 15 show box plots of the comparative quantitative contrasts of the aforementioned areas of interest. Figure 14 depicts only negative values and values equal to zero for all three comparisons ($\Delta T_{o,t,22,15}^C$, $\Delta T_{o,t,42,15}^C$, and $\Delta T_{o,o,42,22}^K$), indicating lower contrasts with increased distance. This reemphasizes the pronounced effect that higher distances can have on recorded infrared radiation by thermal cameras as described by Fouad and Richter [27]. Values sink as low as -4.6 °C for façade elements ($\Delta T_{o,t,22,15}^K$ in Figure 14) and rooftop vent openings ($\Delta T_{o,o,42,22}^K$ in Figure 15). Figure 15 and $\Delta T_{o,o,42,22}^C$ additionally demonstrate how images taken with the same oblique angle suffer less from changes in contrast compared to those acquired with the camera pointing straight down. This supports previous observations of a nadir perspective, resulting in higher contrast deviations.

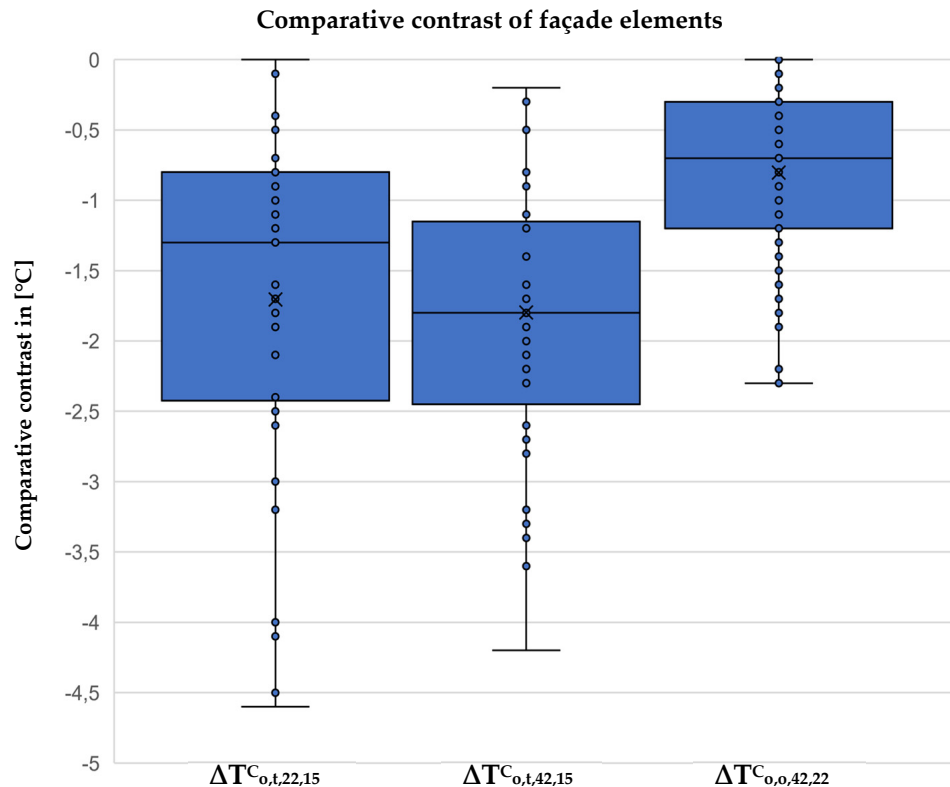


Figure 14. Box plots for the comparative contrasts of façade elements (window, balcony, door, base, insulation).

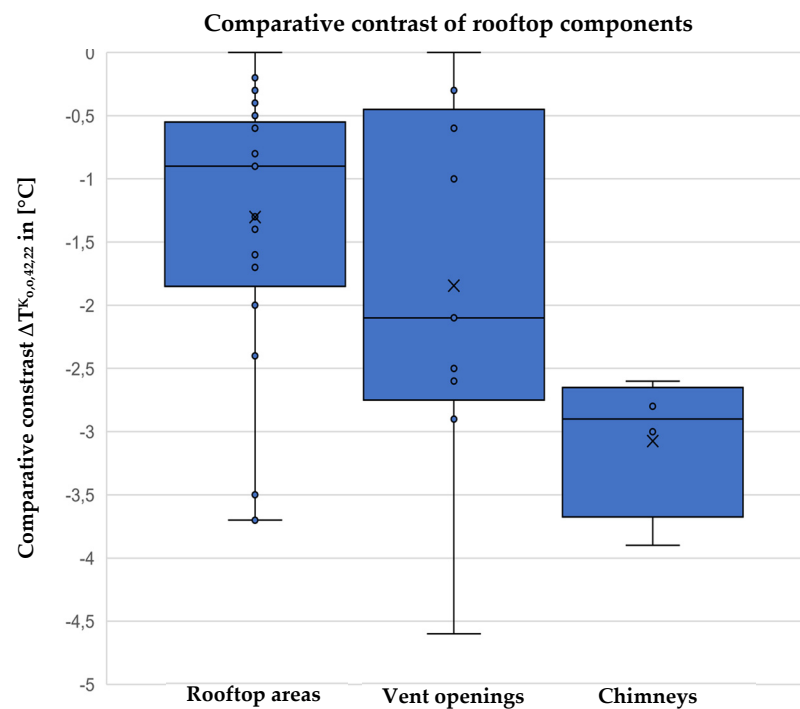


Figure 15. Box plots for the comparative contrasts $\Delta T_{0,0,42,22}^C$ between UAV-based images recorded from a height of 42 m and 22 m of rooftop elements (rooftop areas, vent openings, chimneys).

For the rooftop components in Figure 15, we find that differences of the quantitative contrast between the rooftop covering, vent openings and chimneys are caused by the fact that the roof vent openings and chimneys have much higher thermal losses associated with high temperatures and are therefore more sensitive to changing camera distance. The highest thermal losses are recorded in the chimneys. Accordingly, the greatest deviations in quantitative contrast are caused by changes in camera distance.

As with the comparative temperature difference, contrast is found to be vastly influenced by distance and angle, with greater distances causing decreases in contrast. For rooftops, the contrast is diminished by reflections from the sky occurring in nadir flight mode. Reflections in windows can also have a negative influence. It must again be noted that the aforementioned observations are merely visible trends, not absolute, quantitative statements on influence of the various recording settings, as these would be difficult to make based solely on the analysis of a single dataset.

A final point of contention in thermographic building auditing is the economic feasibility of the implemented method. This is, amongst others, defined by the amount of time involved in image acquisition as it requires a paid expert to do so. A detailed overview of all thermal image acquisitions performed for this case study is provided in Appendix A. Unsurprisingly, the automatically recorded UAV-based method took the least amount of time to record great quantities of images as the flight path was pre-programmed with comparatively high flight speeds. However, the strip flight pattern (which was required to ensure full building coverage) as well as the preparation time for UAV setup both considerably increase the method's duration. Additionally, due to software inaccuracies, some UAV flights were found to take inexplicably longer despite shorter routes (Inaccuracies of the implemented DJI Go 4 App caused recordings at 42 m above ground to take just as long or longer than acquisitions at 22 m, despite shorter distances.). These drawbacks, as well as the necessity for a "stop-and-go" recording process, made the manually UAV-based acquisition mode less time-efficient than even terrestrial acquisition.

4. Conclusions

4.1. Comparison of Acquisition Methods and General Recommendations

Using thermographic UAV-based images for building auditing creates new possibilities for the fast, large-scale energetic assessment of residential districts. The presented study evaluated a dataset of 968 UAV- and ground-based thermal images to identify influences of various methodological implementations on the quality of such images. These included 112 areas of interest with increased temperatures, which were analyzed and evaluated according to five defined quality criteria as well as an additional measure of time efficiency. We evaluated the effects of flight speed, camera distance and angle on the quality of UAV-based thermal images compared to those acquired through classical hand-held camera recordings.

Our case study allows for conclusions to be made regarding the previously mentioned parameters: While flight speeds of up to 5 m/s did not cause any qualitative changes to the thermal images, increasing distances between camera and target objects and changing angles are seen to have a significant negative impact, in particular on UAV-based acquisition methods. These parameter-specific insights influence the outcome of the quality criteria in their assessment of images from each acquisition method.

Previous sections discussed both the three image recording methods implemented in this case study as well as their quality-based evaluation according to the five chosen criteria. This set of tools and the assessment contingent upon them enables a methodological comparison. Table 4 shows such an overview for the three previously discussed methods.

Table 4. Comparison of the strengths and weaknesses of image acquisition methods implemented in this case study by means of previously discussed quality criteria.

Acquisition Method	Automatic UAV Flights	Manual UAV Flights	Hand-Held, Ground-Based Capture
Motion blur	Unaffected (at up to 5 m/s)	Unaffected (stationary)	Unaffected (stationary)
Feature discernibility	Medium (façades less detailed, large distances necessary)	High (same detail throughout, small distances possible)	Medium (non-eye-level areas less details, small distances possible)
Accessibility	Medium (with crosshatch only minor blind spots, inaccessibility of balcony slabs)	High (no blind spots, all areas accessible)	Low (large blind spots, entire envelope parts like rooftops hardly accessible, good accessibility of balcony slabs)
Comp. temperature difference	Weak (large distances necessary)	Strong (small distances possible)	Strong (small distances possible)
Comp. contrast	Weak (though no window reflections, large distances necessary)	Strong (despite pronounced window reflections, small distances possible)	Strong (despite pronounced window reflections, small distances possible)
Time efficiency	Medium (long setup, scalable approach)	Low (long setup and stop-and-go image capture)	Low (stop-and-go image capture on foot)
Overall	Fastest method but with least detail	Slowest method but constant, high detail	Enough detail but accessibility issues

A conclusion can be drawn from the presented overview for the choice of best thermal image acquisition method with regards to building auditing. First and foremost, the above comparison emphasizes how versatile UAV-based acquisition methods are owing to the third degree of freedom they allow. While both the manual and automatic form of implementation have drawbacks with regards to some criteria, combined they fulfill all requirements for a successful and economical thermography-based building assessment.

Manual UAV flights can cover entire building envelopes at close and constant distances without influences in angle, thus guaranteeing images of high quality and contrast. The time-consuming nature of the method limits its economical use to the assessment of individual buildings. When inspecting entire districts, it is therefore prudent to choose the fastest method of acquisition (automatic UAV flights) which, while incapable of offering similarly detailed images, provides enough information to narrow down areas of interest that may require further scrutiny via manual UAV flights. Ground-based thermography via hand-held camera is unable to match the aforementioned owing to the missing degree of freedom that prohibits access to building envelopes of a certain size, such as the ones given in this case study. Its use can therefore not be recommended, unless it is for the inspection of known areas of interest close to the ground.

4.2. Favorable Settings for UAV-Based Acquisition and Specific Recommendations

Automatic UAV-based thermal imaging was found to be most time efficient owing to preprogrammed flight paths and dynamic acquisition although the impact of increased distances and UAV preparation are not to be disregarded. When comparing UAV-based images at flight speeds between 1 and 5 m/s, neither motion blur nor image distortion is found to have occurred. In contrast to observations by Entrop and Vasenev [12] and Zahradník [19], we can therefore conclude that flight speeds of more than 1.5 m/s or 2 m/s are possible with the equipment used in this study. Flight speeds of more than 5 m/s require further investigation and should be examined in future studies, owing to their potential to further increase time efficiency.

Different flight heights and angles lead to deviations in temperature, contrast and the amount of discernible features owing to reflections of infrared radiation or reduced emissivity. Specifically, increased distances between camera and target as well as camera angles of more than 45° are found to negatively influence thermal image quality in the aforementioned aspects. This confirms findings by Fouad and Richter [27] and Ortiz-Sanz et al. [39], respectively.

Evaluating the effects of various camera angles (oblique and nadir) and flight heights (60 m and 48 m) on thermal images acquired in automatic UAV flight leads to the following conclusions: The nadir perspective, while granting detailed views of building rooftops, fails to be of use in the thermal analysis of façades and is associated with increased temperature distortions. Additionally, radiation reflection on rooftops leads to a reduced contrast in nadir images, thus making it more difficult to record thermally conspicuous areas of interest within them. In contrast, recording at a 45° camera angle to the ground enables the analysis of both rooftops and façades. Nadir flights produce thermal images of lower quality, thus deeming the 45° camera angle is more preferable for thermography-based auditing via automatic UAV flight. A camera height of 42 m above the target building allows larger areas to be covered more quickly, but the resulting images suffer from more temperature-related distortions and reduced contrast of both rooftop and façade compared to those acquired at closer distances (such as 22 m). With increasing distance, less thermal anomalies become discernible on the building's envelope.

Based on these observations, we recommend a 45° camera angle and a 22 m distance for the qualitative analysis of buildings using UAVs. However, performing quantitative thermographic studies with the aforementioned settings remains inadvisable due to the distinct temperature and contrast distortions perceptible for instance in window panes. We can therefore only recommend the use of UAV-based thermography for quantitative purposes (such as obtaining U-values) when flying at close range or piloting the drone manually. Table 5 summarizes our suggestions based on the findings of our study with regards to UAV-based thermal image acquisition.

Table 5. Recommendations for UAV settings in UAV-based thermal image acquisition for building auditing deduced from the results and framework conditions of our study; * The usefulness of performing manual flights for rooftop analyses depends on the shape of the rooftop and can make sense in individual cases. If a slanted roof is scanned at a perpendicular angle to the building façade, temperature distortions can be expected to occur, depending on the slant angle.

	Automated Flights				Manual Flights/Recordings
	12 m height above building, 45° camera angle	22 m height above building, 45° camera angle	42 m height above building, 45° camera angle	42 m height above building, 90° camera angle	Up to 15 m horizontal distance, 0° camera angle
Qualitative analysis of the rooftop	Recommended	Recommended	Recommended only for overviews	Recommended only for overviews	Not studied *
Qualitative analysis of the façade	Recommended	Recommended	Recommended only for overviews	Not recommended	Recommended
Quantitative analysis of the rooftop	Recommended	Not recommended	Not recommended	Not recommended	Not studied *
Quantitative analysis of the façade	Not recommended	Not recommended	Not recommended	Not recommended	Recommended

4.3. Critical Review

To conclude, we want to critically reflect on our work. The evaluation of the dataset is influenced by various factors. Overall, the study is limited to data recorded with nine different flight settings on two recording days. For a more comprehensive database, a larger dataset with images from different times of the day and weather conditions could be beneficial. Also, the number of areas of interest considered in the study could be increased. Future studies should additionally examine more flight settings, such as higher flight speeds (>5 m/s), smaller distances (e.g., 20 m) and different camera angles (e.g., 30°). However, it should be noted that some UAV models, like the one implemented in this study, do not allow automatic aerial surveys with the camera angled at less than 40° to the ground. Performing similar studies with other UAVs might therefore be beneficial. Limitations to the flight path caused by the presence of obstacles in a building's vicinity might also be circumvented by using a drone capable of detecting and avoiding such obstructions. In order to increase the number of usable thermographic images, the UAV's path should be aligned to each building's position instead of choosing a heading angle at random to merely cover the area. Furthermore, using different features of FLIR's Thermal Studio software would allow a more balanced assessment of various image aspects. The choice of color distribution along with palette range, for instance, affects the brightness of the thermographic images. In this case, the distribution function "signal linear" was selected to preserve contrast and reduce background effects. However, a simultaneously elicited darkening of the images makes the detection of thermal anomalies more difficult. Implementing other functions that induce contrasting effects, such as "histogram equalization", could further augment the analysis.

Several assumptions of technical and experimental nature need to be addressed as well. First, the use of two different thermal cameras (hand-held and UAV-based) cannot be neglected as a potential source for differences in temperature. However, an exemplary comparison of images recorded with both camera models showed no perceptible distortions to exist—apart from a generally lower resolution apparent in the ground-based images. Other influencing factors depend on the form of image acquisition, such as a slight vignetting indicated by the images' darkened corners and edges of the images collected by drone. Vignetting is caused by variations in temperature between camera components [43]. This

makes the effect a common occurrence in UAV-based acquisition because a drone's propellers induce a lens-cooling slipstream that clashes with the heat internally generated by electronics and gimbal motor [43]. Another observable distortion is a slight drift in temperature caused by a temperature drop during the acquisition time frame. However, the effects from this were found to be negligible for the analysis and aforementioned comparisons. As we opted for a more qualitative-based assessment, the precise distances and angles between camera and building envelope surfaces were not calculated for the case study images. Future studies may therefore elevate the analysis by using photogrammetry to determine such values. This includes pinpointing the exact camera position with relation to the object under scrutiny to identify the precise influence of distance and angle on thermal image quality.

Overall, this work contributes to the joint fields of remote thermography and building auditing by providing a set of tools with which thermal image quality can be assessed. Additionally, specific recommendations are made for various acquisition modes and settings for individual building and district auditing. In the future, we anticipate an increase in quantitative studies to further substantiate current observations regarding the effects of camera distance, angle and speed.

Author Contributions: Conceptualization, Z.M. and A.E.; methodology, Z.M., A.E. and E.V.; formal analysis, Z.M. and A.E.; investigation, Z.M. and A.E.; resources, Z.M., A.E. and E.V.; data curation, A.E.; writing—original draft preparation, Z.M., E.V. and A.E.; writing—review and editing, R.V. and F.S.; visualization, Z.M. and A.E.; supervision, R.V. and F.S. All authors have read and agreed to the published version of the manuscript.

Funding: We acknowledge support by the KIT-Publication Fund of the Karlsruhe Institute of Technology.

Data Availability Statement: All data was obtained in own experiments. All data used for the study can be requested from the authors and is published online at [Zenodo.org](https://zenodo.org) (accessed on 1 January 2020) [34].

Acknowledgments: The authors appreciate the support of Marinus Vogl (Air Bavarian GmbH) in acquiring the thermal images via UAV. Moreover, they thank Harald Schneider (Karlsruhe Institute of Technology) for his advice and assistance. Lastly, they gratefully acknowledge the consent and support of Karlsruher Volkswohnung GmbH within this research project.

Conflicts of Interest: The authors declare no conflict of interest.

Appendix A

Table A1. Overview of thermal image recording parameters.

Flight	Building	Recording Angle [°]	Height above Building [m]	Distance to Façade [m]	Flight Speed [m/s]	Side and Front Overlap [%]	Flight/Recording Time [min]	Recorded Area [m ²]	Number of Images ¹ [-]	Image Rate [Images/min]	Flight Route Length [m]
1	Sophienstr. 201–203	45	22	-	1	10	43	2500	130	3	2730
2	Sophienstr. 201–203	45	22	-	3	10	20	2500	130	6.6	2730
3	Sophienstr. 201–203	45	22	-	5	10	13	2500	130	10	2730
4	Sophienstr. 201–203	45	42	-	3	10	25 ²	2500	104	4.2	2730 ³
5	Sophienstr. 201–203	90 ⁴	22	-	3	10	-	2500	-	-	-
6	Sophienstr. 201–203	90	42	-	3	10	-	2500	-	-	-
1	Volzstr. 2	45	22	-	1	10	29	2000	105	3.6	2275
2	Volzstr. 2	45	22	-	3	10	13	2000	105	8.1	2275
3	Volzstr. 2	45	22	-	5	10	7	2000	105	15	2275

Table A1. Cont.

Flight	Building	Recording Angle [°]	Height above Building [m]	Distance to Façade [m]	Flight Speed [m/s]	Side and Front Overlap [%]	Flight/Recording Time [min]	Recorded Area [m ²]	Number of Images ¹ [-]	Image Rate [Images/min]	Flight Route Length [m]
4	Volzstr. 2	45	42	-	3	10	21	2000	90	4.3	2275
5	Volzstr. 2	90	22	-	3	10	-	2000	-	-	-
6	Volzstr. 2	90	42	-	3	10	-	2000	-	-	-
1	Wichernstr. 4	45	22	-	1	10	34	1700	120	3.5	2045
2	Wichernstr. 4	45	22	-	3	10	15	1700	120	8	2045
3	Wichernstr. 4	45	22	-	5	10	11	1700	120	10.9	2045
4	Wichernstr. 4	45	42	-	3	10	18	1700	98	5.4	2650
5	Wichernstr. 4	90	22	-	3	10	-	1700	-	-	-
6	Wichernstr. 4	90	42	-	3	10	-	1700	-	-	-
1	Wichernstr. 10–18	45	22	-	1	10	40	3600	145	3.6	3870
2	Wichernstr. 10–18	45	22	-	3	10	19	3600	145	7.6	3870
3	Wichernstr. 10–18	45	22	-	5	10	12	3600	145	12.1	3870
4	Wichernstr. 10–18	45	42	-	3	10	22	3600	117	5.3	3870
5	Wichernstr. 10–18	90	22	-	3	10	-	3600	-	-	-
6	Wichernstr. 10–18	90	42	-	3	10	-	3600	-	-	-
7 ⁵	Wichernstr. 4	0	-	4	-	-	15	180	23	1.5	- ⁶
8	Wichernstr. 4	0	-	8	-	-	30	520	48	1.6	-
9	Wichernstr. 4	0	-	15	-	-	14	520 ⁷	22	1.6	-
9	Wichernstr. 10–18	0	-	15	-	-	29	900	46	1.6	-

¹ This refers to all recordings, including those that do not show any areas of interest or are unsuitable for the analysis and were thus sorted out. ² As a result of inaccuracies in the DJI Go 4 UAV software for areas smaller than 20,000 m² (2 ha), the duration of a flight at 42 m is longer than at 22 m. This stands in contrast to the fact that a greater distance should allow for the comparatively smaller object to be captured in less time. ³ As a result of inaccuracies in the DJI Go 4 UAV software for small areas, the distance that needs to be covered for a flight at 42 m height is just as long as for 22 m, even though a greater distance between camera and target should allow for the comparatively smaller object to be captured by means of a shorter flight path. ⁴ The recordings in nadir (90° camera angle) were carried out simultaneously with the recordings at a 45° camera angle and 3 m/s flight speed. Therefore, there is no separate information on flight times. ⁵ Flights 7 to 10 refer to manual UAV-based thermal image acquisition. All other flights were carried out automatically via UAV. ⁶ Precise route information is not available because the recordings were completed by hand and cover only parts of the building envelope. ⁷ The area of the façade was determined for this flight. For flights 1 to 6, on the other hand, the area corresponds to the built-up area of the building. In this context, the built-up area is the area covered by the building [44].

References

- Gade, R.; Moeslund, T.B. Thermal cameras and applications: A survey. *Mach. Vis. Appl.* **2014**, *25*, 245–262. [CrossRef]
- Osornio-Rios, R.A.; Antonino-Daviu, J.A.; de Jesus Romero-Troncoso, R. Recent Industrial Applications of Infrared Thermography: A Review. *IEEE Trans. Ind. Inform.* **2018**, *15*, 615–625. [CrossRef]
- Sarawade, A.A.; Charniya, N.N. Infrared Thermography and its Applications: A Review. In Proceedings of the 2018 3rd International Conference on Communication and Electronics Systems (ICCES), Coimbatore, India, 15–16 October 2018; pp. 280–285. [CrossRef]
- Kirimtat, A.; Krejcar, O. A review of infrared thermography for the investigation of building envelopes: Advances and prospects. *Energy Build.* **2018**, *176*, 390–406. [CrossRef]
- Martin, M.; Chong, A.; Biljecki, F.; Miller, C. Infrared thermography in the built environment: A multi-scale review. *Renew. Sustain. Energy Rev.* **2022**, *165*, 112540. [CrossRef]

6. Bitelli, G.; Conte, P.; Csoknyai, T.; Franci, F.; Girelli, V.A.; Mandanici, E. Aerial Thermography for Energetic Modelling of Cities. *Remote Sens.* **2015**, *7*, 2152–2170. [[CrossRef](#)]
7. Previtali, M.; Barazzetti, L.; Brumana, R.; Roncoroni, F. Thermographic analysis from UAV platforms for energy efficiency retrofit applications. *J. Mob. Multimed.* **2013**, *9*, 66–82. [[CrossRef](#)]
8. Yin, C.; Xiong, Z.; Chen, H.; Wang, J.; Cooper, D.; David, B. A literature survey on smart cities. *Sci. China Inf. Sci.* **2015**, *58*, 1–18. [[CrossRef](#)]
9. Alsamhi, S.H.; Almalki, F.A.; Ma, O.; Ansari, M.S.; Lee, B. Predictive Estimation of Optimal Signal Strength From Drones Over IoT Frameworks in Smart Cities. *IEEE Trans. Mob. Comput.* **2021**, *22*, 402–416. [[CrossRef](#)]
10. Sharma, R.; Arya, R. UAV based long range environment monitoring system with Industry 5.0 perspectives for smart city infrastructure. *Comput. Ind. Eng.* **2022**, *168*, 108066. [[CrossRef](#)]
11. Krawczyk, J.; Mazur, A.; Sasin, T.; Stokłosa, A. Infrared building inspection with unmanned aerial vehicles. *Trans. Inst. Aviat.* **2015**, *240*, 32–48. [[CrossRef](#)]
12. Entrop, A.G.; Vasenev, A. Infrared drones in the construction industry: Designing a protocol for building thermography procedures. *Energy Procedia* **2017**, *132*, 63–68. [[CrossRef](#)]
13. Rakha, T.; Gorodetsky, A. Review of Unmanned Aerial System (UAS) applications in the built environment: Towards automated building inspection procedures using drones. *Autom. Constr.* **2018**, *93*, 252–264. [[CrossRef](#)]
14. Daffara, C.; Muradore, R.; Piccinelli, N.; Gaburro, N.; De Rubeis, T.; Ambrosini, D. A Cost-Effective System for Aerial 3D Thermography of Buildings. *J. Imaging* **2020**, *6*, 76. [[CrossRef](#)]
15. Dahaghin, M.; Samadzadegan, F.; Javan, F.D. Precise 3D extraction of building roofs by fusion of UAV-based thermal and visible images. *Int. J. Remote Sens.* **2021**, *42*, 7002–7030. [[CrossRef](#)]
16. Hou, Y.; Chen, M.; Volk, R.; Soibelman, L. Investigation on performance of RGB point cloud and thermal information data fusion for 3D building thermal map modeling using aerial images under different experimental conditions. *J. Build. Eng.* **2022**, *45*, 103380. [[CrossRef](#)]
17. Benz, A.; Taraben, J.; Debus, P.; Habte, B.; Oppermann, L.; Hallermann, N.; Voelker, C.; Rodehorst, V.; Morgenthal, G. Framework for a UAS-based assessment of energy performance of buildings. *Energy Build.* **2021**, *250*, 111266. [[CrossRef](#)]
18. Mayer, Z.; Heuer, J.; Volk, R.; Schultmann, F. Aerial Thermographic Image-Based Assessment of Thermal Bridges Using Representative Classifications and Calculations. *Energies* **2021**, *14*, 7360. [[CrossRef](#)]
19. Zahradník, D. Roof Leak Detection by Thermography of As-Built Bim. *Int. Arch. Photogramm. Remote Sens. Spat. Inf. Sci.* **2022**, *46*, 251–256. [[CrossRef](#)]
20. Mirzabeigi, S.; Razkenari, M. Automated Vision-Based Building Inspection Using Drone Thermography. In Proceedings of the Construction Research Congress, Arlington, VA, USA, 9–12 March 2022; pp. 737–746. [[CrossRef](#)]
21. Gómez, J.; Tascón, A. Protocolo para el uso de vehículos aéreos no tripulados en la inspección de edificios agroindustriales. *Inf. Constr.* **2021**, *73*, e421. [[CrossRef](#)]
22. Mayer, Z.; Epperlein, A.; Volk, R.; Vollmer, E.; Schultmann, F. Comparison of building thermography approaches using terrestrial and aerial thermographic images. *IOP Conf. Ser. Earth Environ. Sci.* **2022**, *1078*, 012026. [[CrossRef](#)]
23. Google Earth. Karlsruhe. 2022. Available online: <https://earth.google.com/web/@49.0073106,8.36729178,115.40952834a,389.61303477d,35y,16.33359823h,59.7531201t,-0r> (accessed on 12 August 2022).
24. DJI. Matrice 300—DJI. 2022. Available online: <https://www.dji.com/de/matrice300> (accessed on 10 January 2022).
25. FLIR. FLIR XT2 Product Information (Wilsonville, USA). 2021. Available online: <https://www.flir.de/products/xt2/> (accessed on 10 January 2022).
26. FLIR. FLIR T-Series (Wilsonville, USA). 2021. Available online: <https://www.flir.com/instruments/t-series/> (accessed on 10 January 2022).
27. Fouad, N.A.; Richter, T. *Leitfaden Thermografie im Bauwesen: Theorie, Anwendungsgebiete, Praktische Umsetzung*; Fraunhofer IRB Verlag: Stuttgart, Germany, 2012; ISBN 3816784569.
28. Timeanddate. Wetter im Februar 2022 in Karlsruhe, Baden-Württemberg, Deutschland. 2022. Available online: <https://www.timeanddate.de/wetter/deutschland/karlsruhe/rueckblick?month=2&year=2022> (accessed on 12 March 2022).
29. Lucchi, E. Applications of the infrared thermography in the energy audit of buildings: A review. *Renew. Sustain. Energy Rev.* **2018**, *82*, 3077–3090. [[CrossRef](#)]
30. *DIN 4108-2; Wärmeschutz und Energie-Einsparung in Gebäuden—Teil 2: Mindestanforderungen an den Wärmeschutz (May Be Translated as: Thermal Protection and Energy Economy in Buildings—Part 2: Minimum Requirements to Thermal Insulation)*. Deutsches Institut für Normung: Berlin, Germany, 2013.
31. FLIR Systems Inc. User’s Manual Flir Thermal Studio. 2022. Available online: <https://www.sahkonumerot.fi/6708162/doc/operatinginstructions/> (accessed on 12 August 2022).
32. Fouad, N. *Bauphysik-Kalender*; (May Be Translated as: Building Physics Calendar); Ernst. Wilhelm & Sohn (Verlag): Berlin, Germany, 2010; ISBN 978-3-433-02938-1.
33. FLIR Systems Inc. What Happens When I Select Histogram Equalization as the Image Representation in FLIR Tools? 2022. Available online: <https://www.flir.com/support-center/Instruments/what-happens-when-i-select-histogram-equalization-as-the-image-presentation-in-flir-tools/> (accessed on 10 October 2022).

34. Mayer, Z.; Epperlein, A.; Vollmer, E.; Volk, R. *Aerial and Terrestrial Thermal Images of German Multi-Family Buildings Version 1.0*; Zenodo: Geneva, Switzerland, 2022. [CrossRef]
35. Sieberth, T.; Wackrow, R.; Chandler, J.H. Motion blur disturbs—The influence of motion-blurred images in photogrammetry. *Photogramm. Rec.* **2014**, *29*, 434–453. [CrossRef]
36. O'Connor, J.; Smith, M.J.; James, M.R. Cameras and settings for aerial surveys in the geosciences. *Prog. Phys. Geogr. Earth Environ.* **2017**, *41*, 325–344. [CrossRef]
37. Liang, S.; Li, X.; Wang, J. *Advanced Remote Sensing: Terrestrial Information Extraction and Applications*; Elsevier Science & Technology: San Diego, CA, USA, 2012; ISBN 9780123859556.
38. Government of Canada. Spatial Resolution, Pixel Size, and Scale. 2015. Available online: <https://www.nrcan.gc.ca/maps-tools-and-publications/satellite-imagery-and-air-photos/tutorial-fundamentals-remote-sensing/satellites-and-sensors/spatial-resolution-pixel-size-and-scale/9407> (accessed on 30 September 2022).
39. Ortiz-Sanz, J.; Gil-Docampo, M.; Arza-García, M.; Cañas-Guerrero, I. IR Thermography from UAVs to Monitor Thermal Anomalies in the Envelopes of Traditional Wine Cellars: Field Test. *Remote Sens.* **2019**, *11*, 1424. [CrossRef]
40. Böhringer, J.; Bühler, P.; Schlaich, P.; Sinner, D. *Kompendium der Mediengestaltung: Konzeption und Gestaltung. I*; Springer Vieweg: Berlin/Heidelberg, Germany, 2014. [CrossRef]
41. Filippeschi, S.; Leccese, F. Infrared thermography to visualize the texture of historical buildings in Tuscany. In Proceedings of the 8th International Conference on Non-Destructive Investigations and Microanalysis for the Diagnostics and Conservation of the Cultural and Environmental Heritage, Lecce, Italy, 15–19 May 2005. Available online: https://www.academia.edu/29499780/Infrared_Thermography_to_Visualize_the_Texture_of_Historical_Buildings_in_Tuscany (accessed on 1 January 2023).
42. Vollmer, M.; Möllmann, K. *Infrared Thermal Imaging Fundamentals, Research and Applications*; Wiley-VCH. ePDF: Weinheim, Germany, 2017; ISBN 978-3-527-69332-0.
43. Teledyne FLIR. Halo or Vignetting Image on a Vue, Vue Pro, Vue Pro R, Duo, Duo Pro, Duo Pro R, XT or XT2. 2022. Available online: https://flir.custhelp.com/app/answers/detail/a_id/3494/related/1/session/L2F2LzEvdGltZS8xNjY1NjU3Njc0L2dlbi8xNjY1NjU3Njc0L3NpZC9mVW12VnJQZ21RM0xfZ1NXT3FUYldVaUxLYnExUE16dzBfZERHbjB3TEJaY1lnbE9VTkV2bUFzRSU3RXRUb0RSWTNFaXpTbk9hTk5ZaUU3a1FYd0dzendFbHVYdzI1TWFCdkRtWkUxN2hXU1RnelFHRE1FTkh0OVVxdyUyMSUyMQ%3D%3D (accessed on 30 September 2022).
44. *DIN 277:2021-08: DIN 277*; Grundflächen und Rauminhalte im Hochbau. (May Be Translated as: Floor Areas and Volumes in Building Construction). Deutsches Institut für Normung: Berlin, Germany, 2013.

Disclaimer/Publisher's Note: The statements, opinions and data contained in all publications are solely those of the individual author(s) and contributor(s) and not of MDPI and/or the editor(s). MDPI and/or the editor(s) disclaim responsibility for any injury to people or property resulting from any ideas, methods, instructions or products referred to in the content.

Paper D: A Computer Vision Approach for Building Façade Component Segmentation on 3D Point Cloud Models Reconstructed by Aerial Images

This paper was reproduced in its original format with permission from Universitätsverlag der TU Berlin:

Hou, Y., Mayer, Z., Li, Z., Volk, R., Soibelman, L. (2021 - Paper D). A Computer Vision Approach for Building Façade Component Segmentation on 3D Point Cloud Models Reconstructed by Aerial Images. EG-ICE 2021 Proceedings: Workshop on Intelligent Computing in Engineering, 561. Online 18.08.2021:
https://www.researchgate.net/profile/Rebekka-Volk/publication/353768665_A_Computer_Vision_Approach_for_Building_Facade_Component_Segmentation_on_3D_Point_Cloud_Models_Reconstructed_by_Aerial_Images/links/6110f75d1e95fe241abb1b49/A-Computer-Vision-Approach-for-Building-Facade-Component-Segmentation-on-3D-Point-Cloud-Models-Reconstructed-by-Aerial-Images.pdf

A Computer Vision Approach for Building Facade Component Segmentation on 3D Point Cloud Models Reconstructed by Aerial Images

Yu Hou M.Sc.^{a*}, Zoe Mayer M.Sc.^b, Zhaoyang Li^a, Dr. Rebekka Volk^b, Dr. Lucio Soibelman^a
^a University of Southern California, USA, ^b Karlsruhe Institute of Technology, Germany
yuhou@usc.edu

Abstract. Segmenting windows and doors on 3D point cloud models allows for heat loss audits around these areas. Researchers have collected aerial images to reconstruct 3D models for large districts, but easily accessible training datasets with data acquired on ground level cannot be directly used for segmentation on 3D models reconstructed by aerial images. Additionally, building a new dataset is a time-consuming and labour-intensive process. Therefore, we propose a segmentation approach that uses open source training datasets to segment windows and doors on façade images rendered from 3D point clouds. The results show that our approach can make full use of open source datasets to segment windows and doors, and that such trained segmentation models performs differently for different building styles. In addition, different algorithms result in various degrees of accuracy and segmentation on windows performs better than on doors.

1. Introduction

Thermography, a non-destructive inspection technology, is used for heat loss energy audits. However, the most common current data collection approaches only allow individual building energy audit by deploying handheld infrared thermography cameras to collect thermal information from building facades. The biggest downside of current data collection approaches is efficiency. Such approaches also do not consider groups of buildings in large district areas in which interconnected buildings impact each other's thermal behaviors, especially, those connected within the same district heating network. More precisely speaking, if one building that is located in the middle of a heating network has unfixed heat loss issues, it will force buildings located downstream in the network to draw more heat to keep warm, resulting in more energy wasted through the middle-network buildings. Thus, there is a need to investigate novel methods and frameworks for building heat energy audits for large districts. Driven by the need of efficient and thorough energy audits for large districts, researchers have been deploying unmanned aircraft systems (UASs) to improve the data collection process (Hou *et al.*, 2019).

The benefits of using UASs to collect both thermal (infrared spectrum) and RGB (red-green-blue visible light) images include the higher data collection speed and availability of a bird's eye view, which can improve collection efficiency and comprehensively explore high areas of building façades that handheld thermal cameras cannot reach. Thermal and RGB imagery data collected from UASs allow the reconstruction of 3D point cloud models using photogrammetry technology. In order to obtain the 3D point cloud models that can integrate both thermal and RGB information, researchers have deployed different data fusion approaches (Hou *et al.*, 2021; Shahandashti *et al.*, 2010).

Distinguishing windows and other heat loss related building façade elements is an important step for energy audits. Semantic segmentation using 3D point cloud building models fused with thermal information allows researchers to detect heat loss from window and door edges and to monitor thermal bridges and areas of moisture on walls. The first step is to distinguish these façade components. However, in available open source image databases, facade images with their labeled components (the ground truth information) that were taken from the ground cannot be directly used to train a model to segment façade elements either in drone-based aerial images

or in point cloud models reconstructed by these aerial images. To manually label newly captured aerial images and then build a new dataset is a potential option. However, conducting ground truth coding on these aerial images is both time-consuming and labor-intensive. Therefore, studies on the use of open source databases obtained from the ground to train artificial neural network (ANN) models for façade components segmentation using aerial images can provide an alternative that does not require the building of a new database.

To reduce labeling time and maintain the benefits of using UAS-based data collection, we propose a framework to train segmentation models using open source terrestrial image datasets taken from the ground to predict semantic information on building façades. In this paper, we introduce the results of our approach that was tested on two different datasets from Karlsruhe, Germany, one from a university campus, and the other from a central business district (Mayer *et al.*, 2021). The research introduced in this paper was designed to answer the following questions: (1) How does the proposed approach perform on different testing datasets with different building styles? and (2) How does the segmentation accuracy vary for different building components? This paper is organized as follows. We introduce and detail our approach in Section 2. Experiment results are described in Section 3, followed by evaluation and discussion in Section 4. Finally, we present our conclusions in Section 5.

2. Methodology

The proposed approach consists of the following four steps: (1) reconstructing a 3D point cloud model with aerial imagery data, (2) rendering 2D images from the 3D model, (3) training a semantic segmentation ANN model with open source datasets, and (4) predicting segmentation results on the rendered 2D images. We also designed the evaluation and validation metrics for the proposed approach.

Note that with the exception of the 3D models that were reconstructed by ContextCapture, a commercial photogrammetry software kit (Shi and Ergan, 2020; Chen *et al.*, 2020), most of the algorithms used in this study (e.g. Thermal-RGB data fusion, ANN model training, image rendering) were implemented using Python. The involved implementing libraries include Open3D (Zhou *et al.*, 2018), OpenCV (Bradski, 2000), scikit-learn (Pedregosa *et al.*, 2019), and PyRender (Matl, Mahler and Goldberg, 2017).

2.1 Photogrammetry and 3D Point Cloud Model Reconstruction

There are many approaches to detecting defects in building envelopes, such as fan pressurization (blower door test), ultrasound (tone test), and thermography. Thermography, as a non-destructive technique, is considered the most useful method because it can detect thermal values in envelopes allowing for heat loss and moisture detection. However, current thermography methods mostly focus on handheld data collection (Dino *et al.*, 2020; Yang, Su and Lin, 2018), which is not recommended for an energy audit for a group of buildings in a large district. As such, researchers have mounted thermal and RGB cameras on UASs for more efficient large district data collection.

As shown in Figure 1, the data acquisition system used in this study included the drone (DJI M600), camera (FLIR Duo Pro R), control modules, and other equipment. The DJI M600 is a state-of-the-art aerial platform designed for industrial data collection. The FLIR Duo Pro R camera has both photographic and thermal lenses integrated into a single package that enables simultaneous RGB and thermal image data collection. Additionally, the control system allows to remotely operate the drones and the FLIR camera to collect data with the desired flight altitude and camera angles.



(1) Gimbal - Connection to DJI M600; (2) Gimbal - Frame for Camera; (3) FLIR DUO Pro R – Visible Lens Barrel; (4) FLIR DUO Pro R – IR Lens Barrel; (5) FLIR DUO Pro R – Electric Wires; (6) FLIR DUO Pro R – Integration Cable; (7) FLIR DUO Pro R – GPS Antenna Cable; (8) FLIR DUO Pro R – USB Cable.

Figure 1: Cameras Setup for the Unmanned Aircraft System

After both RGB and thermal images with designed image overlapping rates were collected with the drone, images were used to reconstruct 3D point cloud models over the survey areas using the photogrammetry technique. We collected over 10,000 images for both campus and city areas. There were over 12 buildings included for these two areas. Photogrammetry is the technology for 3D modeling of physical objects such as buildings, infrastructures, and their environment through the process of measuring and interpreting overlapped images. There are many well-established photogrammetry commercial software tools. We chose to use ContextCapture since this software provides an application programming interface (API) that support further extended developments, such as extracting parameters of image-orientation estimations to indicate the relative relationships between images and reconstructed 3D models (Fischer, Dosovitskiy and Brox, 2015; Verykokou *et al.*, 2018).

Photogrammetric modeling reconstructed by aerial images can support the investigation of groups of buildings in large districts. As shown in Figure 2 (a), a 3D point cloud model of some residential buildings was reconstructed by a series of aerial RGB images. To audit the heat-related defects of these residential buildings, researchers can also reconstruct a 3D thermal model. Many current approaches directly use thermal images to build thermal-mapping models. We choose to use high-resolution RGB images to reconstruct a 3D RGB model and then project corresponding thermal information onto the RGB model to create a thermal point cloud model (Hou *et al.*, 2021), as the FLIR camera can simultaneously take thermal and RGB images from the same angle and at the same altitude. Additionally, image-orientation estimations provided by ContextCapture support the data fusion process. Figure 2 (b) represents a 3D thermal model of a group of residential buildings created based on the RGB model in Figure 2 (a). In Figure 2 (b), the dark purple color represents a lower thermal value and a lighter yellow color represents a higher value. Another example is a group of 3D models on a campus shown in Figure 2 (c) and (d).

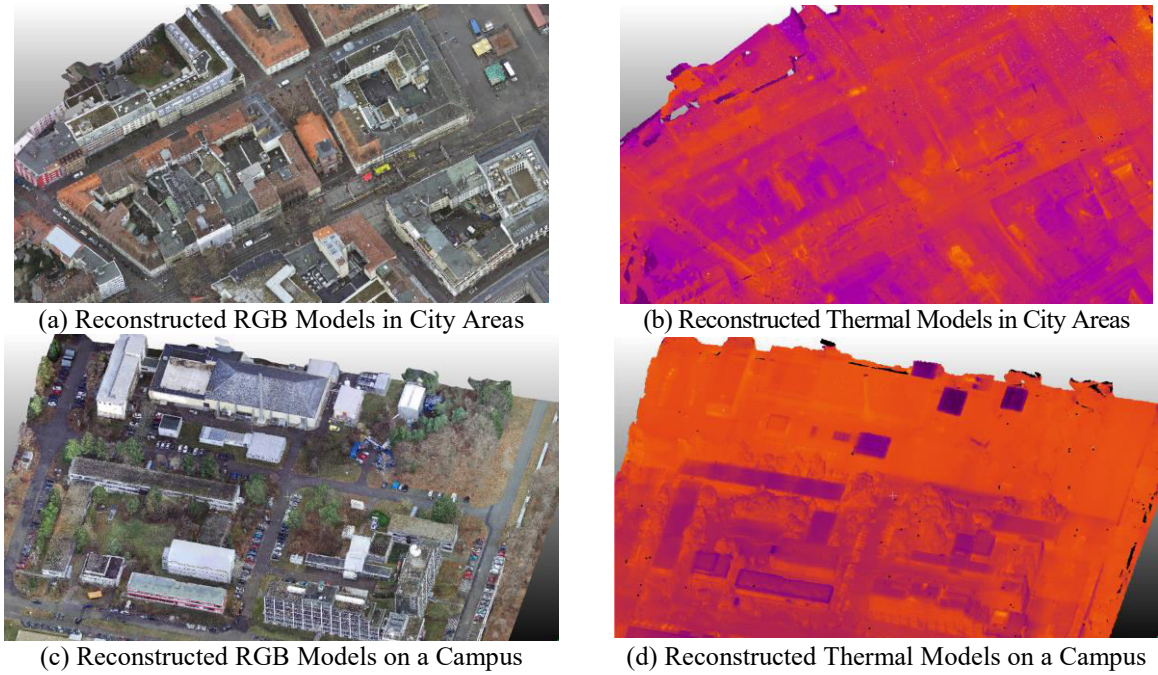


Figure 2: 3D point clouds reconstructed by overlapped images

2.2 Rendering 2D Images from a Reconstructed 3D model

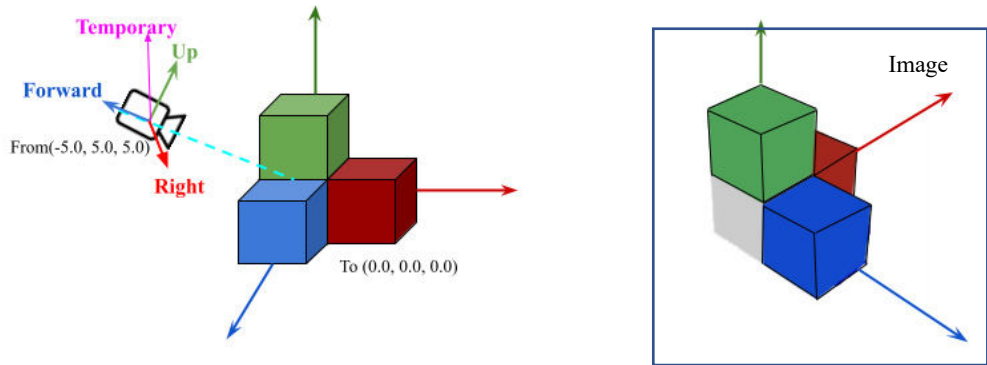
After the development of the 3D point cloud model as described in Section 2.1, the next step focus on how to use the model to audit heat loss. At this step it is important to recognize/classify door and windows elements in the model because those are the most relevant elements when auditing building façade heat loss. Therefore, in this step, we developed a process to render 2D images from the reconstructed 3D models.

We created a virtual camera in the 3D model, which was essential for rendering images that we needed to investigate. In our study, we used the perspective projection, and the default camera position was at the origin and facing the negative Z-axis. To move the camera from its origin position to a position from which the façade image can be rendered, we defined a 4x4 matrix that contains rotation and transformation information, as shown in Eq. (1).

$$\begin{bmatrix} Right_x & Right_y & Right_z & 0 \\ Up_x & Up_y & Up_z & 0 \\ Forward_x & Forward_y & Forward_z & 0 \\ T_x & T_y & T_z & 1 \end{bmatrix} \quad \text{Eq. (1)}$$

First, we defined the *Forward* vector. To set a camera position, the computer must know an initial point, which we refer to as the *From* point. To know the camera's orientation, the computer must also know the point at which the camera looks. We refer to as the *To* point. As shown in Figure 3 (a), as an example, the *From* point is (-5.0, 5.0, 5.0), and the *To* point is (0.0, 0.0, 0.0), and thus we define the *Forward* vector as $Forward = normalize(From - To)$. Next, we define the *Temporary* vector, which does not have to be precise. The typical value is (0, 0, 1). Thus, the *Right* vector is perpendicular to the space that *Forward* and *Temporary* create. Finally, Cartesian coordinates are defined by three mutually perpendicular vectors, and thus we can calculate the *Up* vector based on the *Forward* and *Right* vectors. Note that *Forward*, *Right*, and *Up* vectors are mutually perpendicular, and they are all normalized unit vectors. Therefore, a rendered image by our current camera settings can be shown in Figure 3 (b). Additionally, we need to define the transformation vector *T*, which is

$T = From - Origin$. Since the *Origin* is $(0, 0, 0)$, vector T is the coordinate of the *From* point.



(a) The Camera Aiming at a Point

(b) The Image Can Be Rendered by Such Settings

Figure 3: The Local Coordinate System of the Camera Aiming at a Point

As we have defined the 4x4 rotation and transformation matrix, we can render façade images by the given pairs of *From* and *To* points. After we selected the *From* points on streets and the *To* points inside of buildings, the façade images can be then rendered.

2.3 Training a Semantic Segmentation ANN Model

In this step, we used an open source database to train a segmentation ANN model based on different algorithms. This open source dataset is annotated into eight classes (e.g. Loft, Top, Wall, window, Shop, Door, and Balcony), which is available from the studies of Mathias, *et al.*, 2016 and Simon *et al.*, 2011 and can be freely downloaded from the webpage of *Ecole Centrale Paris Facades Database* (Teboul, 2008). The data contains 400 images for training and 100 images for testing. The images of facades are taken from different cities including Paris, Barcelona, and San Francisco, among others.

Many state-of-the-art ANN algorithms exist to train the segmentation models, including DeepLab, MaskRCNN, and Generative Adversarial Networks (GAN) (Goodfellow *et al.*, 2014). Among these algorithms, GAN can learn density distributions of imagery datasets and explore their internal representations (Hou, *et al.*, 2021). Additionally, as the detailed architecture of a GAN shows in Figure 4, the main difference between the GAN and other ANNs is that the GAN has two separated networks including a generator network and discriminator network; therefore, the GAN architecture is more flexible than other neural network approaches. The function of the discriminator network is to decide if the generated samples are similar to the ground truth samples, and the differences are calculated by the loss function. Further, the backpropagation improves the parameters in generator and discriminator networks based on the loss function. After several epochs, the samples generated by the generator network evolve from random noise to predicted results, and then the model is trained for use in testing datasets. As previously discussed, the GAN architecture is flexible. Thus, it is easy for us to replace the network architecture. We choose to use two different network architectures to build the generator network including “Resnet+9 blocks” and “Unet256”.

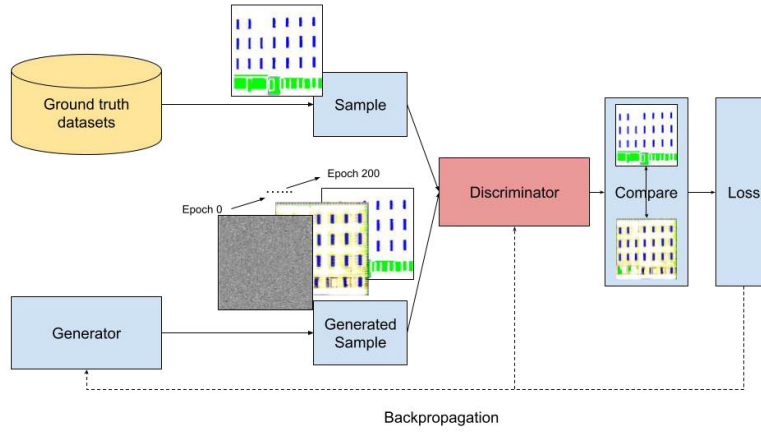


Figure 4: The Detailed Architecture of a GAN

2.4 Segmentation Results and Evaluation of the Proposed Approach

As rendering the façade images and building the semantic segmentation ANN model, we were able to use the trained model to evaluate the segmentation results of the rendered images. We applied trained ANN models (both “Resnet+9 blocks” and “Unet256” versions) on two datasets, including the campus and city areas as shown in Figure 2. As for the evaluation metrics, we chose two evaluation criteria to analyze the performance of the proposed method: (1) an accuracy analysis of the segmentation performance on the open source datasets, and (2) a performance analysis on the rendered images.

We applied four methods to evaluate the segmentation performance on images, including (1) precision, (2) recall, (3) Jaccard/intersection-over-union (IOU), and (4) the dice coefficient /F1-score, as shown in Eqs. (2-5). In these equations, TP (true positive) represents the area of overlap between the predicted segmentation and the ground truth in the images. FP (false positive) represents the areas that belong to the correct class but that the algorithms cannot recognize, and FN (false negative) represents the areas that do not belong to the correct class, but that the algorithms incorrectly recognize them do. Using TP , FP and FN , we can calculate the evaluation metrics. Precision, also known as positive predictive value, is the fraction of the correctly classified area among the actual result area in the ground truth images. Recall, also called sensitivity, is the fraction of the correctly classified pixel area among the predicted result area in the predicted images. Next, IOU, is the fraction of the correctly classified pixel area among the union areas of the actual result areas and predicted result areas. Last, F1 is a harmonic mean that combines precision and recall score.

$$Precision = \frac{TP}{TP+FP} \quad \text{Eq. (2)}$$

$$Recall = \frac{TP}{TP+FN} \quad \text{Eq. (3)}$$

$$IOU = \frac{TP}{TP+FP+FN} \quad \text{Eq. (4)}$$

$$F1 = \frac{2TP}{2TP+FP+FN} \quad \text{Eq. (5)}$$

3. Experiment

Thermography inspection needs a special experimental condition in which the temperature difference between the indoors and outdoors should be at least 10 °C (18 °F) (FLIR Systems, 2011). To meet this requirement, inspections need to be conducted in a hot summer or a cold

winter. However, the sun radiation can cause an inaccurate façade temperature measurement and further impact the cooling energy loss audits. Therefore, thermography inspection on hot days is usually conducted in early morning or late afternoon to avoid sun radiation. However, it is still difficult to guarantee the needed temperature differences during such inspection times in the summer. Considering these facts, we conducted a heat loss inspection on a college campus and in a city area during a cold winter in Karlsruhe, Germany. In collecting data for our experiments, room temperatures were higher (the average temperature was 17 °C (63 °F) for indoor spaces when the research was conducted), and the outside ambient temperatures were lower (the outdoor temperature was -5 °C (23°F) in the early morning).

The open source dataset in which the cameras were set on the ground is annotated into 8 classes. However, we only focused on two categories (doors and windows) related to the heat loss audits for this study. As shown in Figure 5, Figure 5 (a) and (e) are two examples in the open source datasets, (b) and (f) are ground truths for these two examples, (c) and (g) are segmentation results for these two examples, and (d) and (h) are segmentation results using another algorithm.

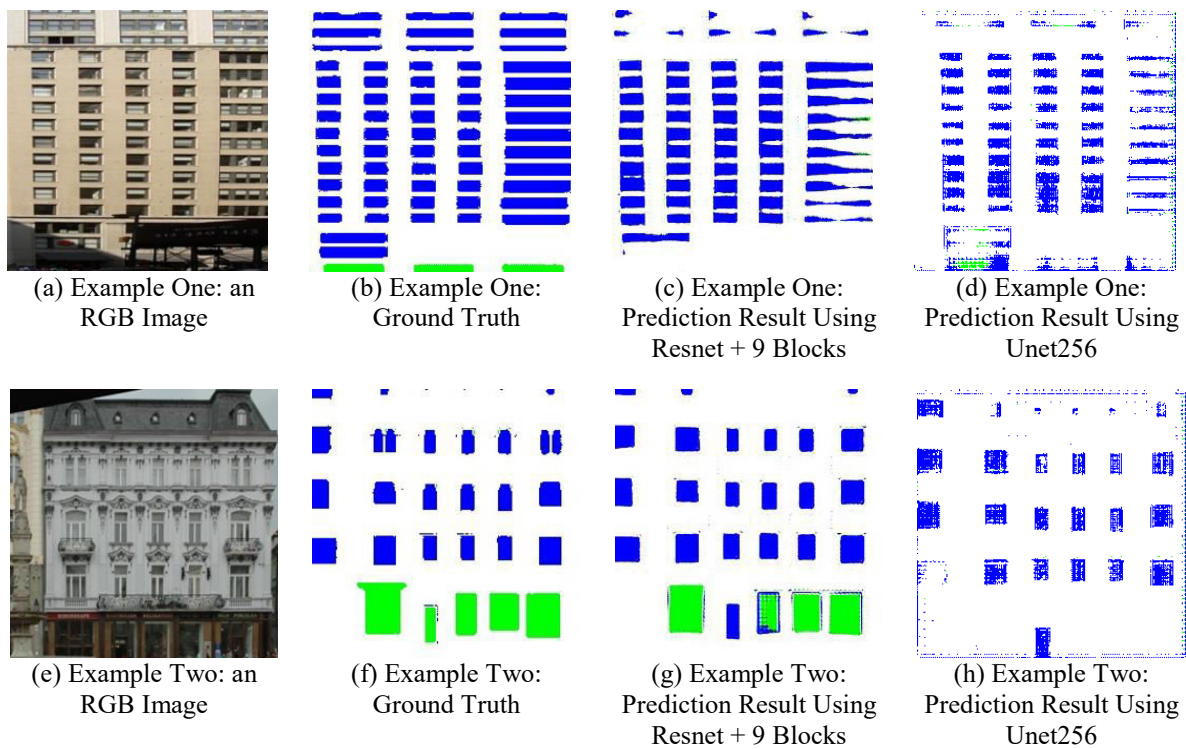


Figure 5: Building the segmentation models

For next step, we used the two segmentation models built using “Resnet” and “Unet” to predict rendered images from the 3D point cloud models. Figure 6 (a) is an example of buildings in a city area, and Figure 6 (b) is another example for the campus buildings. A virtual camera was set in the 3D model, and a façade image with its ground truth were rendered.

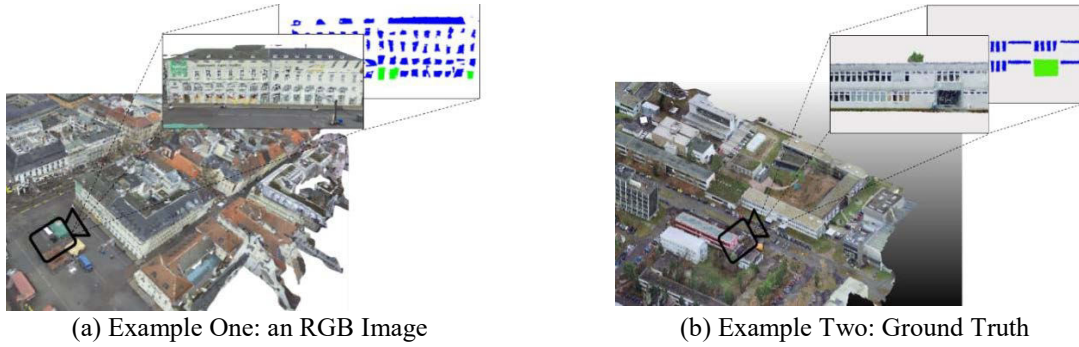


Figure 6: Segmentation on Rendered Images

4. Results and Discussion

Based on the Eqs. (2-5), we conducted accuracy analysis of the segmentation performance for the open source datasets and performance analysis for the rendered images, as shown in Figure 7. We also used the segmentation model trained by open source datasets to predict the segmentation on rendered images, and the accuracy analyses are also shown in Figure 7.

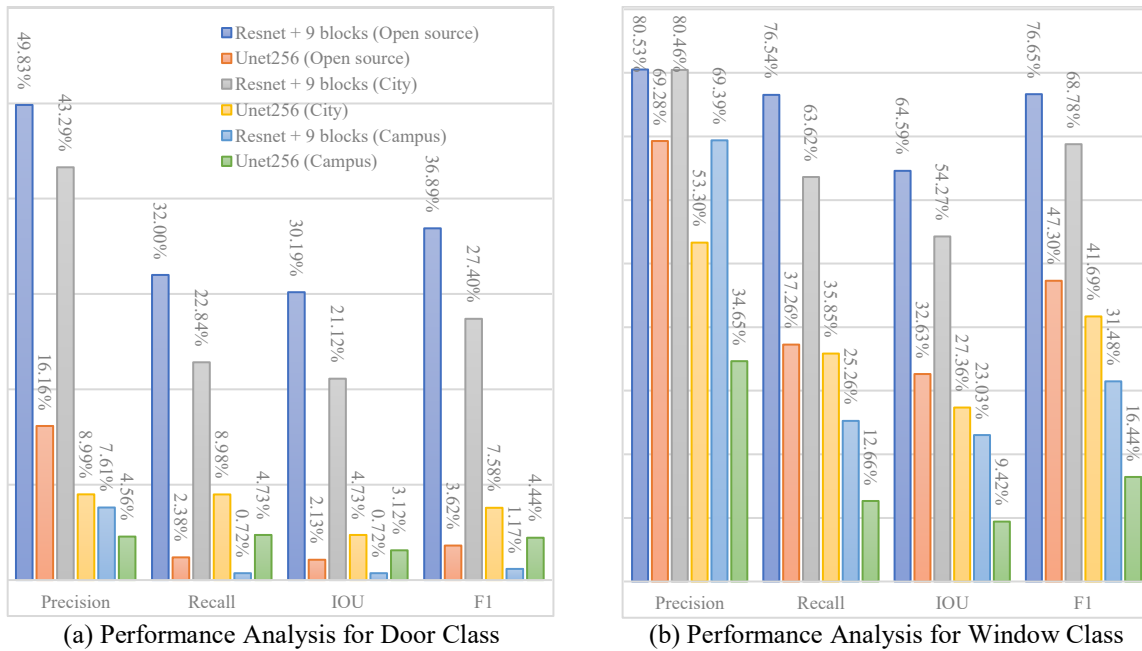


Figure 7: Segmentation Performance Analysis

We also plotted a Precision-Recall curve (PRC) as shown in Figure 8. The blue color represents “Resnet+9blocks” GAN algorithm, and red represents “Unet256” GAN algorithm. As the yellow lines shown in figure (a), the ideal test should have a PRC that passes through the upper right corner representing the 100% precision and 100% recall. In general, the closer the blue or red area is to the yellow lines, the better the performance.

There were some important findings from the results. First, as the results in Figure 7 show, “Resnet+9blocks” outperformed “Unet256” in all cases except predicting door class in rendered images from the campus datasets. Second, in general, predicting window class was more accurate than predicting door class. The blue areas are always on top of the red areas in Figure 8. This is potentially because of the unbalanced datasets. In every image in the datasets, there

were more pixels belonging to window class than pixels belonging to door class. A solution needs to be found for this unbalanced dataset issue in future studies. Third, in general, our proposed approach performed better in city datasets than in campus datasets, potentially because the building styles in the open source are closer to the styles in city datasets.

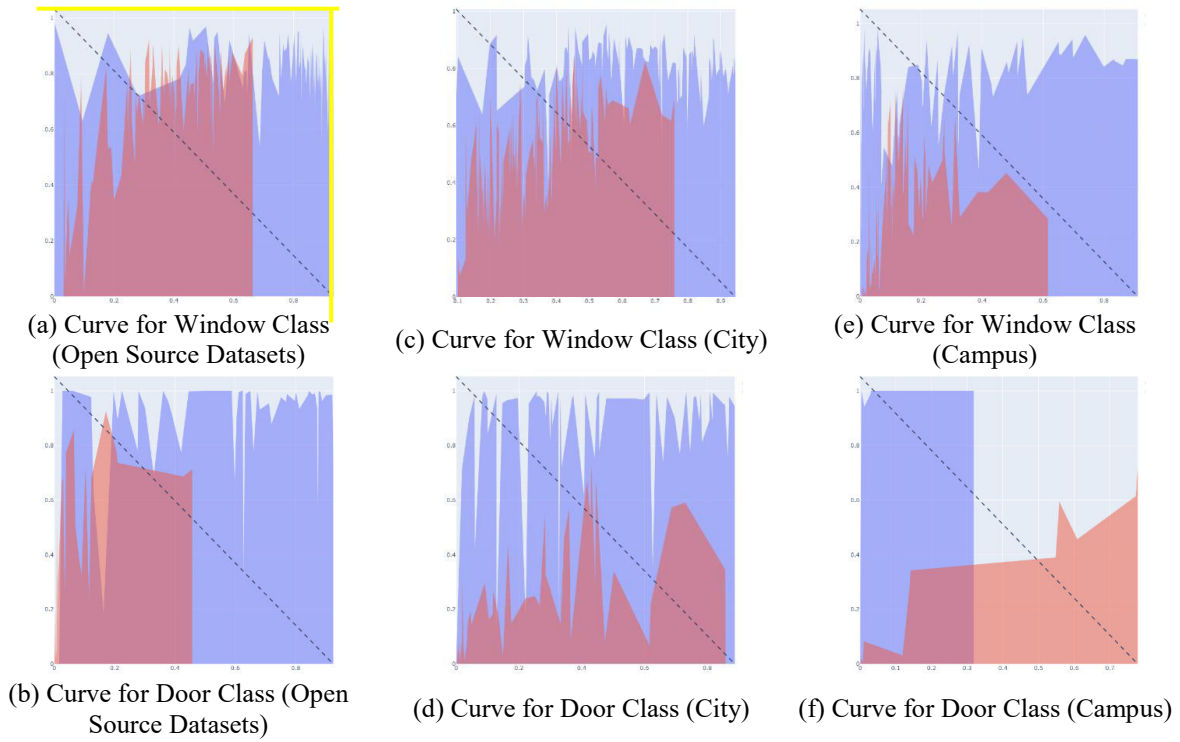


Figure 8: Precision-Recall Curve

5. Conclusion and Outlook

Our results show that a 3D point cloud model can be created using aerial images and that rendered façade images for segmentation can be successfully generated by a virtual camera in the model. As the results show, the segmentation accuracy decreases from the evaluation of the segmentation performance on the open source datasets to the evaluation of the rendered images. Particularly, the performance decreases more when using the “Unet256” algorithm. Second, the accuracy of segmenting windows is higher than segmenting doors. Finally, the results show that the accuracy of semantic segmentation is higher when the approach is conducted on buildings in a city than in a university campus. In the future, there is a need to consider the unbalanced dataset issue related to the higher incidence of windows objects when compared to door objects on existing databases. Additionally, there are two options for improving the segmentation performances; one is by improving the quality of the rendered images, and the other one is by improving the segmentation algorithms.

Acknowledgement

The authors thank the CSC (China Scholarship Council), the KIT International Department, and DAAD (Deutscher Akademischer Austauschdienst, German Academic Exchange Service) for their support. Furthermore, the authors thank Marinus Vogl and Air Bavarian GmbH, his

drone company, for their support with equipment and service. Last, the authors thank Leslie Ramos, Wenyun Lu, and Tianyou Dong for their time and effort in ground truth coding.

References

- Bradski, G. (2000) 'The OpenCV Library', *Dr. Dobb's Journal of Software Tools*.
- Chen, M. et al. (2020) 'Semantic Segmentation and Data Fusion of Microsoft Bing 3D Cities and Small UAV-based Photogrammetric Data', (20220), pp.1–12. doi: arXiv:2008.09648v1.
- Dino, I. G. et al. (2020) 'Image-based construction of building energy models using computer vision', *Automation in Construction*, 116(1). doi: 10.1016/j.autcon.2020.103231.
- Fischer, P., Dosovitskiy, A. and Brox, T. (2015) 'Image orientation estimation with convolutional networks', *German Conference on Pattern Recognition*, pp.368–378. doi: 10.1007/978-3-319-24947-6_30.
- FLIR Systems (2011) An informative guide for the use of thermal imaging cameras for inspecting buildings, solar panels and windmills. *Thermal Image Guidebook for Building and Renewable Energy Applications Content*. Available at: http://www.flirmedia.com/MMC/THG/Brochures/T820325/T820325_EN.pdf (Accessed: 13 June 2020).
- Goodfellow, I. et al. (2014) 'Generative Adversarial Nets', *Advances in neural information processing systems*, pp.2672–2680. doi: 10.1109/ICCVW.2019.00369.
- Hou, Y. et al. (2019) 'Factors affecting the performance of 3D thermal mapping for energy audits in a district by using infrared thermography (IRT) mounted on unmanned aircraft systems (UAS)', in *Proceedings of the 36th International Symposium on Automation and Robotics in Construction, ISARC 2019*, pp.266–273. doi: <https://doi.org/10.22260/ISARC2019/0036>.
- Hou, Y. et al. (2021) 'Automation in Construction Fusing tie points' RGB and thermal information for mapping large areas based on aerial images : A study of fusion performance under different flight configurations and experimental conditions', *Automation in Construction*. Elsevier B.V., 124. doi: 10.1016/j.autcon.2021.103554.
- Hou, Y., Volk, R. and Soibelman, L. (2021) 'A Novel Building Temperature Simulation Approach Driven by Expanding Semantic Segmentation Training Datasets with Synthetic Aerial Thermal Images', *Energies*, 14(2). doi: <https://doi.org/10.3390/en14020353>.
- Mathias, M., Martinović, A. and Van Gool, L. (2016) 'ATLAS: A Three-Layered Approach to Facade Parsing', *International Journal of Computer Vision*, 118(1), pp.22–48. doi: 10.1007/s11263-015-0868-z.
- Matl, M., Mahler, J. and Goldberg, K. (2017) 'An algorithm for transferring parallel-jaw grasps between 3D mesh subsegments', *IEEE International Conference on Automation Science and Engineering, 2017-Augus*, pp.756–763. doi: 10.1109/COASE.2017.8256195.
- Mayer, Z. et al. (2021) 'Thermal Bridges on Building Rooftops - Hyperspectral (RGB + Thermal + Height) drone images of Karlsruhe, Germany, with thermal bridge annotations (Version 0.1.0)', in *Zenodo*. Zenodo. doi: <http://doi.org/10.5281/zenodo.4767772>.
- Pedregosa, F. et al. (2019) 'Generating the blood exposome database using a comprehensive text mining and database fusion approach', *Environmental Health Perspectives*, 127(9), pp.2825–2830. doi: 10.1289/EHP4713.
- Shahandashti, S. M. et al. (2010) 'Data-Fusion Approaches and Applications for Construction Engineering', *Journal of Construction Engineering and Management*, 137(10), pp.863–869. doi: 10.1061/(ASCE)CO.1943-7862.0000287.
- Shi, Z. and Ergan, S. (2020) 'Towards Point Cloud and Model-Based Urban Façade Inspection: Challenges in the Urban Façade Inspection Process', *Construction Research Congress 2020*, p. 385. doi: <https://doi.org/10.1061/9780784482872.042>.

Simon, L. et al. (2011) 'Random Exploration of the Procedural Space for Single-View', *International Journal of Computer Vision*, 93(2), pp.253–271. doi: <https://doi.org/10.1007/s11263-010-0370-6>.

Teboul, O. (2008) Ecole Centrale Paris Facades Database. doi: <http://vision.mas.ecp.fr/Personnel/teboul/data.php>.

Verykokou, S. et al. (2018) 'A Photogrammetry-Based Structure From Motion Algorithm Using Robust Iterative Bundle Adjustment Techniques', *ISPRS Annals of Photogrammetry, Remote Sensing & Spatial Information Sciences*, IV(October), pp.1–2. doi: <https://doi.org/10.5194/isprs-annals-IV-4-W6-73-2018>.

Yang, M. Der, Su, T. C. and Lin, H. Y. (2018) 'Fusion of infrared thermal image and visible image for 3D thermal model reconstruction using smartphone sensors', *Sensors (Switzerland)*, 18(7). doi: [10.3390/s18072003](https://doi.org/10.3390/s18072003).

Paper E: AI-Based Thermal Bridge Detection of Building Rooftops on District Scale Using Aerial Images

This paper was reproduced in its original format with permission from Universitätsverlag der TU Berlin:

Mayer, Z., Kahn, J., Hou, Y., Volk, R. (2021 - Paper E). AI-based thermal bridge detection of building rooftops on district scale using aerial images. Proceedings of the EG-ICE 2021 Work-shop on Intelligent Computing in Engineering proceedings, Berlin, Germany (Vol. 30). Online 18.08.2021: https://www.researchgate.net/profile/Rebekka-Volk/publication/353768496_AI-based_thermal_bridge_detection_of_building_rooftops_on_district_scale_using_aerial_images/links/6110f63f1ca20f6f860ba438/AI-based-thermal-bridge-detection-of-building-rooftops-on-district-scale-using-aerial-images.pdf

AI-based thermal bridge detection of building rooftops on district scale using aerial images

Zoe Mayer M.Sc.^{a*}, Yu Hou M.Sc.^b, Dr. James Kahn^c, Dr. Rebekka Volk^a,
Prof. Dr. Frank Schultmann^a

^aKarlsruhe Institute of Technology, Germany, ^bUniversity of Southern California, USA, ^cHelmholtz AI, Karlsruhe Institute of Technology, Germany
zoe.mayer@partner.kit.edu

Abstract. Thermal bridges are weak areas of building envelopes that conduct more heat to the outside than surrounding envelope areas. They lead to increased energy consumption and the formation of mold. With a neural network approach, we demonstrate a method of automatically detecting thermal bridges on building rooftops from panorama drone images of whole city districts. To train the neural network, we created a dataset including 917 images and 6895 annotations. The images in the dataset contain thermal information for detecting thermal bridges and a height map for rooftop recognition in addition to regular RGB information. Due to the small dataset, our approach currently only has an average recall of 9.4% @IoU:0.5-0.95 (14.4% for large objects). Nevertheless, our approach reliably detects structures only on rooftops and not on other parts of buildings, without any additional segmentation effort of building parts.

1. Introduction

In 2017, building constructions and operations accounted for 36% of global final energy use worldwide and about 40% of energy-related carbon dioxide emissions (GlobalABC, 2018). Thermal energy is a particularly relevant component of this: more than a half of current global household energy use is for space and water heating (IEA, 2014). In addition to high energy standards for new buildings, the energy retrofit of old buildings plays an important role. While new construction adds annually 1% or less to the existing building stock, the other 99% of buildings already existed in the year prior (Power, 2008).

To develop energy-saving approaches for existing buildings in cities, strategies on different aggregation levels can be considered: at the single building scale, the district scale, and the full-city scale. The district scale, the intermediate level between the city and the building scale, is coming increasingly into the focus of building science and urban transition planning. The main strengths of the district scale for the building energy retrofit are summarized by Riechel (2016): Compared to measures for single buildings, measures for whole districts provide the possibility of cost digressions and other economies of scale for energy improvements. For example, the planning and implementation of retrofit measures such as the purchase of retrofit material can be cheaper for a large demand in a small area at the same time. Compared to the city scale, the closeness between habitants and building owners contributes to neighborhood-dynamics in districts. Informal communication among neighbors ("neighborhood gossip") or the copying of a building retrofit in the neighborhood by other owners can have benefits for implementing energy improvement measures. (Riechel, 2016)

There are approaches to systematically use the advantages of the district scale to push urban transition and the retrofit of buildings. One of the most frequently practical and standardized approaches in this field is from Germany called "energetisches Quartierskonzept" (EQ). It describes a policy plan that intends to improve the energy quality of private and public buildings and the energy infrastructure of a whole city district. So far, more than 1,000 EQs have been financially supported by the German government (BES, 2020).

To identify districts with a high need for energy retrofits and to develop effective measures for substantially improving the energy quality of a district, an initial thermal quality analysis of existing buildings is necessary. Currently, such analyses on district scale are expensive and time consuming (Riechel et al., 2016; Neußer, 2017). Therefore, approaches that allow for automatic and simplified analyses are crucial for a higher efficiency of EQs and other retrofit planning approaches.

With the help of unmanned aerial vehicles (UAV, drones), it is possible to collect thermal panorama images of many buildings from different angles with relatively little effort and cost but with a high resolution. A distinction is made between quantitative and qualitative thermography. In quantitative thermography, absolute temperatures are measured as precisely as possible. The process is highly dependent on environmental parameters, the infrared camera used, and the qualifications of the thermography staff. Qualitative thermography, on the other hand, is simpler. It focuses on temperature distributions and differences. Thermal bridges in particular can be easily identified in qualitative images. (Volland et al., 2016)

A thermal bridge is an area of the building envelope that conducts heat easily, thus transporting heat from the warmer inside to the colder outside faster than it does through the adjacent areas. This is caused by different thermal conductivities of used materials or the geometry of constructions. Air leaks can also be subsumed under the term thermal bridge (Schmidt and Windhausen, 2018). Thermal bridges cause high energy losses which can make up to one third of the transmission heat loss of an entire building. Additionally, they lead to the collection of moisture, which in the long term degrades the building fabric or causes mould. A thermal bridge can be seen on a thermographic image as an area with an increased thermal radiation relative to adjacent areas. (Schild, 2018).

2. Research approach

In this study, we analyse how drone-based thermal images can be used for a simple analysis of the thermal quality of building envelopes on district scale. To do so, we investigate the quality of thermal panorama images obtained by drones and analyse how artificial intelligence can help to automatically detect thermal bridges. We focus on thermal bridges on rooftops as they are difficult to access with conventional thermography from terrestrial images.

To motivate our research, we first provide an overview about which publications and studies are known to us in the field of automated computer vision approaches to detect thermal bridges of buildings. We focus on studies that work with imagery data obtained by non-stationary recording approaches - especially with drones - suitable for recording images on district scale.

In the main part of our work, we demonstrate a method to automatically detect thermal bridges on building rooftops in thermal aerial images using a neural network. We employ existing solutions from the domain of object detection to learn to identify the size and location of thermal bridges within each image. For this, we create a dataset of drone images with annotations of thermal bridges on building rooftops. Each image of the dataset consists of a combination of a thermal image, an RGB¹ image recorded from the same angle and converted to the same format, and height information for each pixel (Hou et al., 2021 - a). We select a training dataset for the neural network composed of a subset of the images, and validate our results on the remainder of the dataset.

¹ Red, Green, Blue

3. Related work

Non-stationary thermography with the help of cars and drones for the analysis of buildings is becoming increasingly important in thermography studies. The advantage of drones compared to terrestrial methods is that the entire envelope of buildings (including rooftops) can be thermographically assessed. In addition, the influence of facade covering (e.g. by trees or pedestrians walking past) is less prevalent from the bird's eye view.

Publications in the field of automated thermal bridge detection from thermal images obtained with non-stationary cameras are from Garrido et al. (2018), Macher et al. (2020), Martinez-de Dios and Ollero (2006), and Rakha et al. (2018). To automatically detect thermal bridges these publications work with different threshold approaches for temperature differences in the images. They record close-up images of single buildings from different angles, but do not work with panorama images that cover multiple buildings. Moreover, they use small datasets to validate their approaches and do not focus on entire districts. Garrido et al. (2018) place an infrared camera on the roof of a vehicle to record images at an angle of 45°. The proportion of unrecognized or incorrectly declared thermal bridges is 32% for a test set of three images. Macher et al. (2020) also install their infrared camera on a vehicle and conclude being able to reliably detect thermal bridges between floors and under balconies. No quantitative information is given on the precision of the used algorithm. Martinez-de Dios and Ollero (2006) use a thermal camera placed on a drone helicopter. According to the authors this approach is suitable for detecting thermal bridges on windows. The study lacks precise quality information for evaluating the results. Rakha et al. (2018) also use a drone with a thermal camera to record close-up images of buildings from the air. They state the overall precision of their algorithm of about 75%.

As thermal panorama images contain many different buildings from changing angles and infrastructure in between (e.g. trees, trams, cars, streets, street lights) classic threshold approaches appear unsuitable for the automatic detection of thermal bridges. This is because thermal bridges change in shape from different angles and high temperature differences often occur on objects in the image which are not buildings. For successful thermal bridge detection on panorama images deep learning approaches are very promising, as complex objects such as buildings, certain building parts on that thermal bridges occur (e.g. rooftops), and various thermal bridge types with different shapes can be recognized.

A recent study by Kim et al. (2021) works with a deep learning approach to detect thermal bridges from terrestrial thermographic images. The study uses a method including thermal anomaly area clustering, feature extraction, and an artificial-neural-network-based thermal bridge detection. The average precision of the detection of thermal bridges is for eight test images 89%. However, the images used are close-ups of buildings and cannot be compared to panorama images. To the best of our knowledge there is no study that aims to detect thermal bridges in an entire district on thermal panorama images using deep learning approaches.

4. Dataset

Our dataset of Thermal Bridges on Building Rooftops (TBRR dataset) consists of combined RGB and thermal panorama drone images with a height map (Figure 1). The raw images for our dataset were recorded with a normal (RGB) and a FLIR-XT2 (thermal) camera on a DJI M600 drone. We converted all images to a uniform format of 2400x3200 pixels. They contain RGB, thermal, and GPS information as well as flight altitudes (between 60-80m above ground). The GPS and flight altitude information were used to reconstruct a 3D model out of

the 2D images to create the height map. We hypothesize that this will significantly simplify the task of learning to ignore street-level sections of the images and focus instead on rooftops.

The drone images show parts of the Karlsruhe city centre, east of the market square. The recorded area can be divided into six large city blocks of around 20 buildings per block. Because of a high overlap rate of the images, the same buildings are on average about 20 times on different images, recorded from different angles. The dataset contains a total of 5698 images before preselection. During preselection, all images containing no thermal bridges were filtered out, as well as images that are blurred due to rapid turns or other fast movements of the drone. A total of 917 images remain after preselection.

All images were recorded during a drone flight on March 19, 2019 from 7 a.m. to 8 a.m. At this time, temperatures were between 3.78°C and 4.97°C , humidity between 80% and 98%. There was no rain on the day of the flight, but there was $2.3\text{mm}/\text{m}^2$ 48 hours beforehand.² For recording the thermographic images an emissivity of 1.0 was set. The global radiation during this period was between $38.59\text{ W}/\text{m}^2$ and $120.86\text{ W}/\text{m}^2$, hence the solar radiation was high enough to visually classify the geometric and structural conditions on the RGB images, but not so high that the surface temperatures of thermal bridges and surrounding components change significantly, thus making it difficult to identify thermal bridges. No direct sunlight can be seen visually in any of the recordings.



Figure 1: Drone images of the city centre of Karlsruhe used for the TBBR dataset A) thermal image B) RGB image C) image with height information (height map)

The annotated images of the TBBR dataset contain a total of 6895 annotations. The annotations only include thermal bridges that are easily identifiable, and thus also include thermal bridges that are not annotated. Because of the image overlap each thermal bridge is annotated on average about 20 times from different angles. An example image with annotations is shown in Figure 2. We have published the dataset with further information in Mayer et al. (2021).

² The total absence of moisture can therefore not be fully guaranteed. Moisture falsifies the recording of thermographic images. We recognized puddles on some flat rooftops and removed corresponding images from the dataset during the preselection process; otherwise we could not detect any significant moisture visually on the RGB images.

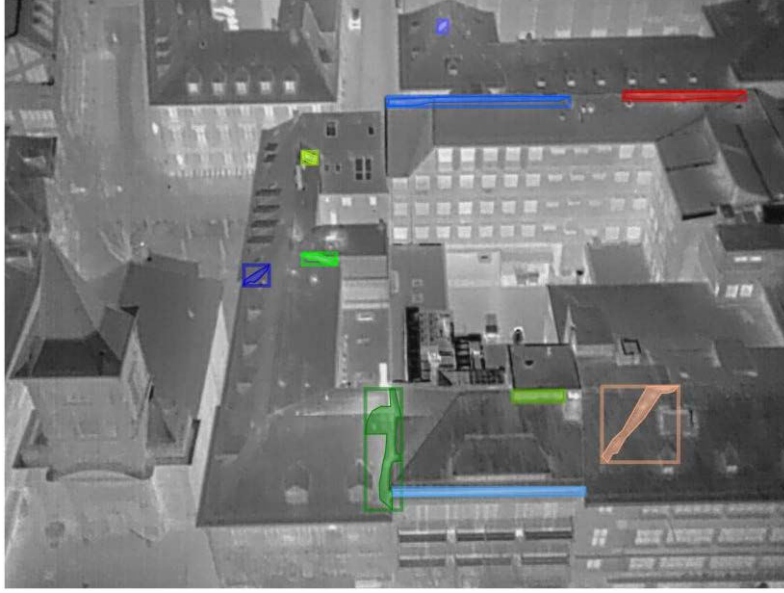


Figure 2: Example of thermal bridge annotations in the TBBR dataset for the example shown in Figure 1. Colours are only for clarity and do not have any other meaning.³

5. Experimental procedure

5.1 Data pre-processing

To prepare the datasets, we align thermal images and height images onto RGB images via a process called image registration (Hou et al., 2021 - a). Since on the collected images, fisheye effects occur (called radial distortion) and the lens is not aligned parallel to the imaging plane (called tangential distortion), we must resolve these two distortions before image registration.

Distortions can be solved by $x_{corr,rad} = x(1 + k_1r^2 + k_2r^4 + k_3r^6)$

$-y_{corr,tang} = y + [p_1(r^2 + 2y^2) + 2p_2xy]$). In these equations, (x, y) represents a point before correction, and (x_{corr}, y_{corr}) represents a point coordinate after correction. Many collected pairs of coordinates of (x, y) and (x_{corr}, y_{corr}) from a collection of calibration images enable the calculation of the distortion coefficients $(k_1, k_2, k_3, p_1, p_2)$. The coefficients (k_1, k_2, k_3) are radial distortion coefficients and (p_1, p_2) are tangential distortion coefficients.

$$x_{corr,rad} = x(1 + k_1r^2 + k_2r^4 + k_3r^6) \quad (1)$$

$$y_{corr,rad} = y(1 + k_1r^2 + k_2r^4 + k_3r^6) \quad (2)$$

$$x_{corr,tang} = x + [2p_1xy + p_2(r^2 + 2x^2)] \quad (3)$$

$$y_{corr,tang} = y + [p_1(r^2 + 2y^2) + 2p_2xy] \quad (4)$$

After undistorting all images, we aligned thermal and height images onto the RGB images using $[x_{thermal}, y_{thermal}] = T_{RGB \rightarrow thermal} * [x_{RGB}, y_{RGB}] - [x_{thermal}, y_{thermal}] =$

³ The borders of the thermal bridge annotations show a slight distortion. The reason for this lies in the data pre-processing and is explained and discussed in more detail in Section 7.

$T_{height \rightarrow thermal} * [x_{height}, y_{height}]$. In these equations, $T_{RGB \rightarrow thermal}$ and $T_{height \rightarrow thermal}$ represent transformation matrices that transform pixels from RGB images to thermal images and pixels from height images to thermal images.

$$[x_{thermal}, y_{thermal}] = T_{RGB \rightarrow thermal} * [x_{RGB}, y_{RGB}] \quad (5)$$

$$[x_{thermal}, y_{thermal}] = T_{height \rightarrow thermal} * [x_{height}, y_{height}] \quad (6)$$

Lastly, we connected the registered thermal and height images to the RGB images to produce single 5-channel images (RGB + thermal + height).

5.2 Neural network details

To identify thermal bridges, we employed a neural network to perform object detection and segmentation. Formally, the task is defined as follows: given a set X containing input images $x_i \in R^{N*H*W*C}$, with image height H , width W , and channels C ; and a corresponding annotation set Y containing bounding boxes $y_{i,box} \in R^{N*4}$, where 4 represents the coordinates of the box's four corners, class labels $y_{i,cls} \in R^N$, and masks $y_{i,mask} \in R^{N*H*W}$, where N is the number of annotated object in the given image; learn the mapping $F: X \rightarrow Y$, where F denotes a neural network.

In this work the neural network is the Mask R-CNN framework (He et al., 2017) with a ResNet-18 (He et al., 2016) backbone implemented in the Detectron2 software package (Wu et al., 2019). We select this architecture for two key reasons: firstly, the ResNet architecture has consistently proven to perform at state-of-the-art (SOTA) levels (e.g. as in Bello et al. (2021)); and secondly, self-supervised training methods offer a means of achieving SOTA performance with limited labelled samples. The latter point is discussed further in section 7 and motivates the use of a neural network over classical approaches.

Figure 3 shows the basic structure of Mask R-CNN. It consists of two stages: the first uses a Region Proposal Network (RPN) to propose candidate regions of interest (ROI); the second uses a (convolutional) backbone to extract features which are then used to perform object classification and bounding box regression, as well as prediction of a binary segmentation mask. The former is performed via fully connected layers on the extracted features, while the latter uses further convolutional layers. In practice, learned features are shared by both stages to speed up processing.

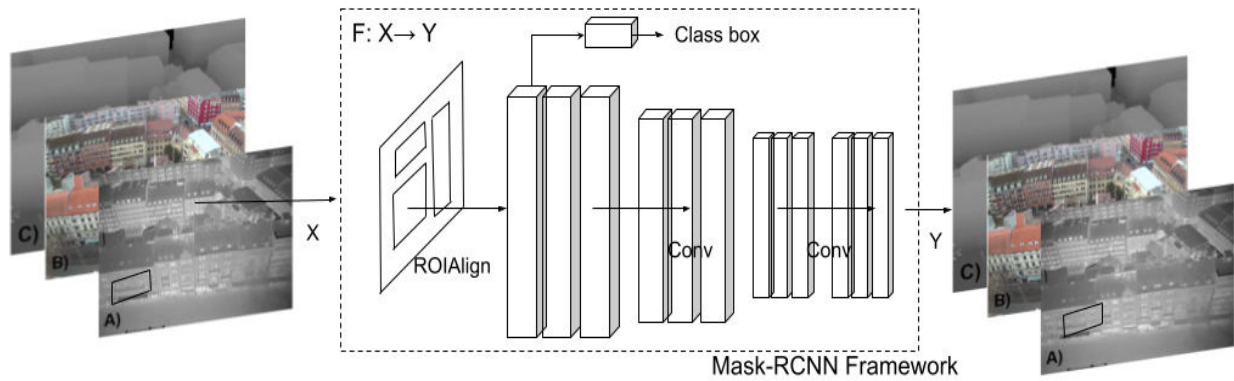


Figure 3: The Mask R-CNN framework

Mask R-CNN uses a multi-task loss on every proposed region of interest: $L = L_{cls} + L_{box} + L_{mask}$. L_{cls} is the categorical cross-entropy loss across $K + 1$ output predictions for K component classes, plus an additional catch-all class for proposed regions containing only background. L_{box} is the bounding box regression (mean squared error) over the predict box corners. L_{mask} is the average binary cross entropy across all pixels in the mask. These are described in further detail in He et al. (2017). Note that for the experiments reported in this work we use a single annotation class (i.e. $K=1$).

The dataset images were split into 717 training images and 200 test images corresponding to five and one of the city blocks described in the section above, respectively. Training was performed for 30,000 iterations at a batch size of eight, with random weight initialisation (i.e. no pre-training). The remaining hyper-parameter configurations were set to the Detectron2 defaults for the “mask_rcnn_R_50_FPN_3x_gn” model from the Detectron2 model zoo templates, with only changes the number of ResNet layers (18) and the pixel value means (130, 135, 135, 118, 118) and standard deviations (44, 40, 40, 30, 21) for (B, G, R, thermal, height) used by Detectron2 to normalise the inputs. These values were calculated from the full set of training images.

6. Results

To evaluate the performance of our training, we use the Average Recall (AR) metric, defined as:

$$AR = \frac{TP}{TP+FN} \quad (7)$$

where TP and FN refer to the number of true positive and false negative object predictions, respectively. The AR measures the probability of objects in an image being detected. Since not every thermal bridge in the dataset is annotated, we do not report any metrics that work with false positives (such as Average Precision). These metrics are guaranteed to underperform as even correctly predicted thermal bridges will be reported as false positives if the corresponding annotation does not exist.

To determine which predicted bounding boxes correspond to correct predictions, the Intersection-over-Union (IoU) is measured between the predicted and ground truth boxes as:

$$IoU = \frac{area(predicted \cap true)}{area(predicted \cup true)} \quad (8)$$

For a given IoU threshold, predicted bounding boxes that have an IoU with an annotated thermal bridge’s bounding box above the threshold are considered true positives. Any annotated thermal bridges without a prediction satisfying this are considered false negatives. Table 1 shows the metric scores for various common variants of the AR metric. An IoU range (i.e. $IoU=0.5:0.95$) indicates the AR is averaged over the given interval. An area of medium or large corresponds to objects of area between 32^2 and 96^2 , and greater than 96^2 pixels, respectively. Max. detections indicates the score given the N highest confidence predictions⁴.

We note immediately the comparatively low scores, which we attribute to the low number of annotated examples relative to the large image sizes and sparsity/small size of thermal bridges. Notably, the network performs better at larger scales, which is likely due to larger

⁴Although often reported in object detection tasks, we do not report small (less than 32^2 pixels) thermal bridges as the smallest present in our dataset is 55^2 pixels.

thermal bridges being less ambiguous with regards to non-thermal bridge heat spots in an image.

An interesting result, however, is the location of predicted thermal bridges, regardless of their accuracy. All predictions are on or overlapping with rooftops, indicating the network has an awareness of sensible locations for thermal bridges. We find that this result is consistent across all test images. We posit that this is due to the inclusion of the height map as a signal to the neural network of where to look for thermal bridges. We plan to perform further ablation studies to confirm this.

Given the dataset was produced by a single fly over of six city blocks, some portions of the test dataset images are also present in the training images from different angles. In these instances we note that the neural network has overfitted those thermal bridges and predicts them with at or near 100% confidence. Nonetheless, the network is able to identify thermal bridges unique to the test dataset, albeit with lower confidence and IoU. We expect this to improve with the training techniques discussed in the next section.

Table 1: Bounding box regression metrics on the test images dataset

Metric	Area	Max. detections	Score
AR @ IoU=0.50:0.95	All	1	0.052
AR @ IoU=0.50:0.95	All	10	0.142
AR @ IoU=0.50:0.95	All	100	0.142
AR @ IoU=0.50:0.95	Medium	100	0.114
AR @ IoU=0.50:0.95	Large	100	0.196

7. Discussion

The Average Recall achieved is not currently suitable for thermal bridge detection; however it does provide a baseline score for prediction with a modern computer vision approach directly on the TBDR dataset. This represents a departure from previous approaches which relied on complex multi-stage solutions (as in Rakha et al. (2018)) or fine-tuning of clustering and feature extraction preprocessing steps (as in Kim et al. (2021)).

A key limitation in this work is the comparatively small number of images available for training. This is due to the time required to manually annotate each image. While we used a total of 917 images, common benchmarks often contain hundreds of thousands (e.g. COCO) or even tens of millions (e.g. Imagenet) of images.

We therefore plan to implement a self-supervised pretext task to maximise the use of collected images. Specifically, we intend to utilise the work from Hou et al. (2021 - b) to first train a neural network to predict thermal images from RGB and use these predicted images, along with the real thermal and the height information, as input to the Mask R-CNN network. This approach is similar to that of the Split-Brain Autoencoder described by Zhang et al. (2017). We hypothesise that the predicted thermal images will be nearly identical to the real thermal images, with only the thermal bridges missing⁵, thus simplifying the network’s task significantly to learn to locate the appropriate differences between the two. If successful, this

⁵ The assumption here is that thermal bridges are only visible from the thermal image, which is of course the original motivation for including thermal images in this project in the first place.

would allow full use of all (non-blurry) drone images captured, not only those on which the laborious task of annotation has been performed.

In order to increase the size of the dataset, it is also possible to use panorama images collected from other sources. Since our approach is based on qualitative thermography, the weather conditions and temperatures when recording new images do not have to be identical to the existing dataset (Volland et al., 2016). However, the temperature contrast of new annotated thermal bridges should be high enough to detect, which is the case when there is a difference of more than 10°C between indoor and outdoor temperatures. The distances of the drone to the buildings can also vary, however thermal images with more than 20m distance to the measurement object should be checked in all individual cases for appropriate quality (Fouad and Richter, 2012).

8. Conclusion

We have reported an overall average recall of 14.2% at IoU:0.5-0.95, and 19.6% at IoU:0.5-0.95 for large thermal bridges. We demonstrated the ability of the neural network to propose predictions in reasonable locations (i.e. rooftops only) which we posited is due to the addition of height information to the input images. While this work has shown a promising first result in identifying individual thermal bridges from drone images, we believe there is still significant potential for improvement to be made using a self-supervised pretext task to maximise the information obtain from the entire set of collected images.

This work focuses on a cost-effective and scalable approach to assess thermal bridges using thermographic images from drones. In future, we intend to use financial and environmental criteria to estimate which buildings in a district the retrofit of thermal bridges is recommended and when buildings should be retrofitted more extensively.

Acknowledgements

This project was performed during a PhD project that is financed with a scholarship according to Landesgraduiertenförderungsgesetz (LGFG), the State Graduate Promotion Act, of the Karlsruhe Institute of Technology (KIT). This work is supported by the Helmholtz Association Initiative and Networking Fund, the Helmholtz AI platform grant, and the HAICORE@KIT partition. Furthermore, we thank Marinus Vogl and the Air Bavarian GmbH for their support with equipment and service for the recording of images and Tobias Beiersdörfer who supported us with the development of the TBBR dataset.

References

- Begleitforschung Energetische Stadtsanierung (BES) (2020): 3. Fachkonferenz der Begleitforschung zum KfW-Förderprogramm Energetische Stadtsanierung Energiewende im Quartier (English: 3rd specialist conference of the accompanying research to the KfW funding program ‘Energy transition in districts’). Berlin.
- Bello, I. et al. (2021). Revisiting resnets: Improved training and scaling strategies. arXiv preprint arXiv:2103.07579.
- Garrido et al. (2018). Thermal-based analysis for the automatic detection and characterization of thermal bridges in buildings. *Energy and Buildings*, 158, 1358–1367. Doi: <https://doi.org/10.1016/j.enbuild.2017.11.031>

- Global Alliance for Buildings and Construction (GlobalABC) (2018). 2018 Global Status Report Towards a zero-emission, efficient and resilient buildings and construction sector. ISBN No: 978-92-807-3729-5.
- He, K. et al. (2017). Mask r-cnn. In Proceedings of the IEEE international conference on computer vision (pp.2961–2969).
- He, K. et al. (2016). Deep residual learning for image recognition. In Proceedings of the IEEE conference on computer vision and pattern recognition (pp.770–778).
- Hou, Y. et al. (2021 - a). Automation in Construction Fusing tie points - RGB and thermal information for mapping large areas based on aerial images: A study of fusion performance under different flight configurations and experimental conditions', Automation in Construction. Elsevier B.V., 124. Doi: 10.1016/j.autcon.2021.103554.
- Hou, Y. et al. (2021 - b). A Novel Building Temperature Simulation Approach Driven by Expanding Semantic Segmentation Training Datasets with Synthetic Aerial Thermal Images. Energies, 14(2). Doi: <https://doi.org/10.3390/en14020353>
- International Energy Agency (IEA) (2014). Energy technology perspectives 2014: Harnessing electricity's potential. OECD/IEA.
- Kim, C. et al. (2021). Automatic Detection of Linear Thermal Bridges from Infrared Thermal Images Using Neural Network. Applied Sciences, 11(3), 931. Doi: <https://doi.org/10.3390/app11030931>
- Macher, H. et al. (2020). Automation of Thermal Point Clouds Analysis for the Extraction of Windows and Thermal Bridges of Building Facades. The International Archives of Photogrammetry, Remote Sensing and Spatial Information Sciences, 43, 287–292. Doi: <https://doi.org/10.5194/isprs-archives-XLIII-B2-2020-287-2020>
- Martinez-De Dios, J. R., and Ollero, A. (2006, July). Automatic detection of windows thermal heat losses in buildings using UAVs. In 2006 world automation congress (pp.1–6). IEEE. Doi: 10.1109/WAC.2006.375998
- Mayer, Zoe, Hou, Yu, Kahn, James, Beiersdörfer, Tobias, & Volk, Rebekka. (2021). Thermal Bridges on Building Rooftops - Hyperspectral (RGB + Thermal + Height) drone images of Karlsruhe, Germany, with thermal bridge annotations (Version 0.1.0) [Dataset]. Zenodo. <http://doi.org/10.5281/zenodo.4767772>
- Neußer, W. (2017). Energetische Quartierssanierung - Ausblick und externe Rahmenbedingungen. (English: District energy improvement - outlook and external conditions.) Information zur Raumentwicklung, 4/2017. BBSR.
- Power, A. (2008). Does demolition or refurbishment of old and inefficient homes help to increase our environmental, social and economic viability. Energy Policy 2008;36: 4487–4501. Doi: <https://doi.org/10.1016/j.enpol.2008.09.022>
- Rakha, T. et al. (2018). Heat mapping drones: an autonomous computer-vision-based procedure for building envelope inspection using unmanned aerial systems (UAS). Technology| Architecture+ Design, 2(1), 30–44. Doi: <https://doi.org/10.1080/24751448.2018.1420963>
- Ren, S. et al. (2016). Faster R-CNN: towards real-time object detection with region proposal networks. IEEE transactions on pattern analysis and machine intelligence, 39(6), 1137–1149. arXiv:1506.01497
- Riechel, R. (2016). Zwischen Gebäude und Gesamtstadt: das Quartier als Handlungsraum in der lokalen Wärmewende. (English: Between the building and the city as a whole: the district as field for action in the local heat transition.) Vierteljahrshefte zur Wirtschaftsforschung, 85(4), 89–101.
- Schild, K. (2018). Wärmebrücken: Berechnung und Mindestwärmeschutz. (English: Thermal bridges: Calculations and minimum requirements) Springer-Verlag. Doi: 10.1007/978-3-658-20709-0
- Schmidt P. and Windhausen S. (2018) Bauphysik-Lehrbuch. (English: Building physics) Bundesanzeiger Verlag, Köln. Doi: https://doi.org/10.1007/978-3-658-21749-5_3-1
- Volland J. et al. (2016). Wärmebrücken: erkennen-optimieren-berechnen-vermeiden. (English: Thermal bridges: recognize-optimize-calculate-avoid) 1. Auflage 420 Seiten Verlagsgesellschaft Rudolf Müller GmbH & Co. KG, 978-3-481-03365-1 (ISBN).

Wu Y. et al. (2019). Detectron2.

Zhang, R., Isola, P., & Efros, A. A. (2017). Split-brain autoencoders: Unsupervised learning by cross-channel prediction. In Proceedings of the IEEE Conference on Computer Vision and Pattern Recognition (pp.1058–1067).

Paper F: Deep Learning Approaches to Building Rooftop Thermal Bridge Detection from Aerial Images

This paper was reproduced in its original format with permission from Elsevier:

Mayer, Z., Kahn, J., Hou, Y., Götz, M., Volk, R., Schultmann, F. (2022 - Paper F). Deep learning approaches to building rooftop thermal bridge detection from aerial images. *Automation in Construction*. Doi: <https://doi.org/10.1016/j.autcon.2022.104690>



Deep learning approaches to building rooftop thermal bridge detection from aerial images

Zoe Mayer^{a,*}, James Kahn^{a,b}, Yu Hou^c, Markus Götz^{a,b}, Rebekka Volk^a, Frank Schultmann^a

^a Karlsruhe Institute of Technology (KIT), Karlsruhe, 76131, Germany

^b Helmholtz AI, Germany

^c Carnegie Mellon University (CMU), USA

ARTICLE INFO

Keywords:

Building analysis
Thermal bridges
Drones
Deep learning
Computer vision
Object detection

ABSTRACT

Thermal bridges are weak points of building envelopes that can lead to energy losses, collection of moisture, and formation of mould in the building fabric. To detect thermal bridges of large building stocks, drones with thermographic cameras can be used. As the manual analysis of comprehensive image datasets is very time-consuming, we investigate deep learning approaches for its automation. For this, we focus on thermal bridges on building rooftops recorded in panorama drone images from our updated dataset of Thermal Bridges on Building Rooftops (TBBRv2), containing 926 images with 6,927 annotations. The images include RGB, thermal, and height information. We compare state-of-the-art models with and without pretraining from five different neural network architectures: MaskRCNN R50, Swin-T transformer, TridentNet, FSAF, and a MaskRCNN R18 baseline. We find promising results, especially for pretrained models, scoring an Average Recall above 50% for detecting large thermal bridges with a pretrained Swin-T Transformer model.

1. Introduction

The emissions of carbon dioxide (CO₂) from the operation of buildings have increased to their highest level yet to around 27% of total global energy-related CO₂ emissions [1]. Thermal energy is particularly pertinent as more than half of global household energy use is for space and water heating [2]. A common reason for heat losses of buildings are thermal bridges. Thermal bridges are areas of the building envelope with low thermal resistance that conduct heat faster from the warmer inside to the colder outside than adjacent areas. Reasons for this are the geometry of constructions, different thermal conductivities of used materials, or air leaks of the building envelope. Energy losses caused by thermal bridges can make up to one third of the transmission heat loss of an entire building [3]. Moreover, they may lead to dampness and mould growth, which in the long term degrades the building fabric and is associated with health concerns caused by poor indoor air quality. For buildings inhabitants, thermal bridges also can lead to uncomfortable spaces due to cold interior surfaces [4,5].

To detect thermal bridges, thermography is currently the state-of-the-art [6]. Recording thermographic images with a terrestrial camera is a method that has been used for building audits and thermal bridge detection for many years [7]. Classical terrestrial thermography,

though, lacks the ability to record rooftops or other parts of high buildings inaccessible from the ground [8]. Moreover, manually recorded thermographic images are not suitable for efficiently analysing the thermal quality of multiple buildings within a short time due to the time-consuming nature of the method and property rights, which only allow the capturing of street-views without owner permissions to enter properties [9,10]. The analysis of many buildings at urban scales, however, is becoming increasingly in demand. Examples include the development of retrofit plans for whole city districts like Community Energy Strategic Planning in the USA [11], Community Energy Planning in Canada [12], Positive Energy Districts in Europe [13], and “energetische Quartierskonzepte” in Germany [14].

To use thermography in urban environments, Unmanned Aerial Vehicles (UAVs, drones)¹ can be used for the scalable and automated recording of building images [8]. In this work, we compare the ability of five popular, state-of-the-art neural network architectures to automatically detect thermal bridges in aerial panorama images obtained using drones. In doing so, we also investigate the benefits of utilising additional height map information. We focus exclusively on thermal bridges of building rooftops as they can be exceptionally well captured from the aerial perspective. To perform this investigation, we utilise open-source computer vision libraries and analyse an updated Thermal

* Corresponding author.

E-mail addresses: zoe.mayer@partner.kit.edu (Z. Mayer), james.kahn@kit.edu (J. Kahn).

¹ Sometimes referred to as Unmanned Aerial Systems (UAS) that also include a drone pilot and the controlling system.

Bridges on Building Rooftops (TBBRv2). We have made the dataset, code, and all neural network configurations used in this work publicly available on Zenodo [15] and <https://github.com/Helmholtz-AI-Energy/TBBRDet>.

2. Related work

Non-stationary thermography with automated thermal bridge detection software has been investigated to speed up and simplify the process of building audits for large building stocks. In 2018, Garrido et al. [16] performed a study where they placed an infrared camera on the roof of a vehicle to record images of a building facade at an angle of 45°. They used an automatic detection approach and characterised thermal bridges based on geometric properties, measured temperature differences, and the calculation of the thermophysical properties of the linear heat transfer. The proportion of false positive detected thermal bridges was 45%, the proportion of missing thermal bridges was 32%, and the dataset used to evaluate the methodology only includes three images shown in the publication. Macher et al. [17] also installed an infrared camera on a vehicle. They intended to detect windows and thermal bridges by taking geometric and thermal characteristics into account and by modelling a thermographic 3D point cloud. For identification they used an iterative histogram approach to analyse global and local temperature maxima. They were able to reliably detect thermal bridges between floors and under balconies, and most windows could also be recognised automatically. The authors stated that windows located on the ground floor or basement are difficult to extract due to the limited field of view of the camera. Windows behind plants or objects cannot be detected in this way either. No quantitative information was given on the precision of the used algorithm.

A disadvantage of thermography with terrestrial vehicles is that no rooftops and only low facades facing the street can be analysed. Drones overcome this limitation. Due to their almost unlimited mobility, the entire outer envelope of a building can be recorded. In addition, the interference due to facade covering by e.g. trees or pedestrians walking past is reduced. Therefore, research is increasingly focusing on non-stationary thermographic audits by drones. Dios and Ollero [18] attempted to automatically detect and quantify heat losses through windows after a thermographic survey of buildings with a drone helicopter. They created heat maps of thermal images and defined a temperature difference of more than 7 °C to the facade as a criterion for a thermal bridge. Thermal irregularities were then classified according to their temperature distributions. This approach was suitable for detecting thermal bridges on windows, however it lacked the precise quantitative information for evaluating the results. Furthermore, this approach is not suitable for a fully automated evaluation. Rakha et al. [19] used a drone with a thermal camera to visually identify areas of thermal anomalies on building envelopes. They worked with a manual temperature thresholding approach and automatic edge filtering to generate a 3D model of a building with its detected thermal bridges. They state the overall precision of their algorithm of about 75%. Mirzabeigi and Razkenari [20] used thermographic cameras installed on a drone to collect close-up images from building sites. They designed a drone flight path for data collection and implemented a computer vision algorithm working with a dynamic thresholding approach to identify thermal anomalies of the building envelope. The study lacks in quantitative information on the quality of the thermal anomaly detection approach.

In all the aforementioned non-stationary thermography studies, thresholding and histogram approaches were applied. While they are applicable to close-up images, they encounter problems in panorama settings, which record multiple buildings and infrastructure in between with varying angles. There is a high likelihood of falsely identify thermal bridges coming from thermal anomalies in the background of buildings or to miss true thermal bridges with irregular shapes due to the varying recording perspectives. To detect thermal bridges only on buildings or specific building parts, like rooftops, a segmentation step

to extract the building or building parts from the rest of the image is usually required, which is computationally expensive for images covering large areas such as a city district.

Supervised learning methods can aid in improving thresholding approaches. Utilising manually annotated training data, they are able to generalise and automatically annotate thermal bridges in previously unseen aerial images. Recently, Barahona et al. [21] used a camera on a car vehicle to detect thermal anomalies on building envelopes, such as thermal bridges, trained on 2000 labelled infrared images. They achieved a precision score of 89.2% and recall of 75.6% on a test dataset of 1184 infrared images. They used supervised learning with a linear model for panorama images to identify those containing anomalies, but segmented the anomalies and particular building components manually in a second, non-trained step to complement their results. Kim et al. [22] focused on terrestrial thermographic images and employed a neural network approach to detect thermal bridges. The study used a multi-step method including thermal anomaly area clustering, feature extraction, and an artificial-neural-network for thermal bridge detection. The average precision and recall of the detected thermal bridges for eight test images was 89% and 87%, respectively. However, the images used in the study are also close-ups of buildings and not panorama images.

Studies using deep learning approaches to detect thermal bridges on aerial thermographic panorama images are not known to the authors. In this study, we present deep learning neural network based approaches for detecting thermal bridges on panorama drone images on rooftops without building part segmentation. In doing so, we build on a previous publication [23] in which the authors presented the first results of the AI-based detection of thermal bridges on rooftops. To maximise the quality of our automated thermal bridge detection results, we use and compare multiple neural network architectures with and without pretraining on an open access dataset.

3. Methods and materials

3.1. Dataset

The dataset used in this study is an updated version of Thermal Bridges on Building Rooftops (TBBRv2) [15], consisting of five channels which are combined RGB² and thermal panorama drone images with a height map. Fig. 1 shows the RGB, thermal, and height map channels of an example image. The raw images for the dataset were recorded early in the morning in March 2019 in the inner city of Karlsruhe, Germany. All images are panorama images that, in addition to the actual objects of interest (buildings), also show the surrounding environment and infrastructure, such as streets, people, cars, trams, and trees.

The recorded area contains six large city perimeter blocks of roughly 20 buildings per block. Each building appears in the dataset around 20 times from different angles due to a high overlap rate during the recording process. The images were recorded with a normal (RGB) and a FLIR-XT2 (thermal) camera on a DJI M600 drone and are converted to a constant format of 2680 × 3370 pixels. Each image contains GPS information and flight altitudes (between 60–80 m above ground).

TBBRv2 contains 926 panorama images and annotations of 6927 thermal bridges on rooftops, split into train and test subsets. The training subset covers five building blocks recorded on 723 images with 5614 annotations, the test subset covers one building block recorded on 203 images with 1313 annotations. The updated TBBRv2 dataset provides more precise annotations due to better overlaps of the five information channels. These annotations only include thermal bridges that are visually clearly identifiable by experts, and thus also include thermal bridges that are not annotated due to being unclear. Because of

² RGB (Red Green Blue) images contain an information channel for each colour.

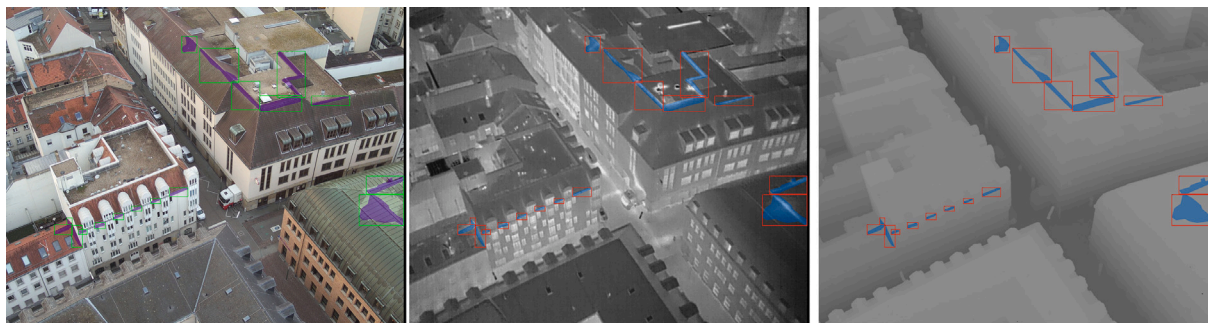


Fig. 1. Example annotations from the TBBRv2 dataset for RGB (left), thermal (centre), and height map (right).

image overlap, each thermal bridge is annotated on average about 20 times from different angles. The original TBBR dataset was published on Zenodo [24], full details of the image recording and dataset creation procedure can be found in Mayer et al. [23].

3.2. Object detection libraries

For the experiments in this paper, two popular computer vision libraries were used: Facebook AI Research's Detectron2 (v0.6) [25] and OpenMMLab's MMDetection (v2.21.0) [26]. Both of these libraries offer a framework within which object detection neural networks can be implemented, evaluated, and visualised. Our intention is to utilise popular, open-source libraries which offer ready-to-use, state-of-the-art (SOTA) object detection neural network architecture implementations. Given the significantly larger choice of object detection model implementations available in MMDetection, this library was used as the main implementation platform for the performed experiments in this work. Detectron2 was used only for comparing the results of this study to former results achieved with the TBBRv1 dataset [23]. There is otherwise no significant difference between the two libraries' capabilities.

3.3. Neural network architectures

While the specific implementations of object detection architectures varies, they predominantly follow the same procedure of first extracting meaningful features from the input image, and then translating these into task-specific predictions. Specifically, one can divide the components into a *backbone* to extract meaningful representations (feature maps) from the image pixels, a *neck* which is commonly used to further extract features for handling objects of different sizes/scales within the image (feature pyramid), and a *head* which uses the extracted features to make the output predictions [27]. In addition, there is generally a region proposal mechanism, which selects specific regions of interest within an image for the head to focus its predictions on. How these components are arranged and implemented in practice we will refer to as the framework.

For the first experiments in this work, performed using Detectron2, a MaskRCNN framework [28] with a ResNet-18 (R18) [29] backbone is used.³ This is chosen for a direct comparison with that of Mayer et al. [23].

For the second experiments using MMDetection, of the implemented frameworks and backbones available, we consider only those with available pretrained models, as is required in our experiments. We first select a MaskRCNN with a ResNet-50 (R50) backbone for our baseline. The MaskRCNN R50 is a standard baseline comparison in object detection tasks. We then selected the following for comparison with the baseline: Swin-T Transformer [30], TridentNet [31], and Feature

Selective Anchor-Free (FSAF) [32], with the explanation for each choice detailed in the following.

Transformer-based computer vision networks have outperformed popular object detection and instance segmentation benchmarks in recent years. In particular, the Shifted Windows (Swin) Transformer [30] and its variants, such as the Swin-V2 [33] and DINO [34], have dominated the popular Common Objects in Context (COCO) [35] object detection and instance segmentation benchmarks. In this work, the Swin-T transformer is tested as an alternative backbone for the MaskRCNN, which is roughly equivalent in size to a ResNet-50. An illustration of a Swin Transformer architecture is shown in Fig. 2.

Given the angled view of building rooftops in TBBRv2, the dataset contains different sized instances of same thermal bridges across multiple images. The TridentNet [31] architecture attempted to adapt the standard ResNet backbone of the Faster-RCNN framework [36] to be scale-aware.⁴ We hypothesise that this will offer an advantage over the regular convolutions used in the baseline model.

The FSAF [32] model is a near-SOTA, single-shot, anchor-free framework, which unlike the Mask/FasterRCNN-based approaches, does not separate the region proposal and feature extraction stages. This has the advantage of removing the dependence on anchor boxes, whose predefined sizes will determine which objects in an image are processed at which scale (which feature map they are associated with). As with the scale-awareness issue that TridentNet attempts to address, this anchor dependence causes the same thermal bridge object, captured at different distances across multiple images, to be redundantly processed by different feature maps within the network. FSAF instead allows the model to dynamically learn the most appropriate feature map.

4. Experimental procedure

The experiments in this work are divided into two parts: first we demonstrate, using Detectron2, the performance improvements due to the updated TBBRv2 dataset and investigate the benefits of the height map inputs, then, using MMDetection, we explore the various object detection frameworks outlined in Section 3.3 to determine the optimal model and performance. An example of the experiment workflow for the pretrained MaskRCNN R50 baseline from MMDetection is shown in Fig. 3. In line with Mayer et al. [23], Average Recall (AR) scores averaged over the intersection over union (IoU) range 0.5 to 0.95 on the test set are used to assess model performance. The AR score is defined as the ratio of correctly identified thermal bridges to all present thermal bridges. The IoU ranges which define what is considered an identified thermal bridge follow those of the commonly used COCO benchmark for object detection [35]. The reported AR score in all cases is that with

³ The 18 in ResNet-18 here indicates the number of convolutional layers within the neural network.

⁴ Scale-awareness means that a model is able to recognise the same object at different scales (sizes) in an image as being the same object, rather than learning each size as its own individual object.

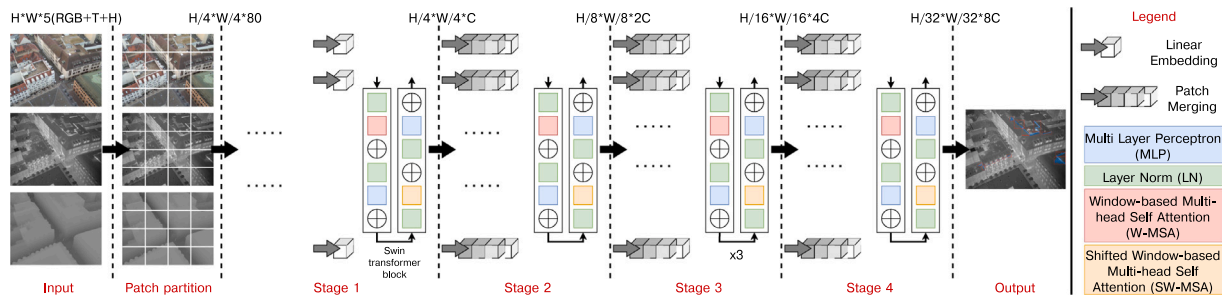


Fig. 2. Swin architecture overview. The input image is divided in 4×4 patches, which are then projected into a linear embedding and passed through successive Swin transformer blocks and patch merging layers until the final output representation of the image which is used to produce thermal bridge predictions. Image adapted from Liu et al. [30], where full details of each component can be found.

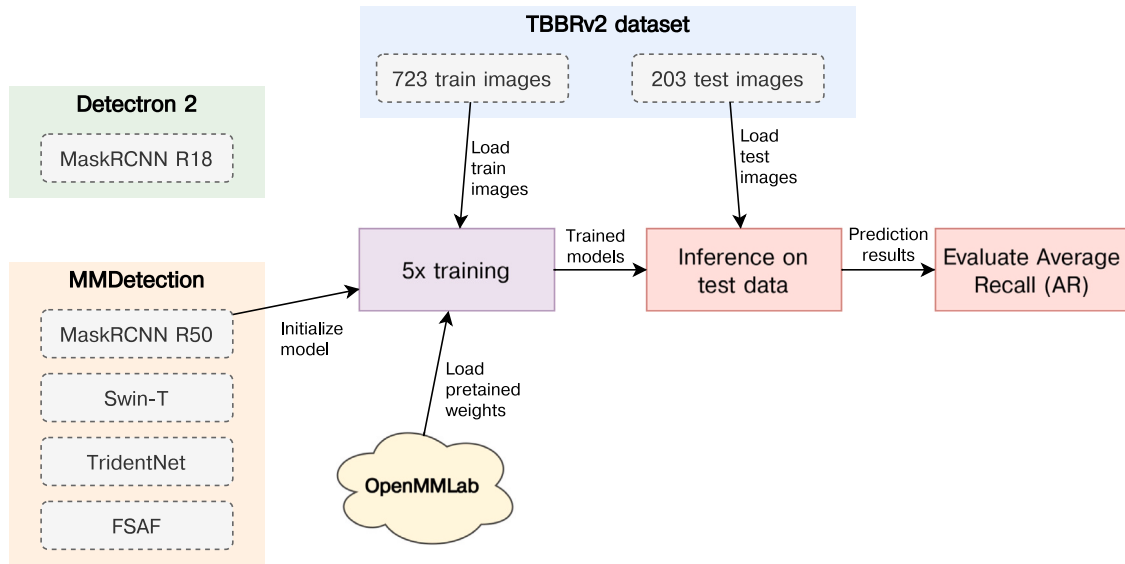


Fig. 3. Example experiment workflow for a pretrained MaskRCNN R50.

the highest AR for the top 100 detections per image (AR@100) across all training epochs. As the Average Precision (AP) penalises finding unannotated but correct thermal bridges, this metric is unsuitable for the TBBR dataset and not used here.

Five trainings are performed for each architecture tested, and the results are used to produce a mean and standard deviation.⁵ We set the following five (randomly chosen) seeds to initialise the neural network weights, listed here for reproducibility: 3000, 10 117, 10 001, 20 770 001, 1 008 111. The same five seeds are used for all architecture trainings. The deterministic flag of MMDetection is also enabled in all experiments to maximise reproducibility. In all cases, the same pixel mean and standard deviation input normalisations are used as in Mayer et al. [23].

All trainings are performed on a single node of the HoreKa super computing system, located at Karlsruhe Institute of Technology (KIT), with four NVIDIA A100 40 GB GPUs in a data-distributed [37] manner. The nodes are reserved exclusively for each individual training and we report the total computing time and energy consumption [38] of the nodes used during training. Full details of all training configurations, along with the code used for training and evaluation, can be found at <https://github.com/Helmholtz-AI-Energy/TBBRDet>. Node hardware specifications are shown in Table A.3.

⁵ While five trainings is not enough for a statistically significant standard deviation, this does provide a useful insight into the fluctuation in performance due to the random seed.

4.1. Detectron2 experiments

The experiments begin with an investigation into the improvements given by the updated alignments in TBBRv2. For this, the MaskRCNN R18 is configured according to Mayer et al. [23], running with the random seed used in that work (56689614). We follow this up with an ablation study in which we remove the height map data from the inputs. All other hyperparameters⁶ are kept fixed, and the five random seeds described above used to estimate the variance in performance. Our aim is to investigate the benefit of height map information in ensuring predicted thermal bridges are located only on building rooftops and not on street level.

4.2. MMDetection experiments

In these experiments, a baseline model is trained using the MMDetection library. For this, the MaskRCNN framework with a ResNet-50 backbone is used. The baseline is trained both from scratch and using pretrained models from the MMDetection model zoo, trained on the popular computer vision benchmark Common Objects in Context (COCO 2017) [35]. The COCO dataset contains scenes with everyday objects in their regular context. We use it as model pretraining for two

⁶ Hyperparameters are all parameters used to configure the architecture and training procedure that are not derived during the training itself. For example the number and type of layers in the network architecture, the random initialisation seeds, etc.

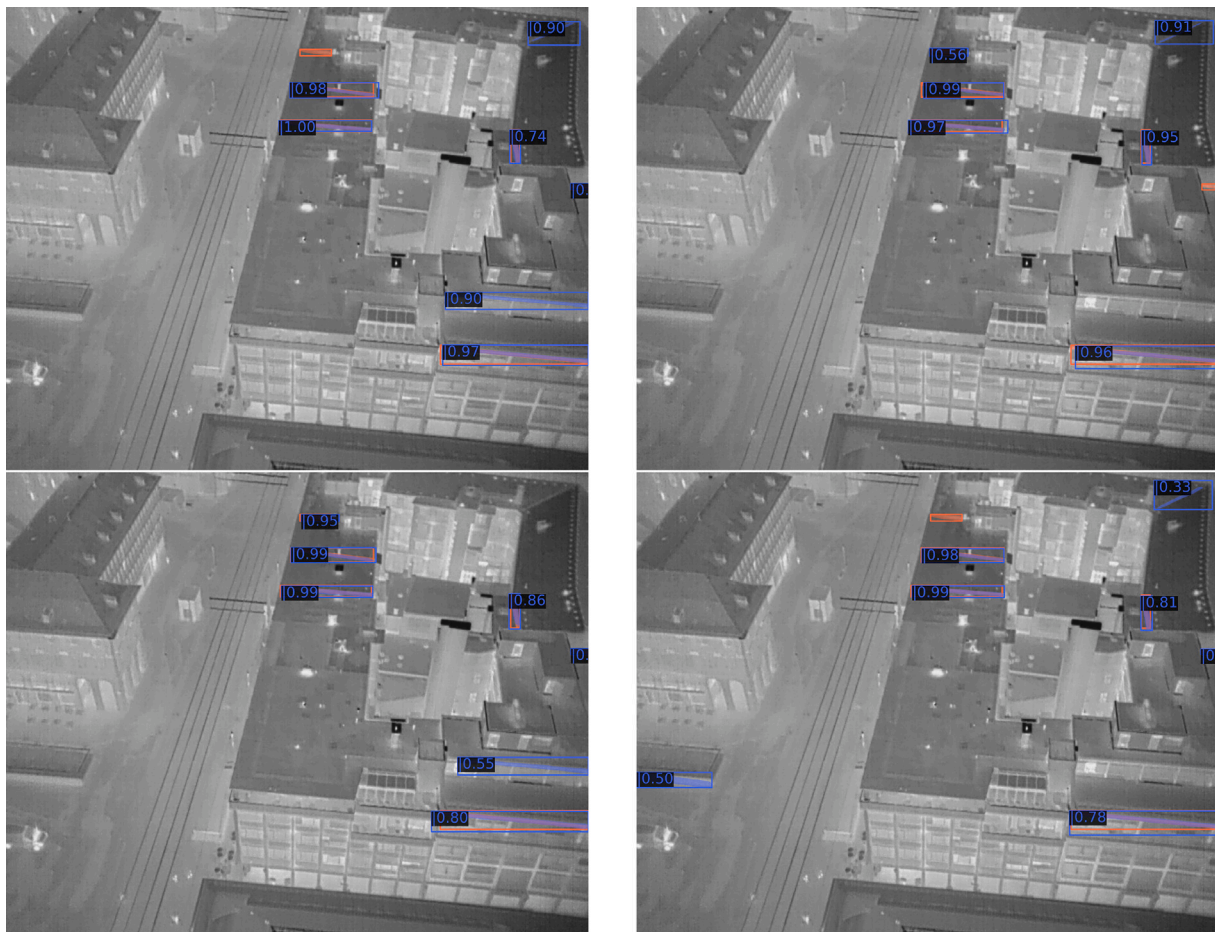


Fig. 4. Example predictions from MaskRCNN R50 baselines, numbers show model prediction scores. Left predictions are based on trainings from scratch and right predictions are based on trainings with pretraining. The top row shows predictions based on trainings with the full RGB + Thermal + Height inputs and bottom based on trainings of the RGB + Thermal ablation study.

reasons: first, OpenMMLab provides COCO pretrained versions of all models implemented in MMDetection, enabling accessible reproduction of our work, and second, the large corpus of everyday objects requires identifying edges, colour changes, etc., which, when finetuned on TBBRv2, we expect will transfer well to identifying thermal bridges on objects.

Using the baseline, the height map ablation study performed with Detectron2 is repeated. Based on both of these experiments' results, we determine the utility of the height map inputs, and proceed with training several other MMDetection architectures for comparison with the baseline.

Given the lack of a validation subset in TBBRv2, for all MMDetection-based experiments we forego hyperparameter optimisation, instead using the model configurations as-is wherever reasonably possible, making changes only to accommodate for the image sizes and extra input channels of our dataset. In particular, for multi-scale trainings, i.e. where inputs images are randomly resized as a form of data augmentation, we adjust the scales to their equivalent from our image sizes. All models are trained for a maximum of 36 epochs. In cases when the memory consumption exceeds that of the GPUs used (e.g. for the Swin Transformer), we use FP16 half precision⁷ (floating point 16) for the neural network weights. According to the benchmarks of mixed precision trainings provided by MMDetection [26], this has a negligible impact on overall performance.

⁷ IEEE 754-2019 [39] compliant binary representation of floating numbers using 16 bits, 1 for the sign, 5 for the exponent and 11 for the significant.

5. Results and discussion

In the following, we present the results of all experiments. We note here that these results are qualitative, in that they allow one to deduce thermal bridge locations and sizes across a large area. Due to high distances (>20 m) and varying recording angles of the drone relative to the buildings, a precise quantitative measurement of the thermal bridges cannot be made [40]. The interpretation of detected thermal bridges, e.g. for characterising them in terms of their risk of mould formation, energy losses, retrofit costs, or retrofit benefits, must be performed in a further step, for example using the methods presented by Mayer et al. [41].

Test results for the bounding box and segmentation AR scores, total node energy consumption in Megajoules (MJ) [38], and computing time in minutes are shown in Tables 1 and 2. We report the AR scores according to the standard object detection COCO benchmark [35]. The total AR is averaged across an Intersection-over-Union (IoU) between the predicted and ground truth thermal bridges of 0.5 to 0.95, at different numbers of top-N (by prediction confidence) predictions: 1, 10, and 100 predictions. An additional score separation into medium (AR_m) and large (AR_l) objects is also given, for objects with an area between 32² and 96² pixels and greater than 96² pixels, respectively. The scores for small detection regions (less than 32² pixels) are not shown as they contain no thermal bridges. In the following subsections interpretations are given for the results of each architecture.

Table 1

Energy usage and bounding box Average Recall scores for each model's training. The ablation column indicates whether height information was excluded from the input. The MaskRCNN R18 architectures were trained using Detectron2. MaskRCNN R18* indicates the model initialised with random seed 56689614, used by Mayer et al. [23]. The best results are marked in bold.

Architecture	Pretrained	Ablation	Energy (MJ)	Time (min)	AR@1	AR@10	AR@100	AR_m@100	AR_l@100
MaskRCNN R18*			20.5	205.5	0.060	0.169	0.169	0.119	0.250
MaskRCNN R18			20.00 ± 0.20	205.3 ± 0.5	0.061 ± 0.002	0.165 ± 0.007	0.166 ± 0.006	0.129 ± 0.007	0.227 ± 0.010
		✓	19.42 ± 0.10	199.7 ± 0.6	0.060 ± 0.005	0.170 ± 0.010	0.170 ± 0.010	0.130 ± 0.020	0.230 ± 0.010
MaskRCNN R50			3.00 ± 0.03	39.5 ± 0.6	0.072 ± 0.008	0.270 ± 0.020	0.308 ± 0.008	0.270 ± 0.020	0.380 ± 0.010
	✓		2.83 ± 0.01	35.6 ± 0.4	0.076 ± 0.008	0.310 ± 0.020	0.370 ± 0.010	0.350 ± 0.020	0.420 ± 0.010
		✓	2.91 ± 0.03	38.1 ± 0.4	0.060 ± 0.010	0.260 ± 0.040	0.304 ± 0.007	0.280 ± 0.020	0.350 ± 0.020
	✓	✓	2.74 ± 0.01	34.5 ± 0.4	0.068 ± 0.004	0.290 ± 0.030	0.360 ± 0.020	0.350 ± 0.020	0.400 ± 0.020
Swin-T			7.90 ± 0.10	125.3 ± 1.3	0.069 ± 0.003	0.239 ± 0.007	0.318 ± 0.004	0.290 ± 0.010	0.370 ± 0.010
	✓		7.09 ± 0.03	107.3 ± 1.9	0.089 ± 0.006	0.380 ± 0.020	0.454 ± 0.007	0.430 ± 0.010	0.507 ± 0.007
TridentNet			4.92 ± 0.08	57.7 ± 1.0	0.031 ± 0.003	0.140 ± 0.010	0.215 ± 0.007	0.160 ± 0.010	0.311 ± 0.010
	✓		4.70 ± 0.10	51.9 ± 0.8	0.060 ± 0.010	0.210 ± 0.040	0.300 ± 0.050	0.220 ± 0.050	0.420 ± 0.070
FSAF			10.20 ± 0.09	103.7 ± 0.3	0.049 ± 0.008	0.150 ± 0.020	0.248 ± 0.008	0.223 ± 0.006	0.300 ± 0.010
	✓		10.00 ± 0.10	102.2 ± 0.3	0.070 ± 0.010	0.270 ± 0.020	0.380 ± 0.010	0.370 ± 0.020	0.410 ± 0.020

Table 2

Segmentation Average Recall scores for each model's training. As both FSAF and TridentNet are object detection architectures only and do not perform instance segmentation, they have no scores to report. Note that the FSAF and TridentNet are object detection frameworks and hence only predict bounding boxes. MaskRCNN R18* indicates the model initialised using the seed 56689614 used by Mayer et al. [23]. The best results are marked in bold.

Architecture	Pretrained	Ablation	AR@1	AR@10	AR@100	AR_m@100	AR_l@100
MaskRCNN R18*			0.040	0.094	0.094	0.069	0.134
MaskRCNN R18			0.037 ± 0.003	0.086 ± 0.002	0.086 ± 0.002	0.067 ± 0.004	0.119 ± 0.006
		✓	0.036 ± 0.001	0.089 ± 0.003	0.090 ± 0.003	0.073 ± 0.008	0.118 ± 0.004
MaskRCNN R50			0.047 ± 0.005	0.179 ± 0.008	0.201 ± 0.009	0.190 ± 0.010	0.225 ± 0.008
	✓		0.047 ± 0.005	0.190 ± 0.020	0.219 ± 0.008	0.217 ± 0.006	0.230 ± 0.020
		✓	0.041 ± 0.009	0.160 ± 0.020	0.191 ± 0.009	0.190 ± 0.010	0.210 ± 0.020
	✓	✓	0.040 ± 0.003	0.180 ± 0.030	0.220 ± 0.020	0.230 ± 0.020	0.220 ± 0.030
Swin-T			0.046 ± 0.002	0.153 ± 0.005	0.206 ± 0.004	0.203 ± 0.006	0.220 ± 0.007
	✓		0.054 ± 0.004	0.230 ± 0.020	0.280 ± 0.010	0.280 ± 0.010	0.280 ± 0.020

5.1. Detectron2 experiments

Comparing the bounding box average recall (AR@100) of the MaskRCNN R18* from Table 1 with that reported in Mayer et al. [23] of 9.4% (14.4% for large regions), we see an almost doubling of the performance. Given all else was equal, we can attribute this improvement to the improved annotations in TBBv2 alone. Looking then at the training of the same model with the five random seeds, we see that they are relatively consistent with the MaskRCNN R18* result. We also observe that the ablation study results without height information are in agreement with those using the full RGB + Thermal + Height inputs, though we do note several falsely predicted thermal bridges on ground-level in the ablation trained model. Given there are only a small number of ground-level predictions, and that there appears to be no significant changes to the overall AR scores, we would therefore expect such false predictions to disappear given a larger training dataset. This is important, as the height map creation procedure used [42] is non-trivial, and therefore an obstacle to the ease of use of the preprocessing during the training procedure.

An interesting finding in the trainings using Detectron2 is the high energy consumption used during training. This was primarily due to extensive training times, which we found difficult to reduce, even when leveraging many dataloader processes to minimise data-loading times. While further expert optimisations are certainly possible to bring this down, we regard this result as a rather significant point against the ease-of-use factor when considering the Detectron2 library.

5.2. MaskRCNN R50 baseline

In all metrics, we observe agreement between the full and ablation trainings without height information. This holds for both trainings from scratch and those using a pretrained model. Fig. 4 shows an example of the predictions on a sample image from the test dataset for all training scenarios. Similar to the Detectron2 trained MaskRCNN R18, we observe several predictions on ground level in the ablation trained models. For this reason, we proceed with the remainder of experiments in this work using the full RGB + Thermal + Height input. However, as the ground-level predictions only detect 16 unique objects appearing across 23 images within the entire test dataset for the ablation training from scratch, we again believe that a larger labelled training dataset would resolve this and allow the RGB + Thermal information to be sufficient. We also observe a significant improvement in performance given by the pretraining, including a 5% to 7% higher score for all AR@100 metrics.

The AR scores significantly outperform the MaskRCNN R18, almost doubling the AR@100. While this is likely due to the increased model size, i.e. more layers, we also note the drastically lower energy consumption due to a significant speedup observed in model training time. This demonstrates an excellent overall out-of-the-box performance of the MMDetection library.

5.3. Comparison with baseline

The pretrained Swin-T transformer achieves the highest AR by a significant margin. Interestingly, the from-scratch training (without

pretraining) only scores as well as the baseline. Transformer-based models are notoriously memory-hungry, and we see this reflected in a longer overall training time and hence larger energy consumption.⁸

The TridentNet architecture performs worse than the baseline on all metrics. We found that the pretrained model was especially unstable during training, regularly suffering from exploding gradients (and hence loss values), only stabilising when the learning rate was turned down an order of magnitude from the default 0.02 to 0.002.

FSAF also performs worse than the baseline in the from-scratch training, but the same when pretrained. Due to its ResNet-101 backbone, the training times were significantly longer, something we see reflected in the fact that it has the largest energy consumption of all MMDetection trainings.

Overall, the use of COCO [35] pretrained model weights proved to be an advantage regardless of the architecture. We therefore recommend this as an essential component in thermal bridge detection when utilising learned object detection approaches, and suggest it as an avenue of investigation for further improving detection performance.

6. Conclusion and outlook

The detection of thermal bridges on building rooftops can be automated by using deep learning approaches on thermographic images. For aerial panorama images, the main advantage of neural networks instead of computer vision approaches working with temperature thresholds is the ability to learn identifying building parts of interest and to include changing shapes of thermal bridges due to different recording angles.

In this study, the best results were achieved with the MMDetection library using a pretrained Swin-T Transformer model, scoring an Average Recall of 50.7% for large thermal bridges. Overall, we find consistently better results for pretrained models than for models without pretraining. Moreover, this work showed the ability of neural networks to propose predictions of thermal bridges only on rooftops by using height information to the input images. While this work has demonstrated promising results in identifying individual thermal bridges from drone images, we believe there is still significant potential for improvement with a larger annotated dataset. A larger dataset would allow for the allocation of a validation subset, enabling tuning of hyperparameters to improve training performance.

While no existing works target the detection of thermal bridges on aerial panorama images with deep learning approaches, we can compare our results with other existing thermal bridge detection procedures. Barahona et al. [21] achieved an Average Recall of 75% for the binary classification of images containing thermal anomalies, however they segmented the anomalies as a subsequent manual step, something that our approach automates entirely. Kim et al. [22] used a multi-step procedure on close-up images to achieve an Average Recall of 87%, which does not deal with the presence of multiple buildings and non-building objects within images. However, both of these works, the latter in particular, represent an optimal benchmark that may be achieved by our approach with the larger dataset proposed above.

Our scoring for this work has only considered the raw Average Recall score across each individual image, yet the images are not independent and instead contain significant overlap. We therefore propose in future to consider the scores across all instances of the same thermal bridge. For this, it is possible to track instances across all images containing the same thermal bridge or to set a threshold for requiring at least two detections of a thermal bridge to count it [43]. Identifying which thermal bridges are matching instances, however, would result in additional effort when creating the dataset.

Further improvements can also be made in the pretraining procedure, which has already proven successful in improving performance.

Performing additional pretraining on existing UAV datasets, such as UAVDT [44] or iSAID [45], is one example that would closer align the pretrained models with the TBBR images. Self-supervised pretraining, used with great success in BERT [46], performed on the larger set of unannotated TBBR images presents another avenue for investigation.

Despite these limitations of our study, we believe we have provided important insights into the benefits of deep learning for automated building analysis in an urban context, which is becoming increasingly important in building and district management. In future, our approach could also be transferred to the analysis of other thermal anomalies on panorama drone images, such as the detection of district heating pipe leakages at ground level.

CRedit authorship contribution statement

Zoe Mayer: Conceptualization, Methodology, Investigation, Data Curation, Writing - Original Draft, Writing - Review & Editing, Project administration. **James Kahn:** Conceptualization, Methodology, Software, Formal analysis, Investigation, Data Curation, Writing - Original Draft, Writing - Review & Editing, Visualization. **Yu Hou:** Methodology, Software, Writing - Original Draft, Writing - Review & Editing, Visualization. **Markus Götz:** Methodology, Writing - Review & Editing, Supervision. **Rebekka Volk:** Conceptualization, Data Curation, Writing - Review & Editing, Supervision, Project administration. **Frank Schultmann:** Writing - Review & Editing, Supervision.

Declaration of competing interest

The authors declare that they have no known competing financial interests or personal relationships that could have appeared to influence the work reported in this paper.

Data availability

All data, code, and configurations used in this work have been made publicly available online.

Acknowledgements

This work is supported by the Helmholtz Association Initiative and Networking Fund under the Helmholtz AI platform grant and the HAICORE@KIT partition. We thank Marinus Vogl and the Air Bavarian GmbH for their support with equipment and service for the recording of images. We also thank Tobias Beiersdörfer for support in the development of the TBBR dataset. All authors approved the version of the manuscript to be published.

Funding

All of the sources of funding for the work described in this publication are acknowledged below:

This work is supported by the Helmholtz Association Initiative and Networking Fund under the Helmholtz AI platform grant and the HAICORE@KIT partition.

Appendix. Training hardware details

See [Table A.3](#).

⁸ Memory itself is has a substantial power draw.

Table A.3
Hardware details for nodes used in all model trainings.

CPU	Intel Xeon Platinum 8368
CPU Sockets per node	2
CPU Cores per node	76
CPU Threads per node	152
Cache L1	64k (per core)
Cache L2	1 MB (per core)
Cache L3	57 MB (shared, per CPU)
Main memory	512 GB
Accelerators	4x NVIDIA A100-40
Memory per accelerator	40 GB
Local discs	960 GB NVMe SSD
Interconnect	InfiniBand

References

- [1] 2021 Global Status Report for Buildings and Construction: Towards a Zero-Emission, Efficient and Resilient Buildings and Construction Sector, Technical Report, United Nations Environment Programme (2021), United Nations, Nairobi, 2021, URL <https://globalabc.org/resources/publications/2021-global-status-report-buildings-and-construction>, accessed 2022-04-22.
- [2] Energy Technology Perspectives 2014, International Energy Agency, 2014, http://dx.doi.org/10.1787/energy_tech-2014-en.
- [3] T.G. Theodosiou, A.M. Papadopoulos, The impact of thermal bridges on the energy demand of buildings with double brick wall constructions, *Energy Build.* 40 (2008) 2083–2089, <http://dx.doi.org/10.1016/j.enbuild.2008.06.006>.
- [4] P. Schmidt, S. Windhausen, *Bauphysik-Lehrbuch: Wärmeschutz - Energieeinsparung - Feuchte- Und Tauwasserschutz - Schallschutz - Raumakustik*, Reguvis Fachmedien GmbH, ISBN: 978-3-8462-0407-8, 2017.
- [5] A. Alhawari, P. Mukhopadhyaya, Thermal bridges in building envelopes – an overview of impacts and solutions, *Int. Rev. Appl. Sci. Eng.* 9 (2018) 31–40, <http://dx.doi.org/10.1556/1848.2018.9.1.5>.
- [6] I. Garrido, M. Solla, S. Lagüela, M. Rasol, Review of InfraRed thermography and ground-penetrating radar applications for building assessment, *Adv. Civ. Eng.* 2022 (2022) e5229911, <http://dx.doi.org/10.1155/2022/5229911>.
- [7] E. Lucchi, Applications of the infrared thermography in the energy audit of buildings: A review, *Renew. Sustain. Energy Rev.* 82 (2018) 3077–3090, <http://dx.doi.org/10.1016/j.rser.2017.10.031>.
- [8] B. Tejedor, E. Lucchi, I. Nardi, Application of qualitative and quantitative infrared thermography at urban level: Potential and limitations, in: D. Bienvenido-Huertás, J. Moyano-Campos (Eds.), *New Technologies in Building and Construction: Towards Sustainable Development*, in: *Lecture Notes in Civil Engineering*, Springer Nature, Singapore, 2022, pp. 3–19, http://dx.doi.org/10.1007/978-981-19-1894-0_1.
- [9] M. Previtali, L. Barazzetti, R. Brumana, F. Roncoroni, Thermographic analysis from uav platforms for energy efficiency retrofit applications, *J. Mob. Multimedia* (2013) 066–082, URL <https://journals.riverpublishers.com/index.php/JMM/index>, accessed 2022-11-08.
- [10] G. Bitelli, P. Conte, T. Csoknyai, F. Franci, V.A. Girelli, E. Mandanici, Aerial thermography for energetic modelling of cities, *Remote Sens.* 7 (2015) 2152–2170, <http://dx.doi.org/10.3390/rs70202152>.
- [11] U.S. Department of Energy (DOE), Guide To Community Energy Strategic Planning, Technical Report, U.S. Department of Energy (DOE), 2013, URL <https://www.energy.gov/eere/slsc/guide-community-energy-strategic-planning>, accessed 2022-11-08.
- [12] Dale Littlejohn, Richard Laszlo, National Report on Community Energy Plan Implementation, Technical Report, Quality Urban Energy Systems of Tomorrow (QUEST), 2015, URL <https://questcanada.org/national-report-on-community-energy-plan-implementation/>, accessed 2022-11-08.
- [13] JPI Urban Europe, SET plan action 3.2, in: *White Paper on PED Reference Framework for Positive Energy Districts and Neighbourhoods*, Technical Report, JPI Urban Europe, 2020, URL <https://jpi-urbaneurope.eu/ped/>, accessed 2022-11-08.
- [14] Federal Ministry of the Interior, Building and Community (BMI), *Energy-Efficient Urban Redevelopment: A Funding Programme for Climate Protection at the Neighbourhood Level*, Technical Report, Federal Ministry of the Interior, Building and Community (BMI), 2020, URL <https://www.bmi.bund.de/SharedDocs/downloads/EN/publikationen/building/energie-efficient-urban-redevelopment.html>.
- [15] Z. Mayer, J. Kahn, Y. Hou, T. Beiersdörfer, M. Götz, R. Volk, Thermal bridges on building rooftops - hyperspectral (RGB thermal height) drone images of Karlsruhe, Germany, with thermal bridge annotations, 2022, <http://dx.doi.org/10.5281/zenodo.6517768>.
- [16] I. Garrido, S. Lagüela, P. Arias, J. Balado, Thermal-based analysis for the automatic detection and characterization of thermal bridges in buildings, *Energy Build.* 158 (2018) 1358–1367, <http://dx.doi.org/10.1016/j.enbuild.2017.11.031>.
- [17] H. Macher, T. Landes, P. Grussenmeyer, Automation of thermal point clouds analysis for the extraction of windows and thermal bridges of building facades, in: *The International Archives of the Photogrammetry, Remote Sensing and Spatial Information Sciences*, Volume XLIII-B2-2020, Copernicus GmbH, 2020, pp. 287–292, <http://dx.doi.org/10.5194/isprs-archives-XLIII-B2-2020-287-2020>.
- [18] J.R.M.-D. Dios, A. Ollero, Automatic detection of windows thermal heat losses in buildings using UAVs, in: *2006 World Automation Congress*, 2006, pp. 1–6, <http://dx.doi.org/10.1109/WAC.2006.375998>.
- [19] T. Rakha, A. Liberty, A. Gorodetsky, B. Kakillioglu, S. Velipasalar, Heat mapping drones: An autonomous computer-vision-based procedure for building envelope inspection using unmanned aerial systems (UAS), *Technol. Archit. + Des.* 2 (2018) 30–44, <http://dx.doi.org/10.1080/24751448.2018.1420963>.
- [20] S. Mirzabeigi, M. Razkenari, Automated vision-based building inspection using drone thermography, in: *20th Annual New York State Green Building Conference*, American Society of Civil Engineers, 2022, pp. 737–746, <http://dx.doi.org/10.1061/9780784483961.077>.
- [21] B. Barahona, R. Buck, O. Okaya, P. Schuetz, Detection of thermal anomalies on building façades using infrared thermography and supervised learning, *J. Phys. Conf. Ser.* 2042 (2021) 012013, <http://dx.doi.org/10.1088/1742-6596/2042/1/012013>.
- [22] C. Kim, J.-S. Choi, H. Jang, E.-J. Kim, Automatic detection of linear thermal bridges from infrared thermal images using neural network, *Appl. Sci.* 11 (2021) 931, <http://dx.doi.org/10.3390/app11030931>.
- [23] Z. Mayer, J. Kahn, Y. Hou, R. Volk, AI-based thermal bridge detection of building rooftops on district scale using aerial images, in: Jimmy Abualdenien, André Borrmann, Lucian-Constantin Ungureanu, Timo Hartmann (Eds.), *EG-ICE 2021 Workshop on Intelligent Computing in Engineering*, Universitätsverlag der TU Berlin, 2021, pp. 497–507, <http://dx.doi.org/10.5445/IR/1000136256>.
- [24] Z. Mayer, Y. Hou, J. Kahn, T. Beiersdörfer, R. Volk, Thermal bridges on building rooftops - hyperspectral (RGB thermal height) drone images of Karlsruhe, Germany, with thermal bridge annotations, 2021, <http://dx.doi.org/10.5281/zenodo.4767772>.
- [25] Y. Wu, A. Kirillov, F. Massa, W.-Y. Lo, R. Girshick, Detectron2, 2019, <https://github.com/facebookresearch/detectron2>, Accessed 2022-11-08.
- [26] K. Chen, J. Wang, J. Pang, Y. Cao, Y. Xiong, X. Li, S. Sun, W. Feng, Z. Liu, J. Xu, Z. Zhang, D. Cheng, C. Zhu, T. Cheng, Q. Zhao, B. Li, X. Lu, R. Zhu, Y. Wu, J. Dai, J. Wang, J. Shi, W. Ouyang, C.C. Loy, D. Lin, MMDetection: Open mmlab detection toolbox and benchmark, 2019, arXiv preprint [arXiv:1906.07155](https://arxiv.org/abs/1906.07155).
- [27] T.-Y. Lin, P. Dollár, R. Girshick, K. He, B. Hariharan, S. Belongie, Feature pyramid networks for object detection, 2016, <http://dx.doi.org/10.48550/ARXIV.1612.03144>, URL <https://arxiv.org/abs/1612.03144>.
- [28] K. He, G. Gkioxari, P. Dollár, R. Girshick, Mask R-CNN, in: *2017 IEEE International Conference on Computer Vision (ICCV)*, 2017, pp. 2980–2988, <http://dx.doi.org/10.1109/ICCV.2017.322>.
- [29] K. He, X. Zhang, S. Ren, J. Sun, Deep residual learning for image recognition, in: *2016 IEEE Conference on Computer Vision and Pattern Recognition (CVPR)*, 2016, pp. 770–778, <http://dx.doi.org/10.1109/CVPR.2016.90>.
- [30] Z. Liu, Y. Lin, Y. Cao, H. Hu, Y. Wei, Z. Zhang, S. Lin, B. Guo, Swin transformer: Hierarchical vision transformer using shifted windows, in: *2021 IEEE/CVF International Conference on Computer Vision*, 2021, pp. 9992–10002, <http://dx.doi.org/10.1109/ICCV48922.2021.00986>.
- [31] Y. Li, Y. Chen, N. Wang, Z.-X. Zhang, Scale-aware trident networks for object detection, in: *2019 IEEE/CVF International Conference on Computer Vision*, 2019, pp. 6053–6062, <http://dx.doi.org/10.1109/ICCV.2019.00615>.
- [32] C. Zhu, Y. He, M. Savvides, Feature selective anchor-free module for single-shot object detection, in: *2019 IEEE/CVF Conference on Computer Vision and Pattern Recognition*, IEEE Computer Society, 2019, pp. 840–849, <http://dx.doi.org/10.1109/CVPR.2019.00093>.
- [33] Z. Liu, H. Hu, Y. Lin, Z. Yao, Z. Xie, Y. Wei, J. Ning, Y. Cao, Z. Zhang, L. Dong, F. Wei, B. Guo, Swin transformer V2: Scaling up capacity and resolution, in: *2022 IEEE/CVF Conference on Computer Vision and Pattern Recognition (CVPR)*, 2022, pp. 11999–12009, <http://dx.doi.org/10.1109/CVPR52688.2022.01170>.
- [34] H. Zhang, F. Li, S. Liu, L. Zhang, H. Su, J. Zhu, L.M. Ni, H.-Y. Shum, DINO: DETR with improved DeNoising anchor boxes for end-to-end object detection, 2022, [arXiv:2203.03605](https://arxiv.org/abs/2203.03605) [cs].
- [35] T.-Y. Lin, M. Maire, S. Belongie, J. Hays, P. Perona, D. Ramanan, P. Dollár, C.L. Zitnick, Microsoft COCO: Common objects in context, in: D. Fleet, T. Pajdla, B. Schiele, T. Tuytelaars (Eds.), *Computer Vision – European Conference on Computer Vision (ECCV) 2014*, Springer International Publishing, Cham, 2014, pp. 740–755, http://dx.doi.org/10.1007/978-3-319-10602-1_48.
- [36] S. Ren, K. He, R. Girshick, J. Sun, Faster R-CNN: Towards real-time object detection with region proposal networks, *IEEE Trans. Pattern Anal. Mach. Intell.* 39 (2017) 1137–1149, <http://dx.doi.org/10.1109/TPAMI.2016.2577031>.
- [37] D. Coquelin, C. Debus, M. Götz, F. von der Lehr, J. Kahn, M. Siggel, A. Streit, Accelerating neural network training with distributed asynchronous and selective optimization (DASO), *J. Big Data* 9 (2022) 14, <http://dx.doi.org/10.1186/s40537-021-00556-1>, [arXiv:2104.05588](https://arxiv.org/abs/2104.05588).

- [38] René Caspart, Sebastian Ziegler, Arvid Weyrauch, Holger Obermaier, Simon Raffener, Leon Pascal Schuhmacher, Jan Scholtyssek, Darya Trofimova, Marco Nolden, Ines Reinartz, Fabian Isensee, Markus Götz, Charlotte Debus, Precise Energy Consumption Measurements of Heterogeneous Artificial Intelligence Workloads, 2022, <http://dx.doi.org/10.48550/arXiv.2212.01698>, arXiv: 2212.01698.
- [39] IEEE Standard for Floating-Point Arithmetic, IEEE Std 754-2019 (Revision of IEEE 754-2008), IEEE Computer Society, 2019, pp. 1–84, <http://dx.doi.org/10.1109/IEEESTD.2019.8766229>.
- [40] N. Fouad, T. Richter, *Leitfaden Thermografie Im Bauwesen, Theorie, Anwendungsgebiete, Praktische Umsetzung*, 2007.
- [41] Z. Mayer, J. Heuer, R. Volk, F. Schultmann, Aerial thermographic image-based assessment of thermal bridges using representative classifications and calculations, *Energies* 14 (2021) 7360, <http://dx.doi.org/10.3390/en14217360>.
- [42] Y. Hou, R. Volk, M. Chen, L. Soibelman, Fusing tie points' RGB and thermal information for mapping large areas based on aerial images: a study of fusion performance under different flight configurations and experimental conditions, *Autom. Constr.* 124 (2021) 103554, <http://dx.doi.org/10.1016/j.autcon.2021.103554>.
- [43] L. Yang, Y. Fan, N. Xu, Video instance segmentation, in: Proceedings of the IEEE/CVF International Conference on Computer Vision, 2019, pp. 5188–5197, URL https://openaccess.thecvf.com/content_ICCV_2019/html/Yang_Video_Instance_Segmentation_ICCV_2019_paper.html, accessed 2022-11-08.
- [44] D. Du, Y. Qi, H. Yu, Y. Yang, K. Duan, G. Li, W. Zhang, Q. Huang, Q. Tian, The unmanned aerial vehicle benchmark: Object detection and tracking, in: V. Ferrari, M. Hebert, C. Sminchisescu, Y. Weiss (Eds.), *Computer Vision – European Conference on Computer Vision (ECCV) 2018*, in: Lecture Notes in Computer Science, Springer International Publishing, Cham, 2018, pp. 375–391, http://dx.doi.org/10.1007/978-3-030-01249-6_23.
- [45] S.W. Zamir, A. Arora, A. Gupta, S. Khan, G. Sun, F.S. Khan, F.Z. 0001, L.S. 0001, G.-S. Xia, X. Bai, iSAID: A large-scale dataset for instance segmentation in aerial images, in: IEEE Conference on Computer Vision and Pattern Recognition Workshops, CVPR Workshops 2019, Long Beach, CA, USA, June 16-20, 2019, Computer Vision Foundation / IEEE, 2019, pp. 28–37, URL http://openaccess.thecvf.com/content_CVPRW_2019/html/DOAI/Zamir_iSAID_A_Large-scale_Dataset_for_Instance_Segmentation_in_Aerial_Images_CVPRW_2019_paper.html, accessed 2022-11-08.
- [46] J. Devlin, M.-W. Chang, K. Lee, K. Toutanova, BERT: Pre-training of deep bidirectional transformers for language understanding, in: Proceedings of the 2019 Conference of the North American Chapter of the Association for Computational Linguistics: Human Language Technologies, Volume 1 (Long and Short Papers), Association for Computational Linguistics, Minneapolis, Minnesota, 2019, pp. 4171–4186, <http://dx.doi.org/10.18653/v1/N19-1423>.

Paper G: Thermal Bridges on Building Rooftops (TBBR)

This paper was reproduced in its original format with permission from Springer Nature:

Mayer, Z., Kahn, J., Götz, M., Hou, Y., Beiersdörfer, T., Blumenröhr, N., ..., Schultmann, F. (2023 - Paper G). Thermal Bridges on Building Rooftops (TBBR). Nature Scientific Data.

Doi: <https://doi.org/10.1038/s41597-023-02140-z>



OPEN

Thermal Bridges on Building Rooftops

DATA DESCRIPTOR

Zoe Mayer^{1,7}✉, James Kahn^{2,3,7}, Markus Götz^{2,3}✉, Yu Hou^{4,5}, Tobias Beiersdörfer¹, Nicolas Blumenröhr^{3,6}, Rebekka Volk¹✉, Achim Streit³ & Frank Schultmann¹

Thermal Bridges on Building Rooftops (TBBR) is a multi-channel remote sensing dataset. It was recorded during six separate UAV fly-overs of the city center of Karlsruhe, Germany, and comprises a total of 926 high-resolution images with 6927 manually-provided thermal bridge annotations. Each image provides five channels: three color, one thermographic, and one computationally derived height map channel. The data is pre-split into training and test data subsets suitable for object detection and instance segmentation tasks. All data is organized and structured to comply with FAIR principles, i.e. being findable, accessible, interoperable, and reusable. It is publicly available and can be downloaded from the Zenodo data repository. This work provides a comprehensive data descriptor for the TBBR dataset to facilitate broad community uptake.

Background & Summary

About 30% of global final energy consumption and 27% of total energy sector emissions stem from building operations. After a short drop during the COVID-19 pandemic, emissions and energy consumption are both now above their pre-COVID level of 2019, showing that no late reduction trend has started¹.

A major field for reducing energy consumption for building operations is the improvement of building envelopes, which is critical for reductions in heating and cooling intensity². A thermal bridge is a discontinuity of a building's envelope, whose thermal properties differ fundamentally from the thermal properties of the adjacent enveloping surface³. With increasing demands on the quality of building envelopes, the minimization of thermal bridges is becoming ever more important, since losses from thermal bridges can account for up to one third of a building's transmission heat loss^{4,5}. Beyond increased energy consumption, thermal bridges can lead to a wide range of problems, from the risk of condensation and mold infestation⁶, to a reduced comfort that occurs due to cold inner surfaces of a building⁷. In summer, thermal bridges lead to increased heat absorption by buildings and thus can increase the need for air conditioning³.

For the detection of thermal bridges of building envelopes, thermography can be reliably used⁸. In recent years, not only individual buildings, but also buildings in their urban context have gained importance for developing adequate retrofit strategies. The New Urban Agenda of the United Nations (UN) puts a spotlight on policies affecting urban structures at all appropriate levels recognizing that building design is one of the "greatest drivers of cost and resource efficiencies"⁹. When studying building stocks in cities, city districts, and villages, thermographic images can be collected with Unmanned Aerial Vehicles (UAVs/drones)^{10,11}. Thermography with drones is especially advantageous because it saves time, resources, and is scalable for large areas compared to classical thermography with static cameras¹⁰. UAV-based thermographic systems are particularly beneficial when examining rooftops, since recordings with hand-held cameras are difficult. Previously, rooftop inspections with thermography had to be carried out on the basis of on-site inspections at night which are particularly labor-intensive, dangerous, and unable to achieve the same coverage feasible with drones¹².

To evaluate large number of thermographic images collected in urban areas, the manual processing of images is time-consuming. The detection of thermal bridges can be automated, but is not trivial. Currently, approaches for automated thermal bridge detection work mostly with temperature threshold values and pattern recognition^{13–16}. It is, however, difficult to find threshold values that can be generally applied to all types of thermal

¹Karlsruhe Institute of Technology, Institute for Industrial Production, 76187, Karlsruhe, Germany. ²Helmholtz AI, Karlsruhe, Germany. ³Karlsruhe Institute of Technology, Steinbuch Centre for Computing, 76344, Eggenstein-Leopoldshafen, Germany. ⁴Western New England University, Department of Construction Management, Springfield, MA, 01119, USA. ⁵Carnegie Mellon University, Civil and Environmental Engineering Department, Pittsburgh, PA, 15213, USA. ⁶Helmholtz Metadata Collaboration, Karlsruhe, Germany. ⁷These authors contributed equally: Zoe Mayer, James Kahn. ✉e-mail: zoe.mayer@partner.kit.edu; markus.goetz@kit.edu; rebekka.volk@kit.edu

Camera	Spectrum (μm)	Image Resolution (px)	FOV ($^\circ$)	Focal Length (mm)	Format
Zenmuse XT2 (RGB)	0.4–0.7	4000 \times 3000	57.12 \times 42.44	8	TIFF
FLIR Tau 2 (thermal)	7.5–13.5	640 \times 512	45.00 \times 37.00	13	TIFF

Table 1. Technical specifications of the cameras used in recording the TBBR raw data. As the thermal camera is less than one year since purchase, it is still factory calibrated (see <https://www.flir.co.uk/support-center/surveillance/infrared-camera-calibration/>).

bridges¹⁷. Patterns and temperatures differ depending on the materials and building components where thermal bridges occur, on environmental conditions, and on recording settings. For example for windows, temperatures on thermographic images appear cooler due to high levels of reflection of glass surfaces¹⁸. Furthermore, misinterpretations, e.g. caused by open windows, can occur with simple threshold methods. Deep learning methods, which can overcome the aforementioned problems, may provide better results, but require annotated image datasets.

In this data descriptor, we present the Thermal Bridges on Building Rooftops (TBBR) dataset. To the best of our knowledge it is the first comprehensive aerial thermographic image dataset, which also provides height mapping information while also being fully annotated for district-scale segmentation of thermal bridges on building rooftops. It is organized and structured according to the FAIR principles¹⁹, i.e. being findable, accessible, interoperable and reusable.

The remainder of the data descriptor is organized as follows: the Methods section describes the environmental conditions and methodological approach in recording the TBBR dataset. Data Records details the organization of the data, including file formats, how the data has been preprocessed and curated, as well as how to obtain it from a publicly available data repository. In the Technical Validation section we highlight data quality aspects of TBBR. Finally, the Usage Notes sections sketches current and prospective use case scenarios for the data with an emphasis on (semi-)automated thermal bridge object detection and instance segmentation.

Methods

The raw images for our dataset were recorded with a Zenmuse XT2 visual (RGB) and a FLIR Tau 2 (thermal, <https://flir.netx.net/file/asset/15598/original/>) camera (see Table 1 for details) on a DJI M600 drone (<https://www.dji.com/de/matrice600>). They were recorded at flight heights between 60–80 m above ground with a flight speed of 1 $\frac{\text{m}}{\text{s}}$ and contain GPS information. The images cover six large blocks of around 20 buildings per block recorded in the city center of the German city Karlsruhe with a total fly-over area of roughly 48500 m^2 (see Fig. 1). Because of a high overlap rate of the images, the same buildings are on average recorded from different angles in different images about 20 times. All images were recorded during drone flights on Tuesday 19th March 2019 from 7am to 8am (UTC + 02:00). At this time, temperatures were between 3.78 $^\circ\text{C}$ and 4.97 $^\circ\text{C}$, and humidity between 80% and 98%. There was no rain on the day of the flights, but there was 2.3 $\frac{\text{mm}}{\text{m}^2}$ 48 hours beforehand. For all images, an exposure time of 1/100 s and ISO speed rating of 128 was used. For recording the thermographic images, an emissivity of 1.0 and an aperture of F1 was set. For the RGB images, an aperture of F1.8 was used. The global radiation during this period was between 38.59 $\frac{\text{W}}{\text{m}^2}$ and 120.86 $\frac{\text{W}}{\text{m}^2}$. No direct sunlight can be seen visually on any of the recordings. Further environmental conditions are shown in Table 2. We do not provide information on the recorded buildings' internal temperatures, for estimates we refer readers to the corresponding German DIN standards²⁰.

The full set of raw images captured contained a total of 5698 images before preselection²¹. Preselection involved the removal of all blurry images, e.g. due to rapid movement or turning of the drone, and all images containing no visible thermal bridges. After preselection a total of 926 images remained.

The RGB and thermal drone images were fused with a computed height map. All images were converted to a uniform format of 4000 \times 3000 px, aligned, and cropped to 3370 \times 2680 px to remove empty borders. The annotations only include thermal bridges that are visually identifiable with the human eye. Because of the aforementioned image overlap, each thermal bridge is annotated multiple times from different angles. For the annotation of the thermal images the image processing program VGG Image Annotator from the Visual Geometry Group, version 2.0.10²², was used. The thermal bridge annotations are outlined with polygon shapes. These polygon lines were placed as close as possible but outside the area of significant temperature increase. If a detected thermal bridge was partially covered by another building component located in the foreground, the thermal bridge was also marked across the covering in case of minor coverings. Adjacent thermal bridges, which affect different rooftop components, were annotated separately. For example, a window with poor insulation of the window reveal located in the area of a poorly insulated roof is annotated individually. There is no overlap between annotated areas. While each image contains annotations, they also include thermal bridges present that are not annotated due to not being clearly identifiable, e.g. too small for accurate identification or unclear due to the camera perspective.

Image preparation. The image registration and alignment procedure is shown in Fig. 2. The procedure involves three main steps:

1. distortion correction,
2. registration and alignment,
3. cropping and stacking.

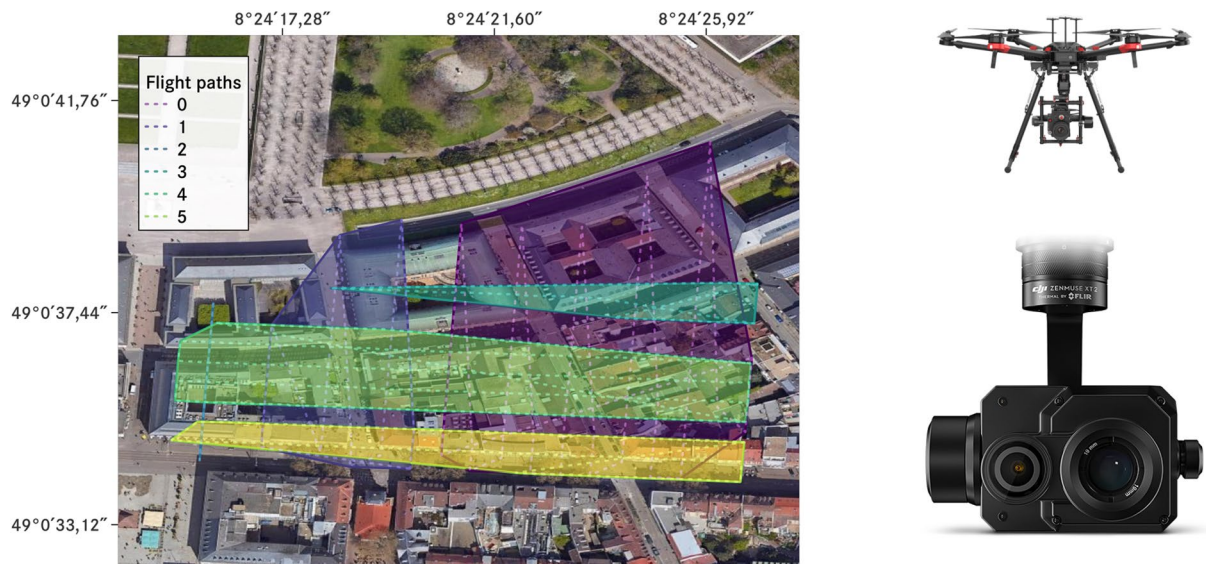


Fig. 1 Geo-located map of drone flyover regions (left, WGS 84 coordinate system, source: Google Maps), DJI M600 drone (upper right), and Zenmuse XT2 camera with a FLIR Tau 2 thermal sensor (lower right). Dashed lines show the flight paths of the drone, polygons the photographed regions. Numbers correspond to identifier of each flight paths, e.g. 2 for Flug1_102 (see Data Records section below). Image source for the drone and camera: © DJI.

Time	Cloud Cover	Pressure (hPa)	Visibility (m)	Wind Speed ($\frac{m}{s}$)	Wind Direction (°)
7am UTC+02:00	overcast	1012.0	29680	0.7	280
8am UTC+02:00	overcast	1012.7	34430	1.1	90

Table 2. Environmental conditions during the fly over on 2019-03-19 as measured by the closest weather station in Rheinstetten N 48°58'21.4"N 8°19'48.4"E (WGS 84 coordinate system, source: DWD OpenData at https://opendata.dwd.de/climate_environment/CDC/observations_germany/climate/hourly/).

The distortion correction procedure used was that established in previous works^{23,24}. In short, a reference image was used to determine distortion coefficients, `cv2.getOptimalNewCameraMatrix()` to find a new camera matrix, and `cv2.undistort()` to correct distortion. All mentioned processing functions are part of the computer vision programming library OpenCV²⁵.

Image registration and alignment was then performed by transforming the RGB and height map images onto the thermal images, as the annotation of thermal bridges was performed on these. A homography matrix was calculated using a total of 316 coordinate pairs from 21 RGB and thermal images. This homography matrix was then used to transform all RGB images in the dataset. Since the height map was created from the RGB images, we also used this homography matrix to transform the height map images.

The final cropping and stacking was performed to create the 5-channel images of the TBBR dataset, output in the NumPy format²⁶. Images are cropped to 3370 × 2680 px to remove large black borders present in thermal images, and subsequently stacked into the channel order [B, G, R, Thermal, Height].

Computation of the height map. Due to the high overlap of images, we can extract similarities from feature points identified in each image and conduct photogrammetry. Photogrammetry allows estimation of the three-dimensional coordinates of points on an object in a generated 3D space involving measurements made on images taken with a high overlap rate. Therefore, we can use this technique to create a 3D point cloud model of the recorded region.

We used the ContextCapture software to perform photogrammetry on the TBBR dataset. ContextCapture provides users with intermediate information necessary to obtain each image's estimated 3D coordinates and orientation^{23,24}. This information allowed estimation of the distance between points in 3D and 2D spaces and to project points from the 3D to the 2D space to generate the height maps. The resulting 2D height map image pixels show the z-axis value (vertical height) of the corresponding 3D point cloud model points, normalized to the 8-bit range of the lowest 3D model point (0) and the drone (255).

Data Records

The Thermal Bridges on Building Rooftops (TBBR) data is publicly available on Zenodo²⁷ and is licensed under Creative Commons Attribution 4.0 International (<http://creativecommons.org/licenses/by/4.0/>). The 926 images in the dataset are made available as a series of compressed archive files totaling 68.5GB. Each compressed archive file corresponds to one of the six flight paths, named Flug1_100 to Flug1_105 respectively

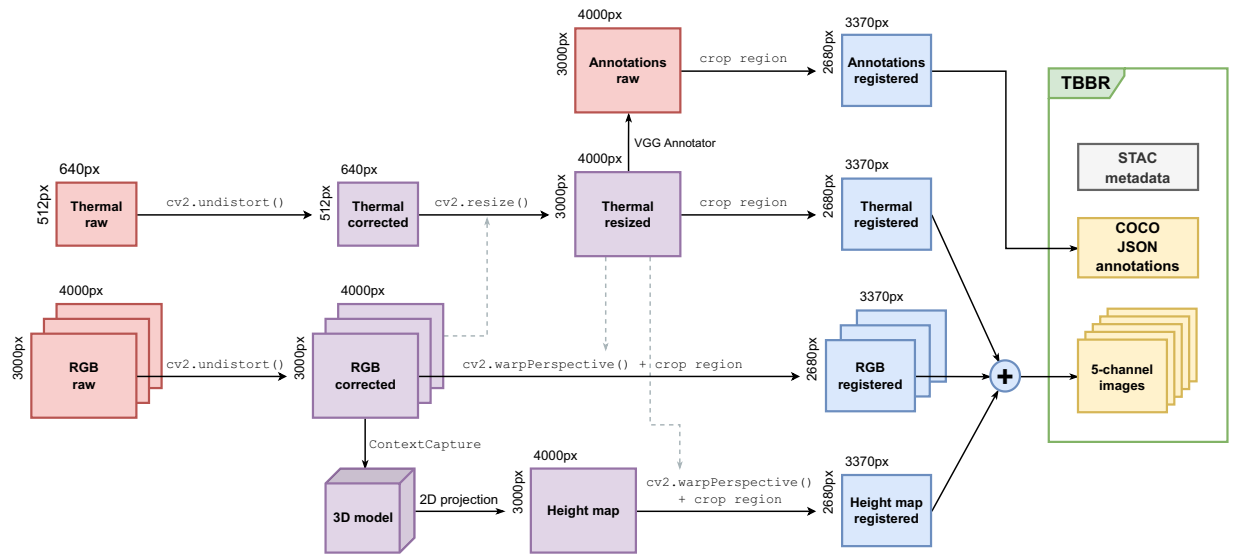


Fig. 2 Image registration and alignment procedure.

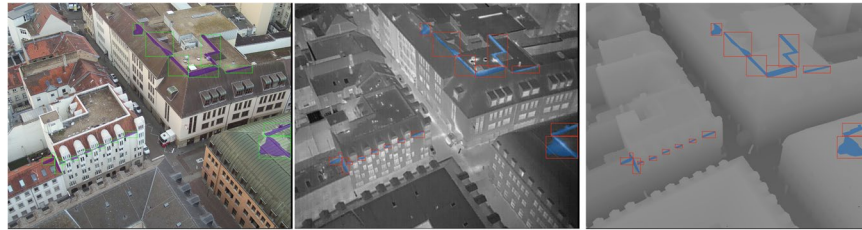


Fig. 3 Example image from the TBBR dataset (Flug_100, ID 523) showing the different channels, RGB (left), thermal (center), and height map (right), including overlaid annotations.

(the word “Flug” means flight in German). The archives contain NumPy²⁶ files (one per image) of shape (2680,3370,5), where the final dimension is the color channel in the format [B, G, R, Thermal, Height]. An example image (Flug_100, ID: 523) is depicted in Fig. 3. Archives were compressed using ZStandard compression²⁸. They can be decompressed by utility software programs, e.g. `tar` or `unzstd`. Corresponding annotations are provided in the COCO JSON format²⁹, which were automatically generated by the VGG Image Annotator.

One of TBBR’s main design objectives was to facilitate (semi-)automated thermal bridges pattern detection algorithms³⁰ (see Usage Notes). In accordance, the data is pre-split into train and test subsets with 723 (5614) and 203 (1313) images (annotations), respectively. There is one annotation COCO JSON for each subset, i.e. one for training (Flug1_100Media to Flug1_104Media) and one for test (Flug1_105Media) data. The latter block is used as a hold-out test dataset to standardize out-of-sample generalization performance assessment.

The experimental metadata was structured with the Spatio Temporal Asset Catalog (STAC) (<https://stacspec.org/en>) specification family. This specification is used to provide a standardized way for describing geo-spatial assets. It defines related JSON object types of `Item`, `Catalog`, and `Collection`, extending `Collection` as the basis. Moreover, STAC objects can be extended with other specifications and enable a mechanism to provide additional metadata. Such an approach addresses the relevance for a common understanding of experimental metadata, which is ideally a widely accepted standard³¹.

The STAC `Collection` JSON object `Flug1_collection_stac_spec` provides information about the recorded images and the environmental conditions during recordings. It also contains information about the overall bounding box of the entire area in which images were recorded. It links to related STAC `Item` JSON objects containing information about the recorded city blocks and the cameras. The objects for the six flight paths, i.e. `Flug1_100_stac_spec`, `Flug1_101_stac_spec`, `Flug1_102_stac_spec`, `Flug1_103_stac_spec`, `Flug1_104_stac_spec`, `Flug1_105_stac_spec`, contain the GeoJSON³² geometry of the respective block and the corresponding bounding box.

The objects containing the camera information, named `Flug1_camera1_stac-spec` for the RGB camera and `Flug1_camera2_stac-spec` for the Thermal camera, are based on an existing STAC extension for camera related metadata. All STAC `Item` objects have a link to the `Flug1_collection_stac_spec` `Collection` object.

Metadata of the archived NumPy files for each image was structured using the Data Package schema from the Frictionless Standards (<https://specs.frictionlessdata.io>). This standard describes a collection of data files.

	Train	Test	Total
Annotated images	723	203	926
Total annotations	5614	1313	6927
Average annotations per image	7.8	6.5	7.5
Rooftop shape	No. of annotations		
Steep roof	3939	895	4834
Flat roof	524	379	903
Mixed shape	1151	39	1190
Rooftop component	No. of annotations		
Rooftop surfaces	437	185	622
Component connections (dormers, ridges, valleys, gables, eaves lines, etc.)	3977	842	4819
Cantilevers (cantilever walls, attics, cantilever floor slabs, etc.)	640	149	789
Windows (reveals, lintels, parapets, dome lights, etc.)	560	137	697

Table 3. TBBR annotation and component overview.

Therefore, metadata about all containerized NumPy files of the six flight paths is provided within a JSON-based file, named `Flug1_100-105_frictionless_standards`.

All files are represented in a standardized way as FAIR Digital Objects (FAIR DOs) to enable machine actionable decisions on the data in the spirit of the FAIR principles³³. This representation further facilitates reproducibility of experiments performed using TBBR and the detection of data errors³⁴. Thus, each file deposited in Zenodo (<https://doi.org/10.5281/zenodo.7022736>)²⁷ was assigned a Persistent Identifier (PID), which is resolvable with the Handle.Net Registry (HNR) (<https://www.handle.net/>). The full list of PIDs are listed in the TBBR Zenodo dataset description²⁷.

Technical Validation

The visual identification process and description of thermal bridges on building rooftops was based on typical patterns described in German DIN standards^{35–37} and thermal infrared inspections³⁸. We note, however, that the interpretation of thermal images for building audits is currently always performed by human operators, which involves a high level of subjectivity¹³.

Thermal bridges occur on different parts of rooftops. Table 3 provides an overview about the different roof types and rooftop components where thermal bridges were annotated.

All preselected images were first manually annotated by a single industrial engineer. Then, following the two-person principle, all annotations were subsequently reviewed independently by an expert supervisor and corrected when necessary.

We qualitatively compare the distributions of thermal and height map values of thermal bridges and background between the train and test subsets. Figure 4 shows the histograms of both distributions within their 8-bit channel ranges of [0,255]. As expected, we observe a uniform distribution of thermal values across background pixels, while there is a distinct peak in warmer pixels for thermal bridges. Similarly, we see the presence of thermal bridges on rooftops only being reflected in the large height map values of thermal bridges, while background pixels are distributed uniformly both at the building level, and to a lesser extent at street level.

To quantitatively compare annotated distributions, we use scale invariant feature transform (SIFT) descriptors³⁹ which has been shown to have a good general robustness across a range of image transformations⁴⁰, e.g. affine transformations, scale changes, and rotations, making it an appropriate comparison for thermal bridge images of rooftops from various distances and angles. Figure 5 shows the average Euclidean distances between all 128 SIFT descriptors for annotated thermal bridges and background pixels across the train and test subsets. We observe a small distance between like classes across both train and test subsets, and larger relative distances for unlike classes, indicating that annotated regions contain distinct features from background in a consistent manner.

Usage Notes

The annotation files contain relative paths to the NumPy files. We recommend the folder structure shown in Fig. 6 for usage of TBBR in conjunction with computer vision libraries such as `Detectron2`⁴¹ or `MMDetection`⁴², or with the provided `TBBRDet` library (see Code Availability).

For image analysis pipelines we recommend to standardize the images, i.e. center it to 0 mean with a standard deviation of 1, to make the different channel ranges of the image data comparable:

$$Z_{(w \times h, c)} = \frac{I_{(w \times h, c)} - \bar{I}_{(c)}}{\sigma(I)_{(c)}}$$

where Z is the transformed data, I the input images, overlines are mean values and σ the standard deviation, subscripts denote shapes of the data. For ease-of-use, we have precomputed the resulting values:

$$\bar{I}_{(5)} = [130.0, 135.0, 135.0, 118.0, 118.0] \quad \sigma(I)_{(5)} = [44.0, 40.0, 40.0, 30.0, 21.0].$$

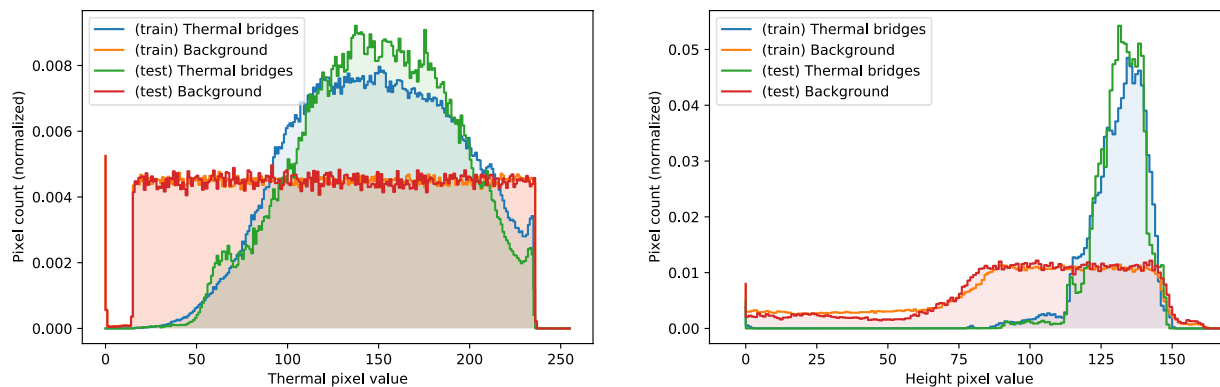


Fig. 4 Histograms of thermal (left) and height map (right) pixel values of thermal bridges and background for both the train and test subsets within their 8-bit channel ranges of [0, 255]. Note that the height map values have been truncated slightly above their maximum at 170 for visual clarity. The zero valued pixel peaks arises from slight (~20 pixels) black borders remaining on the right side of images after cropping.

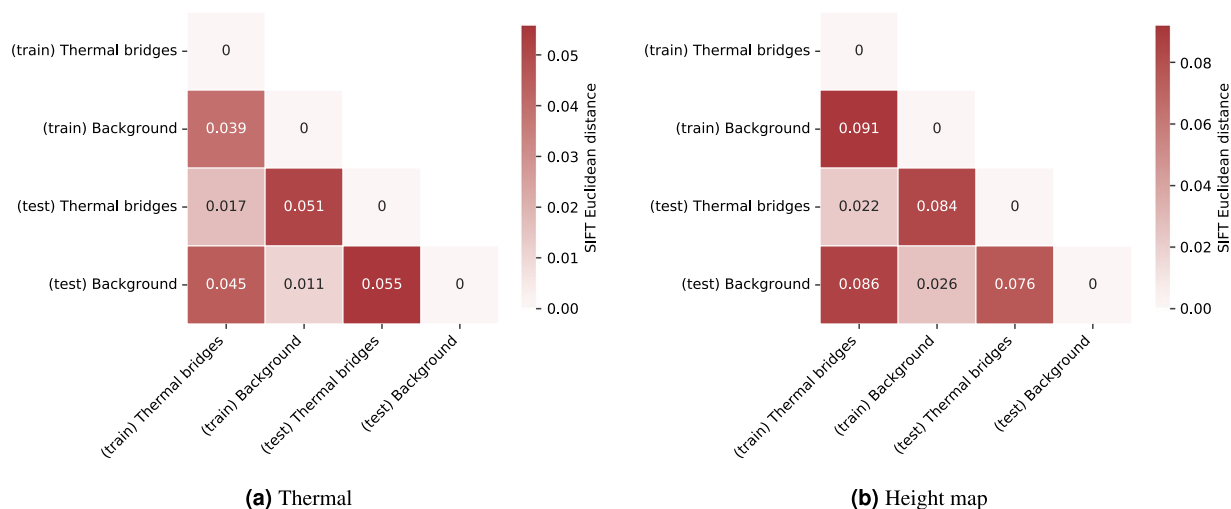


Fig. 5 Euclidean distances between SIFT descriptors for thermal bridges and background annotations between train and test subsets.

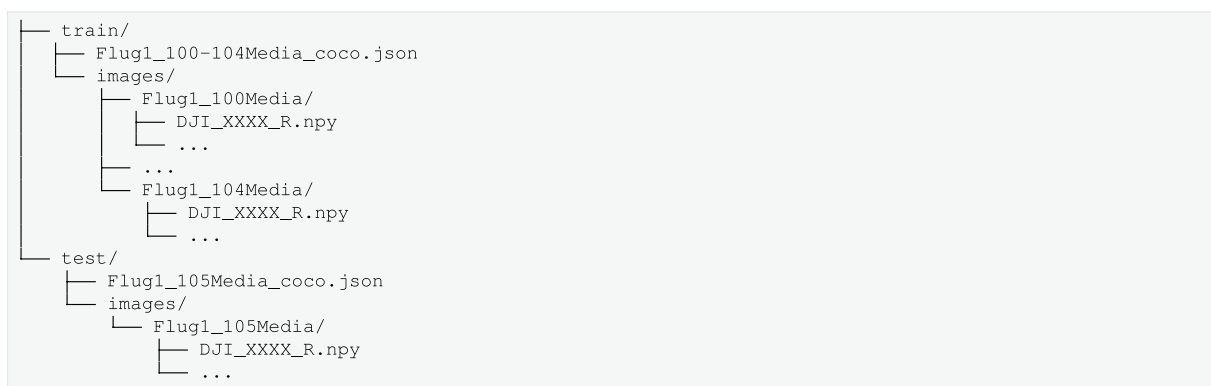


Fig. 6 Recommended folder structure for TBBD dataset.

Code availability

Processing code is publicly available and can be found at <https://github.com/Helmholtz-AI-Energy/TBBDet>. The software is licensed under the Revised Berkley Software Distribution (BSD-3) license (<https://opensource.org/licenses/BSD-3-Clause>). All scripts are implemented with the Python (v.3.6.8) programming language⁴³ and

utilize the PyTorch (v.1.10.2) machine learning framework⁴⁴.

Conceptually, the software provides the following functionalities:

VGG annotation to COCO JSON converter implementing fully automatic conversion from the annotation format generated during the manual labeling process into the COCO JSON format archived on Zenodo.

Dataset mappers for the Detectron2 and MMDetection libraries implementing random-access collections to individual images and corresponding annotations. These are necessary for enabling the loading of five-channel images in each library. Data may be augmented by arbitrary transformations during the loading procedure.

Model configuration for all Detectron2 and MMDetection experiments performed in related works.

Training/evaluation scripts for performing training and evaluation of neural networks for both Detectron2 and MMDetection.

Dataset/experiment utilities for exploring the dataset, calculating image normalization coefficients, combining model scores, and calculating SLURM workload manager system⁴⁵ statistics (consumed energy, runtime, etc.).

For creating, updating, and validating the FAIR DOs, the Typed PID Maker was used. This is a component of the FAIR DO Lab for working on FAIR DO tasks, which is found at <https://github.com/kit-data-manager/FAIR-DO-Lab>.

Received: 12 October 2022; Accepted: 6 April 2023;

Published online: 10 May 2023

References

- International Energy Agency (IEA). Tracking Buildings 2022. Tech. Rep., International Energy Agency (IEA), Paris (2022).
- International Energy Agency (IEA). Building Envelopes. Tech. Rep., International Energy Agency (IEA), Paris (2021).
- Ge, H. & Baba, F. Dynamic Effect of Thermal Bridges on the Energy Performance of a Low-Rise Residential Building. *Energy and Buildings* **105**, 106–118, <https://doi.org/10.1016/j.enbuild.2015.07.023> (2015).
- Schild, K. *Wärmebrücken* (Springer Fachmedien, Wiesbaden, 2018).
- Theodosiou, T. G. & Papadopoulos, A. M. The Impact of Thermal Bridges on the Energy Demand of Buildings with Double Brick Wall Constructions. *Energy and Buildings* **40**, 2083–2089, <https://doi.org/10.1016/j.enbuild.2008.06.006> (2008).
- Fantucci, S., Isaia, F., Serra, V. & Dutto, M. Insulating coat to prevent mold growth in thermal bridges. *Energy Procedia* **134**, 414–422, <https://doi.org/10.1016/j.egypro.2017.09.591> (2017).
- Kalamees, T., Korpi, M., Eskola, L., Kurnitski, J. & Vinha, J. *The Distribution of the Air Leakage Places and Thermal Bridges in Finnish Detached Houses and Apartment Buildings* (Danish Society of Engineers, IDA, 2008).
- Kylili, A., Fokaides, P. A., Christou, P. & Kalogirou, S. A. Infrared thermography (IRT) applications for building diagnostics: A review. *Applied Energy* **134**, 531–549, <https://doi.org/10.1016/j.apenergy.2014.08.005> (2014).
- General Assembly of the United Nations. New Urban Agenda: Resolution Adopted by the General Assembly (2016).
- Ma, L., Li, M., Tong, L., Wang, Y. & Cheng, L. Using Unmanned Aerial Vehicle for Remote Sensing Application. In *2013 21st International Conference on Geoinformatics*, 1–5, <https://doi.org/10.1109/Geoinformatics.2013.6626078> (2013).
- Mayer, Z., Kahn, J., Hou, Y. & Volk, R. AI-based thermal bridge detection of building rooftops on district scale using aerial images. In *EG-ICE 2021 Workshop on Intelligent Computing in Engineering*. Ed.: Jimmy Abualdenien, André Borrmann, Lucian-Constantin Ungureanu, Timo Hartmann, 497 (2021).
- Zhang, J., Jung, J., Sohn, G. & Cohen, M. Thermal Infrared Inspection of Roof Insulation Using Unmanned Aerial Vehicles. *ISPRS - International Archives of the Photogrammetry, Remote Sensing and Spatial Information Sciences* **XL1**, 381–386, <https://doi.org/10.5194/isprsarchives-XL-1-W4-381-2015> (2015).
- Garrido, I., Lagüela, S., Arias, P. & Balado, J. Thermal-Based Analysis for the Automatic Detection and Characterization of Thermal Bridges in Buildings. *Energy and Buildings* **158**, 1358–1367, <https://doi.org/10.1016/j.enbuild.2017.11.031> (2018).
- Macher, H., Landes, T. & Grussenmeyer, P. Automation of Thermal Point Clouds Analysis for the Extraction of Windows and Thermal Bridges of Building Facades. In *The International Archives of the Photogrammetry, Remote Sensing and Spatial Information Sciences*, vol. XLIII-B2-2020, 287–292, <https://doi.org/10.5194/isprs-archives-XLIII-B2-2020-287-2020> (Copernicus GmbH, 2020).
- Rakha, T., Liberty, A., Gorodetsky, A., Kakillioglu, B. & Velipasalar, S. Heat Mapping Drones: An Autonomous Computer-Vision-Based Procedure for Building Envelope Inspection Using Unmanned Aerial Systems (UAS). *Technology: Architecture + Design* **2**, 30–44, <https://doi.org/10.1080/24751448.2018.1420963> (2018).
- Mirzabeigi, S. & Razkenari, M. Automated Vision-Based Building Inspection Using Drone Thermography. In *20th Annual New York State Green Building Conference*, 737–746, <https://doi.org/10.1061/9780784483961.077> (American Society of Civil Engineers, 2022).
- Kim, C., Choi, J.-S., Jang, H. & Kim, E.-J. Automatic Detection of Linear Thermal Bridges from Infrared Thermal Images Using Neural Network. *Applied Sciences* **11**, 931, <https://doi.org/10.3390/app11030931> (2021).
- Flores Larsen, S. & Hongn, M. Determining the infrared reflectance of specular surfaces by using thermographic analysis. *Renewable Energy* **64**, 306–313, <https://doi.org/10.1016/j.renene.2013.11.049> (2014).
- Wilkinson, M. D. *et al.* The FAIR Guiding Principles for scientific data management and stewardship. *Scientific data* **3**, 1–9, <https://doi.org/10.1038/sdata.2016.18> (2016).
- Deutsches Institut für Normung e.V. (DIN). DIN 4108-2:2013-02, Thermal protection and energy economy in buildings - Part 2: Minimum requirements to thermal insulation. Tech. Rep., Beuth Verlag GmbH. <https://doi.org/10.31030/1929159> (2013).
- Kahn, J. *et al.* Hyperspectral (RGB + Thermal) drone images of Karlsruhe, Germany - Raw images for the Thermal Bridges on Building Rooftops (TBBR) dataset, <https://doi.org/10.5281/zenodo.7360996> (2022).
- Dutta, A. & Zisserman, A. The VIA Annotation Software for Images, Audio and Video. In *Proceedings of the 27th ACM International Conference on Multimedia*, MM '19, <https://doi.org/10.1145/3343031.3350535> (ACM, New York, NY, USA, 2019).
- Hou, Y., Volk, R., Chen, M. & Soibelman, L. Fusing tie points' RGB and thermal information for mapping large areas based on aerial images: A study of fusion performance under different flight configurations and experimental conditions. *Automation in Construction* **124**, <https://doi.org/10.1016/j.autcon.2021.103554> (2021).
- Hou, Y., Chen, M., Volk, R. & Soibelman, L. Investigation on performance of RGB point cloud and thermal information data fusion for 3D building thermal map modeling using aerial images under different experimental conditions. *Journal of Building Engineering* **45**, <https://doi.org/10.1016/j.jobee.2021.103380> (2022).
- Bradski, G. The OpenCV library. *Dr. Dobbs' Journal: Software Tools for the Professional Programmer* **25**, 120–123 (2000).
- Harris, C. R. *et al.* Array programming with NumPy. *Nature* **585**, 357–362, <https://doi.org/10.1038/s41586-020-2649-2> (2020).
- Mayer, Z. *et al.* Thermal Bridges on Building Rooftops - Hyperspectral (RGB + Thermal + Height) drone images of Karlsruhe, Germany, with thermal bridge annotations. Zenodo <https://doi.org/10.5281/zenodo.7022736> (2022).
- Collet, Y. & Kucherawy, M. RFC 8878: Zstandard Compression and the 'application/zstd' Media Type. Tech. Rep., Internet Engineering Task Force (IETF). <https://doi.org/10.17487/RFC8878> (2021).

29. Lin, T.-Y. *et al.* Microsoft COCO: Common Objects in Context. In *European conference on computer vision*, 740–755. https://doi.org/10.1007/978-3-319-10602-1_48 (Springer, 2014).
30. Mayer, Z. *et al.* Deep learning approaches to building rooftop thermal bridge detection from aerial images. *Automation in Construction* **146**, 104690. <https://doi.org/10.1016/j.autcon.2022.104690> (2023).
31. Musen, M. A. Without appropriate metadata, data-sharing mandates are pointless. *Nature* **609**, 222–222. <https://doi.org/10.1038/d41586-022-02820-7> (2022).
32. Butler, H. *et al.* The GeoJSON Format. Request for Comments RFC 7946, Internet Engineering Task Force. <https://doi.org/10.17487/RFC7946> (2016).
33. Schwardmann, U. Digital objects – fair digital objects: Which services are required? *Data Science Journal* **19**. <https://doi.org/10.5334/dsj-2020-015> (2020).
34. Berberi, I. & Roche, D. G. No evidence that mandatory open data policies increase error correction. *Nature Ecology & Evolution* 1–4. <https://doi.org/10.1038/s41559-022-01879-9> (2022).
35. Deutsches Institut für Normung e.V. (DIN). DIN EN 13187:1999-05, Thermal performance of buildings - Qualitative detection of thermal irregularities in building envelopes - Infrared method (ISO 6781:1983, modified); German version EN 13187:1998. Tech. Rep., Beuth Verlag GmbH. <https://doi.org/10.31030/8035327> (1999).
36. Deutsches Institut für Normung e.V. (DIN). DIN EN ISO 10211:2018-03, Thermal bridges in building construction - Heat flows and surface temperatures - Detailed calculations (ISO 10211:2017); German version EN ISO 10211:2017. Tech. Rep., Beuth Verlag GmbH. <https://doi.org/10.31030/2522431> (2018).
37. Deutsches Institut für Normung e.V. (DIN). DIN 4108 Beiblatt 2:2019-06, Thermal insulation and energy economy in buildings; Supplement 2: Thermal bridges - Examples for planning and performance, with CD-ROM. Tech. Rep., Beuth Verlag GmbH. <https://doi.org/10.31030/3054799> (2019).
38. Balaras, C. A. & Argiriou, A. A. Infrared thermography for building diagnostics. *Energy and Buildings* **34**, 171–183. [https://doi.org/10.1016/S0378-7788\(01\)00105-0](https://doi.org/10.1016/S0378-7788(01)00105-0) (2002).
39. Lowe, D. G. Distinctive Image Features from Scale-Invariant Keypoints. *International Journal of Computer Vision* **60**, 91–110. <https://doi.org/10.1023/B:VISI.0000029664.99615.94> (2004).
40. Mikolajczyk, K. & Schmid, C. A performance evaluation of local descriptors. *IEEE Transactions on Pattern Analysis and Machine Intelligence* **27**, 1615–1630. <https://doi.org/10.1109/TPAMI.2005.188> (2005).
41. Wu, Y., Kirillov, A., Massa, F., Lo, W.-Y. & Girshick, R. Detectron2 (2019).
42. Chen, K. *et al.* MMDetection: Open MMLab detection toolbox and benchmark. *arXiv preprint arXiv:1906.07155*, (2019).
43. Van Rossum, G. & Drake, F. L. *Python 3 Reference Manual* (CreateSpace, Scotts Valley, CA, 2009).
44. Paszke, A. *et al.* Pytorch: An imperative style, high-performance deep learning library. In Wallach, H. *et al.* (eds.) *Advances in Neural Information Processing Systems* **32**, 8024–8035 (Curran Associates, Inc., 2019).
45. Yoo, A. B., Jette, M. A. & Grondona, M. SLURM: Simple Linux Utility for Resource Management. In Feitelson, D., Rudolph, L. & Schwiegelshohn, U. (eds.) *Job Scheduling Strategies for Parallel Processing*, Lecture Notes in Computer Science, 44–60. https://doi.org/10.1007/10968987_3 (Springer, Berlin, Heidelberg, 2003).

Acknowledgements

This work is supported by the Helmholtz Association Initiative and Networking Fund under the Helmholtz AI platform grant, the HAICORE@KIT partition and Helmholtz Metadata Collaboration grant. We thank Marinus Vogl and the Air Bavarian GmbH for their support with equipment and service for the recording of images.

Author contributions

Z.M., J.K. conceived the experiments, Z.M., J.K., M.G., Y.H., developed the methodology, R.V., Y.H. conducted the data collection, Z.M., J.K., T.B., Y.H., M.G., N.B. analysed, curated, preprocessed and annotated the data, Z.M., J.K., Y.H., M.G., R.V., N.B., A.S., F.S. wrote the manuscript; All authors reviewed the manuscript.

Funding

Open Access funding enabled and organized by Projekt DEAL.

Competing interests

The authors declare no competing interests.

Additional information

Correspondence and requests for materials should be addressed to Z.M., M.G. or R.V.

Reprints and permissions information is available at www.nature.com/reprints.

Publisher's note Springer Nature remains neutral with regard to jurisdictional claims in published maps and institutional affiliations.



Open Access This article is licensed under a Creative Commons Attribution 4.0 International License, which permits use, sharing, adaptation, distribution and reproduction in any medium or format, as long as you give appropriate credit to the original author(s) and the source, provide a link to the Creative Commons license, and indicate if changes were made. The images or other third party material in this article are included in the article's Creative Commons license, unless indicated otherwise in a credit line to the material. If material is not included in the article's Creative Commons license and your intended use is not permitted by statutory regulation or exceeds the permitted use, you will need to obtain permission directly from the copyright holder. To view a copy of this license, visit <http://creativecommons.org/licenses/by/4.0/>.

© The Author(s) 2023

Paper H: Aerial Thermographic Image-Based Assessment of Thermal Bridges Using Representative Classifications and Calculations

This paper was reproduced in its original format with permission from MDPI:

Mayer, Z., Heuer, J., Volk, R., Schultmann, F. (2021 - Paper H). Aerial thermographic image-based assessment of thermal bridges using representative classifications and calculations. *Energies*, 14(21), 7360. Doi: <https://doi.org/10.3390/en14217360>

Article

Aerial Thermographic Image-Based Assessment of Thermal Bridges Using Representative Classifications and Calculations

Zoe Mayer *, Julia Heuer, Rebekka Volk *  and Frank Schultmann 

Karlsruhe Institute of Technology (KIT), Institute for Industrial Production (IIP), Hertzstr. 16, 76187 Karlsruhe, Germany; jc.heuer@gmail.com (J.H.); frank.schultmann@kit.edu (F.S.)

* Correspondence: zoe.mayer@partner.kit.edu (Z.M.); rebekka.volk@kit.edu (R.V.)

Abstract: Since the middle of the 20th century many any buildings were built without any energy standards and still have a comparably poor energy quality. To obtain an overview of the current thermal quality of buildings in a whole city district, it may be promising to work with thermographic images obtained by unmanned aerial vehicles (UAV). Aerial thermography represents a fast and cost-efficient approach compared to traditional terrestrial thermography. In this paper, we describe an approach to finding thermal bridges on aerial thermographic images and characterizing them in terms of their risk of mold formation, energy losses, retrofit costs, and retrofit benefits. To identify thermal bridge types that can be detected reliably on aerial thermographic images, we use a dataset collected with a UAV in an urban district of the German city of Karlsruhe. We classify and characterize 14 relevant thermal bridge types for the German building cohorts of the 1950s and 1960s. Concerning the criterion of mold formation, thermal bridges of window components, basement ceiling slabs, balcony slabs, floor slabs, and attics are found to be particularly relevant to retrofit projects. Regarding energy savings, the retrofit of thermal bridges of window sills, window lintels, and attics shows high potential. The retrofit of attics seems to be less attractive, when also taking into account the necessary retrofit costs.

Keywords: buildings; energy retrofits; thermal bridges; thermography; energy assessment; drones; unmanned aerial vehicles (UAV)



Citation: Mayer, Z.; Heuer, J.; Volk, R.; Schultmann, F. Aerial Thermographic Image-Based Assessment of Thermal Bridges Using Representative Classifications and Calculations. *Energies* **2021**, *14*, 7360. <https://doi.org/10.3390/en14217360>

Academic Editors: Adélio Rodrigues Gaspar and Benedetto Nastasi

Received: 18 August 2021
Accepted: 22 October 2021
Published: 5 November 2021

Publisher's Note: MDPI stays neutral with regard to jurisdictional claims in published maps and institutional affiliations.



Copyright: © 2021 by the authors. Licensee MDPI, Basel, Switzerland. This article is an open access article distributed under the terms and conditions of the Creative Commons Attribution (CC BY) license (<https://creativecommons.org/licenses/by/4.0/>).

1. Introduction

A significant share of global greenhouse gas and in particular CO₂ emissions comes from the building and real estate sector [1]. Most greenhouse gas emissions are not emitted during the construction phase, but during building operation, especially for heating [2]. In many European countries (e.g., Greece, Italy), a major part of the building stock was built without any energy standards [3,4]. In Germany, about 75% of the building stock was built before adoption of the first German thermal insulation regulation of 1979 (“Wärmeschutzverordnung”) and, hence, often is of low energy quality [5,6]. Even today, more than 50 years after the construction of these buildings, their energy quality is significantly worse than that of newer buildings [7].

Buildings that have not yet been retrofitted consume up to five times more heating energy than modern buildings [2]. This is mainly caused by a lack of thermal insulation and thermal bridges. A thermal bridge is an area of the building envelope where heat is transported considerably faster from the warmer inside to the colder outside than in adjacent areas. Reasons are different thermal conductivities of materials, geometries of constructions and components, and air leaks [8,9]. Thermal bridges cause energy losses of up to one third of the transmission heat loss of an entire building [8]. Additionally, they lead to the collection of moisture, which can degrade the building fabric or cause mold formation [8].

To identify weak points of the building envelope such as thermal bridges, an analysis of the thermal quality of buildings is required for an effective and efficient energy retrofit.

Infrared thermal imaging allows conclusions to be drawn with respect to thermal radiation, air leaks, and moisture permeability [10] and, thus, also provides good information for detecting thermal bridges [11]. Thermography for the energy audit of individual buildings is a well-proven technique that has been in use since the early 2000s. Lucchi [12] provides a comprehensive overview of the history and applications of infrared thermography in the energy audit of buildings. Advantages and disadvantages of various thermography approaches are summarized by Kylili et al. [13], who review literature and research in the field of infrared thermography.

To reduce the energy demand of whole building stocks, it is essential to improve the thermal quality not just of individual buildings, but also of entire city districts [14]. Retrofit approaches that focus on districts (communities/neighborhoods) are gaining importance in international retrofit practice [14]. Examples of the simultaneous retrofit planning of many buildings in a district are Community Energy Strategic Planning (CESP) in the USA [15], Community Energy Planning (CEP) in Canada [16], Positive Energy Districts (PED) in Europe [17], and “energetische Quartierskonzepte” (EQ) in Germany [18].

Thermography can also be used for the analysis of buildings in a whole city district. In a detailed thermographic assessment of individual buildings, both exterior and interior images should be recorded in accordance with the German standard DIN EN 13187 (1999) [19] and taking into account background information, such as building materials and construction methods. For the simultaneous assessment of the thermal quality of a large number of individual buildings, such detailed analyses usually are not suitable, as they are very time-consuming and expensive [11].

Outdoor thermography without additional building background information still allows for the detection of thermal bridges, e.g., [10,20]. To audit many buildings within a short time and with high efficiency, moving thermography is gaining importance. However, there are only a few approaches [21–25] that analyze multiple buildings at one time (e.g., in a district) with respect to thermal bridges. Miller and Singh [21], Garrido et al. [22], and Macher et al. [23] placed an infrared camera on the top of a car for the camera to take several pictures of a building façade at an angle of 45°. Their studies focused on the automatic detection of thermal bridges using software. A main disadvantage of their approach is that only façades facing the street can be analyzed and that rooftops can be hardly recorded. According to Macher et al. [23], this approach is especially suited for detecting thermal bridges between floors and under balconies. Miño et al. [24] and Aguerre et al. [25] as well only focus on the street and terrestrial perspective.

For recording images from all different angles of buildings, including rooftops, unmanned aerial vehicles (UAV, pl. UAVs/drones) equipped with thermal cameras can be used [26]. Many scientific publications deal with the ideal framework conditions for recording thermographic images using drones. Vorajee et al. [27] wanted to find a qualified and lightweight infrared camera to detect thermal bridges with drones. Mavromatidis et al. [28] tried to identify possible uses and limits of the combination of thermography and drones regarding the distance between the camera and the object. Entrop and Vasenev [26] developed a protocol for drone flights for the energy audit of buildings based on thermography. Additionally, Benz et al. [29] used drones for the energy audit of buildings and defined a general framework for the assessment of the energy performance of buildings by estimating U-values. They worked with building close-up thermography and tested their approach for a single school building. Hou et al. [30] experimented with different flight patterns and angles for drones with thermographic cameras to record whole city districts as a basis for the analysis of the thermal quality of buildings.

Current publications dealing with the structured analysis of thermal bridges of multiple buildings on thermographic aerial panorama images are not known to the authors. Such a transferable procedure would be helpful in practice for an inexpensive and rapid analysis of a district’s building stock as a basis for the retrofit planning of multiple buildings intended by CESP, CEP, PED, and EQ. Thus, we develop an approach to identifying, classifying, and assessing thermal bridges of building envelopes recorded with thermographic

aerial panorama images on a district scale. This approach is demonstrated for German buildings constructed in the 1950s and 1960s.

2. Methods and Materials

2.1. Procedure

This study aims to investigate how thermal bridges can be detected and assessed in terms of their impact on energy loss, mold growth, and retrofit costs by using outdoor thermographic aerial images of buildings recorded by UAV on the district scale. These recordings are characterized by an increased distance between the infrared camera and the measurement object, changing recording angles depending on UAV flight routes, and the absence of indoor images of buildings.

In the first step of the procedure, it is necessary to record thermographic images with an UAV. For this, an UAV can be programmed to pursue an automatic flight route (e.g., in a mesh grid or a Y-grid) to cover a whole city district from all four cardinal directions [30]. To enhance the quality of the collected images, preprocessing software, e.g., by FLIR [31], is used. With this software, the color scale of thermographic images can be adjusted homogeneously and with a high contrast.

In a next step, thermal bridges can be detected manually on the processed images taking into account different recording/capturing conditions. When selecting images, it should be ensured that the framework conditions for good thermographic practice are fulfilled. This includes suitable weather conditions and recording angles [32]. Good weather conditions means that rain, snow, sun, and wind have to be avoided. The best recording times for images are nights, early mornings, and late evenings of cold winter days. A temperature difference of at least 15 °C from normal indoor temperatures of buildings heated to about 20 °C should be ensured so that temperature gradients can be identified reliably by the human eye [33].

If thermographic images are recorded almost parallel to a building façade (acute angle), misinterpretations of thermal bridges are likely. It is therefore important to sort out images with a small angle (<70°) to the measurement object [10]. To detect thermal bridges, it is necessary to search for high temperature gradients on the buildings. The detected areas on the thermographic images are compared to normal RGB images (recorded with the same UAV or from map service providers) to assure that temperature gradients are not caused by trivial reasons such as open windows or metal constructions.

In order to develop a transferable assessment approach for thermal bridges on thermographic aerial panorama images, thermal bridge types need to be classified and characterized. If no additional information on the buildings in a district is available, assumptions are needed regarding their construction materials and architecture. Thus, this approach is designed for a certain building class with characteristic properties that are needed for the next steps.

This study focuses exclusively on German buildings constructed in the time between 1950 and 1969. Some typical characteristics of this German building age class follow: hardly any constructive thermal insulation; often plastered external walls made of masonry with small cross sections; concrete floors; often flat roofs made of concrete with just a small layer of insulation; wooden windows with small cross sections; and balconies with a continuous floor slab without thermal separation [34]. Buildings of this age class are easily identifiable on aerial images due to their specific characteristics and look.

Analyzing a comprehensive dataset of thermographic aerial UAV images of a German city (Karlsruhe), it was possible to manually identify 14 distinct and relevant thermal bridge types (for details on the dataset, see Section 4). This classification simplifies and is based on the 28 thermal bridge types according to the supplementary sheet 2 of DIN 4108:2019 [35].

In order to characterize the thermal bridge classes concerning the risk of mold growth and potential heat losses, simulation of representative thermal bridges is required. The length of a thermal bridge is defined as the reference value for the simulation (unit: linear

meter). In this way, results can later be transferred to thermal bridges of different lengths, which can be measured, e.g., with measurement tools from map providers or photogrammetry approaches. In this study, the software ThermCad from ROWA-Soft [36] is used. Calculations using this software are based on DIN V 4108-6 [37] and take into account necessary framework conditions in accordance with the supplementary sheet 2 of DIN 4108 [35]. For the materials and quality of building envelope components, all assumptions for the simulation are listed in Appendix A. The simulation uses a relative indoor air humidity of 50% and a relative air humidity on the component surfaces of 80%.

Suitable retrofit options for each thermal bridge type can also be simulated with ThermCad. The individual retrofit recommendations in this study are based on the criteria of preventing mold formation, saving energy, and finding retrofit measures with minimal scope and costs. The cost calculations for retrofits in this study use the BKI database for both old and new buildings from 2020 [38,39], which is standard in Germany. All cost values have been checked by professionals and are based on statistical evaluations of more than 600 billed construction projects accounted in accordance with DIN 276 [40]. Then, all costs are converted to the unit (EUR/linear meter of thermal bridge retrofit) to also refer to the length of a thermal bridge. An overview of our research approach is given in Figure 1.

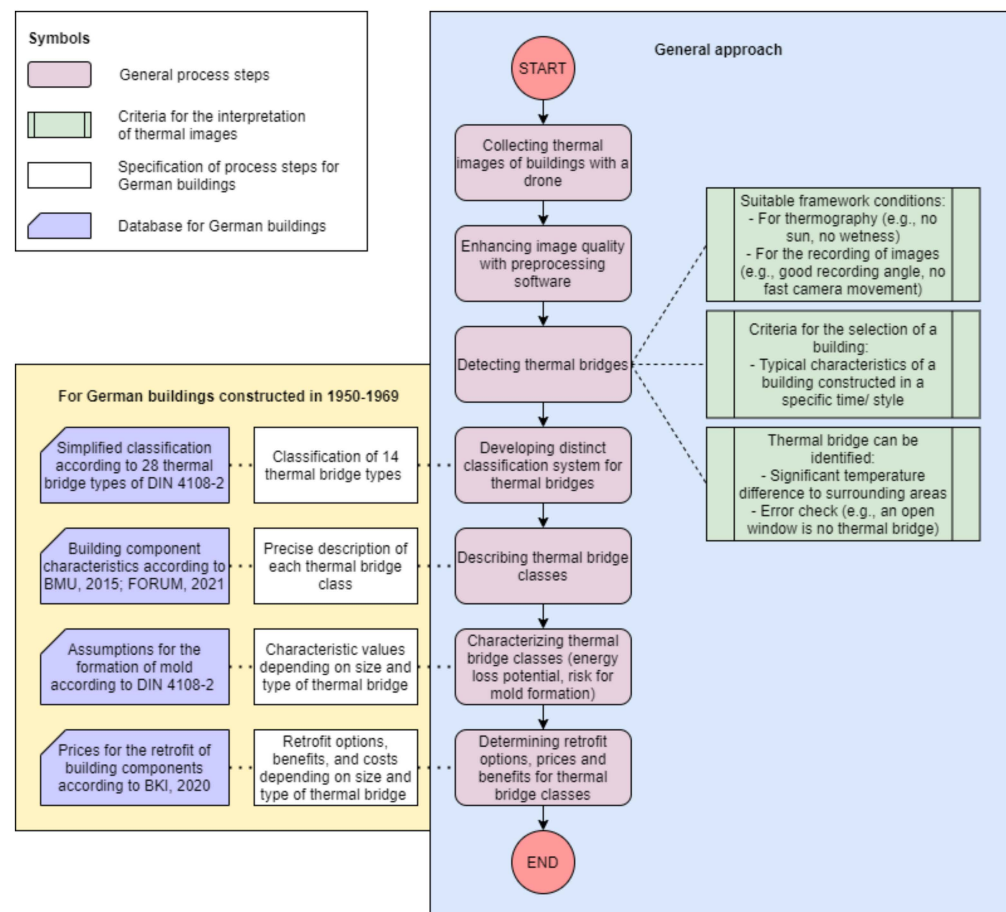


Figure 1. Research approach of this study presented in a flow diagram. The focus of this paper is on buildings constructed in Germany in the time between 1950 and 1969.

2.2. Database

The database of this study consists of thermal drone images recorded with a DJI Matrice 600 Pro drone [41], which is especially suitable for professional aerial photography, combined with the infrared camera DJI Zenmuse XT2 by FLIR [42,43]. This camera system is DJI gimbal combined with a FLIR Duo Pro R camera. The FLIR camera combines both thermal imager and visual camera. The thermal camera contains an uncooled VOx

microbolometer working in the long wavelength range between 7.5 and 13.3 μm . It has a focal length of 13 mm, a sensor width of 10.88 mm and a spatial resolution of 640×512 pixels per image. [42,43]

The area studied is the city district “Innenstadt-Ost” of the German mid-size city Karlsruhe. It is characterized by a particularly large number of typical German multifamily and mixed-use buildings constructed in the 1950s and 1960s with a low thermal quality and a small retrofit progress. In the district, there are primarily apartment buildings for living, commercial and administrative buildings, and university buildings on the Campus South of Karlsruhe Institute of Technology. A map of the area studied is presented in Figure 2.

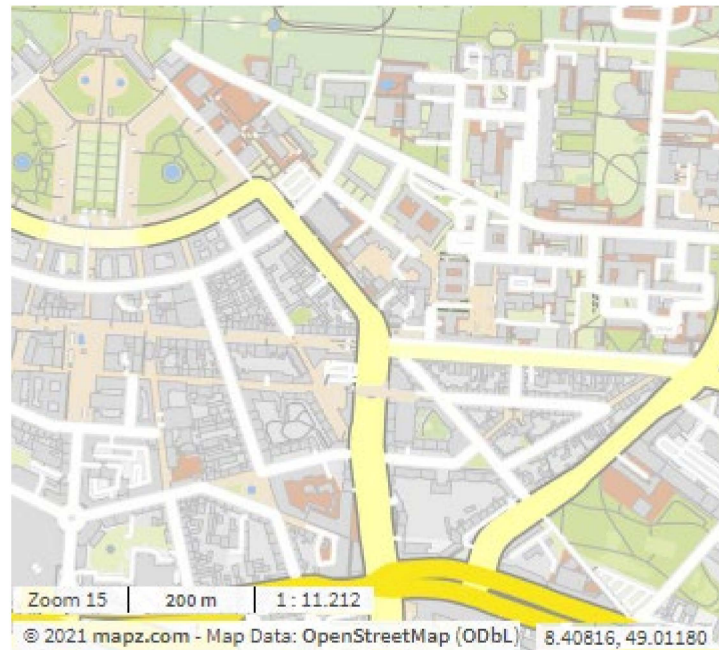


Figure 2. Area where thermal drone images were collected. Map of the city of Karlsruhe, district Innenstadt-Ost [44].

The image data were recorded during 16 drone flights carried out on three consecutive days, 19–21 March 2019. From 1–18 March 2019 in the morning, there were a total of 14 rainy days. In this time period, the average maximum daily temperature was 12 °C and the average minimum daily temperature was 5 °C. During the three days of flight, no rainfall was recorded. The air had relatively constant low temperatures between 2 °C and a maximum of 8.7 °C during the individual flights. In addition, wind speeds were steady at around 5 km/h on 19 March 2019 and around 17 km/h on 20–21 March 2019. The images were recorded in the morning and late evening with a low global radiation of less than 100 W/m².

In sum, the data set contains around 10,000 thermal and RGB images each. The formats of the images are panorama images that cover many different objects in one image and were taken at a height of 60–80 m above ground with a considerable overlap between 80–90%. The extraction of the raw thermal information from the image files depends on the file format and camera manufacturer. Thus, for the processing of the thermographic images, we use the FLIR Tools [31] from FLIR systems. Here, the original gray scale thermal images are colored via the coloring scheme “rainbow” and a temperature scale between −8 and +8 °C. However, it must be noted that truly accurate temperature measurements are difficult to obtain owing to many influencing parameters. An example of a thermographic image of the data set with its corresponding RGB image is shown in Figure 3.

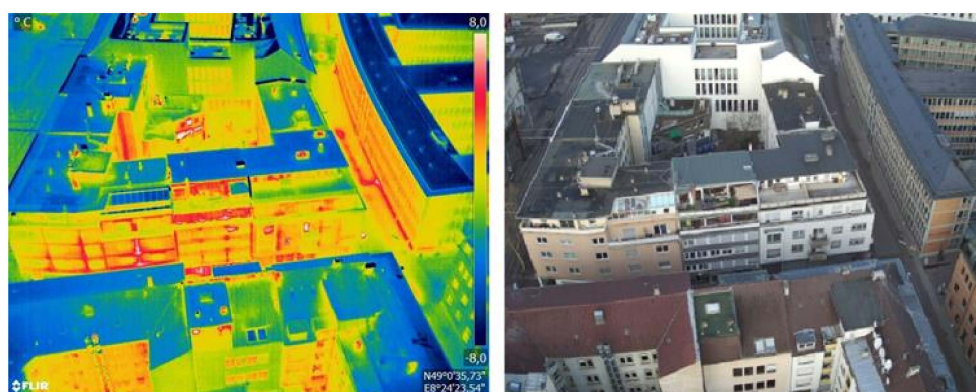


Figure 3. Thermographic aerial panorama image (**left**) with the corresponding RGB aerial panorama image (**right**) of inner-city buildings in Karlsruhe.

2.3. Classification and Assessment of Thermal Bridges in German Buildings Constructed between 1950 and 1969

2.3.1. Types of Thermal Bridges

In the dataset, we manually identified 14 different types of thermal bridges on thermographic images of German buildings constructed between 1950 and 1969. These types of thermal bridges can be categorized according to the building component in which they occur. Explicitly, we identified the types listed in Table 1.

Table 1. Types of thermal bridges sorted by the building parts in which they occur.

Building Part	Type of Thermal Bridge
Thermal bridges of outer walls	Connection of the basement ceiling slab with the outer wall Connection of the wall and the rooftop Connection of an inside wall with the outer wall Connection of a floor slab with the outer wall
Thermal bridge types of balconies	Balcony slab
Thermal bridge types of windows	Roller shutter casing Window lintel Window reveal Window sill
Thermal bridge types of rooftops	Connection between the rooftop and an outer wall (steep roof) Connection of the rooftop and a dormer (steep roof) Roof ridge (steep roof) Connection of a staggered story with the rooftop (flat roof) Connection of an attic with the rooftop (flat roof)

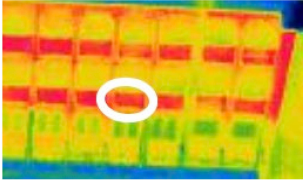
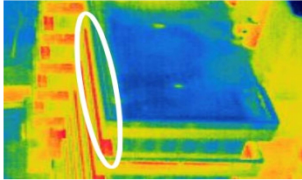
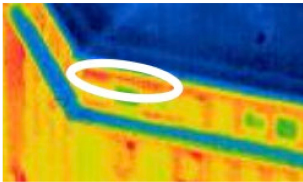
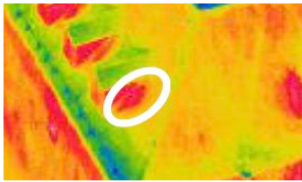

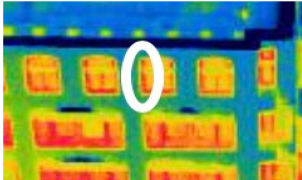
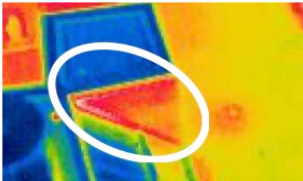
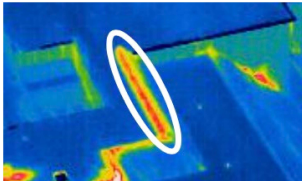
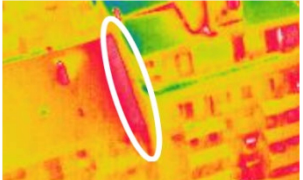
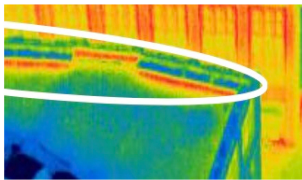
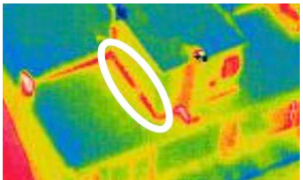
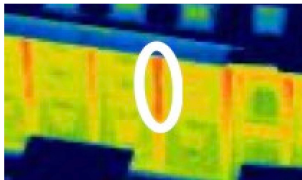
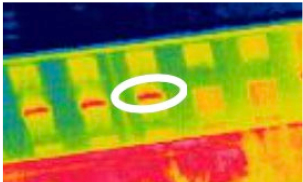
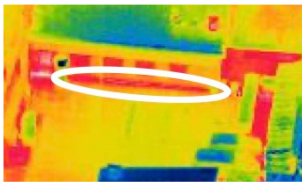
An overview of the 14 thermal bridge types with the corresponding thermographic image excerpts of the dataset is given in Table 2. Detailed descriptions of these thermal bridge types with the panorama images from our database are listed in Appendix B. A list of thermal anomalies that repeatedly appear on thermographic images of our dataset and that should not be misinterpreted as thermal bridges of buildings is given in Appendix C.

2.3.2. Retrofits of Thermal Bridges

Every type of thermal bridge leads to a different energy loss and mold risk and requires individual retrofit measures. Current retrofits for thermal bridges usually include (1) a partial demolition/removal of the old construction components causing a thermal bridge, (2) the installation of new construction components, including insulation material or/and completely new components, and (3) ancillary measures such as the installation of a scaffold or moisture tests [45]. In this study, ancillary measures are not included, as they

usually depend on the framework conditions of the individual buildings and on whether multiple retrofit measures are carried out at the same time.

Table 2. Overview of 14 thermal bridge types of German buildings constructed in the time between 1950 and 1969 with thermographic image excerpts.

Type of Thermal Bridge	Example Image	Type of Thermal Bridge	Example Image
Window sill		Balcony slab	
Window lintel		Dormer	
Floor slab		Window reveal	
Connection wall and rooftop		Roof ridge	
Connection rooftop on wall		Attic	
Staggered story		Inside wall	
Roller shutter casing		Basement ceiling slab	

For all types of thermal bridges in this study, common and simple retrofit measures are considered. For each thermal bridge, one retrofit recommendation is listed in Appendix B, including a list of all required retrofit measures and calculated costs per linear meter of thermal bridge.

2.3.3. Characteristic Values for Thermal Bridges

For the simulation and analysis of the different thermal bridge types and their effects, three characteristic technical values provide information on the risk of mold formation and the energy loss potential. These are:

- The temperature factor $f_{R,si}$ (-) for evaluating internal surface temperatures with regard to the risk of mold formation according to the supplementary sheet 2 of DIN 4108 [35]: A component can be assessed to be free from mold at a relative humidity of higher than 50% regardless of the indoor and outdoor temperatures, if $f_{R,si}$ is higher than 0.7. For a simple assessment approach, it can thus be assumed that if $f_{R,si}$ is lower than 0.7, a retrofit is necessary or should be considered because of a high risk of mold growth and building component deterioration. If $f_{R,si}$ is higher than 0.7, it can be assumed that a retrofit is not necessary to prevent mold growth.
- The thermal bridge loss coefficient Ψ (W/(m*K)) for determining additional heat losses caused by thermal bridges according to DIN EN ISO 10211 [46]: The coefficient Ψ quantifies the additional heat losses through the building envelope caused by a thermal bridge. It refers to linear thermal bridges and depends on the length of a thermal bridge.
- The transmission heat loss per length of thermal bridge q (W/m) (not explicitly defined in standards): The heat loss q also refers to the length of linear thermal bridges and defines the total heat flow through a linear meter of thermal bridge.

Applying the ThermCad simulation tool, all three characteristic values for each type of thermal bridge can be derived both for the original state ($f_{R,si,0}$, Ψ_0 , q_0) and after a retrofit of the thermal bridge according to Section 3 and Appendix B ($f_{R,si,1}$, Ψ_1 , q_1). To quantify the benefit of the considered retrofit recommendation for the individual types of thermal bridges, the reduction of the thermal bridge loss coefficient $\Delta\Psi = \Psi_0 - \Psi_1$ (W/(m*K)) and the reduction of heat flow $\Delta q = q_0 - q_1$ (W/m) after a retrofit are calculated as well.

3. Results

As a result of our study, we provide in Appendix B a detailed thermal bridge catalog for German buildings constructed between 1950 and 1969. This catalog contains comprehensive information on the 14 relevant thermal bridge types identified in this study, provides exemplary aerial thermographic panorama images of each thermal bridge, and describes simple retrofit measures.

For representative thermal bridges (see Table 1), we quantified the characteristic values according to Section 2.3.3 for the 14 thermal bridge types before and after a retrofit, the estimated costs for a retrofit, and the reduction of heat flow per invested Euro of a retrofit (called herein the benefit–cost ratio). These values are listed in Table 3 in descending order of the cost–benefit ratio.

Considering the criterion of mold formation, two thermal bridge types can be assessed to be free from mold with a value of $f_{R,si,0}$ that is significantly higher than 0.7. According to the assessment of examples from the dataset, seven thermal bridge types have a high risk of mold formation with a value of $f_{R,si,0}$ that is clearly lower than 0.7. Five types of thermal bridges have a value of $f_{R,si,0}$ that is very close to 0.7 and can also be assessed to be associated with the risk of mold formation. Figure 4 presents an overview of all thermal bridge types assessed and the criterion of mold formation. With the implementation of the retrofit measures suggested in this study, all simulation values $f_{R,si,1}$ of the 14 thermal bridge types assessed are higher than 0.7 and can be assumed to be free from mold.

Table 3. Characteristic values, estimated costs, and benefit–cost ratios of the retrofits of 14 thermal bridge types in German buildings constructed between 1950 and 1969, prior to and after a retrofit (characteristic values are based on simulations with ThermCad, costs are based on BKI prices as of 2020 [38,39]), sorted according to benefit–cost ratio. The temperature factor is either below (red), near (yellow), or above (green) the mold formation threshold $f_{R,si}$ of 0.7.

Type of Thermal Bridge	Original State before Retrofit			State after Retrofit			Improvement		Estimated Retrofit Costs -	Benefit–Cost Ratio -
	$f_{R,si,0}$	Ψ_0	q_0	$f_{R,si,1}$	Ψ_1	q_1	$\Delta\Psi$	Δq		
	(-)	(W/mK)	(W/m)	(-)	(W/mK)	(W/m)	(W/mK)	(W/m)	(EUR/m)	(W/EUR)
Window sill	0.48	0.18	147.66	0.92	0.08	83.06	0.10	64.60	173.00	0.37
Window lintel	0.42	0.77	142.30	0.74	−0.34	117.60	1.11	24.70	69.20	0.36
Floor slab	0.55	0.70	105.16	0.72	0.09	89.90	0.61	15.26	49.60	0.31
Wall/rooftop	0.68	0.32	66.82	0.88	0.19	57.75	0.13	9.06	34.60	0.26
Rooftop/wall	0.68	0.32	66.82	0.85	0.21	57.96	0.11	8.86	42.60	0.21
Staggered story	0.78	0.28	67.17	0.82	0.23	59.83	0.06	7.34	49.00	0.15
Roller shutter casing	0.70	0.11	121.94	0.85	−0.24	113.14	0.35	8.80	60.00	0.15
Balcony slab	0.58	0.44	102.96	0.74	−0.05	90.87	0.48	12.09	83.64	0.14
Dormer	0.82	0.09	36.34	0.95	0.05	32.01	0.04	4.33	34.60	0.13
Window reveal	0.57	0.10	126.45	0.72	−0.41	118.55	0.51	7.89	69.20	0.11
Roof ridge	0.71	0.06	36.80	0.82	−0.28	30.04	0.34	6.76	69.00	0.10
Attic	0.48	0.25	106.93	0.73	−0.73	82.04	0.99	24.89	280.26	0.09
Inside wall	0.71	0.05	86.45	0.77	−0.23	81.92	0.28	4.52	57.29	0.08
Basement ceiling slab	0.57	0.04	52.97	0.75	−0.46	46.89	0.50	6.08	106.40	0.06

In the analysis, staggered stories and dormers have a comparably low risk of mold formation. The results, however, reveal that window sills and lintels, particularly, and that attics and floor, balcony, and basement ceiling slabs are prone to low temperature factors $f_{R,si,0}$ with a comparably high risk of mold. Thermal bridges on window sills are mainly caused by the construction design for radiator niches—a reduced wall thickness below windows. In a retrofit, the whole area below the window should be insulated to avoid mold formation and heat loss. This would result in a very high improvement with respect to the mold formation risk and the cost–benefit ratio. Window lintels can cause thermal bridges owing to their material that contrasts with surrounding masonry. In a retrofit, insulation with a minimum height of 40 cm is placed onto the lintel and the transition to the surrounding masonry and window frame with an overlap of at least 3 cm on the building outside. Window reveals can cause thermal bridges when the window is not placed in the insulation layer of the building. Similar to thermal bridges at window lintels, they can be retrofitted with an additional outside insulation layer with a minimum 3 cm overlap to the window frame. Attics are the extensions of flat roofs and their connections and different materials used can lead to thermal bridges. In a retrofit, the attic has to be fully covered with insulation and must be placed 50 cm below the roof top. Floor slabs separate different stories and can produce thermal bridges when not properly insulated. A retrofit would incorporate insulation on the outside of façades where the floor slabs adjoin. Basement ceiling slabs separate the unheated basement from the heated ground floor. Without insulation, thermal bridges can also occur. A retrofit includes an 80 cm high insulation with 60 cm above and 20 cm below the lower edge of the basement ceiling slab. The main reason for thermal bridges on balcony slabs is cantilevered slabs that transmit heat to the outside. However, a retrofit is associated with a rather effortful and costly demolition of the balcony combined with an insulation and rebuild of a new balcony.

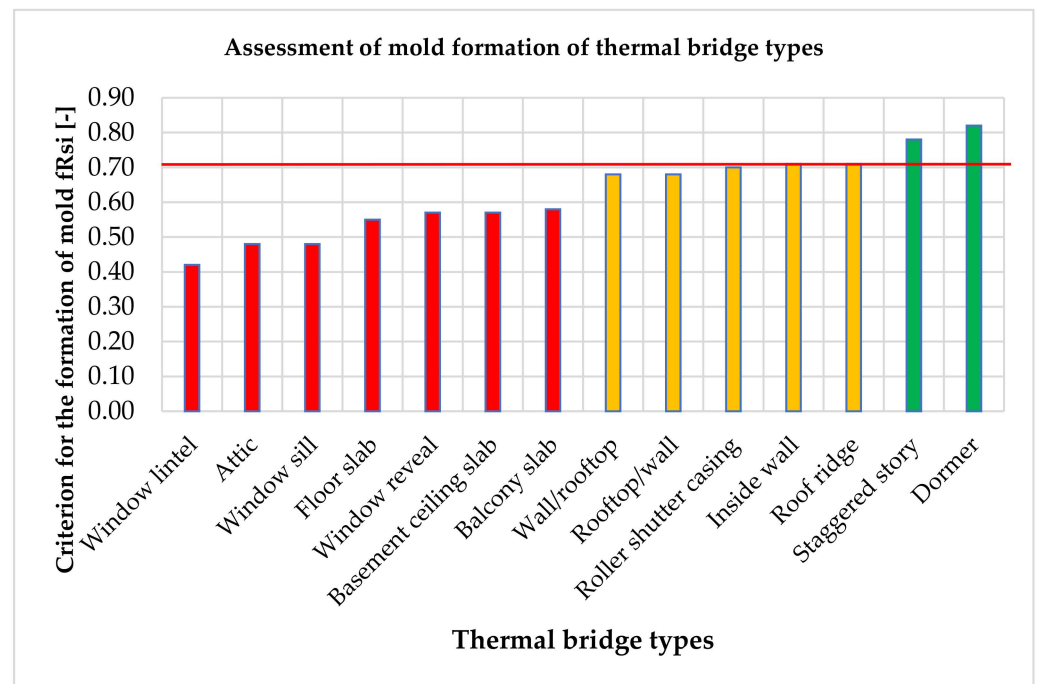


Figure 4. Criterion of mold formation of 14 thermal bridges in German buildings constructed between 1950 and 1969 prior to a retrofit (based on simulations with ThermCad). The red line marks the mold formation criterion of 0.7. Thermal bridge types with a red bar are clearly lower, with a yellow bar close to, and with a green bar clearly higher than 0.7.

After the simulated retrofit, this value increases significantly for window sills, while for the other thermal bridges the value rises to above the 0.7 benchmark. The energy savings of a thermal bridge retrofit is determined by the reduction in the transmission heat flow Δq caused by a retrofit. Besides window sills, the highest savings can be expected for window lintels and attics followed by floors and balcony slabs. With respect to the thermal bridge loss coefficient Ψ , the best retrofit simulation effects can be seen for window lintels, attics, and floor slabs.

The retrofit costs are calculated for the recommended retrofit measures per thermal bridge type. The costs include all retrofit costs per linear meter of the respective thermal bridge. Inflation, tax, depreciation, and interest rates for loans are not considered. Therefore, the expected retrofit costs are comparable with each other. Per linear meter, attics and window sills show the highest estimated retrofit costs, but at least for window sills the benefit–cost ratio is the highest for all thermal bridge types. By considering the retrofit costs of the different thermal bridge types, it becomes clear that retrofits with a high reduction in heat flow often also require higher costs. This relationship is shown in Figures 5 and 6, e.g., by the cost–benefit ratio of the transmission heat flow reduction per invested Euro of a retrofit, sorted in descending order.

The energy savings after a thermal bridge retrofit are determined by the reduction of the transmission heat flow Δq caused by a retrofit. By considering the retrofit costs of the different thermal bridge types, it becomes clear that retrofits with a high reduction of heat flow often require higher costs. This relationship is shown in Figures 5 and 6, e.g., by the cost–benefit ratio of transmission heat flow reduction per invested Euro of a retrofit, sorted in descending order.

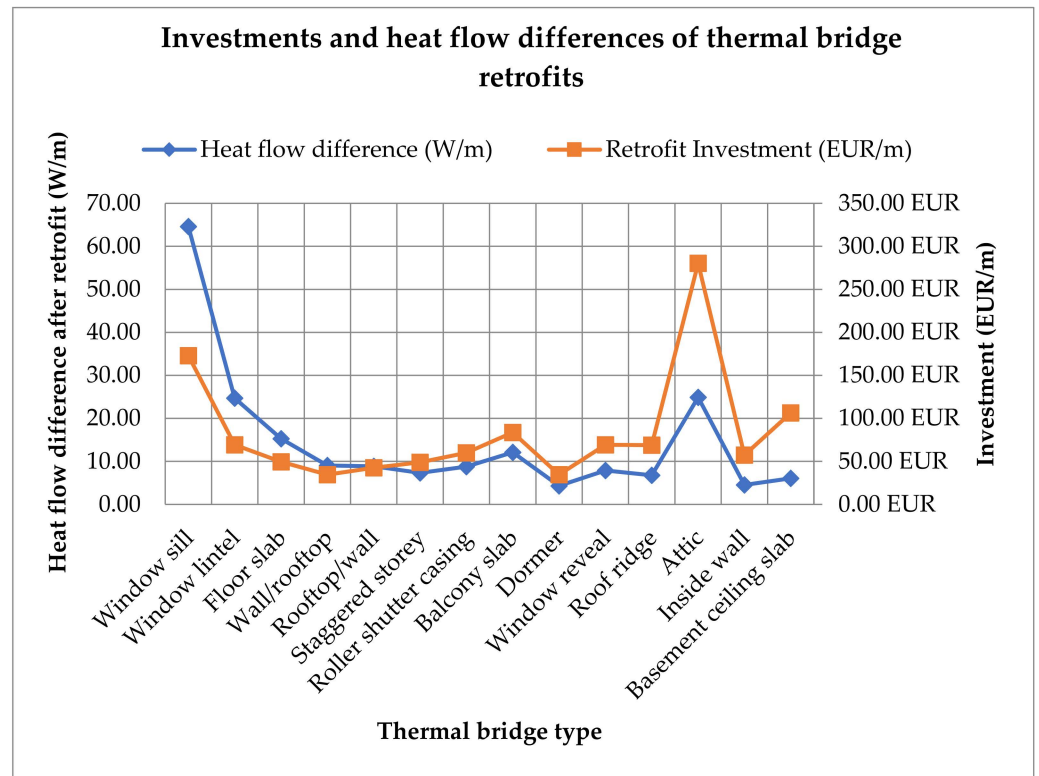


Figure 5. Costs and heat flow differences of the retrofit of 14 thermal bridge types of German buildings constructed between 1950 and 1969.

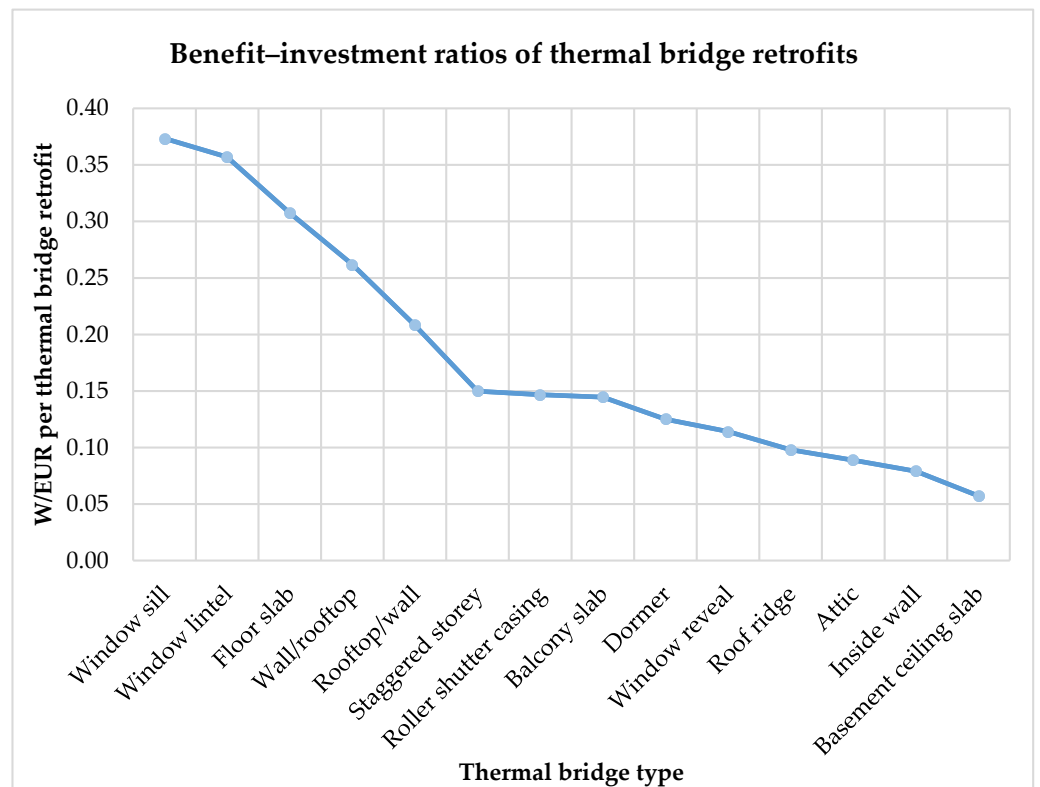


Figure 6. Benefit–cost ratios for energy savings of the retrofits of 14 thermal bridge types of German buildings constructed between 1950 and 1969.

Summarizing, we find that for German buildings constructed in the middle of the 20th century, thermal bridges of window components, floor/basement ceiling/balcony slabs, and attics are particularly relevant to retrofit planning and the criterion of mold formation. Regarding energy savings, the retrofits of thermal bridges of window sills, window lintels, and attics show the highest potentials. When also taking into account the necessary costs for energy savings, the retrofits of window sills and window lintels seem to be most promising. The retrofit of attics seems to be less attractive in this context.

In order to make the approach developed in this paper more comprehensible, a case study for a German building located in the Karlsruhe city center is demonstrated (see also Appendix D). The selected reference building (Figures A29 and A30) is an apartment building located in the Waldhornaße in Karlsruhe. The building consists of four full stories and a roof story with three dormers. The base of the building has a rectangular shaped base. On the west side of the building it is connected to a neighboring building, on the east side partly. There, five types of thermal bridges can be identified at the window, revealing dormers, floor slabs, balcony slabs, and the connection between an outside wall and a roof. By using Google maps and the “measure distance” function [47], we calculated the dimensions of the building and all its components (Table A32). For each component, a typical heat transfer coefficient (U-value) from the 1950s–1960s is determined according to Appendix A. Taking into account the corresponding temperature correction factor and applying the period balance approach (German “Periodenbilanzverfahren”) in accordance with DIN V 4108-6 [37], leads to an associated transmission heat loss per component (Table A33). To calculate the thermal bridge surcharge, we use the exact procedure (German “genaues Verfahren”) [37] (see Appendix D). To determine the state before and after a retrofit (Table A34), the length-related thermal bridge loss coefficients of the associated thermal bridge types (Table 3) are used. The transmission heat loss for the entire reference building is 1042 W/K. The loss due to the thermal bridge areas is around 99 W/K, which corresponds to a share of 9.63% of the heat loss of the entire building. The transmission heat loss of the entire reference building in the state after the thermal bridge retrofit is approximately 906 W/K. The retrofit measures reduce the transmission heat loss by around 136 W/K. This corresponds to a percentage reduction of the transmission heat loss of about 13%.

4. Discussion

This study shows that thermal bridges can be qualitatively detected and quantitatively assessed by analyzing aerial thermal panorama images without using additional building-specific background information.

We demonstrated a simple procedure for the assessment of thermal bridges of German buildings constructed in the decades of the 20th mid-century. For this, we used thermal bridge simulation software and technical standard values for building materials and constructions of the construction period to model and characterize representative thermal bridge types of this building class. As a result of our study, we provide a catalogue of 14 relevant thermal bridge types with exemplary aerial thermal panorama images of German buildings constructed in the 1950s and 1960s. This catalog also provides information on simple retrofit measures, the associated retrofit costs (for Germany), possible energy savings, and the risk reduction of mold formation, by removing a certain thermal bridge type. Similar studies are not known to the authors—only analyses on thermal images from terrestrial street-view and terrestrial perspectives are provided in literature. However, these are not capable for analyzing thermal bridges on rooftops and in upper building areas. Furthermore, in this study we classified the thermal bridges by hand. Inexperienced analyzers could misinterpret some thermal anomalies on the panorama images as thermal bridges (such as ventilation tiles, water pipe aerators, solar systems, lamps, heat build-ups or open windows (see Appendix C). To avoid such misinterpretations, further research could automate the thermal bridge detection with respect to the catalogue developed. Furthermore, in the case study we assume homogeneous construction of the building, meaning

that a certain type of thermal bridge occurs at all comparable building components if it is clearly identifiable on at least one component part. This could be misleading in the case of partial retrofits on a building where some components may have been energetically retrofitted while others have not.

Additionally, we want to note that the thermal bridge surcharge has a negative sign after the retrofit. From a theoretical point of view, the surcharge should actually be approximately zero, as there should be no other thermal bridges after the retrofit. In practice, however, the length-related thermal bridge loss coefficient Ψ also has a negative sign in some cases. This is due to the fact that in this study we want to make sure that the criterion for mold formation of $f_{R,si,1} > 0.7$ is fulfilled. As a consequence, for some thermal bridge retrofits, some areas of the standard cross-section are also affected by the retrofit measures, so that transmission heat loss of the entire building decreases by more than the value of the thermal bridge surcharge in its current state.

The results of our analysis are easy to transfer. To assess a thermal bridge recorded on a thermographic aerial image, only three steps are necessary. First, it must be ensured that the building corresponds to the building class of the 20th mid-century. Second, the thermal bridge must be classified into one of 14 thermal bridge types, whereby our catalog with sample aerial thermal panorama images serves as a classification aid. In the third step, the length of the thermal bridge must be measured with photogrammetric approaches or using measurement tools such as those provided by map services. From this information, conclusions about the retrofit benefit of a thermal bridge for energy savings and avoidance of mold formation can be estimated.

For the planning of retrofits of the 14 thermal bridge types, we state that with regard to the criterion for mold formation, thermal bridges of window components, floor/basement ceiling/balcony slabs, and attics are the most relevant. To maximize energy savings, thermal bridges of window sills, window lintels, and attics are the most relevant.

Finally, we want to critically reflect our approach and results for German buildings constructed during 1950–1969. All quantitative statements in this section are based on theoretical and simplified assumptions. While the recorded infrared energy in a thermal image does originate from the panorama scenes' effective emissivity, it is influenced by ambient temperature, moisture, general surrounding atmosphere, and reflective energy from the background. For the study at hand, however, thermal images are sufficient to qualitatively identify the thermal bridges and their spatial extent. Further studies should include simultaneous thermal images on individual buildings and direct temperature measurements via thermal images, but also incorporate inside and outside temperature measurements of buildings in the scene to quantitatively substantiate our results.

Further work should compare the results of this study with the actual state of buildings (e.g., via onsite inspections) and retrofit options and costs in practice (e.g., retrofit packages, funding schemes, availability of craftspeople, market prices for retrofit materials, and energy). We acknowledge that in practice, the characteristic values of the thermal bridges depend on additional factors such as architectural specifics. Retrofit costs can differ due to regional differences, economies of scale, and additional ancillary costs. It should also be noted that grants and tax benefits for energy retrofits are not taken into account when determining the costs for retrofit measures. It can be assumed that the German subsidy design for energy retrofits would improve the profitability of retrofit measures and be an incentive for more comprehensive retrofits.

We therefore want to point out that our approach is suitable for the quick and easy identification of interesting thermal bridge structures on district scale. We thus found our approach a good instrument for the preselection of relevant buildings and building parts in the context of retrofit planning. In the specific preparation of building retrofit measures, a more comprehensive detailed analysis with background information of each individual building is necessary and recommended.

In following studies, thermal bridge catalogs can be developed for other building classes in Germany and internationally. Due to the simplicity of our approach, we are

convinced that our results can be used to automate the analysis of thermal bridges of buildings on district scale. Current research is already examining automated detection of thermal bridges on panorama drone images and their classification, e.g., [48]. Thus, information on thermal bridges of buildings in urban districts can be collected and assessed in an uncomplicated way as a basis for retrofits in large areas. These results can help to improve and simplify the simultaneous retrofit planning for multiple buildings, such as in the context of CEP, CESP, PED, and EQ.

5. Conclusions

Drone technology allows for the simplified recording of thermographic images of buildings. Compared to terrestrial thermography, aerial images can be recorded faster, at lower cost, and from all angles, including rooftop perspectives. Thermography with drones is therefore very well suited for analyzing buildings in entire districts/neighborhoods/communities. In practical use, aerial thermography has great potential for gaining information on building stocks to prepare retrofits of multiple buildings in the context of CEP, CESP, PED, and EQ. A disadvantage of large-area thermography with drones, however, is the lack of interior thermographic recordings of buildings and of detailed background information on individual building materials and construction methods. Building analysis approaches on the district scale such as the one introduced in this study therefore have to work with simplifying assumptions. Analysis results based on simplifying assumptions can be imprecise and deviate. For this reason, the procedure presented in this study is especially suitable for the identification of interesting thermal bridge structures. Our approach does not replace detailed analyses of buildings and comprehensive planning efforts for the retrofit of thermal bridges.

The results of our study, including a catalogue of 14 relevant thermal bridge types for German buildings from the 1950s and 1960s with exemplary thermographic panorama images, are suitable for practical use. Future studies could focus on developing catalogs for thermal bridges of other German and international building classes. In future, our simple approach will be usable for an automated evaluation of aerial thermal panorama images of buildings. For automation, it is necessary to detect and assign a building to a building class, to detect and assign a thermal bridge to a thermal bridge class, and to measure the length of the respective thermal bridge. For this, computer vision software (e.g., based on deep learning approaches) can be used.

We assume that both drone technology with thermographic cameras and the focus on the district scale will gain importance for the retrofit planning of buildings in future. We hope that with our study we have been able to make a relevant contribution in this field.

Author Contributions: Conceptualization and methodology, investigation, visualization, original draft preparation, writing and editing: Z.M. and J.H.; writing, review, editing, supervision: R.V. and F.S. All authors have read and agreed to the published version of the manuscript.

Funding: The paper was created during a doctoral project financed with a scholarship at Karlsruhe Institute of Technology (KIT) according to the Landesgraduiertenförderungsgesetz—LGFG (State Postgraduate Fellowship Program). And, we acknowledge support by the KIT-Publication Fund of the Karlsruhe Institute of Technology.

Institutional Review Board Statement: Not applicable.

Informed Consent Statement: Not applicable.

Data Availability Statement: The underlying data is referenced throughout the paper. Additional information can be found in the Appendices A and B, see Appendices C and D.

Acknowledgments: The authors appreciate the support of Yu Hou (University of Southern California) and Marinus Vogl (Air Bavarian GmbH) for the collection of drone images. Moreover, they thank Harald Schneider (Karlsruhe Institute of Technology) for advice.

Conflicts of Interest: The authors declare no conflict of interest. The funders had no role in the design of the study; in the collection, analyses, or interpretation of data; in the writing of the manuscript, or in the decision to publish the results.

Appendix A

Table A1. Typical U-values for German buildings constructed in the 1950s–1960s (based on: BMWi and BMU, 2015) [49].

Component	U-Values (1950–1969)	Size
Outer wall, made of vertically perforated brick (VPB)	1.4	0.24 m
Outer wall, wooden structure (dormer)	0.5	0.10 m
Radiator niches	2.8	0.24 m
Wooden windows, 2-layered	2.9	0.07 m
Basement ceiling slab, including floor structure	0.8	0.20 m
Flat roof, massive	0.7	0.20 m
Gable roof, wooden structure	0.7	0.07 m

Table A2. Assumptions for building materials (based on: [50]).

Material	Size	Thermal Conductivity λ
Vertically perforated brick (VPB)	0.24 m	0.460 W/mK
Wood	different sizes	0.100 W/mK
Reinforced concrete	0.20 m	2.300 W/mK
Windows	0.07 m	0.400 W/mK
Façade insulation	different sizes	0.035 W/mK
Perimeter insulation	different sizes	0.040 W/mK

Table A3. List of heat transfer resistances according to the supplementary sheet 2 of DIN 4108 [35].

Heat Transfer Resistances	Temperature (°C)	R_s (m ² K/W)	Illustration Color
Inside–heated	20	0.25	Red
Inside–not heated	10	0.17	Purple
Outside	−5	0.04	Blue

Appendix B

Appendix B.1. Thermal Bridge Types of Outer Walls

Basement ceiling slab

The basement ceiling slab is a horizontal building component that separates the usually unheated basement from the heated ground floor. This component transfers the loads from the ground floor onto the load-bearing basement walls. Therefore, the support of the outer walls is essential to transfer the load [51].

An example of a thermal panorama image shows a thermal bridge in a basement ceiling slab (Figure A1). For the retrofit of this thermal bridge type, it is necessary to install a base insulation in the connection area. This serves to balance the effect of the different specific thermal conductivities and to reduce heat loss. The insulation should be 80 cm high, with 60 cm above and 20 cm below the lower edge of the basement ceiling. An illustration of this retrofit measure is shown in Figure A2. The costs for the retrofit of this thermal bridge type are listed in Table A4 and the change in the characteristic values of heat loss and mold formation of the building component before and after the retrofit is shown in Table A5.

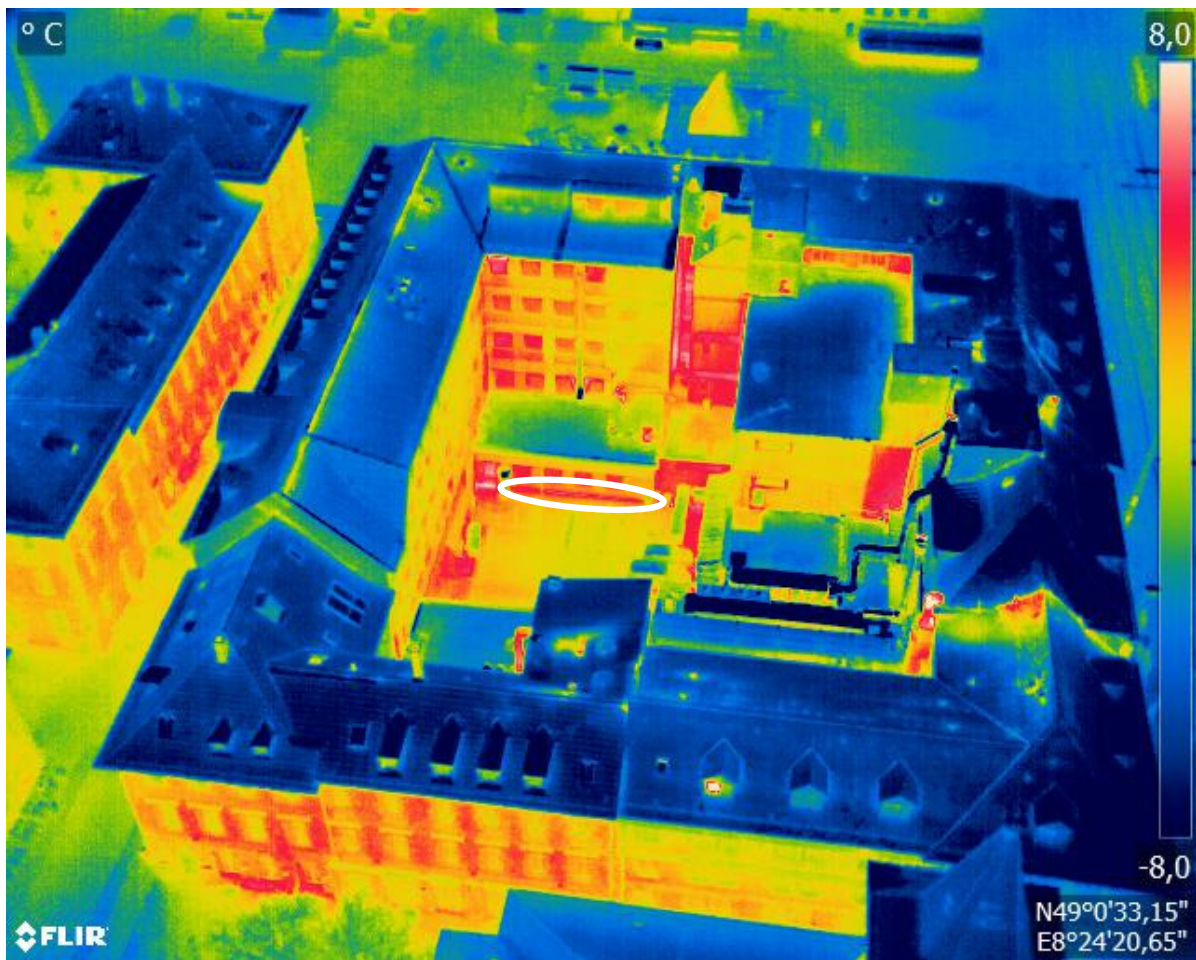


Figure A1. Example: thermal bridge of a basement ceiling slab.

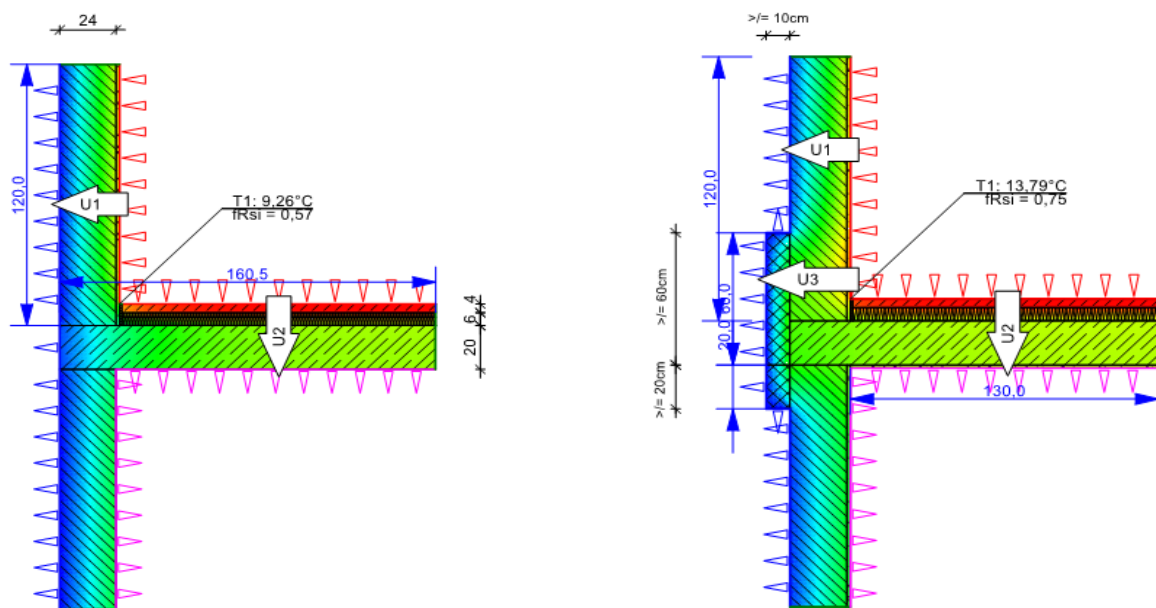


Figure A2. Before and after the thermal bridge retrofit of a basement ceiling slab (created with ThermCad thermal bridge simulation calculator).

Table A4. Retrofit components and costs of the thermal bridge retrofit of a basement ceiling slab [38,39].

Pos. No.	Retrofit Measure * Installation Height: 80 cm	Retrofit Costs per Linear Meter
LB 323-3	Removing old plaster from the building base	11.20 EUR/m
LB 323-6	Removing old plaster base from the wall	11.20 EUR/m
LB 323-68	Preparing base for the thermal insulation system	2.40 EUR/m
LB 323-97	Building base insulation (XPS, 100 mm)	40.00 EUR/m
LB 323-30	Reinforcement fabrics (glass fiber)	8.80 EUR/m
LB 323-67	Plaster (undercoat and finishing plaster)	32.80 EUR/m
Gross total		106.40 EUR/m

* In retrofit practice, a check for possible moisture problems and the need of a base seal is also relevant.

Table A5. Quantifiable results of the thermal bridge retrofit of a basement ceiling slab (ThermCad thermal bridge simulation calculation).

Original State before Retrofit			State after Retrofit			Improvement	
$f_{Rsi, 0}$	Ψ_0	q_0	$f_{Rsi, 1}$	Ψ_1	q_1	$\Delta\Psi$	Δq
(-)	(W/mK)	(W/m)	(-)	(W/mK)	(W/m)	(W/mK)	(W/m)
0.57	0.04	52.97	0.75	-0.46	46.89	0.50	6.08

Floor slab

A floor slab is a horizontal building component that completes a room at the top and constitutes the base of the floor above. It transfers the loads from the stories above onto the load-bearing components and helps in thermal and noise protection. A thermal bridge occurs when the connection depth of the outer wall is not sufficient for the attachment of an additional insulation layer in the binding area. The connection area heats disproportionately more than the standard cross section, so that there is a considerable loss of heat of the reinforced concrete slab. Different materials (masonry and reinforced concrete) with different specific thermal conductivities increase the thermal bridge effect [2].

An example of a thermal bridge of a floor slab is presented in Figure A3. For the retrofit of this thermal bridge type, it is necessary to remove a part of the slab and add a layer of thermal insulation material. The thermal insulation compensates for the effect of the different specific thermal conductivities of masonry and reinforced concrete and, thus, reduces the heat loss. A sufficient embedment depth of the thermal insulation is 5 cm and the thermal insulation should be installed over the entire height of the reinforced concrete ceiling of 20 cm. An illustration of this retrofit measure is shown in Figure A4. The costs for the retrofit of this thermal bridge type are listed in Table A6 and the change in the characteristic values of heat loss and mold formation of the building component before and after the retrofit is shown in Table A7.

Inside wall

Inside walls are vertical components that transfer loads in the longitudinal direction from the components above. They can be attached directly to the outer wall or integrated into the outer wall. From a thermal point of view, the integration of the inner wall into the outer wall is crucial. The thermal bridge effect occurs due to the structural design of the connection details of the inner wall integration and different cross sectional dimensions. Columns integrated into the outer wall are constructively equivalent to inside walls in the outer wall, so that the results achieved here can also be projected and used for column connections [2].

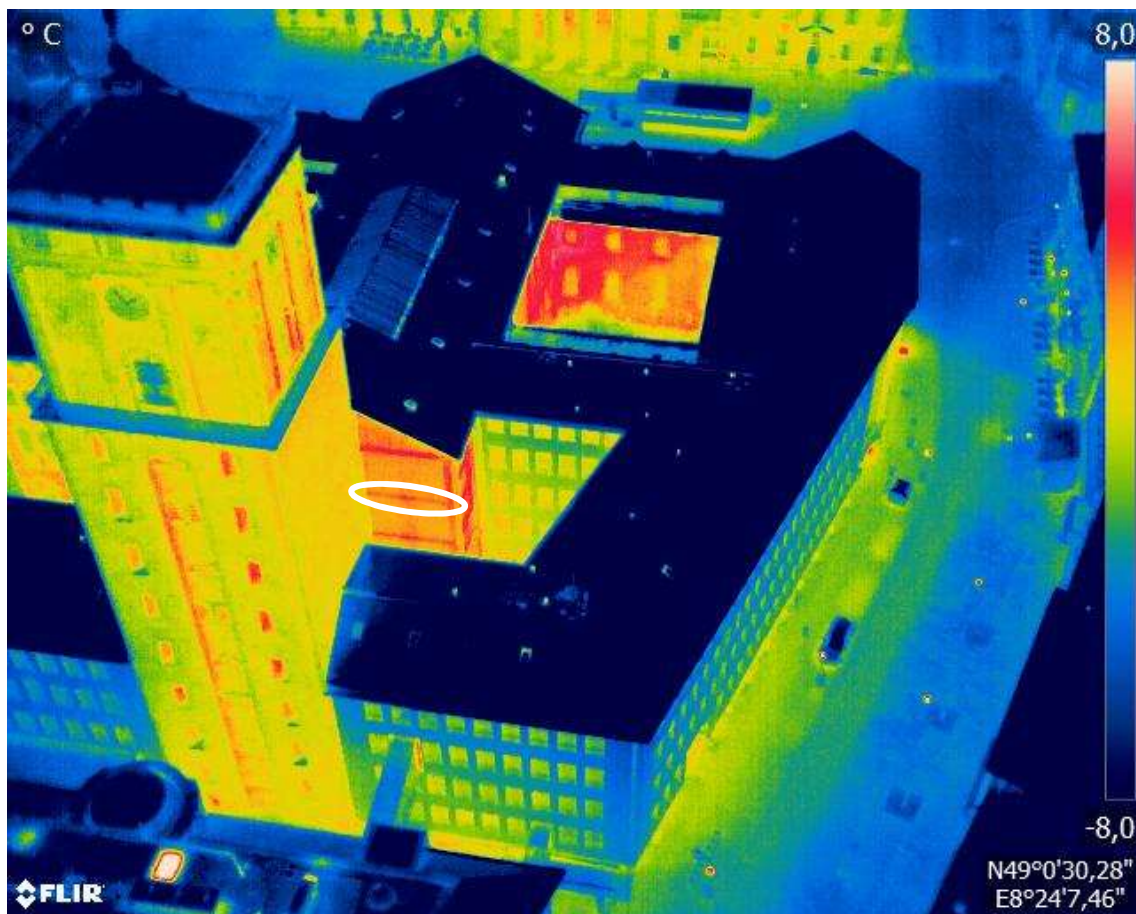


Figure A3. Example: thermal bridge of a floor slab.

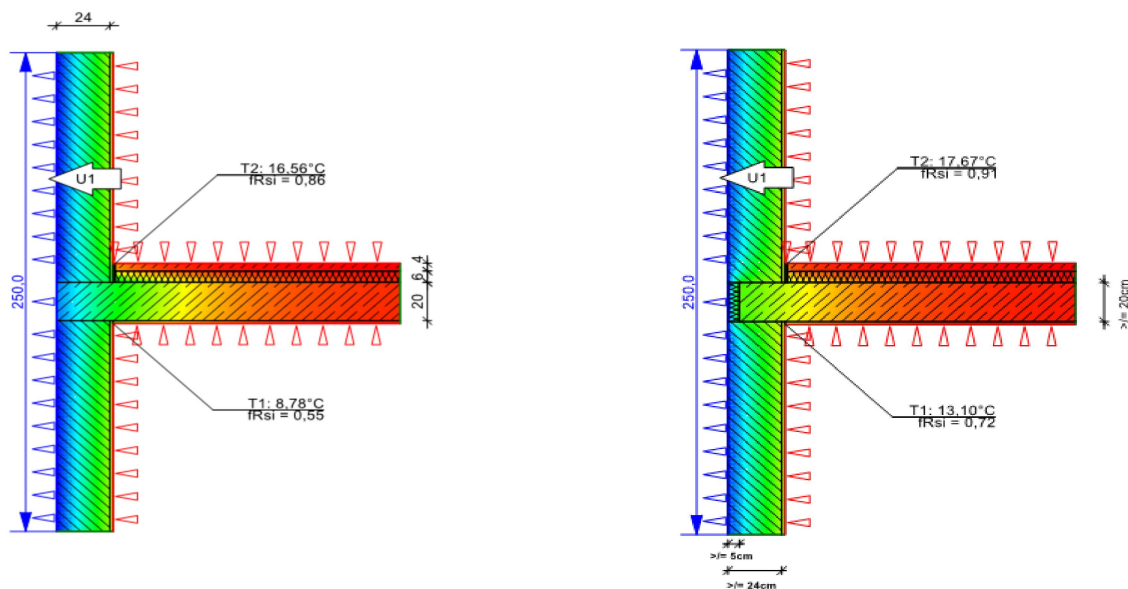


Figure A4. Before and after the thermal bridge retrofit of a floor slab (created with ThermCad thermal bridge simulation calculator).

Table A6. Retrofit components and costs of the thermal bridge retrofit of a floor slab [38,39].

Pos. No.	Retrofit Measure * Installation Height: 20 cm	Retrofit Costs per Linear Meter
LB 323-2	Removing old plaster from the partial area	5.20 EUR/m
LB 323-6	Removing old plaster base from the wall	2.80 EUR/m
LB 313-14	Demolishing old floor slab from the partial area	23.00 EUR/m
LB 323-68	Preparing base for the thermal insulation system	0.60 EUR/m
LB 323-96	Thermal insulation system up to 20 m, PS 50, bonding technique	7.60 EUR/m
LB 323-30	Reinforcement fabrics (glass fiber)	2.20 EUR/m
LB 323-67	Plaster (undercoat and finishing plaster)	8.20 EUR/m
Gross total		49.60 EUR/m

* In retrofit practice, costs for the scaffold are also relevant.

Table A7. Quantifiable results of the thermal bridge retrofit of a floor slab (ThermCad thermal bridge simulation calculation).

Original State before Retrofit			State after Retrofit			Improvement	
$f_{R,si,0}$ (-)	Ψ_0 (W/mK)	q_0 (W/m)	$f_{R,si,1}$ (-)	Ψ_1 (W/mK)	q_1 (W/m)	$\Delta\Psi$ (W/mK)	Δq (W/m)
0.55	0.70	105.16	0.72	0.09	89.90	0.61	15.26

An example of a thermal bridge of an inside wall/column is presented in Figure A5. For the retrofit of this thermal bridge type, it is necessary to break off part of the support or the inner wall and to build a recess into which thermal insulation material can be filled. For a professional retrofit, a sufficient embedment depth of the thermal insulation of 12 cm must be ensured, which should be integrated over the entire width of the inner wall embedment of 24 cm. An illustration of this retrofit measure is shown in Figure A6, the costs for the retrofit of this thermal bridge type are listed in Table A8, and the change in the characteristic values of heat loss and mold formation of the building component before and after the retrofit is shown in Table A9.

Table A8. Retrofit components and costs of the thermal bridge retrofit of an inside wall [38,39].

Pos. No.	Retrofit Measure * Installation Height: 24 cm	Retrofit Costs per Linear Meter
LB 323-2	Removing old plaster from the partial area	6.24 EUR/m
LB 323-6	Removing old plaster base from the wall	3.36 EUR/m
LB 312-5	Demolishing old outer masonry	14.57 EUR/m
LB 323-68	Preparing base for the thermal insulation system	0.72 EUR/m
LB 323-87	Thermal insulation system up to 20 m, PS 50, Bondig technique	19.92 EUR/m
LB 323-30	Reinforcement fabrics (glass fiber)	2.64 EUR/m
LB 323-67	Plaster (undercoat and finishing plaster)	9.84 EUR/m
Gross total		57.29 EUR/m

* In retrofit practice costs for scaffold are also relevant.

Table A9. Quantifiable results of the thermal bridge retrofit of an inside wall (ThermCad thermal bridge simulation calculation).

Original State before Retrofit			State after Retrofit			Improvement	
$f_{R,si,0}$ (-)	Ψ_0 (W/mK)	q_0 (W/m)	$f_{R,si,1}$ (-)	Ψ_1 (W/mK)	q_1 (W/m)	$\Delta\Psi$ (W/mK)	Δq (W/m)
0.71	0.05	86.45	0.77	-0.23	81.92	0.28	4.52

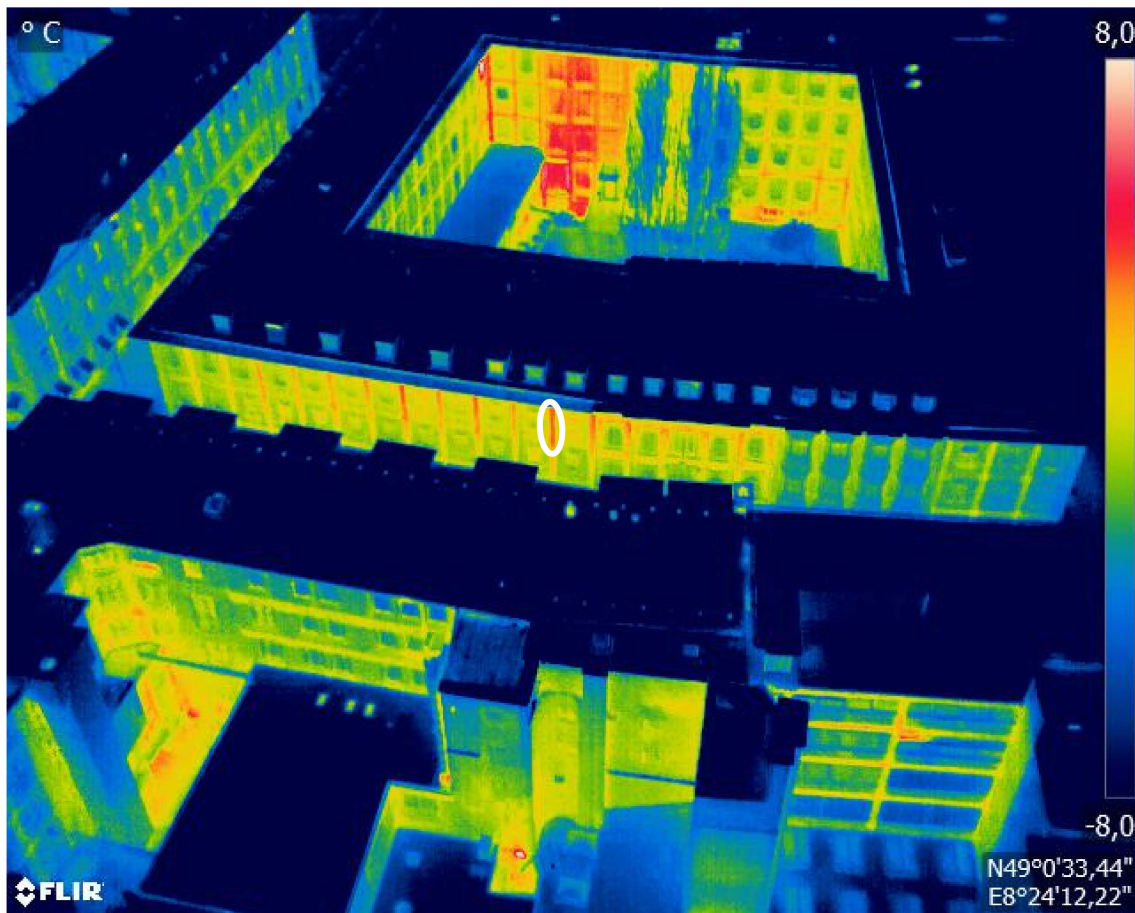


Figure A5. Example: thermal bridge of an inside wall/column.

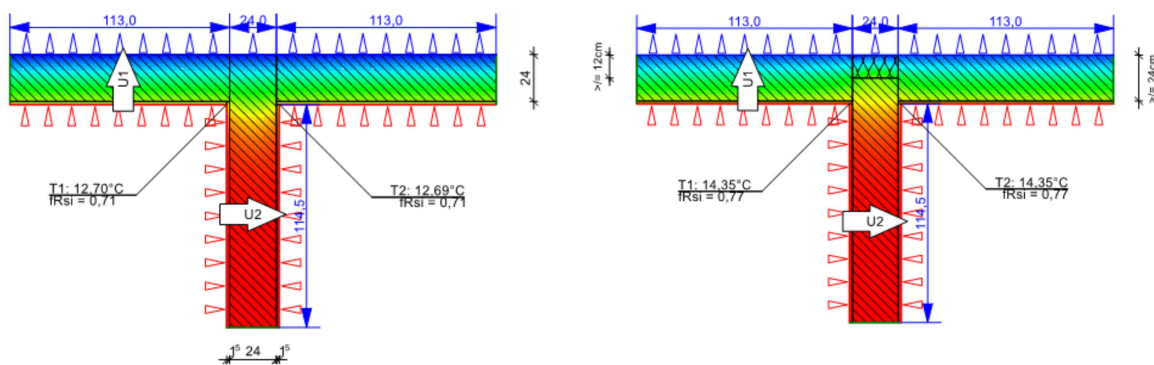


Figure A6. Before and after the thermal bridge retrofit of an inside wall (created with ThermCad thermal bridge simulation calculator).

Connection wall and rooftop

The connection between the outer wall and the rooftop is difficult for the insulation work due to different geometric conditions and changing angles. If the insulation is missing or incorrectly attached, this connection is a thermally weak point of the façade. A thermal bridge can occur due to the structural design of the external wall in the area of the connection to the roof. Due to static requirements, a reinforced concrete ring anchor in the area of the thermal bridge is needed but has a different material compared to the rest of the standard cross-section of the outer wall. There is a significant loss of heat in the area of the ring anchor. This effect is reinforced by the different thermal conductivities of the

various materials that are installed in the connection area (usually masonry and reinforced concrete) [51].

An example for a thermal bridge of a connection between a wall and a rooftop is presented in Figure A7. For the retrofit of this thermal bridge type, it is necessary to apply thermal insulation material in the connection area along the ring anchor. The necessary insulation should be a total of 20 cm high and installed in the direct connection area to the roof. An illustration of this retrofit measure is shown in Figure A8, the costs for the retrofit of this thermal bridge type are listed in Table A10 and the change in the characteristic values heat loss and criterion for mold formation of the building component before and after the retrofit is shown in Table A11.

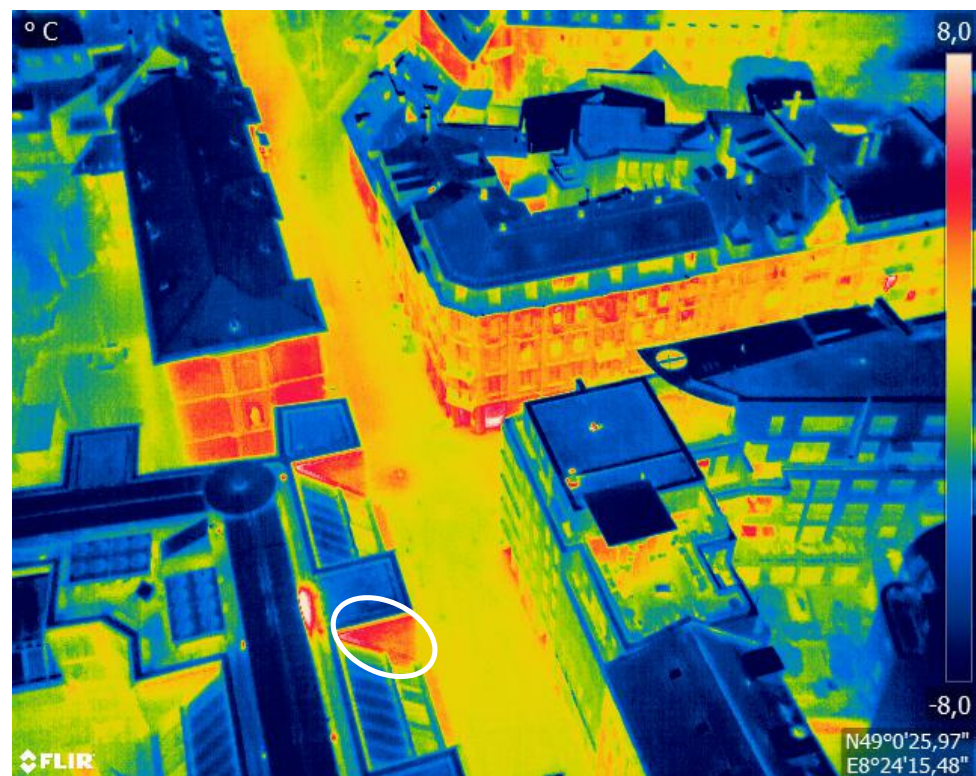


Figure A7. Example: thermal bridge of a connection between a wall and a rooftop.

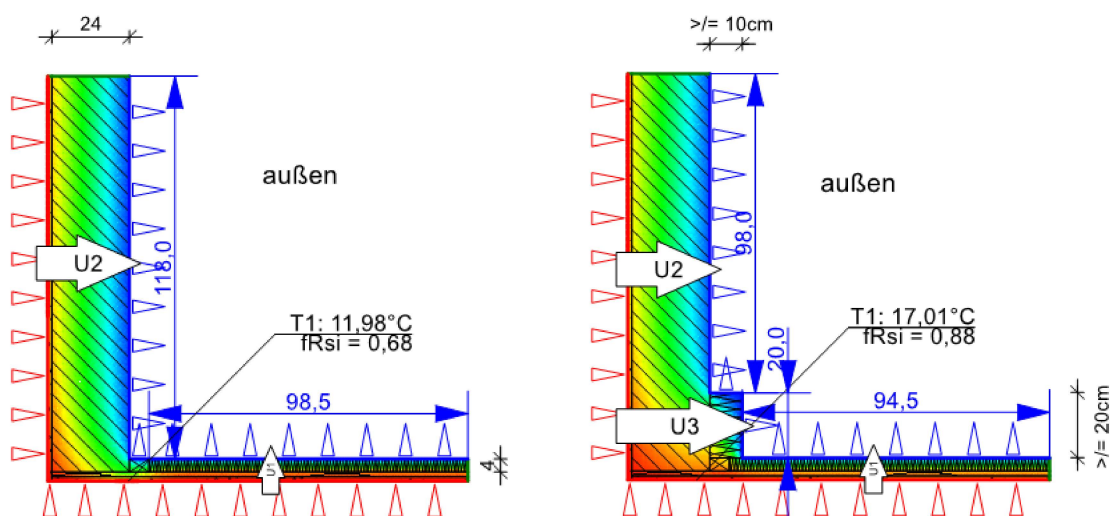


Figure A8. Before and after scheme of the thermal bridge retrofit of a connection between a wall and a rooftop (created with ThermCad thermal bridge simulation calculator).

Table A10. Retrofit components and costs of the thermal bridge retrofit of a connection between a wall and a rooftop [38,39].

Pos. No.	Retrofit Measure * Installation Height: 20 cm	Retrofit Costs per Linear Meter
LB 323-2	Removing old plaster from the partial area	5.20 EUR/m
LB 323-6	Removing old plaster base from the wall	2.80 EUR/m
LB 323-68	Preparing base for the thermal insulation system	0.60 EUR/m
LB 323-86	Thermal insulation system up to 20 m, PS 50, bonding technique	15.60 EUR/m
LB 323-30	Reinforcement fabrics (glass fiber)	2.20 EUR/m
LB 323-67	Plaster (undercoat and finishing plaster)	8.20 EUR/m
Gross total		34.60 EUR/m

* In retrofit practice, costs for the scaffold are also relevant.

Table A11. Quantifiable results of the thermal bridge retrofit of a connection between wall and rooftop (ThermCad thermal bridge simulation calculation).

Original State before Retrofit			State after Retrofit			Improvement	
$f_{R,si,0}$ (-)	Ψ_0 (W/mK)	q_0 (W/m)	$f_{R,si,1}$ (-)	Ψ_1 (W/mK)	q_1 (W/m)	$\Delta\Psi$ (W/mK)	Δq (W/m)
0.68	0.32	66.82	0.88	0.19	57.75	0.13	9.06

Appendix B.2. Thermal Bridge Types of Balconies

Balcony slab

Balconies are outdoor elements and permanently exposed to changing weather conditions. A thermal bridge can occur especially in cantilevered balcony slabs of old reinforced concrete buildings, which are designed as an extension of the story ceiling without thermal decoupling. The cause of the thermal bridge is the structural design of the connection details of the balcony slab and the associated heating of the external components [8].

An example of a thermal bridge of a balcony slab is presented in Figure A9. This type of thermal bridge can only be retrofitted if the existing balcony slab is completely demolished. The thermal bridge can then be removed by inserting an insulating element between the floor slab and the new balcony slab. An illustration of this retrofit measure is shown in Figure A10, the costs of the retrofit of this thermal bridge type are listed in Table A12, and the change in the characteristic values of heat loss and mold formation of the building component before and after the retrofit is shown in Table A13.

Table A12. Retrofit components and costs of the thermal bridge retrofit of a balcony slab [38,39].

Pos. No.	Retrofit Measure * Installation Height: 20 cm	Retrofit Costs per Linear Meter
LB 313-7	Demolishing old balcony slab	22.00 EUR/m
LB 313-89	Cleaning concrete surfaces	0.24 EUR/m
LB 013-128	Thermal insulation element for the balcony connection	4.20 EUR/m
LB 013-84	Reinforced concrete prefabricated component, balcony slab	45.20 EUR/m
LB 013-65	Side rails for the balcony slab	4.40 EUR/m
LB 013-61	Slab, in-situ concrete, SB2, C25/30	7.60 EUR/m
Gross total		83.64 EUR/m

* In retrofit practice, costs for the scaffold are also relevant.



Figure A9. Example: thermal bridge of a balcony slab.

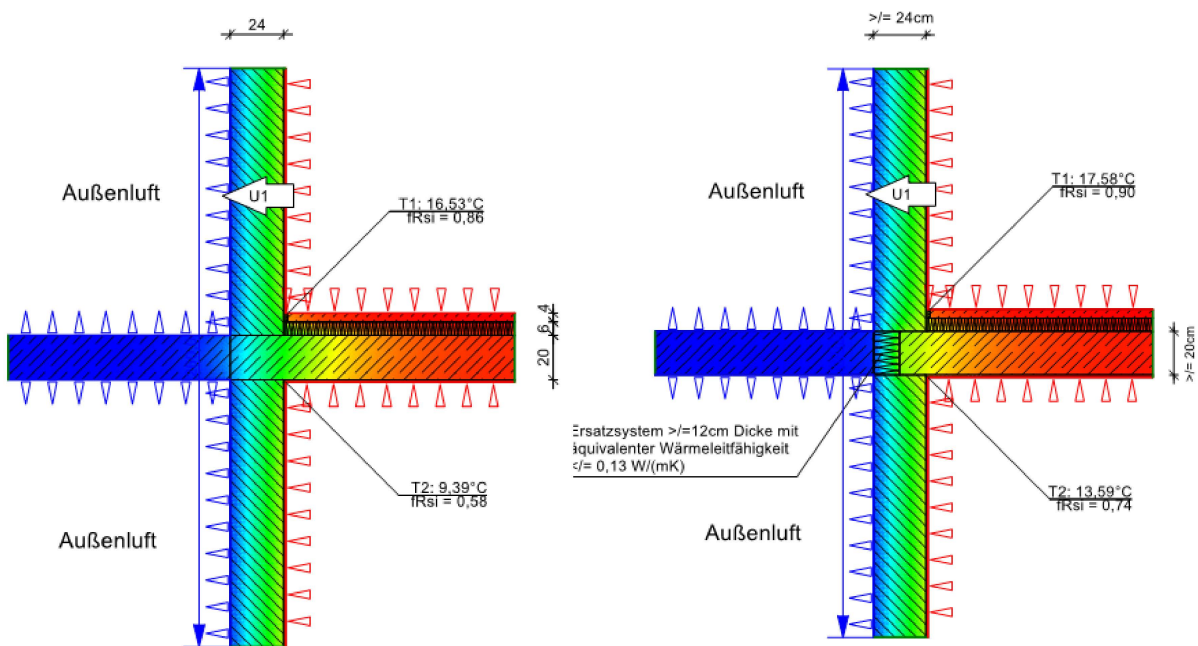


Figure A10. Before and after the thermal bridge retrofit of a balcony slab (created with ThermCad thermal bridge simulation calculator).

Table A13. Quantifiable results of the thermal bridge retrofit of a balcony slab (ThermCad thermal bridge simulation calculation).

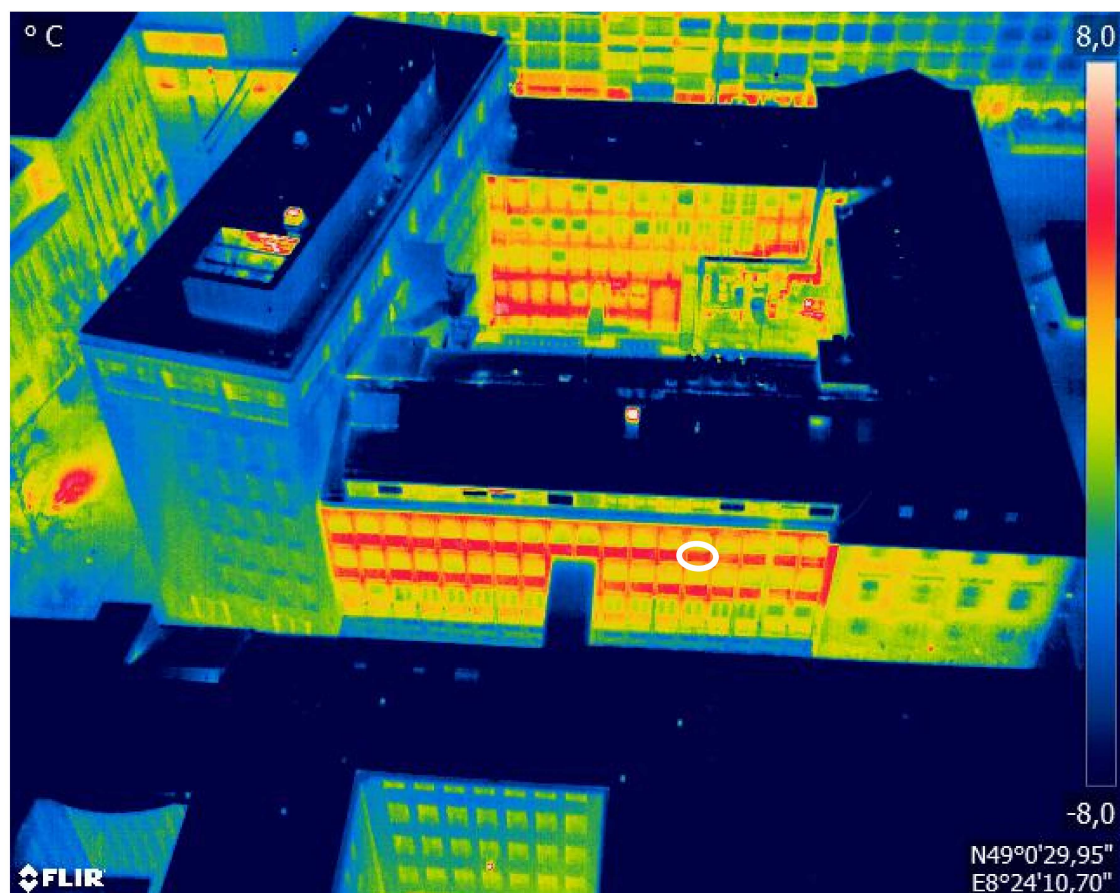
Original State before Retrofit			State after Retrofit			Improvement	
$f_{R,si,0}$ (-)	Ψ_0 (W/mK)	q_0 (W/m)	$f_{R,si,1}$ (-)	Ψ_1 (W/mK)	q_1 (W/m)	$\Delta\Psi$ (W/mK)	Δq (W/m)
0.58	0.44	102.96	0.74	-0.05	90.87	0.48	12.09

Appendix B.3. Thermal Bridge Types of Windows

Window sill

A window sill is the part of a wall below a window. Thermal bridges in these areas are caused by radiator construction designs. In old buildings, the positioning of radiators directly below a window is usual. This is due to the poor quality of old windows and supposed to prevent drafts caused by convection of cold air. In addition, the heat emissions by the radiator can circulate better on the window than on a wall due to a temperature difference. In order to save space and enable easier installation of the windows, the wall thickness in the area of windows in old buildings is often reduced, which is called “radiator niche” [9].

An example of a thermal bridge of a window sill is presented in Figure A11. For the retrofit of this thermal bridge type, it is necessary to insulate the entire area below a window. For this purpose, thermal insulation material should be installed for compensating for the effect of the different specific thermal conductivities. An illustration of this retrofit measure is shown in Figure A12, the costs of the retrofit of this thermal bridge type are listed in Table A14, and the change in the characteristic values of heat loss and mold formation of the building component before and after the retrofit is shown in Table A15.

**Figure A11.** Example: thermal bridge of a window sill.

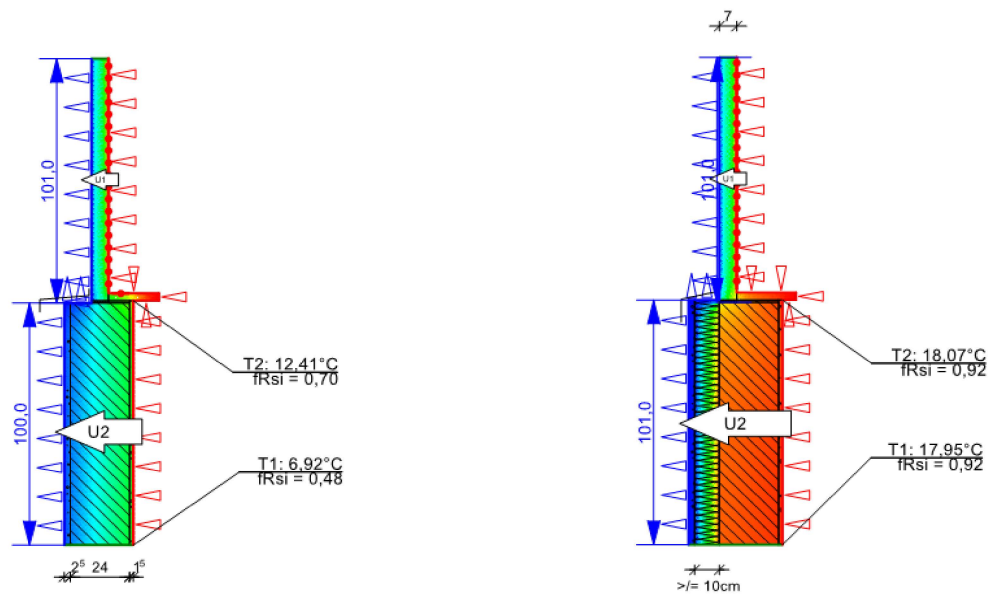


Figure A12. Before and after the thermal bridge retrofit of a window sill (created with ThermCad thermal bridge simulation calculator).

Table A14. Retrofit components and costs of the thermal bridge retrofit of a window sill [38,39].

Pos. No.	Retrofit Measure * Installation Height: 100 cm	Retrofit Costs per Linear Meter
LB 323-2	Removing old plaster from the partial area	26.00 EUR/m
LB 323-6	Removing old plaster base from the wall	14.00 EUR/m
LB 323-68	Preparing base for the thermal insulation system	3.00 EUR/m
LB 323-86	Thermal insulation system up to 20 m, PS 100, bonding technique	78.00 EUR/m
LB 323-30	Reinforcement fabrics (glass fiber)	11.00 EUR/m
LB 323-67	Plaster (undercoat and finishing plaster)	41.00 EUR/m
Gross total		173.00 EUR/m

* In retrofit practice, costs for the scaffold are also relevant.

Table A15. Quantifiable results of the thermal bridge retrofit of a window sill (ThermCad thermal bridge simulation calculation).

Original State before Retrofit			State after Retrofit			Improvement	
$f_{R,si,0}$ (-)	Ψ_0 (W/mK)	q_0 (W/m)	$f_{R,si,1}$ (-)	Ψ_1 (W/mK)	q_1 (W/m)	$\Delta\Psi$ (W/mK)	Δq (W/m)
0.48	0.18	147.66	0.92	0.08	83.06	0.10	64.60

Window reveal

Every window has at least one connection joint in the area where the window frame and the outer wall connect. The anchoring of the window frame in the lateral surface of the outer wall can be the cause of a thermal bridge. These so-called window reveals exist both on the inside and on the outside of windows. If the window is not installed within the insulation layer, the side connection joint of the window to the outer wall is exposed. It is important to note that there are two possible vertical thermal bridge areas per window [2].

An example of a thermal bridge of a window reveal is presented in Figure A13. For the retrofit of this thermal bridge type, it is necessary to apply additional thermal insulation material in the connection area of the window reveal. The main purpose of this is to compensate for the effect of the different specific thermal conductivities of masonry and

wood/glass. The necessary insulation should be 40 cm long in total and installed in the direct connection area of the window reveal. It is important to ensure that the window frame is insulated by at least 3 cm so that the lateral connection joint between the window and the outside wall is not exposed. An illustration of this retrofit measure is shown in Figure A14, the costs of the retrofit of this thermal bridge type are listed in Table A16, and the change in the characteristic values of heat loss and mold formation of the building component before and after the retrofit is shown in Table A17.

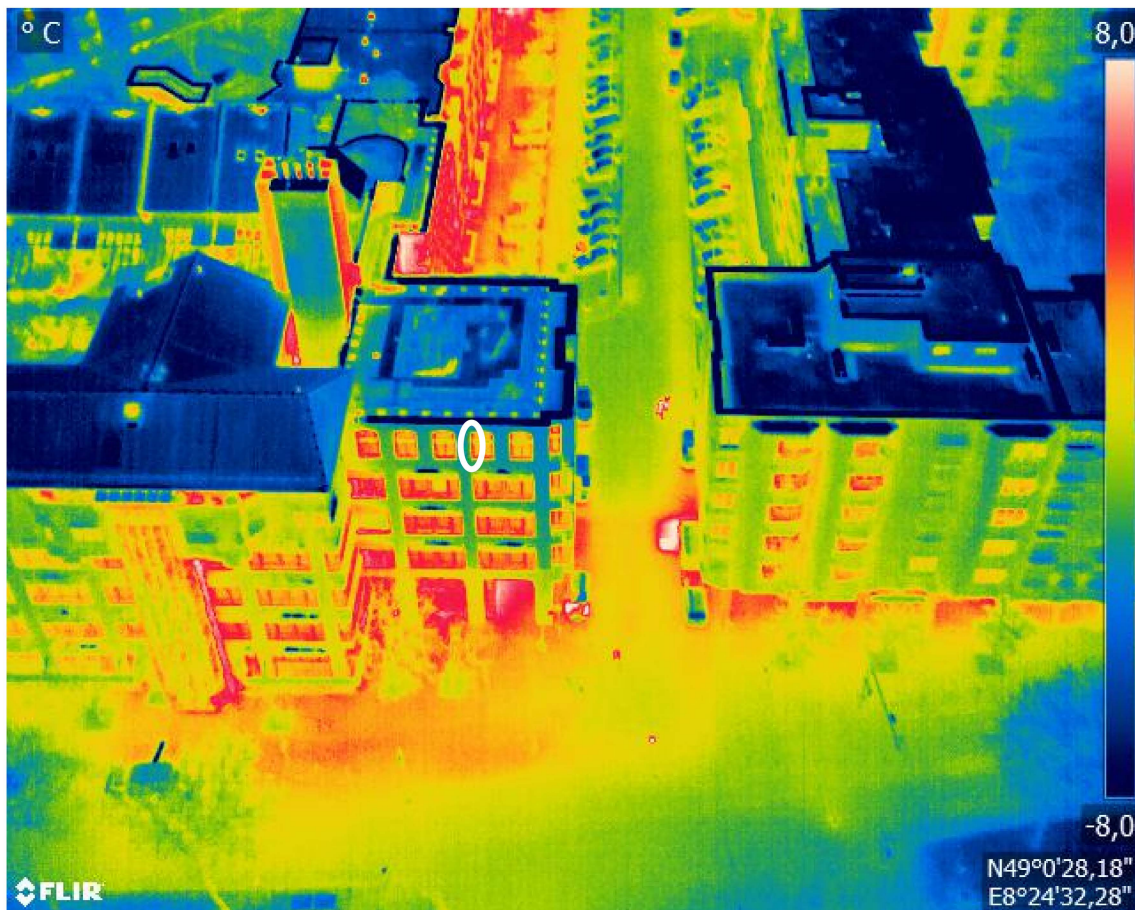


Figure A13. Example: thermal bridge of a window reveal.

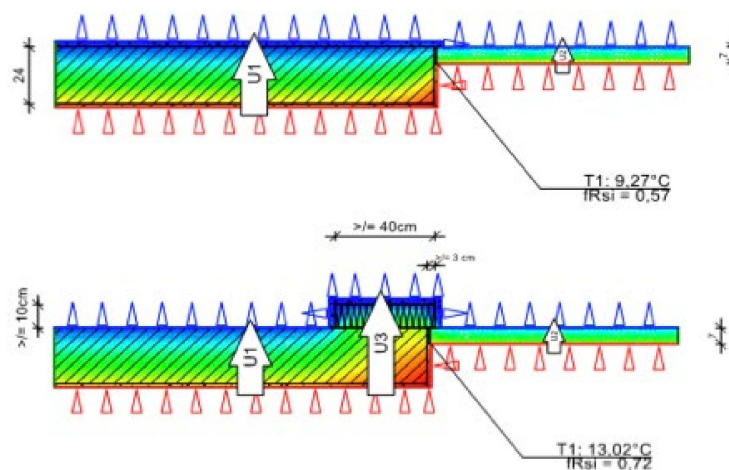


Figure A14. Before and after the thermal bridge retrofit of a window reveal (created with ThermCad the thermal bridge simulation calculator).

Table A16. Retrofit components and costs of the thermal bridge retrofit of a window reveal [38,39].

Pos. No.	Retrofit Measure * Installation Height: 40 cm	Retrofit Costs per Linear Meter
LB 323-2	Removing old plaster from the partial area	10.40 EUR/m
LB 323-6	Removing old plaster base from the wall	5.60 EUR/m
LB 323-68	Preparing base for the thermal insulation system	1.20 EUR/m
LB 323-86	Thermal insulation system up to 20 m, PS 100, bonding technique	31.20 EUR/m
LB 323-30	Reinforcement fabrics (glass fiber)	4.40 EUR/m
LB 323-67	Plaster (undercoat and finishing plaster)	16.40 EUR/m
Gross total		69.20 EUR/m

* In retrofit practice, costs for the scaffold are also relevant.

Table A17. Quantifiable results of the thermal bridge retrofit of a window reveal (ThermCad thermal bridge simulation calculation).

Original State before Retrofit			State after Retrofit			Improvement	
$f_{R,si,0}$ (-)	Ψ_0 (W/mK)	q_0 (W/m)	$f_{R,si,1}$ (-)	Ψ_1 (W/mK)	q_1 (W/m)	$\Delta\Psi$ (W/mK)	Δq (W/m)
0.57	0.10	126.45	0.72	-0.41	118.55	0.51	7.89

Window lintel

Windows have a horizontal lintel above the corresponding wall opening, which diverts the incoming loads from above to the side of the window. In the area of lintels, different materials are located next to each other. Usually, masonry is used as the outer wall and reinforced concrete as the actual lintel of this construction element. Due to this construction, a thermal bridge can occur on the contact surface [51].

An example of a thermal bridge of a window lintel is presented in Figure A15. For the retrofit of this thermal bridge type, it is necessary to install thermal insulation material along the lintel. This should compensate for the effect of the different specific thermal conductivities of masonry and reinforced concrete. It is important to use thermal insulation with a height of at least 40 cm that should not only cover the lintel, but also the transition to the masonry. It is crucial that the window frame is insulated by at least 3 cm, in analogy to the retrofit of a window reveal. An illustration of this retrofit measure is shown in Figure A16, the costs of the retrofit of this thermal bridge type are listed in Table A18, and the change in the characteristic values of heat loss and mold formation of the building component before and after the retrofit is shown in Table A19.

Table A18. Retrofit components and costs of the thermal bridge retrofit of a window lintel [38,39].

Pos. No.	Retrofit Measure * Installation Height: 40 cm	Retrofit Costs per Linear Meter
LB 323-2	Removing old plaster from the partial area	10.40 EUR/m
LB 323-6	Removing old plaster base from the wall	5.60 EUR/m
LB 323-68	Preparing base for the thermal insulation system	1.20 EUR/m
LB 323-86	Thermal insulation system up to 20 m, PS 100, bonding technique	31.20 EUR/m
LB 323-30	Reinforcement fabrics (glass fiber)	4.40 EUR/m
LB 323-67	Plaster (undercoat and finishing plaster)	16.40 EUR/m
Gross total		69.20 EUR/m

* In retrofit practice, also costs for the scaffold are relevant.

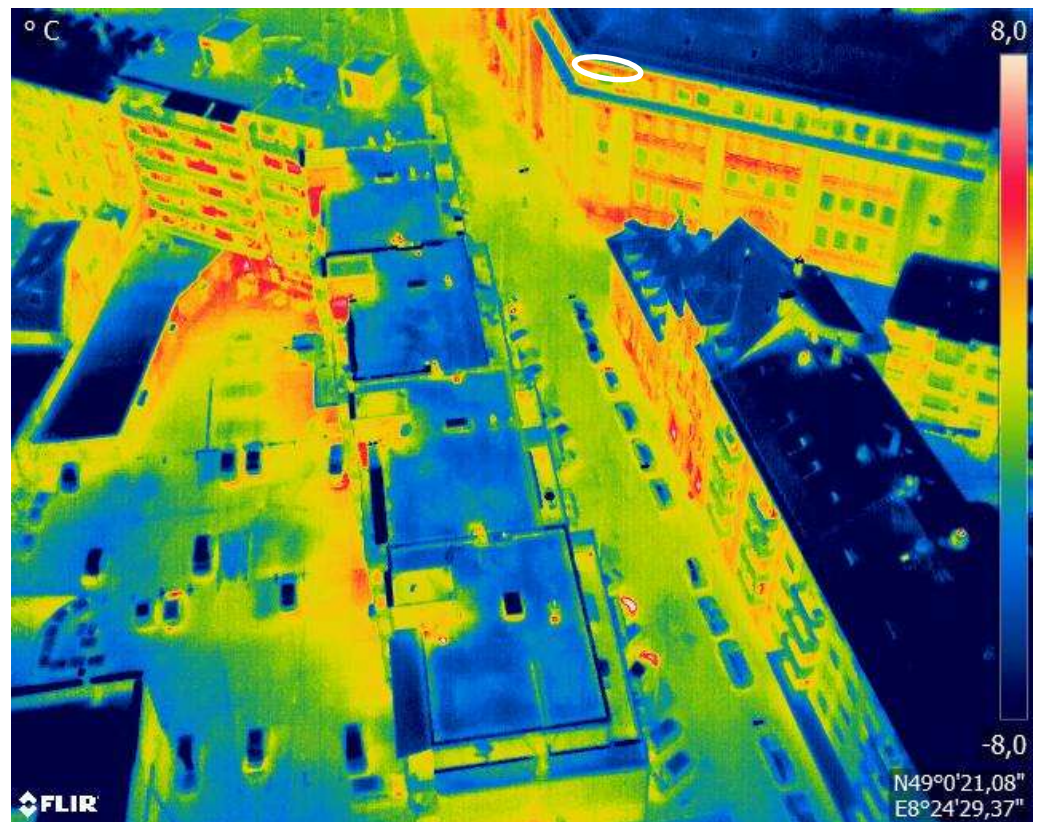


Figure A15. Example: thermal bridge of a window lintel.

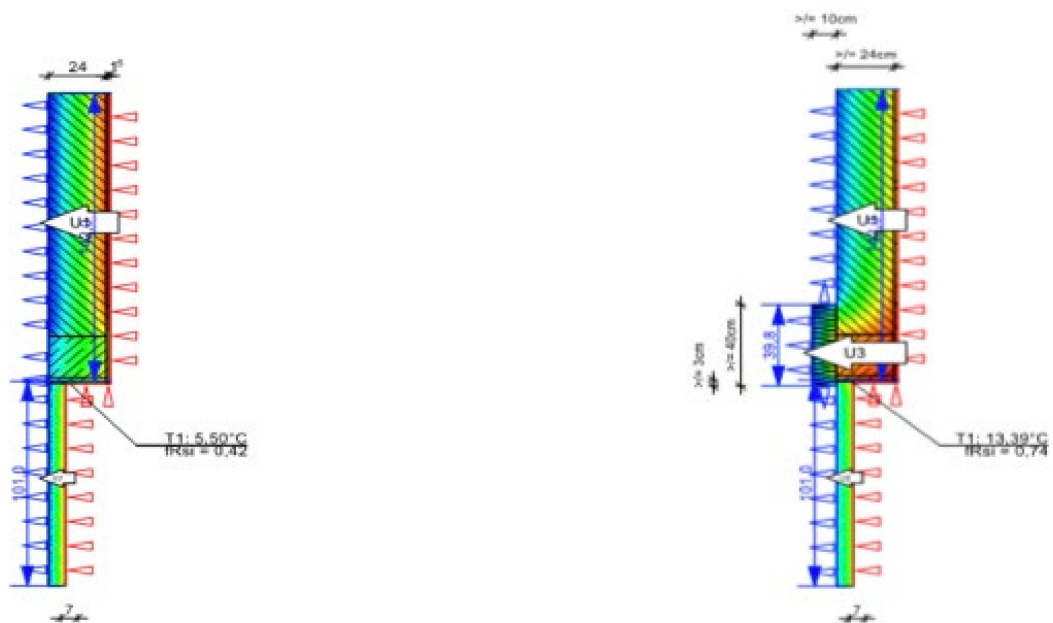


Figure A16. Before and after the thermal bridge retrofit of a window lintel (created with ThermCad thermal bridge simulation calculator).

Table A19. Quantifiable results of the thermal bridge retrofit of a window lintel (ThermCad thermal bridge simulation calculation).

Original State before Retrofit			State after Retrofit			Improvement	
$f_{R,si,0}$	Ψ_0	q_0	$f_{R,si,1}$	Ψ_1	q_1	$\Delta\Psi$	Δq
(-)	(W/mK)	(W/m)	(-)	(W/mK)	(W/m)	(W/mK)	(W/m)
0.42	0.77	142.30	0.74	-0.34	117.60	1.11	24.70

Roller shutter casing

In most existing buildings, the roller shutter casing is integrated into the outer wall. In this area of the façade, the outer wall has a significantly smaller cross section than the remaining almost homogeneous outer wall. In addition, the insulating effect of the façade is reduced by the roller shutter casing. Due to different materials, this thermal bridge is reinforced by different specific thermal conductivities. The thermal bridge effect is most intense when the roller shutters are down, as then there is an air-filled space within the façade [51].

An example of a thermal bridge of a roller shutter casing is presented in Figure A17. For the retrofit of this thermal bridge type, it is necessary to add additional thermal insulation material to the roller shutter casing. The insulation is used to compensate for the effect of the different specific thermal conductivities of the roller shutter box and the outer wall and to reduce heat loss. This measure can be carried out very quickly and easily without removing the roller shutter. The insulation material can be pushed into the roller shutter box from the inside, with a length of about 80 cm being required. It is important to choose the insulation thickness such that the roller shutter can still be moved after the retrofit. An illustration of this retrofit measure is shown in Figure A18, the costs of the retrofit of this thermal bridge type are listed in Table A20, and the change in the characteristic values of heat loss and mold formation of the building component before and after the retrofit is shown in Table A21.

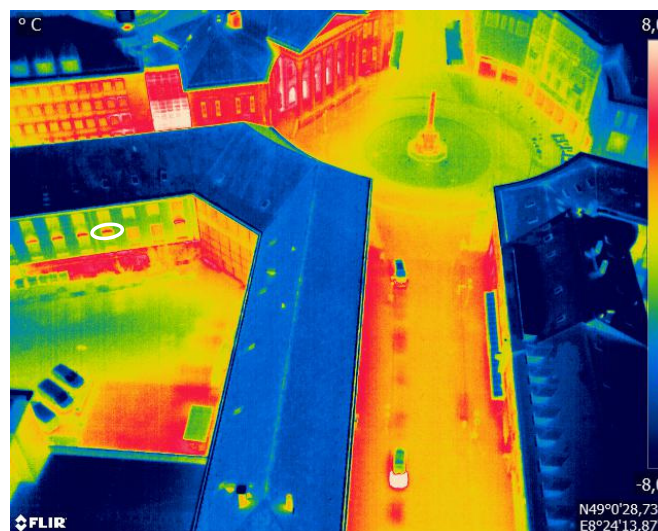


Figure A17. Example: thermal bridge of a roller shutter casing.

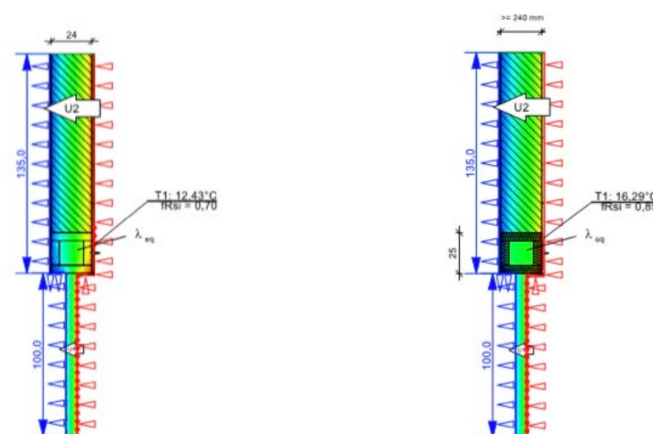


Figure A18. Before and after the thermal bridge retrofit of a roller shutter casing (created with ThermCad thermal bridge simulation calculator).

Table A20. Retrofit components and costs of the thermal bridge retrofit of a roller shutter casing [38,39].

Pos. No.	Retrofit Measure * Installation Height: 80 cm	Retrofit Costs per Linear Meter
LB 330-7	Insulating roller shutter casing	60.00 EUR/m
Gross total		60.00 EUR/m

* In retrofit practice, a check for possible moisture problems and the need of a base seal is also relevant.

Table A21. Quantifiable results of the thermal bridge retrofit of a roller shutter casing (ThermCad thermal bridge simulation calculation).

Original State before Retrofit			State after Retrofit			Improvement	
$f_{R,si,0}$ (-)	Ψ_0 (W/mK)	q_0 (W/m)	$f_{R,si,1}$ (-)	Ψ_1 (W/mK)	q_1 (W/m)	$\Delta\Psi$ (W/mK)	Δq (W/m)
0.70	0.11	121.94	0.85	-0.24	113.14	0.35	8.80

Appendix B.4. Thermal Bridge Types of Rooftops

Flat roof: Attic

An attic is an extension of the actual flat roof. The connection between a flat roof and an attic leads to geometric changes and can cause a thermal bridge. The connection area warms disproportionately more compared to the standard cross section, so that a significant heat loss occurs. This thermal bridge effect is reinforced by different materials used for the attic and roof surfaces [51].

An example of a thermal bridge of an attic is presented in Figure A19. For the retrofit of this thermal bridge type, it is necessary to completely cover the attic with thermal insulation material. This compensates for the effect of the different specific thermal conductivities and minimizes the heat loss and other negative effects of the thermal bridge. For a retrofit, the thermal insulation material must be introduced directly above the roof insulation and run around the entire attic. It is important that the insulation on the façade side is attached up to at least 50 cm below the upper edge of the reinforced concrete ceiling. An illustration of this retrofit measure is shown in Figure A20, the costs of the retrofit of this thermal bridge type are listed in Table A22, and the change in the characteristic values of heat loss and mold formation of the building component before and after the retrofit is shown in Table A23.

Table A22. Retrofit components and costs of the thermal bridge retrofit of an attic [38,39].

Pos. No.	Retrofit Measure * Installation Height: 162 cm	Retrofit Costs per Linear Meter
LB 323-2	Removing old plaster from the partial area	42.12 EUR/m
LB 323-6	Removing old plaster base from the wall	22.68 EUR/m
LB 323-68	Preparing base for the thermal insulation system	4.86 EUR/m
LB 323-86	Thermal insulation system up to 20 m, PS 100, bonding technique	126.36 EUR/m
LB 323-30	Reinforcement fabrics (glass fiber)	17.82 EUR/m
LB 323-67	Plaster (undercoat and finishing plaster)	66.42 EUR/m
Gross total		280.26 EUR/m

* In retrofit practice, the bitumen waterproofing is replaced, if necessary, to prevent moisture problems.

Table A23. Quantifiable results of the thermal bridge retrofit of an attic (ThermCad thermal bridge simulation calculation).

Original State before Retrofit			State after Retrofit			Improvement	
$f_{R,si,0}$ (-)	Ψ_0 (W/mK)	q_0 (W/m)	$f_{R,si,1}$ (-)	Ψ_1 (W/mK)	q_1 (W/m)	$\Delta\Psi$ (W/mK)	Δq (W/m)
0.48	0.25	106.93	0.73	-0.73	82.04	0.99	24.89



Figure A19. Example: thermal bridge of an attic.

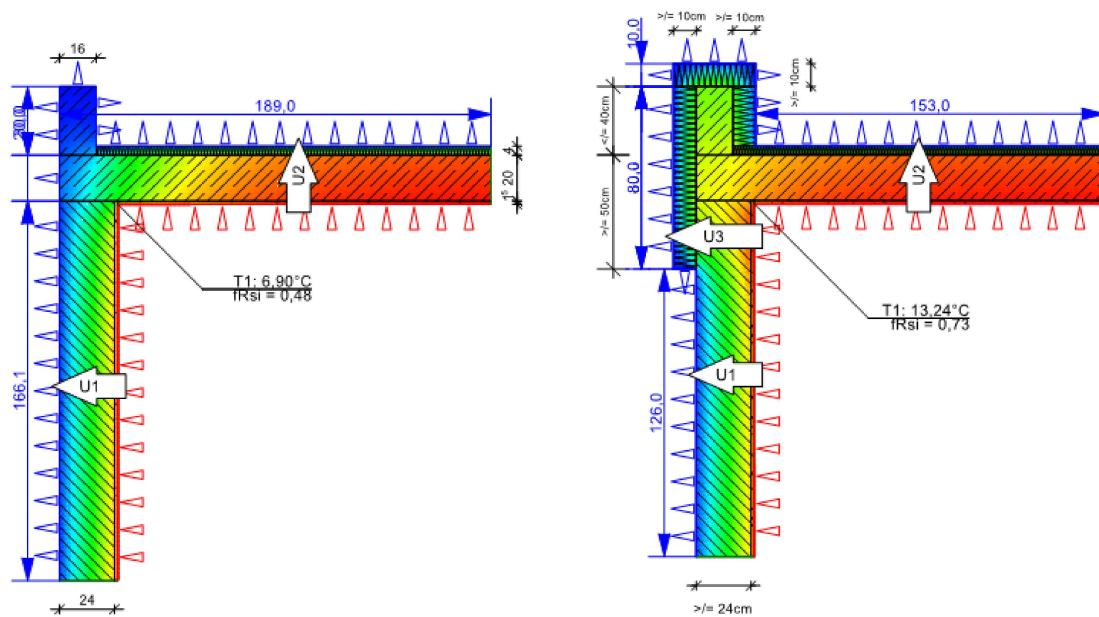


Figure A20. Before and after the thermal bridge retrofit of an attic (created with ThermCad thermal bridge simulation calculator).

Flat roof: Staggered story

A staggered story is an additional top story set back from the outer walls of the building. A thermal bridge can occur at the connection between a flat roof and a staggered story, if the insulation in this area is missing or incorrectly applied. The thermal bridge effect can be reinforced by the different materials used for the staggered story and the roof surface [51].

An example of a thermal bridge of a staggered story is presented in Figure A21. For the retrofit of this thermal bridge type, it is necessary to demolish a part of the roof structure and install new thermal insulation material in the connection area. The thermal insulation reduces the negative effects of the thermal bridge in the edge area. Due to the necessary partial removal of the existing roof covering, this retrofit is time-consuming and there is a risk of moisture problems. The insulation should be 20 cm long in total and installed in the direct connection area to the rising components of the staggered story. An illustration of this retrofit measure is shown in Figure A22, the costs of the retrofit of this thermal bridge type are listed in Table A24, and the change in the characteristic values of heat loss and mold formation of the building component before and after the retrofit is shown in Table A25.

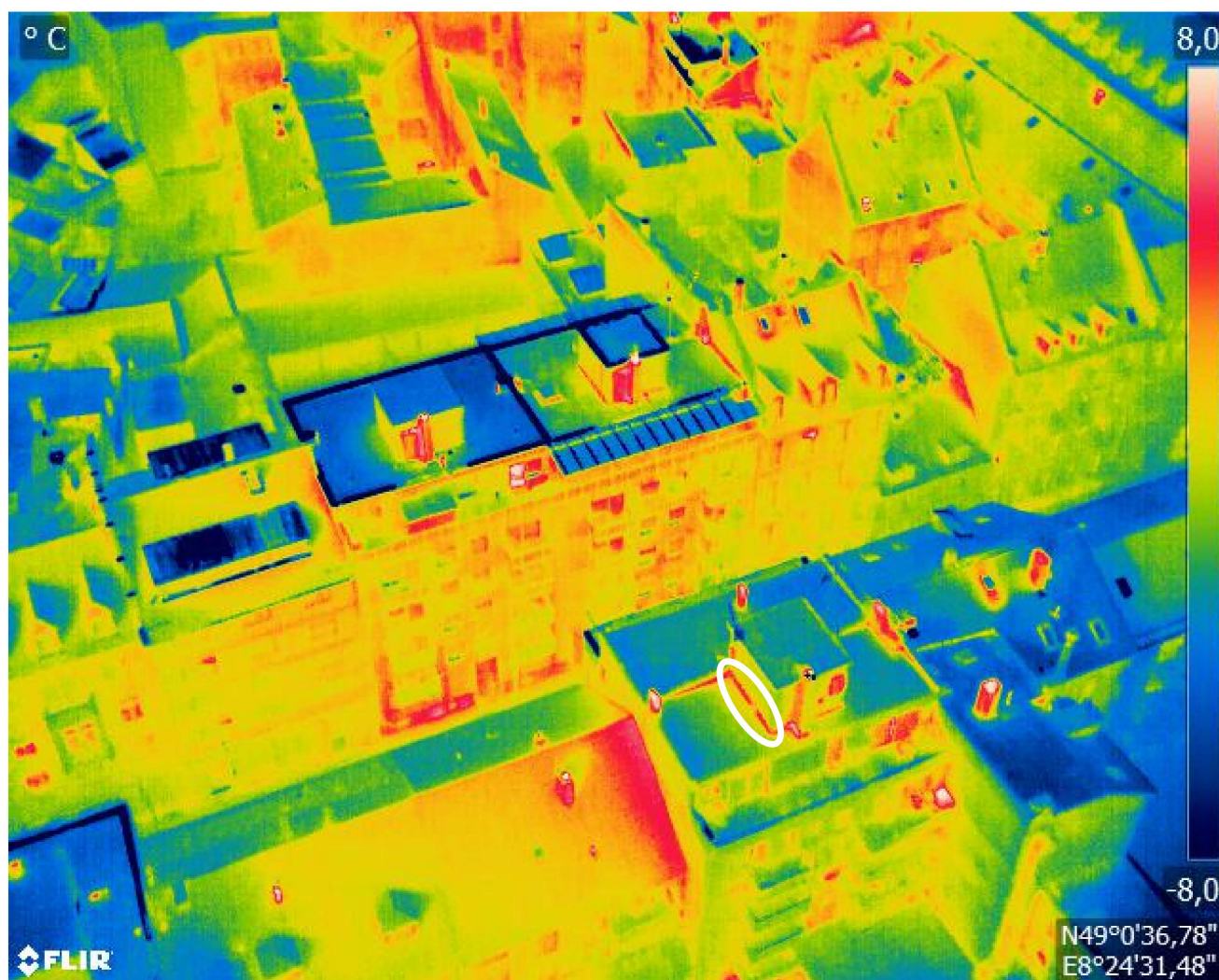


Figure A21. Example: thermal bridge of a staggered story.

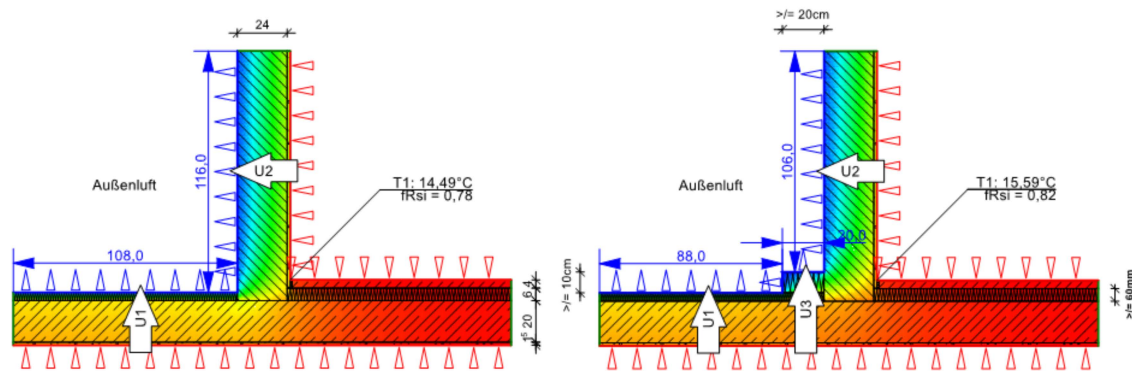


Figure A22. Before and after the thermal bridge retrofit of a staggered story (created with ThermCad thermal bridge simulation calculator).

Table A24. Retrofit components and costs of the thermal bridge retrofit of a staggered story [38,39].

Pos. No.	Retrofit Measure * Installation Height: 100 cm	Retrofit Costs per Linear Meter
LB 321-5	Removing and reattaching roof paving	11.80 EUR/m
LB 321-4	Removing and reattaching gravel filling	10.20 EUR/m
LB 321-10	Demolishing old trickle protection mat	2.00 EUR/m
LB 321-9	Removing old filter layer	0.80 EUR/m
LB 321-27	Thermal insulation, DAA, CG, up to 140 mm	16.40 EUR/m
LB 321-35	Roof waterproofing PYE PV250 S5, upper layer	3.40 EUR/m
LB 310-15	Percolating layer, fleece-laminated	3.40 EUR/m
LB 321-40	New trickle protection mat	1.00 EUR/m
	Gross total	49.00 EUR/m

* In retrofit practice, the bitumen waterproofing is replaced, if necessary, to prevent moisture problems.

Table A25. Quantifiable results of the thermal bridge retrofit of a staggered story (ThermCad thermal bridge simulation calculation).

Original State before Retrofit			State after Retrofit			Improvement	
$f_{R,si,0}$ (-)	Ψ_0 (W/mK)	q_0 (W/m)	$f_{R,si,1}$ (-)	Ψ_1 (W/mK)	q_1 (W/m)	$\Delta\Psi$ (W/mK)	Δq (W/m)
0.78	0.28	67.17	0.82	0.23	59.83	0.06	7.34

Steep roof: Roof ridge

A gable roof has a ridge where the two sloping roof surfaces connect. The ridge has high demands on the quality of the roof insulation work due to the different geometric conditions. If the insulation is missing or incorrectly installed, this area can become a significant thermal bridge within the roof structure. In addition, the air leakage potential increases considerably due to changes in the angle [2].

An example of a thermal bridge of a roof ridge is presented in Figure A23. For the retrofit of this thermal bridge type, it is necessary to install thermal insulation material as under-rafter insulation below the ridge. This reduces the effect of the geometric discontinuity and the heat loss through the thermal bridge area. For a professional retrofit, a sufficient width of the thermal insulation of 30 cm must be ensured, which should be attached directly to the ridge. It is important that the thermal insulation is applied on both sides of the ridge. An illustration of this retrofit measure is shown in Figure A24, the costs of the retrofit of this thermal bridge type are listed in Table A26, and the change in the

characteristic values of heat loss and mold formation of the building component before and after the retrofit is shown in Table A27.

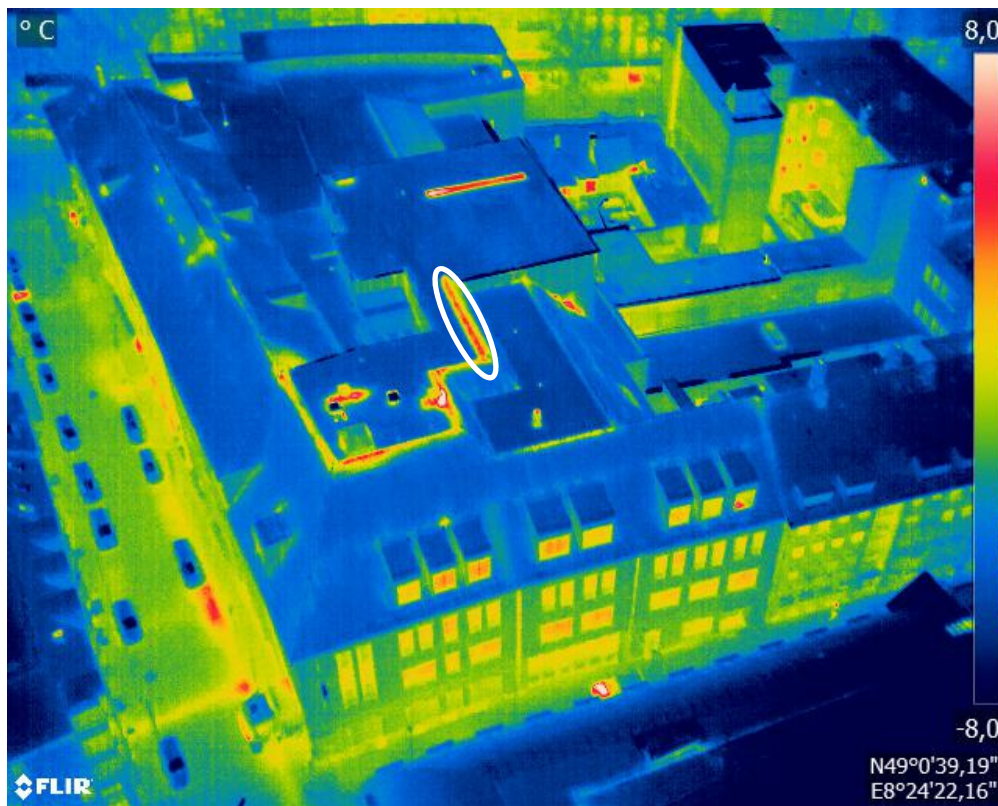


Figure A23. Example: thermal bridge of a roof ridge.

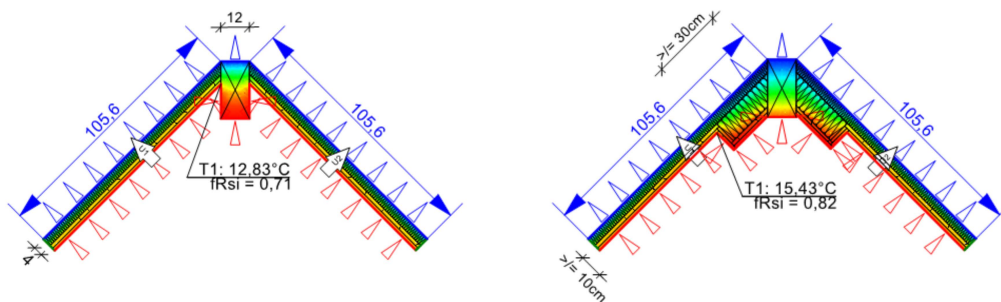


Figure A24. Before and after the thermal bridge retrofit of a roof ridge (created with ThermCad thermal bridge simulation calculator).

Table A26. Retrofit components and costs of the thermal bridge retrofit of a roof ridge [38,39].

Pos. No.	Retrofit Measure * Installation Height: 60 cm	Retrofit Costs per Linear Meter
LB 320-11	Demolishing old roof boarding	10.80 EUR/m
LB 320-8	Removing old roof lathing	2.40 EUR/m
LB 320-37	Bottom rafter insulation, MW 035, 100 mm	29.40 EUR/m
LB 320-64	Vapor barrier, variable humidity	4.80 EUR/m
LB 320-72	Cross-laths, dry, 30 × 50 mm, roof	3.00 EUR/m
LB 320-82	Boarding OSB/3 humidity range, 25 mm	18.60 EUR/m
Gross total		69.00 EUR/m

* In retrofit practice, costs for the scaffold are also relevant.

Table A27. Quantifiable results of the thermal bridge retrofit of a roof ridge (ThermCad thermal bridge simulation calculation).

Original State before Retrofit			State after Retrofit			Improvement	
$f_{R,si,0}$ (-)	Ψ_0 (W/mK)	q_0 (W/m)	$f_{R,si,1}$ (-)	Ψ_1 (W/mK)	q_1 (W/m)	$\Delta\Psi$ (W/mK)	Δq (W/m)
0.71	0.06	36.80	0.82	-0.28	30.04	0.34	6.76

Steep roof: Dormer

The connection between the rooftop and a dormer has high demands on the quality of insulation work due to the geometrical conditions. If the insulation is missing or incorrectly applied, this connection leads to a thermal bridge within the roof cladding. Due to different angles, the thermal bridge potential also increases considerably. The thermal bridge effect is reinforced by the different specific thermal conductivities of wood and masonry [2].

An example of a thermal bridge of a dormer is presented in Figure A25. For the retrofit of this thermal bridge type, it is necessary to install additional thermal insulation material along the connection area from the dormer to the rooftop. This serves to balance the effect of the different specific thermal conductivities of masonry and wood and to reduce heat loss. The necessary insulation should be 20 cm high and installed in the direct connection area to the roof. An illustration of this retrofit measure is shown in Figure A26, the costs of the retrofit of this thermal bridge type are listed in Table A28, and the change in the characteristic values of heat loss and mold formation of the building component before and after the retrofit is shown in Table A29.

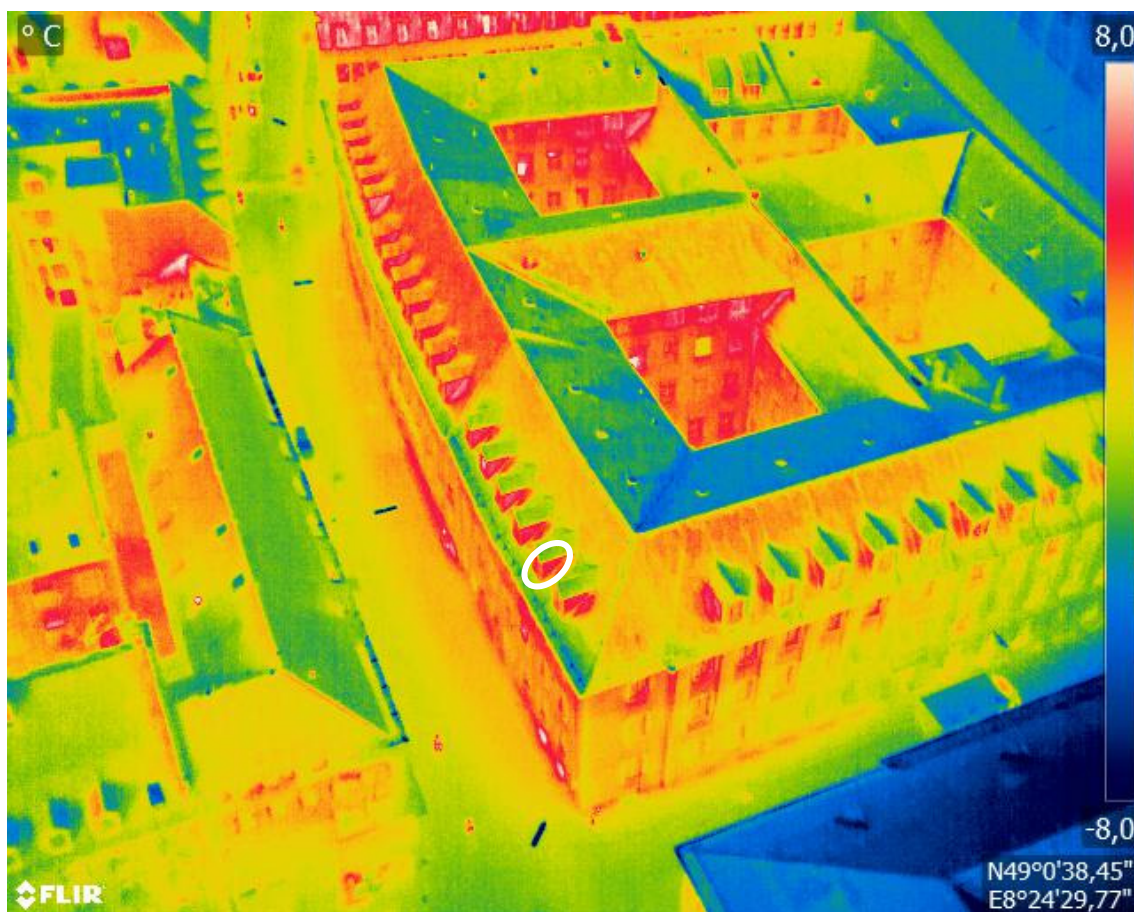


Figure A25. Example: thermal bridge of a dormer.

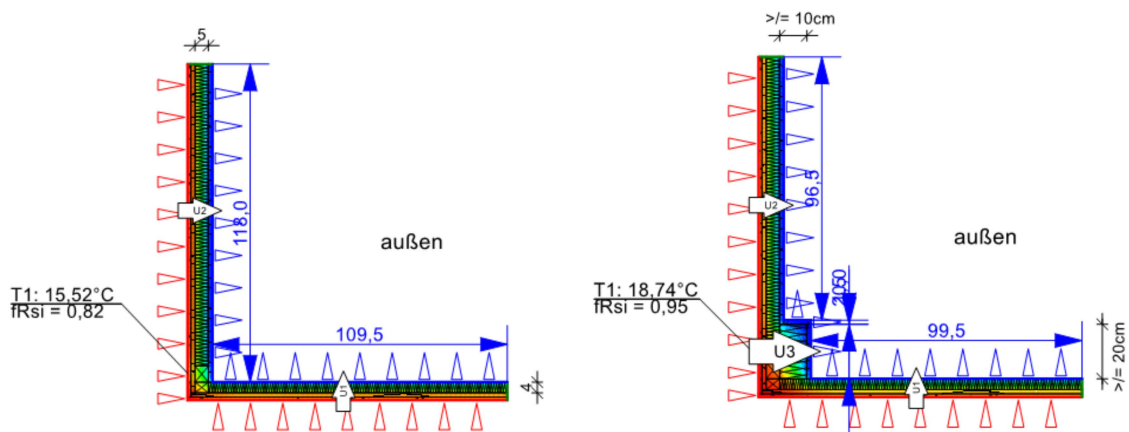


Figure A26. Before and after the thermal bridge retrofit of a dormer (created with ThermCad thermal bridge simulation calculator).

Table A28. Retrofit components and costs of the thermal bridge retrofit of a dormer [38,39].

Pos. No.	Retrofit Measure * Installation Height: 20 cm	Retrofit Costs per Linear Meter
LB 323-2	Removing old plaster from the partial area	5.20 EUR/m
LB 323-6	Removing old plaster base from the wall	2.80 EUR/m
LB 323-68	Preparing base for the thermal insulation system	0.60 EUR/m
LB 323-86	Thermal insulation system up to 20 m, PS 100, bonding technique	15.60 EUR/m
LB 323-30	Reinforcement fabrics (glass fiber)	2.20 EUR/m
LB 323-67	Plaster (undercoat and finishing plaster)	8.20 EUR/m
Gross total		34.60 EUR/m

* In retrofit practice, costs for the scaffold are also relevant.

Table A29. Quantifiable results of the thermal bridge retrofit of a connection of a rooftop on a wall (ThermCad thermal bridge simulation calculation).

Original State before Retrofit			State after Retrofit			Improvement	
$f_{R,si,0}$ (-)	Ψ_0 (W/mK)	q_0 (W/m)	$f_{R,si,1}$ (-)	Ψ_1 (W/mK)	q_1 (W/m)	$\Delta\Psi$ (W/mK)	Δq (W/m)
0.82	0.09	36.34	0.95	0.05	32.01	0.04	4.33

Steep roof: Connection between a rooftop and a wall

Due to the different geometric conditions, the connection between a rooftop and an outer wall is associated with high demands on the quality of the insulation work. If the roof insulation is missing or incorrectly installed, this connection causes a thermal bridge. In addition, the thermal bridge potential increases considerably due to the angle of the roof and different materials of the two components [51].

An example of a thermal bridge of a connection between a rooftop and a wall is presented in Figure A27. For the retrofit of this thermal bridge type, it is necessary to demolish part of the roof structure and install additional thermal insulation material in the connection area to reduce the negative effects of the thermal bridge in the edge area. The partial removal of the existing roof structure makes the retrofit very complex and is associated with the risk of moisture problems if the vapor barrier is damaged. For the retrofit, it is important to use a sufficiently long thermal insulation layer of 30 cm, which is installed in the direct connection area to the outer wall. An illustration of this retrofit measure is shown in Figure A28, the costs of the retrofit of this thermal bridge type are

listed in Table A30, and the change in the characteristic values of heat loss and mold formation of the building component before and after the retrofit is shown in Table A31.



Figure A27. Example: thermal bridge of a connection between a rooftop and a wall.

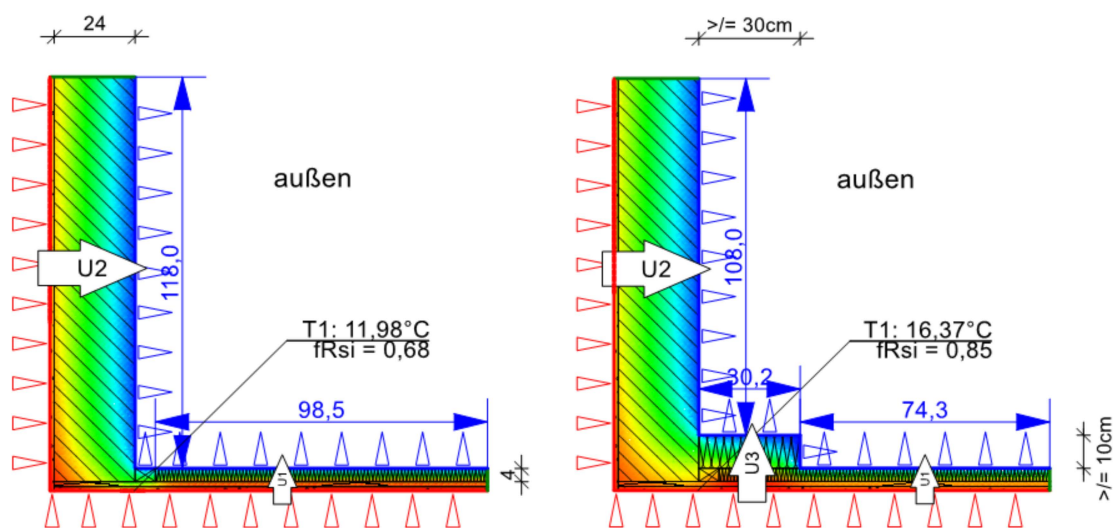


Figure A28. Before and after the thermal bridge retrofit of a connection between a rooftop and a wall (created with ThermCad thermal bridge simulation calculator).

Table A30. Retrofit components and costs of the thermal bridge retrofit of a connection between a rooftop and a wall [38,39].

Pos. No.	Retrofit Measure * Installation Height: 30 cm	Retrofit Costs per Linear Meter
LB 320-2	Removing and reattaching roof covering	6.00 EUR/m
LB 320-8	Removing old roof lathing	1.20 EUR/m
LB 320-20	Demolishing old underlay sill	1.80 EUR/m
LB 320-11	Demolishing old roof boarding	5.40 EUR/m
LB 320-37	Bottom rafter insulation, MW 035, 100 mm	15.00 EUR/m
LB 320-79	Roof boarding, coniferous wood, 24 mm peg	8.10 EUR/m
LB 320-68	Underlay sill, ventilated roof	2.70 EUR/m
LB 320-74	Roof lathing, dry	2.40 EUR/m
	Gross total	42.60 EUR/m

* In retrofit practice, costs for the scaffold are also relevant.

Table A31. Quantifiable results of the thermal bridge retrofit of a connection between a rooftop and a wall (ThermCad thermal bridge simulation calculation).

Original State before Retrofit			State after Retrofit			Improvement	
$f_{R,si,0}$ (-)	Ψ_0 (W/mK)	q_0 (W/m)	$f_{R,si,1}$ (-)	Ψ_1 (W/mK)	q_1 (W/m)	$\Delta\Psi$ (W/mK)	Δq (W/m)
0.68	0.32	66.82	0.85	0.21	57.96	0.11	8.86

Appendix C

Thermal anomalies on aerial thermographic images that can be misinterpreted as thermal bridges:

- Ventilation tiles on gable roofs: Ventilation tiles help ventilating the roofing in order to prevent the formation of mold and moisture problems. These additional but small heat losses cannot be avoided or retrofitted and can be neglected in accordance with the supplementary sheet 2 of DIN 4108 [35]. In thermograms, they appear as small hot dots on rooftops.
- Water pipe aerators: Pipe aerators for wastewater downpipes must also be routed over the roof. They prevent overpressure or underpressure in the sewage system in order to protect the residents from harmful sewer gases. Because of the sewage's own temperature, there is little heat loss, which is released into the environment via the pipe aerator and can also be neglected according to the supplementary sheet 2 of DIN 4108 [35]. In thermograms, these also appear as small hot dots on rooftops.
- Solar systems: Photovoltaic systems on roofs can radiate a lot of heat for a long time after sunset. The roof can then be falsely rated as having a very low energy quality. At night, this phenomenon is reversed in PV systems. Then, they appear comparatively cold due to the very high reflection. If there is a photovoltaic system, no conclusions can be drawn with respect to the thermal quality of the roof below.
- Lamps: Lamps and neon signs that are attached to the building and operated with old, conventional light sources appear as small flat areas that have a higher temperature than the remainder of the exterior façades.
- Constructions with heat build-ups: Constructions such as small inner courtyards or arcade constructions lead to heat build-ups. Due to their protected construction, heat is retained here particularly well and warm air cannot flow easily. These constructions are often visible in thermograms as areas with increased temperature, but they are not thermal bridges and do not need to be retrofitted.

- Open windows: Through open windows, high amounts of thermal energy can be transported. On thermograms, open windows can be misinterpreted as thermal weak points of the façade.

Appendix D

Case study: Exemplary thermal bridge assessment of a German building constructed in the 1950s/1960s using thermographic aerial images:



Figure A29. Reference building for an exemplary thermal bridge assessment (north orientation).



Figure A30. Thermographic aerial images of the reference building (north, east, and west orientation).

Table A32. Building size characteristics of the reference building [47].

Building Size Characteristics	Size	Unit
Width	11.40	M
Length	15.40	M
Floor area	175.56	M
Width of jutting edge	6.45	M
Height to roof edge	11.00	M
Building height	14.00	M

Table A32. Cont.

Building Size Characteristics	Size	Unit
Number of stories	4 full stories + 1 additional roof story	-
Number of windows	20	Pieces
Window sizes	1.76 × 1.38 (length × height)	M
Number of French windows	13	pieces
French window sizes	1.76 × 2.31 (length × height)	m
Number of dormers	3	pieces
Size dormer (south)	10.4 × 1.5 × 3 (length × height × width)	m
Size dormer (north 1)	4.5 × 1.5 × 3 (length × height × width)	m
Size dormer (north 2)	4.2 × 1.5 × 3 (length × height × width)	m

Table A33. Area sizes, U-values, temperature adjustment factors, and transmission heat losses of components of the reference building [37,47,49].

Building Component	Area (m ²)	U-Value (W/m ² K)	Temperature Adjustment Factor F_{ix} (-)	Transmission Heat Loss H_T (W/K)
Outside wall north	104.85	1.4	1.0	146.79
Outside wall east	80.63	1.4	1.0	112.88
Outside wall south	84.52	1.4	1.0	118.33
Outside wall west	0.00	1.4	1.0	0.00
Basement wall above ground north	5.70	1.4	1.0	7.98
Basement wall above ground east	3.23	1.4	1.0	4.52
Basement wall above ground south	5.70	1.4	1.0	7.98
Basement wall above ground west	0.00	1.4	1.0	0.00
Basement wall underneath ground north	22.80	1.4	0.6	19.15
Basement wall underneath ground east	12.90	1.4	0.6	10.84
Basement wall underneath ground south	22.80	1.4	0.6	19.15
Basement wall underneath ground west	0.00	1.4	0.6	0.00
Ground floor slab	176.70	1.2	0.4	84.82
Windows north	40.55	2.9	1.0	117.60
Windows east	0.00	2.9	1.0	0.00
Windows south	60.88	2.9	1.0	176.55
Windows west	0.00	2.9	1.0	0.00
Rooftop	136.80	0.7	1.0	95.76
Dormer north	22.05	0.5	1.0	11.03
Dormer east	0.00	0.5	1.0	0.00
Dormer south	20.10	0.5	1.0	10.05
Dormer west	0.00	0.5	1.0	0.00

To calculate the thermal bridge surcharge, we use the high precision method (German “genaues Verfahren”) [37]:

$$H_T = \sum_i H_{T,i} + H_{TB} = \sum_i (F_{x,i} * U_i * A_i) + \sum_j (\Psi_j * l_j)$$

H_T : Transmission heat loss (W/K)
 $H_{T,i}$: Transmission heat loss of building component I (W/K)
 H_{TB} : Additional transmission heat loss caused by thermal bridges (W/K)
 $F_{x,i}$: Temperature correction factor of building component i (-)
 U_i : Heat transmission coefficient of building component i (W/(m²K))
 A_i : Area size of building component i (m²)
 Ψ_j : The thermal bridge loss coefficient of thermal bridge j (W/(mK))
 l_j : Length of thermal bridge j (m)

Table A34. Transmission heat losses caused by thermal bridges and total transmission heat losses of the reference building before and after a retrofit [37,47,49].

	l_i	Ψ_0	Ψ_1	$H_{TB,0,i} = \Psi_{0,i} * l_i$	$H_{TB,1,i} = \Psi_{1,i} * l_i$
Thermal bridges	(m)	(W/mK)	(W/mK)	(W/K)	(W/K)
Window reveal	115.26	0.10	−0.41	11.53	−47.26
Dormer	37.10	0.09	0.05	3.34	1.86
Floor slab	96.30	0.70	0.09	67.41	8.67
Connection wall/roof	6.00	0.32	0.19	1.92	1.14
Balcony slab	32.70	0.44	−0.05	14.39	−1.64
$H_{TB} = \sum H_{TB}$				98.58	−37.23
$H_T = F_{xi} * U_i * A_i$				943.40	943.40
$H_T = H_{T,i} + H_{TB}$				1041.99	906.17

References

- Global Alliance for Buildings and Construction (GlobalABC). *Global Status Report towards a Zero-Emission, Efficient and Resilient Buildings and Construction Sector*; GlobalABC: Paris, France, 2018; ISBN 978-92-807-3729-5.
- Haefele, G.; Oed, W.; Sabel, L. *Hauserneuerung: Instandsetzen Modernisieren Energiesparen Umbauen*, 17th ed.; (May Be Translated As: Building Retrofits: Repairing, Modernizing, Saving Energy, Reconstructing); Ökobuch: Staufen bei Freiburg, Germany, 2019; ISBN 978-3-936896-49-7.
- Theodoridou, I.; Papadopoulos, A.; Hegger, M. A typological classification of the Greek residential building stock. *Energy Build.* **2011**, *43*, 2779–2787. [CrossRef]
- Ballarini, I.; Corgnati, S.P.; Corrado, V. Use of reference buildings to assess the energy saving potentials of the residential building stock: The experience of TABULA project. *Energy Policy* **2014**, *68*, 273–284. [CrossRef]
- Diefenbach, N. Basisdaten für Hochrechnungen mit der Deutschen Gebäudetypologie des IWU: Neufassung Oktober 2013. IWU, Darmstadt. (May Be Translated as: Basic Data for Projections with the German Building Typology of the IWU: New version October 2013.). Available online: https://www.iwu.de/fileadmin/publikationen/energie/klima_altbau/2013_IWU_Diefenbach_Basisdaten-f%C3%BCr-Hochrechnungen-mit-der-Deutschen-Geb%C3%A4udetypologie-des-IWU-2013.pdf (accessed on 15 June 2021).
- Kreditanstalt für Wiederaufbau (KfW). Einflussfaktoren auf die Sanierung im deutschen Wohngebäudebestand. IWU, Darmstadt. (May Be Translated as: Factors Influencing the Renovation of the German Residential Building Stock). 2016. Available online: https://www.kfw.de/PDF/Download-Center/Konzernthemen/Research/PDF-Dokumente-alle-Evaluationen/Einflussfaktoren-auf-die-Sanierung-im-deutschen-Wohngeb%C3%A4udebestand_2016.pdf (accessed on 25 April 2021).
- Cischinski, H.; Diefenbach, N. Datenerhebung Wohngebäudebestand 2016. IWU, Darmstadt. (May Be Translated as: Data Collection of Residential Buildings in 2016). 2018. Available online: https://www.iwu.de/fileadmin/user_upload/dateien/gebaeudebestand/prj/Endbericht_Datenerhebung_Wohngeb%C3%A4udebestand_2016.pdf (accessed on 15 June 2021).
- Schild, K. *Wärmebrücken: Berechnung und Mindestwärmeschutz*, 1st ed.; (May Be Translated as: Thermal bridges: Calculation and Minimum Requirements for Thermal Insulation); Springer Fachmedien Wiesbaden GmbH: Wiesbaden, Germany, 2018. [CrossRef]
- Schmidt, P.; Windhausen, S. *Bauphysik-Lehrbuch: Wärmeschutz—Energieeinsparung—Feuchte- und Tauwasserschutz—Schallschutz—Raumakustik*, 1st ed.; (May be translated as: Building physics textbook: Thermal insulation—energy saving—moisture and condensation protection—sound insulation—room acoustics.); Bundesanzeiger: Köln, Germany, 2018; ISBN 978-3-8462-0407-8.
- Fouad, N.; Richter, T. *Leitfaden Thermographie im Bauwesen: Theorie, Anwendungsgebiete, Praktische Umsetzung*, 4th ed.; (May be Translated as: Thermography Guideline for Construction: Theory and Practice); Fraunhofer IRB: Stuttgart, Germany, 2012; ISBN 3816784569.

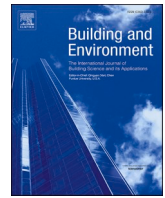
11. Kiritat, A.; Krejcar, O. A review of infrared thermography for the investigation of building envelopes: Advances and prospects. *Energy Build.* **2018**, *176*, 390–406. [[CrossRef](#)]
12. Lucchi, E. Applications of the infrared thermography in the energy audit of buildings: A review. *Renew. Sustain. Energy Rev.* **2018**, *82*, 3077–3090. [[CrossRef](#)]
13. Kylili, A.; Fokaides, P.; Christou, P.; Kalogirou, S. Infrared thermography (IRT) applications for building diagnostics: A review. *Appl. Energy* **2014**, *134*, 531–549. [[CrossRef](#)]
14. Umweltbundesamt (UBA): Kohlendioxid-Emissionen im Bedarfsfeld „Wohnen. (May Be Translated as: Carbon Dioxide Emissions in the Housing Sector). 2021. Available online: <https://www.umweltbundesamt.de/daten/private-haushalte-konsum/wohnen/kohlendioxid-emissionen-im-bedarfsfeld-wohnen> (accessed on 25 May 2021).
15. US Department of Energy (DOE). Guide to Community Energy Strategic Planning. 2013. Available online: https://www.energy.gov/sites/prod/files/2014/05/f15/cesp_guide.pdf (accessed on 30 August 2021).
16. Littlejohn, D.; Laszlo, R. National Report on Community Energy Plan Implementation. Quality Urban Energy Systems of Tomorrow (QUEST). 2015. Available online: https://questcanada.org/wp-content/uploads/2018/08/National-Report-on-Community-Energy-Plan-Implementation_Full_Report_2015.pdf (accessed on 12 September 2021).
17. Urban Europe (UE). White Paper on PED Reference Framework for Positive Energy Districts and Neighbourhoods. 2020. Available online: <https://jpi-urbaneurope.eu/ped/> (accessed on 30 August 2021).
18. Kreditanstalt für Wiederaufbau (KfW). Merkblatt Energetische Stadtsanierung—Zuschuss. 432 Zuschüsse für Quartierskonzepte und Sanierungsmanager. (May Be Translated As: Leaflet on Urban Energy Improvement—Grant. 432 Grants for District Plans and Redevelopment Managers) Frankfurt. 2015. Available online: [https://www.kfw.de/PDF/Download-Center/F%C3%B6rderprogramme-\(Inlandsf%C3%B6rderung\)/PDF-Dokumente/6000002110_M_432_Energetische_Stadtsanierung_Zuschuss.pdf](https://www.kfw.de/PDF/Download-Center/F%C3%B6rderprogramme-(Inlandsf%C3%B6rderung)/PDF-Dokumente/6000002110_M_432_Energetische_Stadtsanierung_Zuschuss.pdf) (accessed on 12 January 2021).
19. DIN EN 13187:1999-05. *Wärmetechnisches Verhalten von Gebäuden—Nachweis von Wärmebrücken in Gebäudehüllen—Infrarot-Verfahren (ISO 6781:1983, Modifiziert); Deutsche Fassung EN 13187:1998*; (May Be Translated as: Thermal Performance of Buildings—Qualitative Detection of Thermal Irregularities in Building Envelopes—Infrared Method (ISO 6781:1983, Modified); German Version EN 13187:1998; DIN: Berlin, Germany, 1999. [[CrossRef](#)]
20. Fouad, N.; Richter, T. *Bauphysik-Kalender 2012: Schwerpunkt: Gebäudediagnostik*; (May Be Translated as: Building Physics Calendar 2012: Focus: Building Diagnostics); Verlag für Architektur und technische Wissenschaften GmbH & Co. KG: Berlin, Germany, 2012.
21. Miller, J.; Singh, N. Kinetic Super-Resolution Long-Wave Infrared (KSR LWIR) Thermography Diagnostic for Building Envelopes: Scott AFB, IL. Engineer Research and Development Center Champaign II Construction Engineering Research Lab. 2021. Available online: <https://erdc-library.erdcresearch.dren.mil/jspui/bitstream/11681/19958/1/ERDC-CERL-TR-15--18.pdf> (accessed on 18 June 2021).
22. Garrido, I.; Lagüela, S.; Arias, P.; Balado, J. Thermal-based analysis for the automatic detection and characterization of thermal bridges in buildings. *Energy Build.* **2018**, *158*, 1358–1367. [[CrossRef](#)]
23. Macher, H.; Landes, T.; Grussenmeyer, P. Automation of Thermal Point Clouds Analysis for the Extraction Of Windows and Thermal Bridges of Building Facades. *ISPRS—Int. Arch. Photogramm. Remote Sens. Spat. Inf. Sci.* **2020**, *XLIII-B2-2*, 287–292. [[CrossRef](#)]
24. Miño, J.A.P.Y.; Dupont, N.; Beckers, B. Pixel-by-pixel rectification of urban perspective thermography. *Remote Sens. Environ.* **2021**, *266*, 112689. [[CrossRef](#)]
25. Aguerre, J.P.; Nahon, R.; Garcia-Nevado, E.; La Borderie, C.; Fernández, E.; Beckers, B. A street in perspective: Thermography simulated by the finite element method. *Build. Environ.* **2018**, *148*, 225–239. [[CrossRef](#)]
26. Entrop, A.G.; Vasenev, A. Infrared drones in the construction industry: Designing a protocol for building thermography procedures. *Energy Procedia* **2017**, *132*, 63–68. [[CrossRef](#)]
27. Vorajee, N.; Mishra, A.K. Analyzing capacity of a consumer-grade infrared camera in South Africa for cost-effective aerial inspection of building envelopes. *Front. Arch. Res.* **2020**, *9*, 697–710. [[CrossRef](#)]
28. Mavromatidis, L.; Dauvergne, J.-L.; Saleri, R.; Batsale, J.-C. *First Experiments for the Diagnosis and Thermophysical Sampling Using Pulsed IR Thermography from Unmanned Aerial Vehicle (UAV)*; Taylor & Francis: Bordeaux, France, 2014. [[CrossRef](#)]
29. Benz, A.; Taraben, J.; Debus, P.; Habte, B.; Oppermann, L.; Hallermann, N.; Voelker, C.; Rodehorst, V.; Morgenthal, G. Framework for a UAS-based assessment of energy performance of buildings. *Energy Build.* **2021**, *250*, 111266. [[CrossRef](#)]
30. Hou, Y.; Volk, R.; Chen, M.; Soibelman, L. Fusing tie points’ RGB and thermal information for mapping large areas based on aerial images: A study of fusion performance under different flight configurations and experimental conditions. *Autom. Constr.* **2021**, *124*, 103554. [[CrossRef](#)]
31. FLIR Systems Inc. FLIR Tools. 2021. Available online: <https://www.flir.de/products/flir-tools/> (accessed on 10 July 2021).
32. Fouad, U.-P.D.-I.N.A.; Richter, I.T. *Infrarot-Thermografie in der Praxis*; John Wiley & Sons: Hoboken, NJ, USA, 2012. [[CrossRef](#)]
33. Fouad, N. *Bauphysik-Kalender 2017: Schwerpunkt: Gebäudehülle und Fassaden*; (May be Translated as: Building Physics Calendar 2017: Focus: Building Envelope and Façades.); Wilhelm Ernst & Sohn: Hoboken, NJ, USA, 2017. [[CrossRef](#)]
34. Stadt Essen (City of Essen). Gebäudetypologie für die Stadt Essen. (May be Translated as: Building Typology for the City of Essen). 2015. Available online: https://www.alt-bau-neu.de/_database/_data/datainfopool/Gebaedetypologie_Essen.pdf (accessed on 17 April 2021).

35. DIN 4108 Beiblatt 2. *Wärmeschutz und Energieeinsparung in Gebäuden—Beiblatt 2: Wärmebrücken—Planungs- und Ausführungsbeispiele*; (May be Translated as: Thermal Insulation and Energy Economy in Buildings; Supplement 2: Thermal Bridges—Examples for Planning and Performance); DIN: Berlin, Germany, 2004.
36. ROWA Soft GmbH. *ThermCAD Wärmebrückensimulationsberechnung*; (May be Translated as: Thermal Bridge Calculation Tool); ROWA Soft GmbH: Altenburg, Germany, 2021. Available online: <http://www.rowasoftgmbh.de/de/produkte/produktdetails/thermcad> (accessed on 10 May 2021).
37. DIN V 4108-6:2003-06: *Wärmeschutz und Energie-Einsparung in Gebäuden—Teil 6: Berechnung des Jahresheizwärme- und des Jahresheizenergiebedarfs*; (May be Translated as: Thermal Protection and Energy Economy in Buildings—Part 6: Calculation of Annual Heat and Energyconsumption); DIN: Berlin, Germany, 2003.
38. BKI Baukosteninformationszentrum. *BKI Baukosten 2020 Altbau: Statistische Kostenkennwerte für Positionen*; (May be Translated as: BKI Construction Prices 2020 Old Buildings: Statistical Price Parameters); BKI: Stuttgart, Germany, 2020; ISBN 978-3-945649-95-4.
39. BKI Baukosteninformationszentrum. *BKI Baukosten 2020 Neubau: Statistische Kostenkennwerte für Positionen*; (May be Translated as: BKI Construction Prices 2020 New Buildings: Statistical Price Parameters); BKI: Stuttgart, Germany, 2020; ISBN 978-3-945649-89-3.
40. DIN 276. *Kosten im Bauwesen*; (May be translated as: Building Costs); DIN: Berlin, Germany, 2018.
41. SZ DJI Technology Co. Ltd. *Matrice 600 Pro: User Manual*; Version 1.0; DJI: Shenzhen, China, 2018; Available online: <https://www.dji.com/de/matrice600-pro> (accessed on 25 October 2021).
42. FLIR Systems, Inc. Duo Pro R: User Guide Version 1, August 2017. 2017. Available online: <https://www.flir.com/products/duo-pro-r/> (accessed on 25 October 2021).
43. SZ DJI Technology Co. Ltd. *Zenmuse XT 2: User Manual*; Version 1.0; DJI: Shenzhen, China, 2018; Available online: <https://www.dji.com/zenmuse-xt2> (accessed on 25 October 2021).
44. Mapsz Editor (n.d.). Karlsruhe, Germany. Available online: <https://mapz.com/map> (accessed on 25 October 2021).
45. Deutsche Energie-Agentur (dena). *Wärmebrücken in der Bestandssanierung: Leitfaden für Fachplaner und Architekten*; (May be Translated as: Thermal Bridges and the Retrofit of Existing Buildings: Guidelines for Specialist Planners and Architects); Dena: Berlin, Germany, 2015. Available online: https://www.dena.de/fileadmin/dena/Publikationen/PDFs/2019/8179_Leitfaden_Waermebuecken_Bestandssanierung.pdf (accessed on 27 July 2021).
46. DIN EN ISO 10211:2008-04. *Wärmebrücken im Hochbau—Wärmeströme und Oberflächentemperaturen—Detaillierte Berechnungen*; (May be Translated as: Thermal Bridges in Building Construction—Heat Flows and Surface Temperatures—Detailed Calculations (ISO 10211:2007); German Version EN ISO 10211:2007/DIN; DIN: Berlin, Germany, 2008.
47. Google Maps. 2021. Available online: <https://www.google.de/maps> (accessed on 27 July 2021).
48. Mayer, Z.; Kahn, J.; Hou, Y.; Volk, R. AI-based thermal bridge detection of building rooftops on district scale using aerial images. In Proceedings of the EG-ICE 2021 Workshop on Intelligent Computing in Engineering proceedings, Berlin, Germany, 30 June–2 July 2021; 1427. [[CrossRef](#)]
49. Bundesministerium für Wirtschaft und Energie (BMWi); Bundesministerium für Umwelt, Natur, Bau und Reaktorsicherheit (BMU). *Bekanntmachung der Regeln zur Datenaufnahme und Datenverwendung im Wohngebäudebestand*; (May be Translated as: Announcement of the Rules for Data Acquisition and Data Use in the Residential Building Stock); BMWi: Munich Germany, 2015. Available online: https://www.bbsr-energieeinsparung.de/EnEVPortal/DE/EnEV/Bekanntmachungen/Download/WGDataaufnahme2013.pdf;jsessionid=5176E5F904AEFBDEA192EC019F60DC57.live21322?__blob=publicationFile&v=5 (accessed on 18 March 2021).
50. Forum. EnEV 2014 im Gebäudebestand. (May Be Translated as: Energy Saving Ordinance 2014 for the Building Stock). 2021. Available online: https://www.forum-verlag.com/media/pdf/lp_1391_Gebaude-aus-den-Baujahren-1960--1969.pdf (accessed on 10 May 2021).
51. Gabriel, I.; Ladener, H. *Vom Altbau zum Effizienzhaus: Modernisieren und Energetisch Sanieren*, 13th ed.; Staufen bei Freiburg May be Translated as: From the Old to the Efficient Building: Modernizing and Energetic Retrofitting; Ökobuch: Freiburg im Breisgau, Germany, 2018; ISBN 978-3-936896-75-6.

Paper I: Analysis of Financial Benefits for Energy Retrofits of Owner-Occupied Single-Family Houses in Germany

This paper was reproduced in its original format with permission from Elsevier:

Mayer, Z., Volk, R., Schultmann, F. (2022 - Paper I). Analysis of financial benefits for energy retrofits of owner-occupied single-family houses in Germany. *Building and Environment*, 211, 108722. Doi: <https://doi.org/10.1016/j.buildenv.2021.108722>



Analysis of financial benefits for energy retrofits of owner-occupied single-family houses in Germany

Zoe Mayer^{*}, Rebekka Volk, Frank Schultmann

Karlsruhe Institute of Technology (KIT), Institute for Industrial Production (IIP), Hertzstr. 16, 76187, Karlsruhe, Germany

ARTICLE INFO

Keywords:

Buildings
Single-family houses
Energy retrofits
Financial incentives
Optimization models
Energy policy

ABSTRACT

In many industrialized countries, a significant number of buildings were constructed prior to any energy-related building construction standards. Today, single-family houses (SFH/pl. SFHs) from this time still have a comparably poor thermal quality. This paper aims to examine and model the incentive effects of the German energy retrofit funding schemes for owners of SFHs constructed shortly before the introduction of the first German thermal insulation ordinance in 1979. We develop a novel mixed-integer economic optimization model that determines the financially optimal energy retrofit configuration for owner-occupied SFHs. In a case study, we consider German framework conditions such as governmental incentives, standards, regulations, retrofit costs, and energy prices. We calculate economic burdens and benefits in 48 different retrofit scenarios for two representative SFHs constructed in the 1960s and 1970s. In the majority of cases, the return on investment is positive. For heating system retrofits, energy savings are comparatively small, but the cost-benefit ratios of retrofits are better than for measures on the building envelope. Overall, we find retrofits to decrease operational costs to between 15% and 62% of the initial value. The financial incentive effect of the German funding instruments can lead to financially optimal savings of CO₂ emissions in the range of 82–94%, however our findings show that the conditions of the German funding programs are not designed to maximize CO₂ savings per funded euro. We show that the funding invested to reduce the annual tons of CO₂ ranges from 493 € to 3747 € in our case study.

1. Introduction

In the European Union (EU), building stock accounts for roughly 40% of the final energy consumption, and roughly 36% of CO₂ emissions [1]. Thus, the reduction of buildings energy demands is a key element in the climate protection strategy of the EU to be implemented by Member States [2]. The German Government has declared its aim to reach an almost climate-neutral building stock by 2050. Specifically, the primary energy demand of buildings should be reduced by 80% compared to 2008 through energy savings and renewable energy supply [3]. Due to the low deconstruction and replacement rates and an increasing demand for residential area per capita [4], high energy standards for new buildings are not enough to reduce the energy demand of the building stock. Instead, retrofits of buildings with low energy standards are important. As in the rest of the EU, the retrofit rate in Germany has stagnated at around 1% per year [5,6], and the retrofit of building components or technical building equipment typically only takes place at least 30 years after installation [7]. Even for heating systems with a

significantly shorter lifetime, experts usually expect its retrofit only 30 years after its installation [8]. To achieve the German climate goals for the building stock by 2050, it is crucial to accelerate retrofits, especially those with significant primary energy and CO₂ savings.

For many years, international research has given relatively little attention to retrofit strategies for single-family houses (SFH/pl. SFHs). Lately, this has increased following the political interest due to the large potential for energy and CO₂ savings in many countries, especially in Europe [9–11]. In Germany, SFHs account for more than half of the residential building stock [12]. Of these, 87% are occupied by their owners and only 13% are rented [13]. About two thirds of the SFHs in Germany were built before the first German Heat Insulation Ordinance (Wärmeschutzverordnung) in 1979 and about one third was built between 1958 and 1978 with an often low energy quality [12,14]. Even today, about 50 years after their construction, their energy quality is significantly worse than that of newer buildings because of various deficits in their building envelopes and technical equipment. Their heating systems especially require energy retrofits [15].

^{*} Corresponding author.

E-mail address: zoe.mayer@partner.kit.edu (Z. Mayer).

In Germany, financial profitability appears to be a main driver for energy retrofits. This is highlighted by various studies by Stieß et al. (2010) [16], Gossen and Nischan (2014) [17] and Renz and Hacke (2016) [18] evaluating the motivations of energy retrofit clients via qualitative interviews and surveys. In all three studies, economic reasons such as a long-term reduction in energy costs, the reduction of operating costs, and short amortization periods were mentioned by almost all participants as major motivating factors for their energy retrofits.

To increase the economic incentives of energy retrofits, there are a variety of funding instruments for retrofitters in Germany. The largest and most popular funding programs for residential buildings are coordinated by the Kreditanstalt für Wiederaufbau (KfW), which is a public German banking group [19–21]. The funding programs “Energy Efficient Retrofit” and “Energy Efficient Building” for the period between 2005 and 2017 supported energy retrofit measures of about 2.8 million residential units. In total, 73 million € was invested, contributing to annual CO₂ savings of more than seven million tons [22,23]. Moreover, other smaller funding programs at the federal level are provided by the Bundesamt für Wirtschaft und Ausfuhrkontrolle (BAFA), the Federal Office for Economics and Export Control [3]. The BAFA funds particularly innovative heating systems with renewable energies [24]. Runst (2016) [25] analyzed the financial incentives of KfW and BAFA for energy retrofits of buildings for building owners. He summarized publications on payback periods for energy-related building retrofits and found that retrofit measures are in general not profitable for building owners despite KfW and BAFA funding. In 2020, the conditions of the KfW and BAFA funding system were updated and new tax advantages for energy retrofits of owner-occupied SFHs were introduced [26]. No studies are known to the authors providing information about the recent incentive effects of the German funding system since 2020 for climate-friendly retrofits from the financial perspective of self-using SFH owners.

Other European countries (e.g. Italy, Greece, UK, Ireland, Cyprus) provide similar financial incentives as part of their national building retrofit strategies [2]. As in Germany, these incentives have different forms such as funding schemes, grants and tax exemptions, or reductions that directly and indirectly reduce the retrofit costs to stimulate energy efficiency retrofits in residential and non-residential buildings [27,28]. Due to their high relevance and large investments from the public treasury, there are a variety of European studies investigating the best design of such funding instruments. The studies deal with, for example, regional and building specific differences for the funding design of a country [29,30], the comparison of different financial initiatives among selected European countries [28], the financial attractiveness of investments in the presence and absence of incentive schemes for building retrofits [27], and building owner preferences for different structures of financial incentives [31].

This study investigates the incentive effect of the German funding system of 2020 on the comprehensive energy retrofit of owner-occupied SFHs constructed between 1958 and 1978. Moreover, we analyse how much CO₂ can be saved with a financially optimal retrofit of these buildings from the perspective of the owners. For this, we develop an economic optimization model that provides information on the maximum possible financial savings of a building retrofit from the perspective of a self-using SFH owner.

Many existing models for energy retrofits of residential buildings focus on optimizing retrofit measures. Wang et al. (2014) [32] present an optimization model with a differential evolution algorithm to identify optimal retrofit measures that maximize both energy savings and economic benefits during a selected time period and with a fixed available budget. Kumbaroğlu and Madlener (2012) [33] develop an optimization model with a techno-economic evaluation method for the energy retrofit of buildings to find the optimal set of retrofit measures with maximum net present value for a case study building. Financial incentives for building owners and users are also considered to evaluate investment alternatives. Ruparathna et al. (2017) [34] propose a fuzzy logic-based

life cycle cost analysis approach for building energy retrofits to estimate the overall costs of energy retrofit alternatives and to facilitate the selection of those with lowest costs. Simulations are used to compute expected net present values for retrofit alternatives. Penna et al. (2015) [30] develop a genetic algorithm and simulation model to investigate promising energy efficiency measures related to the building envelope and the thermal-conditioning system with respect to multiple competing objectives (Pareto approach). Their objectives are the economic performance, energy consumption, and thermal comfort of a building. However, the model does not consider retrofit measures with renewable energies. Asadi et al. (2011) [35] develop a multi-objective optimization model to select retrofit measures to minimize the energy use in a cost-effective manner, while satisfying several occupants' requirements. This model includes all technically feasible combinations concerning windows, insulation materials for the building envelope, and solar collectors, without being confined to a small set of predefined retrofit scenarios. It is implemented with a Tchebycheff programming simulation technique which is complex and difficult to extend. Rosso et al. (2020) [36] also implement a multi-objective optimization of building retrofits to minimize investment, energy demand or operational energy cost, and CO₂ emissions. To identify the optimal retrofit measures, they use a genetic algorithm with active archive and non-dominated sorting. Antipova et al. (2014) [37] develop a fast mixed-integer linear program that identifies the alternatives with the lowest environmental impact. The program can be adapted to different climatic zones, but is limited to a few retrofit measures only. It considers different wall insulation materials, exchange of windows, and the installation of solar panels, while the replacement of the heating system or the installation of a ventilation system are missing. Jafari and Valentin (2017) [38] optimize the life-cycle cost for a specific building during its service life with respect to retrofit measures based on available equity. They use a simplified prediction method for the building's energy demand by integrating dynamic and static modeling and incorporating energy retrofitting decision-making uncertainties. However, only limited retrofit measures for a specific project are considered. Wu et al. (2015) [39] present a multi-objective optimization (trade-off) to minimize life cycle cost and greenhouse gas emissions via retrofits. Their approach consists of a dynamic energy demand simulation to depict a wide range of existing buildings. It is combined with a mixed-integer linear program.

The approaches by Wang et al. (2014) [32], Kumbaroğlu and Madlener (2012) [33], Ruparathna et al. (2017) [34], Antipova et al. (2014) [37], Jafari and Valentin (2017) [38], and Wu et al. (2016) [39] can be used or extended for German retrofitting projects. Moreover, they can be transferred to different building types and all of them include economic objective functions, among others. Only Kumbaroğlu and Madlener (2012) [33] quantify the CO₂ savings through the retrofit, whereby Wu et al. (2016) [39] quantify and maximize the savings of all greenhouse gases. Coupling effects¹ are only considered by Kumbaroğlu and Madlener (2012) [33]. Only Ruparathna et al. (2017) [34] and Jafari and Valentin (2017) [38] differentiate between equity and debt capital. No existing model is known to the authors that performs an economic optimization covering German buildings and German framework conditions of energy standards, retrofit costs, different financing alternatives and the funding systems of the BAFA, KfW, and German tax benefits. Thus, we develop an innovative optimization model for the economic assessment and selection of energy retrofits under German conditions. The model is capable of the following (requirements):

¹ Coupling effect [40,41]: Energy retrofits are often planned when conventional retrofits are necessary anyway. The coupling effect has an impact on the cost planning of a retrofit, since often only additional energy-related costs of a retrofit measure are relevant then to a building owner. These costs can be considerably lower, if retrofit measures are coupled.

- Modeling German residential buildings, their building components, their retrofit status, and their energy performance
- Evaluating different retrofit measures and prices for the most common retrofit measures (insulation and retrofit of the building envelope components, exchange of the heating system with different technologies, installation of a ventilation system, auxiliary measures)
- Considering the coupling effect
- Integrating German tax advantages and public subsidies on federal level (KfW, BAFA) into the cost-benefit optimization
- Taking into account the technical standards, minimum requirements, and laws for energy retrofits in Germany
- Distinguishing different financing alternatives (with/without equity of different amounts)
- Allowing program implementation with a short computing time to allow multiple optimization runs for different scenarios

The output of the model provides information on financially optimal retrofit measures and their CO₂ impacts. In a case study, we apply the model to two representative buildings of the largest cohort of German SFHs from the 1960s and 1970s according to the European TABULA building typology [12].

2. Methods and theory

The concept of the optimization model is developed as a mixed-integer problem (MIP/pl. MIPs) in Section 2.1 and specified in a case study with data for two German buildings, German framework conditions, and exemplary retrofit scenarios in Section 2.2. The case study is implemented as a program in GAMS [42], a programming language that has the advantage of describing an optimization problem in a way that is very similar to its mathematical description. For solving MIPs, GAMS uses branch and bound algorithms. Appendix 1 contains detailed information on the database used in the case study. Appendix 3 contains our annotated code with all constraints in detail.

2.1. The optimization model

2.1.1. Target function and model structure

The target function TF describes the financial perspective of a self-using SFH owner. In the considered time period tp [a], owners want to maximize the savings of energy costs after the retrofit (compared to before) sav [€], the financial benefits or tax advantages for the retrofit $benef$ [€] minus the investments for the retrofit measures inv [€] and the costs for a potentially necessary credit $cred$ [€]. All components of the target function depend on the vector variable mes [–], representing a bundle of selected retrofit measures. The amount of financial benefits depends on the vector variable $prog$ [–] representing a bundle of selected funding programs/tax benefits. The target function describes the return on investment (ROI/pl. ROIs) for an energy retrofit. The ROI is a main economic decision criterion that is suitable for planning energy retrofits [43].

The target function is formulated as:

$$\max TF(mes) = \sum_{ip} sav(mes) + benef(mes, prog) - \left(inv(mes) + \sum_{ip} cred(mes, prog) \right) [\text{€}] \quad (1)$$

To model the selected bundle of retrofit measures mes , the model uses an n -dimensional vector of binary variables of n individual retrofit measure (e.g. insulation of the walls, replacement of the heating with a heat pump). These equal 1 if a measure according to the optimization function is optimal and 0 if not. Similarly, the vector $prog$ corresponds to an m -dimensional binary vector for retrofit funding programs, indicating whether a funding program is optimal for a maximized ROI. The

constraints of this optimization model are calculations for the investment costs, financial benefits, and performance values (e.g. boiler efficiencies, heat distribution losses, wall insulation quality) depending on every possible combination of the n retrofit measures. With this information, it is possible to calculate the expected annual energy demand, costs, and CO₂ emissions prior to and after energy retrofits according to technical standards, described in Section 2.1.2 and Appendix 1. Furthermore, the model allows the inclusion of information on building parts that must be retrofitted/replaced anyway due to defects (coupling effect), which is often the initial motivation for building owners to plan comprehensive retrofits [40,41].

The outputs of the model are the maximized variables of the target function which are the optimal ROI TF , a bundle of optimal retrofit measures mes , financial savings sav , suggestions for the optimal funding programs/tax benefits $prog$ and the amount of financial benefits $benef$, as well as investment and credit costs inv and $cred$. Additionally the output provides information on energy/CO₂ performance values of the building after retrofit and the comparison to the building performance before retrofit. An overview of the model components is illustrated in Fig. 1.

2.1.2. Technical model to calculate the heating needs of an SFH

The basic structure to calculate the energy needs of a building within the model is based on the TABULA calculation method for energy use from heating and domestic hot water [45]. It applies the seasonal method according to the standard EN ISO 13790 [46] of the German institute for standardization (DIN). This standard specifies calculation methods for determining the annual energy requirement for space heating and cooling of a residential building, assuming a constant indoor temperature. The methods include the calculation of the heat transfer through the building envelope by transmission and ventilation. The heat balance of the building also includes the contribution of internal and solar heat. To achieve a fast computation time for the optimization model, we developed an MIP without non-linear equations by modifying the TABULA approach. The calculation equations (Eq. (2) – Eq. (13)) and their modifications are listed in Table 1. The modifications particularly affect the calculations of the energy needs for heating and hot water, the non-renewable energy needs for the heating system, and the needs for delivered energy for heating and ventilation (in Eq. (6), Eq. (8) and Eq. (10)). For these modifications, we used simplified, linear factors and standard values of DIN 4108-6 [47] for annual period accounting, with a heating period of 185 days for an averaged climate² as well as standard values of DIN 4701-10 [48]. Moreover, to linearize all equations we used fixed efficiency parameters, loss parameters, and specific energy needs.³ Fig. 2 schematically illustrates the implemented calculation of the thermal energy balance of a building and the subsequent primary energy needs of the building's heating system in the optimization problem. The model focuses on retrofit measures on the building envelope and fixed installed technical equipment; the exchange of appliances like more efficient appliances (e.g. efficient dishwashers, shower heads, fridges) are not considered. The calculation procedure and references are explained in detail in Appendix 1 in the context of to the case study described in Section 2.2.

2.2. Case study for German buildings from the 1960s and 1970s

2.2.1. Considered buildings

Two German SFHs are examined that are representative of SFHs construction for the decades 1958–1968 and 1969–1978. Both buildings are modeled with their average energy quality in 2017. In terms of

² For our program, we used climate values for Germany according to our case study.

³ For our program, we used values that rely on estimators on technical standards deduced from market investigation of currently available building components in Germany according to our case study.

Target function

Maximizing the savings of energy costs and financial benefits (subsidies) minus the initial investments and credit costs of a retrofit within a certain planning time period

Model parameters

<u>Input mask for model/ optimization parameters adaptable by the user</u>	<u>Calculation parameters</u>	<u>Characteristics of the considered SFHs</u>
<p>Includes:</p> <ul style="list-style-type: none"> - Selecting a single family house - Selecting building components with retrofit necessities - Building specific conditions (available building infrastructure) - Owner specific conditions (considered planning time period, equity, annual taxes) 	<p>Includes:</p> <ul style="list-style-type: none"> - Energy prices for energy sources - CO₂-factors for energy sources - Primary energy factors for energy sources - Interest rate for private credits - Market dynamics (annual price changes for energy sources, annual change of CO₂-factors of energy sources) - Technical standard parameters (energy efficiency of modern heat boilers, energy performing factors of modern heat pumps, shares of energy need covered by solar systems, distribution losses of heating pipes, heat recovery efficiency factors of ventilation, auxiliary electricity energy needs of the heating and ventilation systems) 	<p>Includes:</p> <ul style="list-style-type: none"> - Areas of building envelope components (roof, walls, floors, windows, door) - Quality parameters of building envelope components (U-values, g-values, assumption on the air tightness of the building envelope) - Quality parameters for the technical building system (energy source of the heating system, efficiency of the heating system, quality of the heating pipes, existstance of a solar system, existstance of a modern ventilation system with heat recovery, area-specific el. auxiliary energy need) - Other building characteristics (room height, shape of the roof)

Constraints (calculations for every possible combination of retrofit measure)

<u>Investment for retrofit</u>	<u>Building performance after retrofit</u>	<u>Financial benefits</u>
<p>Takes into account:</p> <ul style="list-style-type: none"> - Calculation of investments for the retrofit of building components depending on the retrofit quality (e.g. U-value of a wall insulation) - Considering full costs and additional energy-quality-related investment costs for every building component - Calculation of the sum of additional costs and the sum of full costs for the whole retrofit 	<p>Takes into account:</p> <ul style="list-style-type: none"> - Annual need for delivered energy - Annual primary energy need - Annual CO₂-emissions - Annual energy costs - Comparison of performance before retrofit with performance after retrofit 	<p>Takes into account:</p> <ul style="list-style-type: none"> - Credit benefits and investent benefits - Minimum standards for receiving funding (e.g. technical minimum requirements for retrofitted components) - Requirements for the combination of programs

Output variables

<ul style="list-style-type: none"> - Maximized target function with financial savings/ additional expenditure for the considered time period after retrofit - Suggestions for optimal retrofit measures - Suggestions for optimal financial benefit programs/ tax advantages - Performance characteristics of the optimally retrofitted building (annual energy costs, annual CO₂-emissions, annual energy needs) - Comparison values to indicate performance differences before and after the optimal retrofit - Amount of optimal retrofit invests (full costs and additional costs for every retrofitted building component)
--

Fig. 1. Model components of the optimization model including model input parameters, calculation modules, and model outputs. Details for the implementation of this model for German buildings are introduced in the case study in Section 2.2. (Explanations [44]: U-value [W/(m²K)]: coefficient for thermal transmittance through building components mainly between indoor and outdoor/g-value [-]: coefficient commonly used in Europe to measure the solar energy transmittance of windows. A g-value of 1 describes full transmittance, while a value of 0 describes zero transmittance).

quantity and energy needs, both SFHs are representative of the important German building category of SFHs from the 1960s and 1970s with respect to the CO₂ reduction potential (Section 1). The underlying data for the buildings' modelings are based on the TABULA building typology, which provides a comprehensive and validated database [49]. A brief description of the buildings is shown in Table 2. Their detailed technical building data is listed in Appendix 1 (Table A1.1). For our optimization program, we further assume that the considered buildings

can be connected to a district heating system, that gas heating infrastructure is locally available, that the property's soil allows deep drilling and is large enough to install ground collectors and ground probes for heat pumps, and that there is enough space for the installation of a solar system on the building's property.

2.2.2. Financial benefits and tax advantages for energy-related retrofits

In the case study, we include financial benefits from the KfW bank

Table 1

New simplified calculation method for the building performance for energy, CO₂ emissions, and energy costs [45–48].

Parameter	Equation	Notation
Heat transfer coefficient by transmission H_{tr} (Eq. (2)) (TABULA, 2013)	$H_{tr} = \sum_{\text{envelope part } i} b_i * U_i * A_i + thf * A_{env} \left[\frac{W}{K} \right]$	b : Standard soil adjustment factor [–] U : U-value [W/m ² K] A : Size of an area [m ²] thf : Standard thermal bridging surcharge factor [W/m ² K] A_{env} : Area of the building envelope [m ²]
Heat transfer coefficient by ventilation H_{ve} (Eq. (3)) (TABULA, 2013)	$H_{ve} = c_{p,air} * (n_{air,acc} + n_{air,inf}) * A_{ref} * h_{room} \left[\frac{W}{K} \right]$	$c_{p,air}$: Volume-specific heat capacity of air [Wh/m ³ K] $n_{air,acc}$: Air change rate by use [1/h] $n_{air,inf}$: Air change rate by infiltration [1/h], A_{ref} : Reference area of the building [m ²] h_{room} : Height of the buildings' rooms [m]
Solar heat load during heating season Q_{sol} (Eq. (4)) (TABULA, 2013)	$Q_{sol} = g_{window} * F_{sh} * (1 - F_F) * F_W * \sum_{\text{cardinal direction } i} A_{window,i} * I_{sol,i} \left[\frac{kWh}{a} \right]$	g_{window} : g-value of the windows [–] F_{sh} : External shading [–] F_F : Frame area fraction [–] F_W : Non-perpendicular [–] $A_{window,i}$: Area size of windows [m ²] $I_{sol,i}$: Solar global radiation [kWh/m ² a]
Internal heat gain Q_{int} (Eq. (5)) (TABULA, 2013)	$Q_{int} = f_{ii} * d_{hs} * \varphi_{int} * A_{ref} \left[\frac{kWh}{a} \right]$	f_{ii} : Conversion factor for converting days into hours [kh/d] d_{hs} : Length of the heating season [d/a] φ_{int} : Average thermal output of internal heat sources [W/m ²] A_{ref} : Reference area of the building [m ²]
Energy need for heating Q_H (Eq. (6)) (DIN 4108-6 modified)	$Q_H = c_{dd} * (H_{tr} + \eta_{ve} H_{ve}) - c_{he} * (Q_{sol} + Q_{int}) \left[\frac{kWh}{a} \right]$	c_{dd} : Factor considering the temperature difference between inside and outside [kKh/a] c_{he} : Utilization rate of heat gains [–] η_{ve} : Efficiency factor of the ventilation system [–]
Energy need for hot water Q_W (Eq. (7)) (DIN V 4701-10)	$Q_W = q_W * A_{ref} \left[\frac{kWh}{a} \right]$	q_W : Energy need for hot water [kWh/m ² a] A_{ref} : Reference area of the building [m ²]
Non-renewable energy need for the heating system Q_E (Eq. (8)) (DIN V 4701-10 modified)	$Q_E = \frac{\left(\frac{\eta_{sol} * Q_H + \eta_{sw} * Q_W}{\eta_p} \right)}{\eta_h} \left[\frac{kWh}{a} \right]$	η_{sol} : Factor for a possible reduction of the heating energy need by the use of a solar thermal system [–] η_{sw} : Factor for a possible reduction of the energy need

Table 1 (continued)

Parameter	Equation	Notation
Auxiliary electrical energy need for the heating and ventilation system Q_{aux} (Eq. (9)) (TABULA, 2013)	$Q_{aux} = aux_{el} * A_{ref} \left[\frac{kWh}{a} \right]$	hot water by the use of a solar thermal system [–] η_h : Efficiency rate of the heating generation system [–] (For heat pump: Annual performance factor, for boilers and district heat: Annual efficiency rate) η_p : Factor for the thermal quality of the heating pipes in the building [–] aux_{el} : Factor for the auxiliary energy need of the heating system and the ventilation system [kWh/m ² a]
Need for delivered energy for heating and ventilation Q_{del} (Eq. (10)) (TABULA, 2013 modified)	$Q_{del} = Q_E + Q_{aux} \left[\frac{kWh}{a} \right]$	
Total primary energy need for the heating system PE (Eq. (11)) (TABULA, 2013)	$PE = Q_E * f_{PE} + Q_{aux} * f_{PE,el} \left[\frac{kWh}{a} \right]$	f_{PE} : Primary energy factor of the used energy source [–]
Total CO ₂ emissions of the heating system CO_2 (Eq. (12)) (TABULA, 2013)	$CO_2 = Q_E * f_{CO_2} + Q_{aux} * f_{CO_2,el} \left[\frac{g}{a} \right]$	f_{CO_2} : CO ₂ factor of the used energy source [g/kWh]
Total energy costs of the heating system C (Eq. (13)) (TABULA, 2013)	$C = Q_E * p + Q_{aux} * p_{el} \left[\frac{€}{a} \right]$	p : Energy price of the used energy source [€/kWh]

and the BAFA as well as tax benefits (status: 03/2020). An overview of the funding programs, their allowed combinations, and minimum standards are summarized in Table 3. In general, combining two funding instruments for a single measure is not possible, while a combination of grants and credits is allowed. Some funding instruments are only applicable in combination with other instruments. We only consider support programs for retrofit measures and funding conditions relevant to the focus of this study. We do not consider retrofit measures that do not affect a building's thermal energy needs such as retrofitting of electric or water distribution systems. For more details, we refer to the explanations of the funding programs and their funding guidelines [19, 24, 26].



2.2.3. Retrofit measures and standards

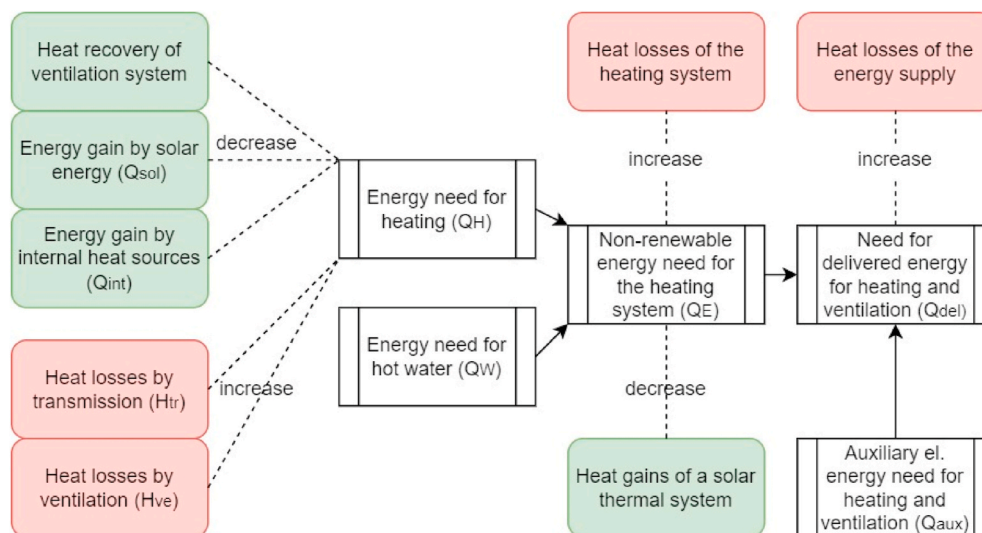
The retrofit measures included in the case study that can be freely combined with each other are:

- Façade:
 - o New windows (2 panes/3 panes),
 - o new door,
 - o insulation of the walls (U-value between 0.1 and 0.24 W/m²K),
 - o insulation of the roof (U-value between 0.1 and 0.3 W/m²K),

Table 2

Basic characteristics of the considered German SFHs of the construction decades 1958–1968 and 1969–1978 [49].

Characteristics	SFH_E	SFH_F
		
Number of existing buildings in Germany	1.509 million	1.507 million
Year of construction	1958–1968	1969–1978
Reference floor area	121.2 m ²	173.2 m ²
Area of the building envelope	463.8 m ²	549.2 m ²

**Fig. 2.** Overview of the energy losses and energy gains of a building (own illustration).

- o insulation of the floor (U -value between 0.1 and 0.3 W/m²K)
- Heating system:
 - o Replacement of the heating system with a heat pump (with a ground probe/with a ground collector/for outside air) both for heating and hot water,
 - o with a fossil fuel-based district heating system,
 - o with a boiler (gas condensing boiler/oil condensing boiler/pellet boiler),
 - o with an optional solar system (for hot water only or for the full heating system) suitable for the building
- Others:
 - o Renewal of heating pipes,
 - o installation of a central ventilation system with heat recovery

In Germany, the technical requirements for thermal energy retrofits are regulated in the German Building Energy Act (Gebäudeenergiegesetz (GEG)) [50], which relies on the previous Energy Saving Ordinance (Energieeinsparverordnung (EnEV)) [51]. It defines retrofit obligations of energy-related components of buildings as well as their minimum energy standards. In our program, the quality parameters for retrofitted building components are estimated average values according to standards of currently available building components in Germany. All energy values used comply with the GEG 2020. The detailed measures, standards, and minimum requirements of our program are listed in the database in [Appendix 1 \(Table A1.2\)](#). For further information on the qualitative scope of the retrofit measures that are not important for the thermal modeling (e.g. average sizes and standard construction material

of retrofit measures) we refer to the studies by Hinz [40,41], which are introduced in the following section.

2.2.4. Retrofit costs

The cost functions for the energy retrofit of building components for the case study relate to the component surfaces and the building reference area, and are based on Hinz (2015) [41]. The database relies on a very comprehensive and high-quality study about German energy retrofits evaluating retrofit projects of 1200 residential buildings, of which approx. 780 are single and two-family houses. The costs for heat pumps also rely on Hinz (2012) [40]. We adjusted these values to the first quarter of 2020 by using the same construction price index for the maintenance of residential buildings including the value added tax of Destatis [52], as in Hinz et al. (2012) [40], and multiply all costs by a factor of 1.182. More recent retrofit cost data was not available for all considered retrofit measures. In our model, we differentiate between full retrofit costs and additional retrofit costs. This difference takes into account the coupling principle. The full retrofit costs describe the whole energy-related and energy-unrelated investments. The additional costs only quantify the additional costs for a higher energy quality than the current minimum standard. All modeled cost functions are listed in [Appendix 1 \(Table A1.2\)](#).

2.2.5. Scenario definition

We define 48 different scenarios ($4 \times 3 \times 4$ alternatives) for each building: First, we consider four planning periods of 5, 10, 15, and 20 years that lie within the range of usual economic planning. Second, we

Table 3

Overview of German subsidy instruments for the thermal energy-efficient retrofit of owner-occupied SFHs [19,24,26] (Explanations: KfW standard [19]: KfW standards were defined by the KfW bank and indicate the thermal quality of a building according to its annual primary energy requirement and transmission heat loss. CO₂ emissions are not relevant. The lower the standard, the lower the primary energy requirement of a building).

Name	Object of the program	Allowed combinations with other programs	Maximum credit per building and interest rate	Direct financial benefit per building	Financially supported measures and funding conditions
KfW 151/152	-Retrofit with high efficiency KfW standard -Single energy efficiency measures	Possible with: KfW 167, KfW 431	-Up to 120,000 €/SFH for efficiency standard of at least KfW 115 for max. 30 years -max. 50,000 €/SFH for single measures for max. 30 years 0.75% per year (fix for 10 years)	-KfW 55: 40% of retrofit costs, max. 48,000 €/SFH -KfW 70: 35% of retrofit costs, max. 42,000 €/SFH -KfW 85: 30% of retrofit costs, max. 36,000 €/SFH -KfW 100: 27.5% of retrofit costs, max. 33,000 €/SFH -KfW 115: 25% of retrofit costs, max. 30,000 €/SFH -Single measures: 20% of retrofit costs, max. 10,000 €/SFH	-Insulation of walls: Max. allowed U-value [W/m ² K]: 0.2 -Insulation of roofs: Max. allowed U-value [W/m ² K]: 0.14 -Insulation of floor ceilings: Max. allowed U-value [W/m ² K]: 0.25 -Renewal of windows: Max. allowed U-value [W/m ² K]: 0.95 -Renewal of doors: Max. allowed U-value [W/m ² K]: 1.3 -Installation/renewal of energy-efficient ventilation systems -Renewal of heating systems: Connection to district heating network and heat exchanger, pellet boilers, gas condensing boiler, heat pumps, solar systems (a single measure financial support for a heating system with only renewable energies is not possible. For this it needs the BAFA program as described below.) -Insulation of heating pipes Same as BAFA program for heating with renew. energies
KfW 167	-Heating systems with renewable energies	Possible with: KfW 151/152, KfW 430, KfW 431, BAFA program for heating with renew. Energies	-Up to 50,000 €/SFH for max. 10 years 1% per year	–	Same as BAFA program for heating with renew. energies
KfW 430	See KfW programs 151/152	See KfW program 151/152	–	See KfW program 151/152	Same as KfW 151/152
BAFA heating with renew. energies	-Heating systems with renew. Energies	- Possible with: KfW 167, KfW 431	–	-Solar systems (without retrofit of the heating system): 30% of retrofit costs -Hybrid heating system (combination of solar and pellet), pellet boilers and heat pumps: 35% of retrofit costs/SFH (45% if existing system works with oil) -max. 50,000 €/SFH	-Pellet boiler: Minimum efficiency factor: 89% -Heat pumps: Minimum annual performing factor for air [-]: 3.5, Minimum annual performing factor for ground heat [-]: 3.8 -Insulation of heating pipes in combination with the retrofit of the heating system with Solar systems, heat pumps and pellet boilers Same as all measures and conditions of KfW 151/152 + BAFA program for heating with renew. Energies + KfW 431
Tax benefits 2020	-All kinds of energy efficiency measures -Alternative to all the programs of KfW and BAFA described in this table	–	–	-20% of retrofit costs, max. 40,000 €/SFH tax deductible within 3 years The collective income tax, reduced by the other tax reductions: 1. Year: Tax reduced by 7% of the retrofit costs, max. 14,000 €/SFH, 2. Year: Tax reduced by 6% of the retrofit costs, max. 12,000 €/SFH, 3. Year: Tax reduced by 6% of the retrofit costs, max. 12,000 €/SFH	Same as all measures and conditions of KfW 151/152 + BAFA program for heating with renew. Energies + KfW 431

consider building owners with no (0€), medium (25.000€), and high equity (100.000€) available for the retrofit investment; if higher investments are optimal the model calculates respective credits by a private bank or funding programs as described in Section 2.2.6. Third, we consider four different packages (P1–P4) of necessary retrofit measures to take into account the coupling effect. These necessary retrofits cover defect/old building components that have to be retrofitted anyway. In addition to the necessary retrofit measures, which are specified in the individual retrofit packages, any other additional retrofit measures described in Section 2.2.3 can be selected within the framework of the optimization. The packages cover common retrofit necessities for SFHs. They also cover different parts of the building and different extents of retrofit efforts.

These are:

- (P1) No retrofit necessary,

- (P2) Retrofit of the building envelope necessary (including the insulation of walls and roof, and the exchange of windows and the door),
- (P3) Retrofit of the heating system necessary (including the exchange of the heat generator and the insulation of heating pipes), and
- (P4) Full retrofit necessary (including the envelope as described in (P2), the insulation of floors, the replacement of the heating system as described in (P3), and the installation of a new ventilation system).

2.2.6. Further data and assumptions

The data used on prices for energy sources and price changes for the considered planning periods, primary energy factors, CO₂ factors, and factor changes for the considered planning period are summarized in Table 4 and in more detail in Appendix 1 (Table A1.3). For credits that do not belong to the funding instruments but are offered by a private bank we calculate with an interest rate of 1.2%, which corresponds to the effective annual construction interest rate of the common credit

Table 4

Boundary conditions for the case study (primary energy factors and CO₂ factors [56,57]; CO₂ factor growth rates [58]; prices [59,60]; price growth rates [61]).

Energy source	Oil	Gas	District heat	Pellets	Electric energy
Primary energy factors [–]	1.1	1.1	1.3	0.2	1.8
CO ₂ factors [–]	310	240	280	40	550
Rates of annual CO ₂ factor growth [–]	1	1	1	1	0.966
Prices [€/kWh]	0.0413	0.0661	0.0907	0.0477	0.3071
Rates of annual price growth [–]	1.05	1.011	1.005	1	0.997

institutions in Germany (e.g. local credit institutes such as Sparkasse and Volksbank [e.g. [53–55]]). The costs for a credit follow the nominal credit costs and we assume that the credit is paid back within the considered time period. For state credits from KfW funding programs that expire after 10 years, we assume constant interest rates for the planning periods of 15 and 20 years. We do not consider opportunity profits if the equity is used for investments other than a retrofit. We assume that the annual tax obligations of a retrofitter are higher than the possible tax benefits of a retrofit.

3. Results

Both case study buildings show very similar results and patterns across the evaluated retrofit scenarios. There are minor differences regarding optimal retrofit measures, optimal financial benefit programs, and quantitative results. Detailed optimization results are listed in Appendix A2.

3.1. Optimization results for SFH_E and SFH_F

3.1.1. Selected retrofit measures

For both building types, the installation of a pellet heating system with a solar system for hot water was selected as optimal in all optimization scenarios except for package P1 (no retrofit necessity) over a planning period of 5 years. For packages P1 and P3, no additional measures for the building envelope are recommended. For retrofit packages P2 and P4, with comprehensive retrofit necessities of the building envelope, insulation of the roof, walls, and floor for both buildings with the highest U-value of 0.1 W/m²K is optimal. For all

scenarios where windows are renewed, 2-pane windows are optimal. Only for a planning time of 20 years, the use of 3-pane windows is preferred to 2-pane windows for both building types.

3.1.2. Selected benefit programs

For all considered optimization scenarios, the use of tax benefit programs and private credits plays no role. Instead, the program 430 and the programs 151/152 respectively are optimal for all optimization scenarios with comprehensive retrofits of the building envelope (packages P2 and P4). For packages P1 and P3, where only a renewal of the heating system is recommended, the program of BAFA (combined with the KfW 167 program in the scenarios with required credits) is optimal.

3.1.3. Target function/return on investment

Overall, almost all optimal calculated energy retrofits lead to large savings, offsetting the retrofit investments within 20 years. Even extensive retrofits can be attractive from an economical point of view (Fig. 3). For SFH_E with full equity financing and optimal measures, all retrofit packages lead to a positive ROI within 20 years. Only for SFH_F, no positive target function can be found with a full retrofit (P4) within 20 years.

The financial cost-benefit ratio for measures on the heating system is comparably better than for measures on the building envelope. While retrofits without retrofit necessity (P1) or with a necessary retrofit of the heating system have a positive ROI after 10 years already, the retrofit packages with extensive retrofits of the building envelope (P2, P4) have a positive ROI only after a longer period of time. For all scenarios, it is clear that credit costs are negligible compared to the total costs; they are less than 3% of the investments in all scenarios, even for planning times of 20 years. We can see that with current interest rates, the available retrofit equity has a small impact on the total ROI value. To better illustrate the results in the following result sections, we work with average values (average ROI with differing funding periods between 5 and 20 years) for the retrofit scenarios with different amounts of equity (Fig. 4, Fig. 5, Fig. 6).

3.1.4. Investment and financial benefits

The optimal investments for the retrofits of the two buildings reach about 104,000 € for the SFH_E and up to about 110,000 € for the SFH_F in the scenarios with necessity for full retrofit (Fig. 4). As expected, in the scenarios with no or just a few retrofit necessities (P1, P3) investments are lower. The financial benefits of KfW, BAFA and tax

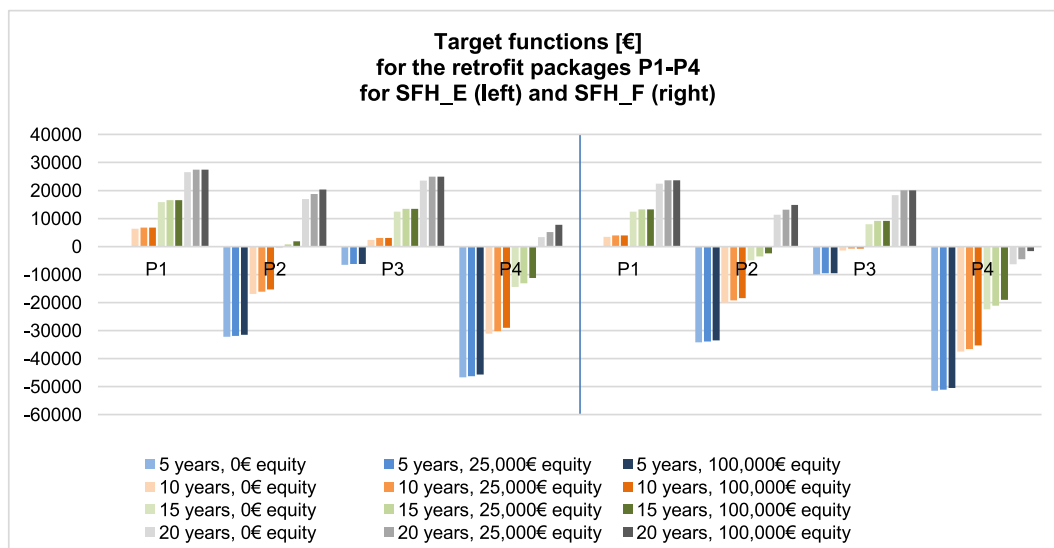


Fig. 3. Target function value (return on investment) of the optimization scenarios for different retrofit packages (P1–P4) and different equities, aggregated with respect to financing periods (between 5 and 20 years).

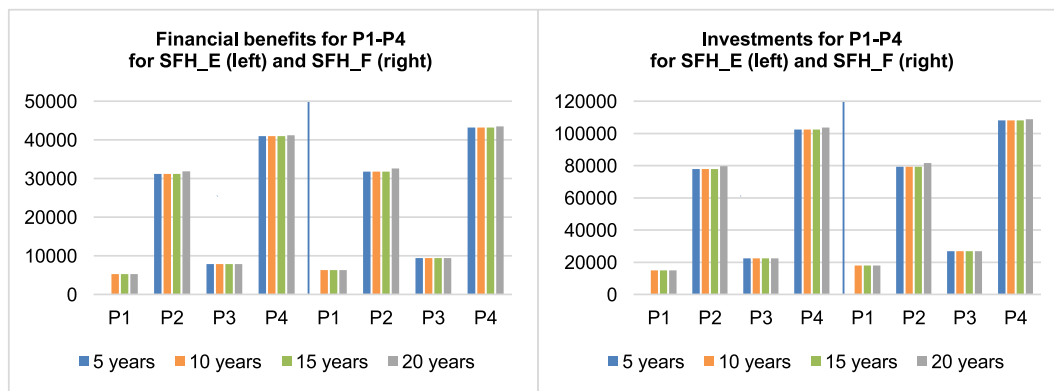


Fig. 4. Investments and financial benefits (of KfW, BAFA, and tax benefits) for optimal retrofits (average values for scenarios with different amounts of equity between 0 €, 25,000 €, and 100,000 €).

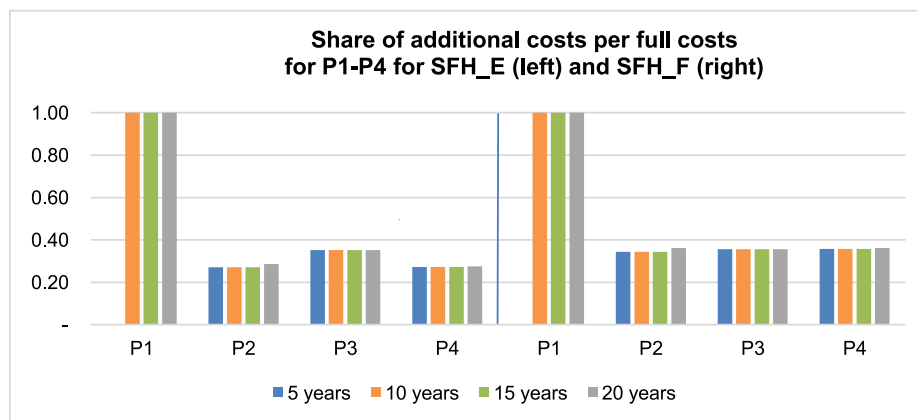


Fig. 5. Shares of additional energy-related costs per full costs of conventional retrofits for economically optimal retrofits (average for scenarios with different amounts of equity between 0 €, 25,000 €, and 100,000 €).

benefits reach up to about 41,500 € for SFH_E and up to about 44,000 € for SFH_F for the full retrofit scenarios (P4) (Fig. 4). All optimal retrofit measures and funding programs recommended by the program are broken down for all scenarios in Appendix A2.1.

Fig. 5 shows that the energy-related additional costs for a higher/optimal energy standard after retrofit are only a small share (27–36%) of the full costs when conventional retrofits are necessary anyway (P2–P4).

3.1.5. Performance indicators

The performance indicators in the optimization are the annual savings in energy (delivered and primary energy), annual CO₂ emissions, annual energy costs (heating) and the KfW standard. The performance values of the buildings in the initial state before retrofits calculated by the program are shown in Table 5.

The performance after an optimal retrofit according to the model is shown in Fig. 6 as the proportion of the original energy demand.

For all scenarios with recommended measures, considerable CO₂ savings can be achieved, with the optimal solution having only 7–18% of the original annual emissions. Large savings in delivered energy can only be achieved if the building envelope is retrofitted (P2, P4). Here, the savings of delivered energy are up to 90%. In the scenarios with heating system retrofits only, the possible delivered energy savings are comparably small. The savings of primary energy need are up to 95%. Correspondingly, the reduction in energy costs is significant for all scenarios where retrofit measures are recommended. The reduction in operational costs is greatest when measures lead to a reduction of the energy need (in the scenarios with a retrofitted envelope). For all scenarios with recommended measures, the new operational costs are

between 15% and 62% of the initial value.

3.2. Result analysis

The case study shows that most economic retrofits of SFHs from the 1960s and 1970 can lead to considerable CO₂ savings, even within a short period of 5–10 years. A reduction in annual CO₂ emissions down to 7–18% of the of pre-retrofit emissions was found for all scenarios for a 10-year planning period, and for a 5-year planning period with retrofit necessities. Within 20 years, all energy retrofits of the two SFH representatives are amortized or almost amortized through energy savings, even in a scenario with a full retrofit necessity. Under the given framework conditions, retrofit measures that exceed the regulated minimum energy standard of building components prove to be optimal in almost all scenarios (see bold retrofit measures listed in Table A2.1). In the scenarios with retrofit necessities, the financial funding compensates for the additional energy costs of the retrofit measures in almost all cases. This is not the case for scenarios without retrofit necessity (P1) where the energy-related additional costs are equivalent to the full costs.

The conditions of German funding programs are not designed to maximize the CO₂ savings of an energy retrofit. There are considerable differences in the funding efficiencies for saved emissions per euro of financial benefit for the individual scenarios (Fig. 7). The funding invested to reduce an annual ton of CO₂ ranges from 493 € (in P1) to 3747 € (in P4). While the replacement of the heating system in our study leads to high CO₂ savings, additional measures on the building envelope (P2, P4) only lead to relatively small reductions, but are highly

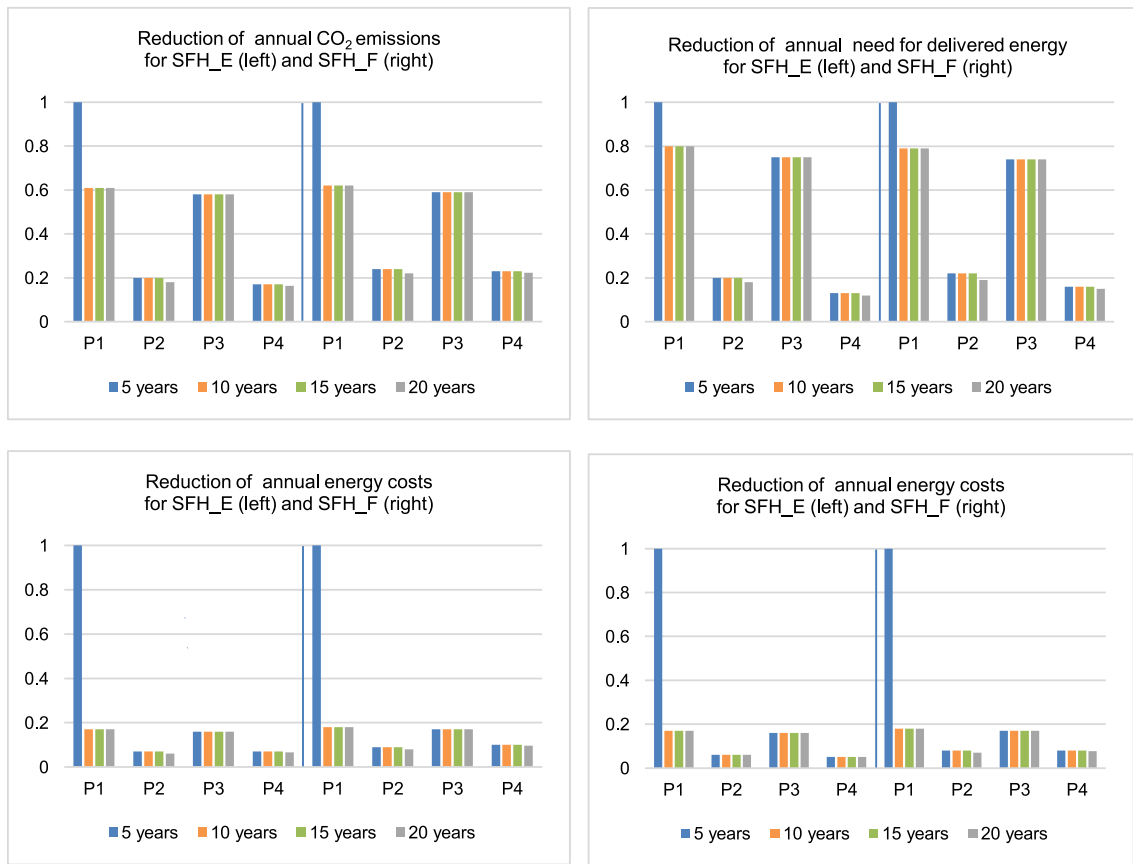


Fig. 6. Annual reductions of CO₂ emissions, delivered energy need, primary energy need, and energy costs for the reference year 2020 (average for scenarios with different amounts of equity between 0€, 25,000 €, and 100,000€).

Table 5
Characteristic values for SFH_E and SFH_F for the initial state without retrofit measures.

	SFH_E	SFH_F
Annual delivered energy need [kWh]	52,385	49,768
Annual primary energy need [kWh]	58,175	55,533
Annual energy costs [€]	3653	3561
Annual CO ₂ emissions [kg]	12,817	12,293
KfW standard	613	515

subsidized.

3.3. Model validation and program computing time

To validate the technical model, with its simplified assumptions for the calculation of the energy needs of the considered buildings, we compared it with calculations and empirical values from TABULA [49]. For both considered SFHs, TABULA provides data for three different energy performance levels (V1, V2, V3) achieved by different retrofit alternatives, which we tested with our model. A performance comparison (Table 6, Fig. 8) shows that our simplified procedure provides

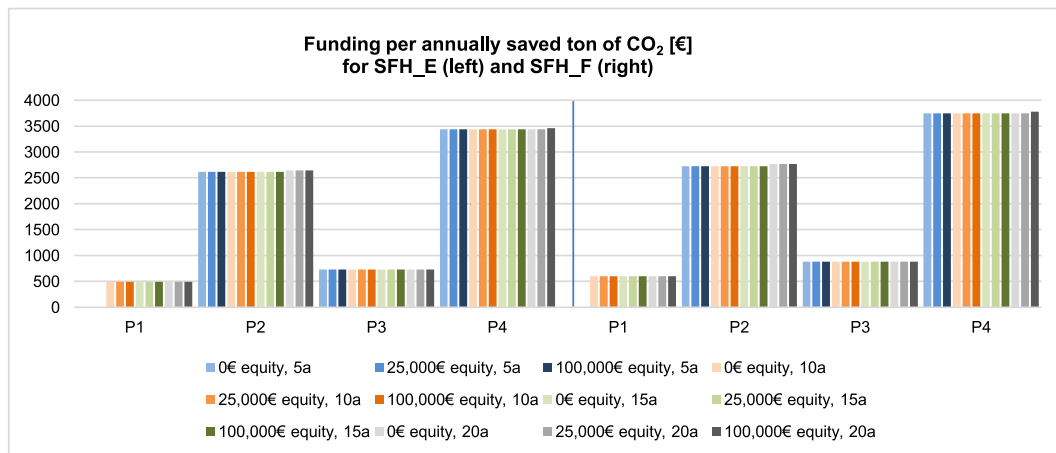


Fig. 7. Amount of funding [€] per annually saved ton of CO₂ emissions (average for scenarios with different amounts of equity (0 €, 25,000 € and 100,000 €) and investment periods (5, 10, 15 and 20a).

structurally comparable values like those given by the TABULA Web tool [49], whose calculation approach is based on German DIN standard calculations, for the two considered SFHs. However, the theoretical calculations deviate from empirically averaged recorded values for these three energy performance levels. User behavior plays a major role, particularly in the case of low energy performance buildings, where users tend toward energy-saving behavior, for example by reducing average room temperature or by not heating unused building areas [45]. This is indicated by “the broad spread of consumption values which can be observed in thermally similar buildings and which is the result of different thermal comfort levels” [45].

For the three given energy performance levels and two building types, the most significant differences for the calculated and empirical energy needs occur for energetically poorly performing buildings (V1) (Table 6). The average inaccuracy between TABULA calculations and empirical values is 24%. With 27%, our new linearized method is only about 3% worse than the TABULA calculation method. However, our program has the advantage of a low complexity and a very fast computing time (0.5–3.5 s in all 96 case study scenarios) compared to non-linear problems (hours to days).

3.4. Sensitivity analysis

There are several parameters in the model implemented in our case study program that could be considered for a sensitivity analysis which are neither covered by scenarios of our case study nor are fixed building parameters. These are: energy prices, energy factors and CO2 factors, changes in prices and factors within the planning time, and technical parameters. As the energy prices are part of the target function and highly relevant to calculate the return on investment, we selected them for our sensitivity analysis. We increased and decreased the energy prices by 10% (90 and 110% of the standard price level) in all scenarios.

Our analysis found that with these price changes, the program results remain structurally the same (Fig. 9). Only individual optimal retrofit measures are slightly different within a scenario (e.g. recommendation of 3-pane windows instead of 2-pane windows). For scenarios with a longer time period, changes of the target function are higher. This is to be expected, as higher/lower savings over a longer time due to changed energy prices compound over time. The target functions are on average significantly below/above 10% if the prices are adjusted by the same percentage, showing a relatively high sensitivity of the model to energy prices. With an increase in energy prices by 10%, the average target

function is 26% above the average target function value at normal energy prices. With a decrease in prices by –10%, it is at 26% below average. However, we want to point out that with values around zero, even small absolute changes lead to large percentage deviations.

The detailed results of the sensitivity analysis for all scenarios are shown in Appendix 2.

4. Discussion

The developed model complements existing models by introducing a simple approach to approximate the energy demand of residential buildings with a fast computing time. It is able to model energy retrofits for German buildings within German framework conditions, and provides decision support for the most economic retrofit measures for buildings from the perspective of self-using SFH owners. The case study shows that energy retrofits for the two analyzed German SFHs are financially attractive, having short time spans of 10–20 years for positive return on investments, even in scenarios with comprehensive retrofit necessities of the buildings. Since these two buildings are representative for SFHs for the 1960s and 1970s, comparable results can be assumed for many other buildings of this age group.

Looking at the energy and CO2 savings of retrofits in our case study, we see that for heating system retrofits, energy savings are comparably small but they lead to higher operational CO2 and cost saving than retrofit measures on the building envelope. Large energy savings of up to 90% can only be achieved by retrofit of the building envelope. Our study shows that the conditions of German funding programs are not designed to maximize CO2 savings per funded euro. The funding invested to reduce an annual ton of CO2 ranges from 493 € to up to 3747 €. When prioritizing CO2 savings for climate protection strategies, it might make sense to adjust the German funding conditions of BAFA, KfW and tax advantages to focus more on CO2 emissions.

When looking at financial criteria for retrofit planning, it becomes clear that the amount of available equity for retrofits investments plays a minor role of less than 3% of the investment sum. Tax incentives do not appear financially attractive for retrofit measures that lead to the achievement of a defined KfW energy quality standard, or for the replacement of the heating system with a renewable energy-based system. In our case studies, the funding programs by the KfW and BAFA offer better funding options as selected by the optimization model. Comparing the results of our case study for the new funding conditions for energy retrofits of SFHs in Germany since 2020, we state a much

Table 6
Need for delivered energy calculated with our simplified approach compared to calculated and measured values according to TABULA [49].

Building	SFH_E			SFH_F				
	Technical standard (U-values [W/m ² K])	New simplified approach	TABULA calculated	TABULA empiric data	Technical standard (U-values [W/m ² K])	Simplified Approach	TABULA calculated	TABULA measured
V1: Annual delivered energy without retrofit	Roof (0.8), Wall 1 (1.2), Wall 2 (0.8), Floor (1.08), Windows (2.8), Door (3) Old gas boiler from 1987 to 1994	432.22 kwh/m ² (179%)	407.3 kwh/m ² (169%)	241.4 kwh/m ² (100%)	Roof (0.5), Wall 1 (1), Floor 1 (0.77), Floor 2 (1), Windows (2.8), Door (3) Old gas boiler from 1987 to 1994	287.35 kwh/m ² (133%)	313.9 kwh/m ² (146%)	215.4 kwh/m ² (100%)
V2: Annual delivered energy with good quality retrofit	Roof (0.41), Wall 1 (0.23), Wall 2 (0.21), Floor (0.31), Windows (1.3), Door (1.3) Gas boiler from 1995	155.53 kwh/m ² (102%)	173.1 kwh/m ² (113%)	152.8 kwh/m ² (100%)	Roof (0.18), Wall 1 (0.22), Floor 1 (0.28), Floor 2 (0.3), Windows (1.3), Door (1.3) Gas boiler from 1995	96.64 kwh/m ² (77%)	132.4 kwh/m ² (105%)	125.5 kwh/m ² (100%)
V3: Annual delivered energy with very high quality retrofit	Roof (0.14), Wall 1 (0.13), Wall 2 (0.12), Floor (0.23), Windows (0.8), Door (0.8) Gas condensing boiler with high efficiency, ventilation system with 80% heat recovery, solar system for hot water covering 60% of heat production	69.23 kwh/m ² (112%)	59.6 kwh/m ² (96%)	62.0 kwh/m ² (100%)	Roof (0.09), Wall 1 (0.13), Floor 1 (0.21), Floor 2 (0.23), Windows (0.8), Door (0.8) Gas condensing boiler with high efficiency, ventilation system with 80% heat recovery, solar system for hot water covering 60% of heat production	55.35 kwh/m ² (112%)	46.8 kwh/m ² (95%)	49.3 kwh/m ² (100%)

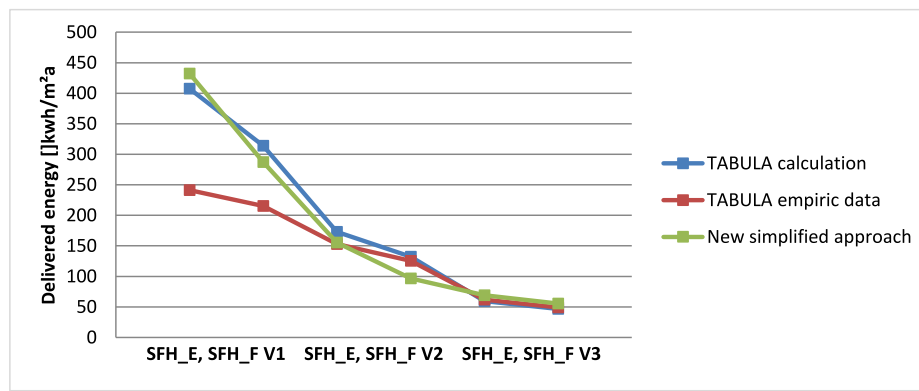


Fig. 8. Comparison of the new simplified approach for the calculated and measured (empiric) delivered energy need according to TABULA [49] for different retrofit qualities V1, V2, and V3 and the two considered SFHs.

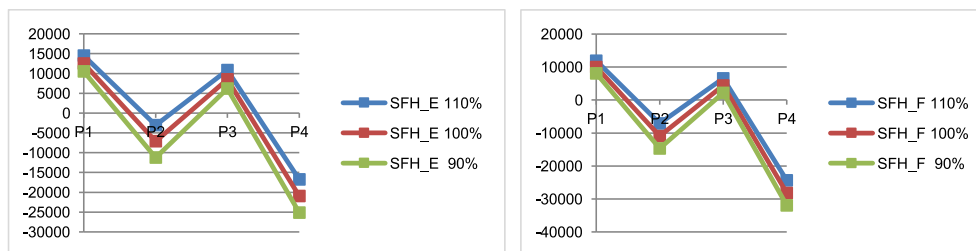


Fig. 9. Optimization results for different energy price levels (110% of prices and 90% of prices) – average target functions for the retrofit scenarios for the four retrofit packages.

better profitability than Runst (2016) [25], who found that retrofit measures are in general not profitable for building owners despite previous KfW and BAFA funding conditions.

We also want to highlight the shortcomings and possible improvements of our developed model. The model only includes retrofit measures on the building envelope or fixed installations/equipment relevant to the thermal energy demand of SFHs. Furthermore, the embodied energy and embodied emissions of the retrofit measures are also excluded. As described in Section 3.3., financial, energy, and CO₂ savings are systematically overestimated, in particular for buildings with low energy quality. This is a problem that affects all calculation approaches that do not take into account data for user behavior. For buildings with a low energy performance level, it appears that calculated energy needs are higher than empirically measured energy needs. To include the impact of user behavior, respective correction factors could potentially improve modeling results. Here, we decided not to include such factors, as German DIN standards and German funding conditions are based on theoretically calculated needs for standardized behaviour. Furthermore, there are also no generalizable correction factors that can be applied linearly and that are scientifically well-founded. TABULA (2017) currently only provides correction factors for exemplary buildings and exemplary retrofit measures [49].

For the cost calculation of retrofit measures as of 2020, we mainly used a database from 2015 from a comprehensive study. Since no current database of comparable quality and information is available, we used an adjustment factor for the cost of retrofit measures from the Federal Statistical Office. This does not take into account potentially differing price increases for different measures. The data could be updated with newer and more precise values.

In our model we do not consider the increased building values (asset) through investments. This leads to a systematic underestimation of the financial benefits of energy retrofits. Also, we neglected stochastic elements e.g. of costs due to possible defects of building technology or increasing maintenance costs for building technology with increasing

age. As these effects are difficult to quantify, we decided to exclude these aspects.

Furthermore, the annual thermal building energy need was calculated via a simplification (linearization). This differs from current standard approaches and from the real energy consumption (Section 3.3). To improve our model, a higher modeling complexity working with energy demands instead of energy needs could be beneficial, e.g. based on detailed BIM⁴-based simulations via EnergyPlus (E+) or Integrated Environmental Solutions Virtual Environment (IES VE) that are closer to measurements. The consideration of non-linear equations, smaller time intervals (monthly/daily/hourly instead of annually) or of sector coupling between electricity and heat generation would be interesting and could also lead to more precise results. However, this would increase the computing time of the model significantly.

Since 2021, there is a new CO₂ emission pricing system in Germany with about 25 €/ton of emitted CO₂ (rising up to 55 €/ton CO₂ in 2025). This leads to increased costs of oil by about 0.8 cents/kWh and of gas by 0.5 cents/kWh and a reduction in electricity costs is planned, but not further specified yet [62,63]. Therefore, its effect is still unclear and cannot be considered currently, but should be taken into account in subsequent studies.

In future, the objective function of the model could be transformed into a multi-criteria problem including thermal or aesthetic comfort for example. A more complex economic objective is also possible, as described in e.g. the European Energy Performance of Buildings Directive [64], which takes into account a life cycle assessment of buildings and building components.

In a further step, the model results could be scaled up to Germany's owner-occupied residential buildings, helping to design German "Energiewende" transition paths for the SFH stock. This could be simulated for example by considering the willingness to pay or invest by

⁴ BIM = Building Information Modeling.

different sinus milieu groups of SFH owners, neighborhood effects, regional differences in economic prosperity, and other influential factors on energy retrofit implementation. With a modified database, SFHs and funding schemes of other countries could also be analyzed with our model.

5. Conclusions

To investigate the incentive effect of the German funding system as of 2020 for energy retrofits of owner-occupied SFHs constructed in the time between 1958 and 1978, we developed an optimization model and performed a case study utilizing it. We included the funding schemes of the Kreditanstalt für Wiederaufbau banking group (KfW) and the Federal Office for Economics and Export Control (Bundesamt für Wirtschaft und Ausfuhrkontrolle (BAFA)) as well as tax benefits. Our case study uses two representative SFHs from the 1960s and 1970s show that retrofits of SFHs in Germany can significantly lower the energy demand of buildings in a financially optimal scenario for owners. Moreover, we analyzed how much CO₂ can be saved with a financially optimal retrofit of these buildings from the perspective of self-using SFH owners. We found that the financial incentive effect of the German funding instruments can lead to financially optimal annual CO₂ emissions of 7–18% of the original annual emissions. Yet, it is clear that the conditions of German funding programs are not designed to maximize CO₂ savings per funded euro. The funding invested to reduce an annual ton of CO₂ ranges from 493 € to up to 3747 € in our study. Since the KfW and BAFA programs are not only aiming at reduced energy demand/consumption, but also a means to achieve the national climate goals, it is necessary to consider an adaptation of the German funding schemes focusing more on CO₂ reduction potentials instead of energy savings.

We showed that the current funding schemes lead to positive return on investments in most of the considered scenarios and investment periods of our study. From the economic perspective, the amount of available equity for retrofits investments plays a minor role. In our case study, we found that the funding programs by the KfW offer better funding options for comprehensive retrofits than tax benefits, as higher subsidies are granted with higher energy standards of the whole building.

Overall, from the theoretical perspective of our model we find that the funding conditions in Germany are already very attractive to motivate SFH owners of buildings from the 1960s and 1970s to save energy and CO₂ with comprehensive retrofits. If we consider the low rate of building retrofits in Germany (around 1%), then we can conclude that this low rate is likely not caused by the lack of attractive funding conditions for this building class.

Finally, we would like to highlight that the investigation of the funding conditions for SFHs constructed before any energy regulation standards in other European countries would be very beneficial towards helping achieve climate their goals. For this, the systematics of our simple model can be adopted and our case study program easily modified. This would also likely be beneficial for other pre-energy regulation building classes within Germany as well.

Funding

No funding was received for this work.

CRediT authorship contribution statement

Zoe Mayer: Writing – review & editing, Visualization, Validation, Methodology, Investigation, Funding acquisition, Writing – original draft, Formal analysis, Conceptualization. **Rebekka Volk:** Supervision, Writing – original draft, Writing – review & editing. **Frank Schultmann:** Writing – review & editing, Supervision.

Declaration of competing interest

The authors declare that they have no known competing financial interests or personal relationships that could have appeared to influence the work reported in this paper.

Funding information/Acknowledgments

The study was performed during a doctoral project that is financed by a scholarship according to Landesgraduiertenförderungsgesetz (LGFG), the State Graduate Funding Act of the Karlsruhe Institute of Technology (KIT).

Appendix A. Supplementary data

Supplementary data to this article can be found online at <https://doi.org/10.1016/j.buildenv.2021.108722>.

References

- [1] Tsemekidi-Tzeiranaki, S. et al. (2019). reportAnalysis of the Annual Reports 2018 under the Energy Efficiency Directive, EUR 29667 EN, Publications Office of the European Union, Luxembourg, 2019, ISBN 978-92-76-00173-7, Doi: 10.2760/22313, JRC115238.
- [2] M. Economidou, et al., Review of 50 years of EU energy efficiency policies for buildings, Energy Build. 110322 (2020), <https://doi.org/10.1016/j.enbuild.2020.110322>.
- [3] Bundesministerium für Wirtschaft und Energie (BMWi), Zweiter Fortschritts-Bericht zur Energiewende - Die Energie der Zukunft - Berichtsjahr 2017, 2019. Berlin. (May be translated as: Second progress report for Energy transition - energy of the future - reporting year 2017) Online 28.11.2021: <https://www.bmwi.de/Redaktion/DE/Publikationen/Energie/fortschrittsbericht-monitoring-energiewende.html>.
- [4] Statistisches Bundesamt (destatis), Gebäude und Wohnungen - Bestand an Wohnungen und Wohngebäuden - Bauabgang von Wohnungen und Wohngebäuden - Lange Reihen ab 1969 – 2020 (May be translated as: Buildings and apartments stock of apartments and residential buildings - construction of apartments and residential buildings - Time line 1969 – 2020). Online 28.11.2021, https://www.destatis.de/DE/Themen/Gesellschaft-Umwelt/Wohnen/Publikationen/Downloads-Wohnen/fortschreibung-wohnungsbestand-pdf-5312301.pdf?__blob=publicationFile, 2020.
- [5] Deutsches Institut für Wirtschaftsforschung (DIW), Wärmemonitor 2018: Steigender Heizenergiebedarf, Sanierungsrate Sollte Höher Sein, 2019. Berlin. (May be translated as: Heat monitor 2018: Increasing heating energy demand, retrofit rate should be higher.) Online 28.07.2021: https://www.diw.de/document/s/publikationen/73/diw_01.c.676231.de/19-36-1.pdf.
- [6] European Commission (EC), Communication from the Commission to the European Parliament. Renovation Wave for Europe - greening our buildings, creating jobs, improving lives, COM/2020/662 final Document 52020DC0662. Online 1.12.2021: <https://eur-lex.europa.eu/legal-content/EN/TXT/?uri=CELEX:52020DC0662>, 2020.
- [7] Kreditanstalt für Wiederaufbau (KfW), Monitoring der KfW-Programme „Energieeffizient Sanieren“ und „Energieeffizient Bauen“ 2017. IWU, Darmstadt, Fraunhofer IFAM, Bremen (May be translated as: Monitoring of the KfW programs “Energy-efficient retrofit” and “Energy-efficient construction” 2016) Online 28.11.2021: <https://www.kfw.de/PDF/Download-Center/Konzerntemen/Research/PDF-Dokumente-alle-Evaluationen/Monitoring-der-KfW-Programme-EBS-2017.pdf>, 2018.
- [8] Bundesinstitut für Bau-, Stadt- und Raumforschung (BBSR), Kurzgutachten zu einem Sanierungsfahrplan im Wohngebäudebestand, IWU, Darmstadt, 2013 (May be translated as: Brief report on a renovation roadmap in existing residential buildings.) Online 28.11.2021: https://www.iwu.de/fileadmin/publikationen/gebäudebestand/prj/Kurzgutachten_Sanierungsfahrplan.pdf.
- [9] K. Gram-Hanssen, Retrofitting owner-occupied housing: remember the people, Build. Res. Inf. 42 (2014) 393–397, <https://doi.org/10.1080/09613218.2014.911572>.
- [10] K. Gram-Hanssen, Existing buildings—users, renovations and energy policy, Renew. Energy 61 (2014) 136–140, <https://doi.org/10.1016/j.renene.2013.05.004>.
- [11] Gram-Hanssen, et al., Local strategies to promote energy retrofitting of single-family houses, Energy Effic. 11 (8) (2018) 1955, <https://doi.org/10.1007/s12053-018-9653-5>.
- [12] T. Loga, et al., Deutsche Wohngebäudetypologie. Beispielhafte Maßnahmen zur Verbesserung der Energieeffizienz von typischen Wohngebäuden, Institut Wohnen und Umwelt, Darmstadt/Germany. (May be translated as: German residential building typology. Exemplary measures to improve the energy efficiency of typical residential buildings), Online 1.12.2021: https://www.episcope.eu/downloads/public/docs/brochure/DE_TABULA_TypologyBrochure_IWU.pdf, 2015.
- [13] Statistisches Bundesamt (Destatis) (2019). Statistisches Jahrbuch 2019 - Wohnen. ISBN: 978-3-8246-1086-0. (May be translated as: Statistics for 2019 - Housing).

- Online 8.12.2021: https://www.destatis.de/DE/Themen/Querschnitt/Jahrbuch/jb-wohnen.pdf?_blob=publicationFile.
- [14] Kreditanstalt für Wiederaufbau (KfW) (2016). Einflussfaktoren auf die Sanierung im deutschen Wohngebäudebestand. IWU, Darmstadt. (May be translated as: Influential factors on the renovation in the German residential building stock.) Online 28.11.2021: https://www.kfw.de/PDF/Download-Center/Konzernthemen/Research/PDF-Dokumente-alle-Evaluationen/Einflussfaktoren-auf-die-Sanierung-im-deutschen-Wohngeb%C3%A4udebestand_2016.pdf.
- [15] H. Cischinski, N. Diefenbach, Datenerhebung Wohngebäudebestand 2016, IWU, Darmstadt, 2018 (May be translated as: Data collection of residential buildings in 2016.) Online 28.07.2021: https://www.iwu.de/fileadmin/user_upload/dateien/gebäudebestand/prj/Endbericht_Datenerhebung_Wohngeb%C3%A4udebestand_2016.pdf.
- [16] Stieß, I. et al. (2010). Handlungsmotive, -hemmnisse und Zielgruppen für eine energetische Gebäudesanierung. Ergebnisse einer standardisierten Befragung von Eigenheimsanierern. Frankfurt am Main. (May be translated as: Motives, obstacles and target groups for an energetic building retrofit. Results of a standardized survey of retrofitters.) Online 28.07.2021: http://www.isoepublikationen.de/publikationen/publikation-detail/?tx_refman_pi1%5Brefman%5D=354&tx_refman_pi1%5Bcontroller%5D=Refman&tx_refman_pi1%5Baction%5D=detail&cHash=75e2c320a175a52f327e678e4bdd61dc.
- [17] Gossen, M., and Nischan, C. (2014). Regionale Differenzen in der Wahrnehmung von energetischen Sanierungen. Ergebnisse einer qualitativen Befragung von privaten GebäudeeigentümerInnen zu energetischer Sanierung in zwei unterschiedlichen Regionen, Gebäude-Energiewende, Arbeitspapier, 1. (May be translated as: Regional differences in the perception of energy-related retrofits. Results of a qualitative survey of private building owners on energy-efficient retrofit in two different regions, building energy transition, working paper, 1st.) Online 28.07.2021: https://www.gebaeude-energiewende.de/data/gebEner/user_upload/Dateien/GEW_API_Ergebnisbericht_Interviews_final_141126.pdf.
- [18] Renz, I. and Hacke, U. (2016). Einflussfaktoren auf die Sanierung im deutschen Wohngebäudebestand. Ergebnisse einer qualitativen Studie zu Sanierungsanreizen und-hemmnissen privater und institutioneller Eigentümer. IWU, Darmstadt. (May be translated as: Influential factors on the retrofit in the German residential building stock. Results of a qualitative study on incentives and barriers to retrofit of private and institutional owners.) Online 28.07.2021: https://www.kfw.de/PDF/Download-Center/Konzernthemen/Research/PDF-Dokumente-alle-Evaluationen/Einflussfaktoren-auf-die-Sanierung-im-deutschen-Wohngeb%C3%A4udebestand_2016.pdf.
- [19] Kreditanstalt für Wiederaufbau (KfW) (online: 2020). Förderkredite und Zuschüsse für bestehende Immobilien. (May be translated as: Loans and grants for existing real estate.) Online 28.07.2021: <https://www.kfw.de/inlandsfoerderung/Privatepersonen/Bestandsimmobilie/F%C3%B6rderprodukte/F%C3%B6rderprodukte-f%C3%BCr-Bestandsimmobilien.html>.
- [20] Kreditanstalt für Wiederaufbau (KfW) (online: 2020), Evaluationen Energieeffizient Bauen und Sanieren (May be translated as: Evaluations of energy-efficient building constructions and retrofits.) Online 28.07.2021, <https://www.kfw.de/KfW-Konzern/Service/Download-Center/Konzernthemen/Research/Evaluationen/Evaluationen-Energieeffizient-Bauen-und-Sanieren/>.
- [21] Institut der Deutschen Wirtschaft (IW), Gutachten im Rahmen des Forschungsprogramms „Handwerk und Energiewende im Gebäudesektor“. Köln, 2017 (May be translated as: Expert opinion as part of the research program "Crafts and the energy transition in the building sector".) Online 28.07.2021, https://www.iwkoeln.de/fileadmin/publikationen/2017/317876/IW-Gutachten_2017_Energetische_Foerderung.pdf.
- [22] N. Diefenbach, Monitoring der KfW-Programme „Energieeffizient Sanieren“ und „Energieeffizient Bauen“ 2017, IWU, Darmstadt, 2018 (May be translated as: Monitoring of the KfW programs “Energy-efficient retrofit” and “Energy-efficient construction” 2017.) Online 28.07.2021: <https://www.kfw.de/PDF/Download-Center/Konzernthemen/Research/PDF-Dokumente-alle-Evaluationen/Monitoring-der-KfW-Programme-EBS-2017.pdf>.
- [23] Kreditanstalt für Wiederaufbau (KfW), Monitoring der KfW-Programme „Energieeffizient Sanieren“ und „Energieeffizient Bauen“ 2017, IWU, Darmstadt, Fraunhofer IFAM, Bremen, 2018 (May be translated as: Monitoring of the KfW programs “Energy-efficient retrofit” and “Energy-efficient construction” 2016) Online 28.07.2021: <https://www.kfw.de/PDF/Download-Center/Konzernthemen/Research/PDF-Dokumente-alle-Evaluationen/Monitoring-der-KfW-Programme-EBS-2017.pdf>.
- [24] Bundesamt für Wirtschaft und Ausfuhrkontrolle (BAFA) (online: 2020). Heizen mit Erneuerbaren Energien. (May be translated as: Heating with renewable energies.) Online 28.07.2021: https://www.bafa.de/DE/Energie/Heizen_mit_Erneuerbaren_Energien/heizen_mit_erneuerbaren_energien_node.html;jsessionid=EAA4476C1EBD21FBC7040BF8BE972452.1_cid362.
- [25] P. Runst, Kurswechsel in der deutschen Klimapolitik am Beispiel der energetischen Gebäudesanierung, Wirtschaftsdienst 96 (5) (2016) 340–343 (May be translated as: Strategy change in German climate policy using the example of energy-efficient building retrofits.) Online 15.02.2021: <https://link.springer.com/content/pdf/10.1007/s10273-016-1979-z.pdf>.
- [26] Einkommensteuergesetz (EStG) § 35c (2020). Steuerermäßigung für energetische Maßnahmen bei zu eigenen Wohnzwecken genutzten Gebäuden. (May be translated as: Tax reduction for energetic measures in buildings used for own residential purposes.) Online 28.07.2021: https://www.gesetze-im-internet.de/estg/_35c.html.
- [27] M. Menicou, et al., Economic evaluation of financial incentive schemes for energy retrofit projects in residential buildings, J. Sustain. Architect. Civ. Eng. 16 (3) (2016) 32–45, <https://doi.org/10.5755/j01.sace.16.3.16200>.
- [28] G. Trotta, et al., Energy efficiency in the residential sector: identification of promising policy instruments and private initiatives among selected European countries, Energy Effic. 11 (8) (2018) 2111–2135, <https://doi.org/10.1007/s12053-018-9739-0>.
- [29] L. Di Pilla, et al., Optimizing the distribution of Italian building energy retrofit incentives with Linear Programming, Energy Build. 112 (2016) 21–27, <https://doi.org/10.1016/j.enbuild.2015.11.050>.
- [30] P. Penna, et al., Multi-objective optimization for existing buildings retrofitting under government subsidization, Sci. Technol. Built. Environ. 21 (6) (2015) 847–861, <https://doi.org/10.1080/23744731.2015.1028867>.
- [31] M. Collins, et al., Financial Incentives for Residential Energy Efficiency Investments in Ireland: Should the Status Quo Be Maintained? ESRI WP562, 2017. May 2017, <http://hdl.handle.net/10419/174295>.
- [32] B. Wang, et al., A multi-objective optimization model for the life-cycle cost analysis and retrofitting planning of buildings, Energy Build. 77 (2014) 227–235, <https://doi.org/10.1016/j.enbuild.2014.03.025>.
- [33] G. Kubaroglu, R. Madlener, Evaluation of economically optimal retrofit investment options for energy savings in buildings, Energy Build. 49 (2012) 327–334, <https://doi.org/10.1016/j.enbuild.2012.02.022>.
- [34] R. Ruparathna, et al., Economic evaluation of building energy retrofits: a fuzzy based approach, Energy Build. 139 (2017) 395–406, <https://doi.org/10.1016/j.enbuild.2017.01.031>.
- [35] E. Asadi, et al., Multi-objective optimization for building retrofit strategies: a model and an application. <https://doi.org/10.1016/j.enbuild.2011.10.016>, 2011.
- [36] F. Rosso, et al., Multi-objective optimization of building retrofit in the Mediterranean climate by means of genetic algorithm application, Energy Build. (2020), <https://doi.org/10.1016/j.enbuild.2020.109945>, 109945.
- [37] E. Antipova, et al., Multi-objective optimization coupled with life cycle assessment for retrofitting buildings, Energy Build. 82 (2014) 92–99, <https://doi.org/10.1016/j.enbuild.2014.07.001>.
- [38] A. Jafari, V. Valentin, An optimization framework for building energy retrofits decision-making, Build. Environ. 115 (2017) 118–129, <https://doi.org/10.1016/j.buildenv.2017.01.020>.
- [39] R. Wu, et al., Multiobjective optimisation of energy systems and building envelope retrofit in a residential community, Appl. Energy 190 (2017) 634–649, <https://doi.org/10.1016/j.apenergy.2016.12.161>.
- [40] Hinz, E. (2012). Kosten energierelevanter Bau- und Anlagenteile bei der energetischen Modernisierung von Altbauten. IWU, Darmstadt. (May be translated as: Costs of energy-relevant building and plant components in the energy retrofit of old buildings.) Online 28.07.2021: https://www.bbsr.bund.de/BBSR/DE/Veroeffentlichungen/ministerien/BMVB/Online/2012/DL_ON072012.pdf;jsessionid=71E2323DCD432802330804D93853755F.live!1291?_blob=publicationFile&v=2.
- [41] Hinz, E. (2015). Kosten energierelevanter Bau- und Anlagenteile bei der energetischen Modernisierung von Altbauten. IWU, Darmstadt. (May be translated as: Costs of energy-relevant building and plant components in the energy retrofit of old buildings.) Online 28.07.2021: https://www.iwu.de/fileadmin/publikationen/handlungslogiken/2015_IWU_Hinz_Kosten-energierelevanter-Bau-und-Anlagenteile-bei-der-energetischen-Modernisierung-von-Altbauten.pdf.
- [42] GAMS Development Corp. (online: 2021). GAMS Studio. Online 10.12.2021: <https://www.gams.com/products/gams/gams-language/>.
- [43] S.F. Tadeu, et al., A comparison between cost optimality and return on investment for energy retrofit in buildings-A real options perspective, Sustain. Cities Soc. 21 (2016) 12–25, <https://doi.org/10.1016/j.scs.2015.11.002>.
- [44] VFF Merkblatt ES.01, Energetische Kennwerte von Fenstern, Türen und Fassaden. (May be translated as: Energy parameters of windows, doors and facades), AC-Code, 2018. DE45962974.
- [45] TABULA, TABULA Calculation Method – Energy Use for Heating and Domestic Hot Water, 2013. Online 28.07.2021, https://www.episcope.eu/fileadmin/tabula/public/docs/report/TABULA_CommonCalculationMethod.pdf.
- [46] DIN EN ISO 13790:2008-09, Energieeffizienz von Gebäuden - Berechnung des Energiebedarfs für Heizung und Kühlung. (May be translated as: energy performance of buildings - calculation of energy use for space heating and cooling), 2008.
- [47] DIN V 4108-6:2003-06, Wärmeschutz und Energie-Einsparung in Gebäuden - Teil 6: Berechnung des Jahresheizwärme- und des Jahresenergiebedarfs. (May be translated as: thermal protection and energy economy in buildings - Part 6: calculation of annual heat and energy use), 2003.
- [48] DIN V 4701-10:2003-08, Energetische Bewertung heiz- und raumlufttechnischer Anlagen - Teil 10: Heizung, Trinkwassererwärmung, Lüftung. (May be translated as: Energy efficiency of heating and ventilation systems in buildings - Part 10: Heating, domestic hot water supply, ventilation), 2003.
- [49] TABULA Web Tool, Developed within the framework of the Intelligent energy Europe projects TABULA and EPISCOPE, Online 28.07.2021, <http://webtool.building-typology.eu/#bm>, 2017.
- [50] Gebäudeenergiegesetz (GEG), Gesetz zur Einsparung von Energie zur Nutzung erneuerbarer Energien zur Wärme- und Kälteerzeugung in Gebäuden, Bearbeitungsstand 01.11.2020. (May be translated as: Law on saving energy for the use of renewable energies for heating and cooling of buildings. Processing status 01/11/2020.) Online 28.07.2021: <http://www.gesetze-im-internet.de/geg/>, 2020.
- [51] Energieeinsparverordnung (EnEV) (2015). Energieeinsparverordnung vom 24. Juli 2007 (BGBl. I S. 1519), die zuletzt durch Artikel 3 der Verordnung vom 24. Oktober 2015 (BGBl. I S. 1789) geändert worden ist. (May be translated as: Energy Saving Ordinance of July 24, 2007 (Federal Law Gazette I p. 1519), which was last amended by Article 3 of the Ordinance of October 24, 2015 (Federal Law Gazette I

- p. 1789.) Online 28.07.2021: https://www.gesetze-im-internet.de/enev_2007/BJNR151900007.html.
- [52] Statistisches Bundesamt (Destatis) (2020). Preisindizes für die Bauwirtschaft. Fachserie 17, Reihe 4 02/2020. (May be translated as: Price indices for the construction industry.) Online 28.07.2021: https://www.destatis.de/DE/Themen/Wirtschaft/Preise/Baupreise-Immobilienpreisindex/Publikationen/Downloads-Bau-und-Immobilienpreisindex/bauwirtschaft-preise-2170400203214.pdf;jsessionid=42B5FB00C084DCF86569A2D1976159C7.internet8731?_blob=publicationFile.
- [53] Sparkasse Koblenz (online: 2020), Modernisierungskredit (May be translated as: Retrofit credit). Online 1.2.2021, <https://www.sparkasse-koblenz.de/de/home/privatkunden/kredite-und-finanzierungen/modernisierungskredit.html>.
- [54] Mainzer Volksbank (online: 2020), Baufinanzierung (May be translated as: Construction loans). Online: 1.2.2021: <https://www.mvb.de/privatkunden/baufinanzierung/immobilie-kaufen/baufi-10-jahre.html>.
- [55] Sparkasse Heinsheim (online, Baufinanzierung (May be translated as: Construction loans). Online: 1.2.2021: <https://www.kreissparkasse-heinsberg.de/de/home/privatkunden/kredite-und-finanzierungen/baufinanzierung/baufilead.html>, 2020.
- [56] DIN V 18599-1:2018-09 (2018). Energetische Bewertung von Gebäuden - Berechnung des Nutz-, End- und Primärenergiebedarfs für Heizung, Kühlung, Lüftung, Trinkwarmwasser und Beleuchtung - Teil 1: Allgemeine Bilanzierungsverfahren, Begriffe, Zonierung und Bewertung der Energieträger. (May be translated as: Energy efficiency of buildings - Calculation of the net, final and primary energy demand for heating, cooling, ventilation, domestic hot water and lighting - Part 1: General balancing procedures, terms and definitions, zoning and evaluation of energy sources).
- [57] Bundesamt für Wirtschaft und Ausfuhrkontrolle (BAFA) (2019 b). Merkblatt zu den CO₂-Faktoren. Energieeffizienz in der Wirtschaft – Zuschuss und Kredit. (May be translated as: Leaflet on CO₂ factors. Energy efficiency in business - grant and credit.) Online 28.11.2021: http://www.mediagnose.de/wp-content/uploads/2020/02/eew_merkblatt_co2.pdf.
- [58] Icha, P. (2020). Entwicklung der spezifischen Kohlendioxid-Emissionen des deutschen Strommix in den Jahren 1990 -2019. Umweltbundesamt, Dessau-Roßlau. (May be translated as: Development of the specific carbon dioxide emissions of the German electricity mix in the years 1990-2019) Online 28.11.2021: https://www.umweltbundesamt.de/sites/default/files/medien/1410/publikationen/2020-04-01_climate-change_13-2020_strommix_2020_fin.pdf.
- [59] Verbraucherzentrale Nordrhein-Westfalen (VZ NRW) (2020): Datentabellen „Energiepreise in NRW“ Stand Juli 2020. (May be translated as: Data tables for energy prices in NRW as of July 2020.) Online 28.07.2021: <https://www.verbraucherzentrale.nrw/sites/default/files/2020-12/Datentabelle%20VZ-NRW%20November%202020.pdf>.
- [60] Energieeffizienzverband für Wärme, Kälte und KWK (AGFW) (2020). Statistik Heizkostenvergleich in Anlehnung an VDI2067 zum Stichtag 01.04.2020. (May be translated as: Statistics on heating cost comparison based on VDI2067 as of April 1st, 2020.) Online 08.07.2021: https://www.fernwaerme-info.com/fileadmin/Redakteure/fernwaerme-info/F%C3%B6rderung_und_Kosten/Heizkostenvergleich/Heizkostenvergleich_Webexemplar.pdf.
- [61] Bundesministerium für Wirtschaft und Energie (BMWi) (2015). Hintergrundpapier zur Energieeffizienzstrategie Gebäude. IWU, ifeu, PROGNOSE, Berlin, Heidelberg, Darmstadt, 131. (May be translated as: Paper on the energy efficiency strategy for buildings.) Online 28.07.2021: https://www.bmwi.de/Redaktion/DE/Downloads/E/energieeffizienzstrategie-hintergrundinformation-gebäude.pdf?_blob=publicationFile&v=5n.
- [62] Bundesministerium für Wirtschaft und Energie (BMWi), Bundesministerium für Umwelt, Naturschutz, Bau und Reaktorsicherheit (BMU) (2020). Bundeskabinett beschließt höheren CO₂-Preis, Entlastungen bei Strompreisen und für Pendler (May be translated as: Federal cabinet decides on higher CO₂ prices, relief for electricity prices and for commuters) Online 28.07.2021: <https://www.bmwi.de/Redaktion/DE/Pressemitteilungen/2020/20200520-bundeskabinett-beschliesst-hoeheren-co2-preis.html>.
- [63] Bundesministerium für Umwelt, Naturschutz und nukleare Sicherheit, Fragen und Antworten zur CO₂ Bepreisung zum 1. Januar 2021 (May be translated as: Questions and answers about CO₂ pricing as of January 1, 2021.) Online 28.07.2021: <https://www.bmu.de/service/haeufige-fragen-faq/fragen-und-antworten-zur-einfuehrung-der-co2-bepreisung-zum-1-januar-2021/>, 2021.
- [64] EPBD, Directive 2010/31/EU of the European Parliament and of the Council of 19 May 2010 on the energy performance of buildings (recast), Online 28.07.2021, <http://eurlex.europa.eu/LexUriServ/LexUriServ.do?uri=OJ:L:2010:153:0013,2010,0035:EN:PDF> Only in the Appendix.

Eidesstattliche Versicherung

gemäß § 13 Abs. 2 Ziff. 3 der Promotionsordnung des Karlsruher Instituts für Technologie für die KIT-Fakultät für Wirtschaftswissenschaften

1. Bei der eingereichten Dissertation zu dem Thema CONCEPTS AND TOOLS TO IMPROVE THE THERMAL ENERGY PERFORMANCE OF BUILDINGS AND URBAN DISTRICTS - DIAGNOSIS, ASSESSMENT, IMPROVEMENT STRATEGIES, AND COST-BENEFIT ANALYSES handelt es sich um meine eigenständig erbrachte Leistung.
2. Ich habe nur die angegebenen Quellen und Hilfsmittel benutzt und mich keiner unzulässigen Hilfe Dritter bedient. Insbesondere habe ich wörtlich oder sinngemäß aus anderen Werken übernommene Inhalte als solche kenntlich gemacht.
3. Die Arbeit oder Teile davon habe ich bislang nicht an einer Hochschule des In- oder Auslands als Bestandteil einer Prüfungs- oder Qualifikationsleistung vorgelegt.
4. Die Richtigkeit der vorstehenden Erklärungen bestätige ich.
5. Die Bedeutung der eidesstattlichen Versicherung und die strafrechtlichen Folgen einer unrichtigen oder unvollständigen eidesstattlichen Versicherung sind mir bekannt. Ich versichere an Eides statt, dass ich nach bestem Wissen die reine Wahrheit erkläre und nichts verschwiegen habe.

Belehrung:

Die Universitäten in Baden-Württemberg verlangen eine Eidesstattliche Versicherung über die Eigenständigkeit der erbrachten wissenschaftlichen Leistungen, um sich glaubhaft zu versichern, dass der Promovend die wissenschaftlichen Leistungen eigenständig erbracht hat.

Weil der Gesetzgeber der Eidesstattlichen Versicherung eine besondere Bedeutung beimisst und sie erhebliche Folgen haben kann, hat der Gesetzgeber die Abgabe einer falschen eidesstattlichen Versicherung unter Strafe gestellt. Bei vorsätzlicher (also wissentlicher) Abgabe einer falschen Erklärung droht eine Freiheitsstrafe bis zu drei Jahren oder eine Geldstrafe.

Eine fahrlässige Abgabe (also Abgabe, obwohl Sie hätten erkennen müssen, dass die Erklärung nicht den Tatsachen entspricht) kann eine Freiheitsstrafe bis zu einem Jahr oder eine Geldstrafe nach sich ziehen.

Die entsprechenden Strafvorschriften sind in § 156 StGB (falsche Versicherung an Eides Statt) und in § 161 StGB (fahrlässiger Falscheid, fahrlässige falsche Versicherung an Eides Statt) wiedergegeben.

§ 156 StGB: Falsche Versicherung an Eides Statt: Wer vor einer zur Abnahme einer Versicherung an Eides Statt zuständigen Behörde eine solche Versicherung falsch abgibt oder unter Berufung auf eine solche Versicherung falsch aussagt, wird mit Freiheitsstrafe bis zu drei Jahren oder mit Geldstrafe bestraft.

§ 161 StGB: Fahrlässiger Falscheid, fahrlässige falsche Versicherung an Eides Statt: Abs. 1: Wenn eine der in den § 154 bis 156 bezeichneten Handlungen aus Fahrlässigkeit begangen worden ist, so tritt Freiheitsstrafe bis zu einem Jahr oder Geldstrafe ein. Abs. 2: Straflosigkeit tritt ein, wenn der Täter die falsche Angabe rechtzeitig berichtigt. Die Vorschriften des § 158 Abs. 2 und 3 gelten entsprechend.

Karlsruhe, Germany, 15.05.2023

Zoe Mayer